A CFD MODELLING SYSTEM FOR AIR FLOW AND HEAT TRANSFER IN VENTILATED PACKING SYSTEMS DURING FORCED-AIR COOLING OF FRESH PRODUCE

A thesis presented in partial fulfilment of the requirements for
the Degree of Doctor of Philosophy in Food Engineering
at Massey University

Qian Zou
M.AppSci.(Hons)

2002

ABSTRACT

Forced-air cooling is the common method for precooling horticultural produce. Ventilated packaging systems are often used to facilitate cooling efficiency. A computational fluid dynamics (CFD) modelling system was developed to simulate airflow and heat transfer processes in the layered and bulk packaging systems during the forced-air cooling of fresh produce.

Airflow and heat transfer models were developed using a porous media approach. The areas inside the packaging systems were categorised as solid, plain air, and produce-air regions. The produce-air regions inside the bulk packages or between trays in the layered packages were treated as porous media, in which the volume-average transport equations were employed. This approach avoids dealing with the situation-specific and complex geometries inside the packaging systems, and therefore enables the development of a general modelling system suitable for a wide range of packaging designs and produce.

The calculation domains were discretised with a block-structured mesh system that was referenced by global and local grid systems. The global grid system specifies the positions of individual packages in a stack, and the local grid system describes the structural details inside individual package. The solution methods for airflow and heat transfer models were based on SIMPLER (Semi-Implicit Method for Pressure-Linked equations Revised) method schemes, and the systems of linear algebraic equations were solved with GMRES (Generalised Minimum Residual) method.

A prototype software package CoolSimu was developed to implement the solution methods. The software package hid the core components (airflow and heat solvers) from user, so that the users without any knowledge of CFD and heat transfer can utilise the software to study cooling operations and package designs. The user interaction components in CoolSimu enable users to specify packaging systems and cooling conditions, control the simulation processes, and visualise the predicted airflow patterns and temperature profiles.

When the predicted and measured product centre temperatures were compared during the forced-air cooling of fresh fruit in several layered and bulk packaging systems, good agreements between the model predictions and experimental data were obtained. Overall, the developed CFD modelling system predicted airflow patterns and temperature profiles with satisfactory accuracy.

ACKNOWLEDGEMENTS

I would like to thank the following persons for their guidance and help during the course of this project:

Dr Linus U. Opara, formerly Senior Lecturer, Institute of Technology and Engineering, Massey University, Chief Supervisor.

Professor Robert McKibbin, Institute of Information and Mathematical Sciences, Massey University, Chief Supervisor.

Professor Donald Cleland, Institute of Technology and Engineering, Massey University, Supervisor.

I would like to acknowledge the advice and assistance of Dr David Tanner, formerly Director of Fresh Technology, Massey University.

Finally, I wish to express my gratitude to my family, my parents and parents-in-law for their help and encouragement, and especially my wife Binglan for her endless support, understanding, and love.

TABLE OF CONTENTS

LIST OF FIGURES

LIST of TABLES

CHAPTER 1
INTRODUCTION

The horticultural industries make significant contributions to the New Zealand economy. In the last two decades horticultural export earnings increased from less than $200 million in 1980 to $ 1,700 million in 1999 (Ministry of Agriculture and Forestry, 2000). Recent industry studies have predicted that export returns will more than double again by 2010 (Ministry of Agriculture and Forestry, 2000). To maintain and increase their share of the highly competitive global market, the New Zealand horticultural industries have to produce and market products with the highest possible quality.

Effective temperature management is essential to maintain product quality. The temperature of horticultural produce at harvest is close to that of ambient air. Rapid reduction of produce temperature to the optimum storage condition results in the desired produce quality and prolonged storage life. Rapid cooling after harvest is generally referred to as precooling (Wills *et al.*, 1998). Forced-air cooling (pressure cooling) is often adopted for precooling of horticultural produce. Forced-air cooling involves creating a pressure gradient to force cold air through container vents. The rate of cooling is significantly increased as the surface area available for heat transfer is enlarged by forcing air through packages and thus around each item of produce rather than only over the package surfaces. The time needed for forced-air cooling is only 10-25 percent of that for room cooling (Mitchell 1992; Watkins, 1989).

During forced-air cooling, it is crucial to achieve fast and uniform cooling throughout stacks of bins or pallets. The cooling rates of products inside the packages depend mainly on heat transfer between cooling medium (air) and products in the packages. The heat transfer processes are closely related to airflow transport within the packaging systems.

Apart from its influence on the heat transfer processes, air distribution plays a crucial role in produce weight loss due to water vapour mass transfer between product and air. Other important quality-related factors, such as the concentrations of gases

(oxygen, nitrogen, carbon dioxide, ethylene, etc.) in the storage atmosphere and inside the produce, are also affected by air movement.

The heat and airflow transport processes are affected by the following factors:

- Materials and configurations of the produce packaging systems (trays, cartons, bins, palletisation patterns, stacking patterns, etc.)
- Characteristics of produce (dimensions, thermal properties, etc.)
- Cooling conditions (inlet airflow rates, inlet air temperature, inlet air moisture content, etc.)

Forced-air cooling requires the produce packages to be ventilated. Effective container venting is essential for efficient forced-air cooling. Cold air must be able to pass through all parts of the package so that all items of produce can be cooled evenly. As packages are usually stacked or palletised during forced-air cooling, the stack patterns should also allow a substantial amount of the airflow to be uniformly distributed over the whole packaging system.

A packaging system needs to be carefully evaluated before implementation to ensure the most efficient cooling operation. Ventilated packaging has been used by the New Zealand fresh fruit industries for a long time. A recent trend is to apply different packaging designs for different markets and consumer groups; consequently more new packaging systems need to be assessed in shorter periods of time. The traditional trial-and-error method for packaging re-development is no longer suitable. Prediction tools are therefore needed to examine the effects of a newly-proposed package on the cooling rate of the produce.

It is usually considered expensive, time-consuming and situation-specific to use only experimental methods for studying heat and airflow transfer processes. Furthermore it may be difficult to achieve a complete understanding of the phenomena by examining a large amount of experimental data. Alternatively, mathematical modelling is, overall, a cost-effective strategy for predicting the airflow patterns and temperature variation in controlled environments such as ventilated packages. If information on packaging systems, cooling conditions, and produce properties are used as model input data, the results obtained can predict the effects of these factors on the airflow

patterns and the product cooling rate. In this case, experiments may still have to be conducted for model verification.

Computational Fluid Dynamics (CFD) provides a sophisticated but economic tool for modelling airflow and heat transfer. CFD employs numerical methods to solve the fundamental fluid transport equations that are derived from the laws of conservation of mass, momentum and energy. The increasing capacity and decreasing cost of modern computers have made the application of CFD modelling more and more efficient and popular.

The overall aim of this project is to develop a CFD modelling system for simulating airflow and heat transfer processes to predict airflow patterns and temperature profiles in ventilated packaging systems during the forced-air cooling of fresh produce. Such a modelling system will find practical applications in evaluating forced-air cooling operations and assessment of cooling performance of alternative packaging designs for a range of horticultural commodities. In order to facilitate wider applications and use of the proposed system, user-friendly interfaces will be designed and incorporated, such that even users without any knowledge of CFD can find the prediction tools easy to use.

The rest of this thesis is organised as follows:

Chapter 2 reviews the literature on CFD, porous media methods, and the mathematical models for airflow and heat transfer in the air-based cooling of fresh produce.

Chapter 3 discusses the forced-air cooling systems for horticultural crops, and defines the exact system to be modelled in this study.

Chapter 4 presents the conceptual models for airflow in layered and bulk packaging systems, and then develops the corresponding CFD models for airflow.

Chapter 5 presents the conceptual models for heat transfer in layered and bulk packaging systems, and then develops the corresponding CFD models for heat transfer.

Chapter 6 deals with the solution methods of the air and heat transfer models.

Chapter 7 describes the user-friendly software package 'CoolSimu', which implements the solution procedures of the airflow and heat transfer models.

Chapter 8 presents the predicted airflow patterns and temperature profiles, and compares the predicted temperature profiles with experimental data for model validation.

Chapter 9 concludes this thesis by summarising the model development, implementation, and validation, and discussing the further work needed for model improvement and industrial applications.

Appendix A presents the details on how the algebraic discretisation equations are derived from the partial different equations in the airflow and heat transfer models.

CHAPTER 2
LITERATURE REVIEW

2.1 Introduction

This review focuses on the principles of Computational Fluid Dynamics (CFD), transport phenomena in porous media, and the mathematical models for airflow and heat transfer processes in air-based cooling of fresh produce. Five classes of relevant literature were reviewed: (a) general modelling methodology; (b) basic principles of CFD; (c) porous media approach; (d) modelling of airflow; (e) modelling of heat transfer during produce cooling.

2.2 Modelling Methodology

Harper & Wanninger (1969) defined mathematical models as the equations that simulate real world situations, because they behave in a manner analogous to the actual situations. Application of mathematical models reduces the scope and cost of experimentation, as modelling allows more alternatives to be considered which may be difficult or expensive to test (Levine, 1997).

2.2.1 Modelling Procedure

Meerschaert (1993) identified five main stages in a modelling process: asking the questions, selecting a modelling approach, formulating the model, solving the model, and answering the questions. The starting steps are to examine the real world system to be modelled, and to identify the problems to be solved. These would enable the modeller to decide on the objectives of modelling, the required accuracy, and the type and size of computer envisaged (Touber, 1984). Cleland (1990) introduced a general system for equation development suitable for modelling in the area of refrigeration. The sequence of model development for complex problems in engineering science is summarised in Figure 2.1 (Kleinsteuer, 1997).

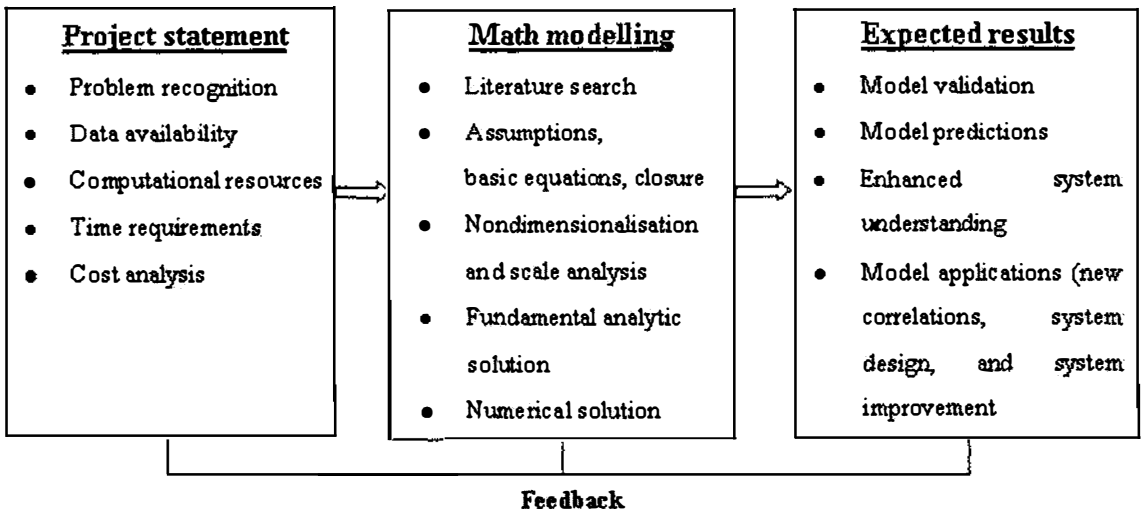

Figure 2.1 Sequence of model development (Kleinsteuer, 1997).

2.2.2 Types of Models

- **Steady-state and unsteady-state models**

According to whether the modelled systems change with time or not, models can be classified as steady state and dynamic (unsteady-state).

Steady-state models are suitable for modelling systems whose major parameters do not change with time. Steady-state models are also used to assess the performance of a system under different sets of operating conditions (Touber, 1984). Steady-state modelling may be applied to describe time-averaged behaviour of a transient system, while heat and mass accumulation in the system is negligible. Steady-state models generally demand less computational time and a small amount of input data, as the time-variability in system parameters is not considered.

Dynamic models are applied to assess how the time-variable effects, such as heat load, environmental conditions and start-up transients, influence normal system operation; accordingly advanced control strategies or detailed controllers may be developed (Cleland & Cleland, 1989). Dynamic models are usually considered closer to real world situations because most of them are time-dependent. However, as one more dimension (time) has to be dealt with mathematically, the dynamic modelling approach requires

more input data (initial conditions) and more computational capacity while solving the models.

- **Zoned and fully distributed models**

Based on the approaches for modelling positional variation of variables (space discretisation), models are divided into zoned and fully distributed models.

In zoned models, the space to be modelled is divided into several zones. For each zone an ordinary differential equation is adequate for each variable as the conditions within the zone are assumed to be uniform. Movement of fluid within a region may be defined by a plug-flow pathway, and the position of zones is arranged along the flow pathway through the system in a sequential fashion (Amos, 1995). Generally, only temperature and fluid concentration are solved in zoned models, while fluid velocity is defined with experimental data instead of by solving the momentum conservation equations. A single-zoned model is the simplest case in which the whole calculation region is treated as uniform.

Fully distributed models are also called fluid dynamic models, and use partial differential equations (PDEs) to formulate the full position-variability. These PDEs describe heat, mass, and momentum conservation within the considered region. This approach is usually able to simulate the real world more accurately than the zoned models, since fewer assumptions are needed to develop a fully distributed model. Finite-difference, finite-element, and finite-volume methods are the most commonly used numerical tools for solving the transport equations. Fully distributed modelling requires much larger computer memory and computational time than zoned modelling.

2.3 Principles of Computational Fluid Dynamics

Computational Fluid Dynamics (CFD) modelling is the process of representing a fluid flow problem by mathematical equations based on the fundamental laws of physics, and then solving those equations numerically using computer to predict the variation of the relevant parameters within the flow field (Jones & Whittle, 1992). The use of CFD

involves three main steps: the definition of problem, its solution, and analysis of the results (Scott & Richardson, 1997).

To define a problem, one firstly defines the boundary and/or initial conditions of a fluid field, and determines the flow characteristics that include dimensionality, compressibility, viscosity, dependence of time, variation of temperature, and existence of turbulence, etc. Based on the analysis, proper differential and auxiliary algebraic equations are chosen to formulate the transport phenomena of interest. The process of CFD solution consists of two stages: (a) discretisation in which the continuous partial differential equations and auxiliary (boundary and initial) conditions are converted into a discrete system of algebraic equations; (b) solution process in which an equation solver is used to solving the system of algebraic equations (Fletcher, 1988a). While analysing a CFD prediction, the output data are usually presented in graphic forms that are easily interpreted. Experimental validation is considered essential before final application of simulation results.

2.3.1 Fundamental Fluid Transport Equations

The starting point of CFD is the fundamental equations of fluid dynamics that describe the transport phenomena based on the conservation laws.

- **General transport equations**

All the conservation equations, also known as field equations, represent the variation of solution variables in space and time. These basic equations for incompressible, viscous flow and the energy equation for solid are presented as follows (Yuan, 1967; Fletcher, 1988a, 1988b; Ferziger & Peric, 1997).

(a) Continuity equations (mass conservation equation)

$$\nabla \cdot \mathbf{v} = 0 \tag{2.1}$$

where:

$\mathbf{v}$ = velocity vector ($m \cdot s^{-1}$).

(b) Navier-Stokes equations (momentum conservation equations) for fluid with constant viscosity

$$\rho_f \frac{\partial \mathbf{v}}{\partial t} + \rho_f \nabla \cdot (\mathbf{vv}) = \rho_f \mathbf{g} - \nabla p + \mu \nabla^2 \mathbf{v} \tag{2.2}$$

where:

t	=	time (s).
ρ_f	=	fluid density (kg m^{-3}).
$\mathbf{g}$	=	gravitational constant (m s^{-2}).
p	=	fluid pressure (N m^{-2}).
μ	=	fluid dynamic viscosity (N s m^{-2}).

(c) Equation for energy conservation

$$\rho_f C_P \frac{\partial T_f}{\partial t} + \rho_f C_P \nabla \cdot (\mathbf{v} T_f) = \nabla \cdot (K_f \nabla T_f) \tag{2.3}$$

where:

T_f	=	fluid temperature (K).
ρ_f	=	fluid density (kg m^{-3}).
C_P	=	fluid constant-pressure specific heat capacity (J $kg^{-1}K^{-1}$).
K_f	=	fluid thermal conductivity (W $m^{-1}K^{-1}$).

(d) Fourier equation for heat conduction (equation for energy conservation in solid)

$$\rho_s C_s \frac{\partial T_s}{\partial t} = \nabla \cdot (K_s \nabla T_s) \tag{2.4}$$

where:

T_s	=	solid temperature (K).
ρ_s	=	solid density (kg m^{-3}).
C_s	=	solid specific heat capacity (J kg^{-1} K^{-1}).
K_s	=	solid thermal conductivity (W m^{-1} K^{-1}).

- **Auxiliary conditions**

Many transport phenomena in the area of agricultural and food engineering may be described by the same set of equations. Differences in the results obtained stem from auxiliary conditions, e.g. boundary and initial conditions of the problem. Only unsteady flow modelling requires the initial conditions that specify initial values of velocity components, temperature, turbulence quantities for turbulent flows, and other solved-for quantities everywhere in solution region. The boundaries that are commonly encountered in practical flows are inflow, outflow, and wall (Awbi, 1989; Versteeg & Malalasekera, 1995; Ferziger & Peric, 1999).

For an inflow boundary, distribution of all solved-for variables (velocity components, temperature, turbulence quantities, etc.) must be given. It is often better to obtain the inlet conditions from experimental data than to use assumed values (Awbi, 1989; CHAM, 1995; Versteeg & Malalasekera, 1995).

Outflow boundaries are usually positioned at locations where flow is approximately unidirectional and where surface stresses take known values. The common outflow boundaries include external flows far from solid objects and fully-developed internal flows out of a duct. In these cases, boundary conditions are the specified pressure and zero gradients of velocity, temperature, and turbulence quantities along the flow direction. The longitudinal velocity may be derived from mass conservation for the whole flow field. The pressure may be fixed at a certain value, e.g. atmospheric pressure. The exit temperature can be calculated from the energy conservation of the entire domain of interest by taking into account the heat transfer across all boundaries (Awbi, 1989; CHAM, 1995; Versteeg & Malalasekera, 1995).

The no-slip boundary condition is used to specify the fluid velocity on a wall, i.e., the fluid moves at the same velocity as the wall (Awbi, 1989; CHAM, 1995; Versteeg & Malalasekera, 1995).

2.3.2 Discretisation Methods

After the mathematical model has been established, a suitable discretisation method is selected to approximate the differential equations with systems of algebraic equations. The most important discretisation methods are the finite difference (FD), finite volume (FV), and finite element (FE). In practice, all of the above methods can be applied to discretise spatial derivatives, but only the finite difference method is used for time discretisation (Fletcher, 1988a).

- **Finite difference method**

When applying the finite difference method, the solution domain is mapped with a grid. At each grid point, the partial derivatives in the PDEs are replaced by algebraic approximations in terms of nodal values of the solution functions. The result is one algebraic equation per grid node for each variable, in which the variable values at the node and a number of its neighbour nodes are unknowns in the equation. The approximations to the first and second derivatives of the variables are usually obtained by Taylor series expansion or polynomial fitting (Anderson *et al.*, 1984).

The FD method has only been applied to structured grids. The grid lines serve as local coordinates. This method is considered the easiest one for simple geometries. It is especially easy to employ high-order schemes on regular grids. The disadvantages of the FD method are that the conservation is not automatically enforced, and the restriction to simple geometries makes it difficult to deal with complex flows (Ferziger & Peric, 1999).

- **Finite volume method**

Patankar & Spalding (1972) firstly proposed the finite volume method. Patankar (1980) and Versteeg & Malalasekera (1995) introduced the details on the application of the FV approach in CFD. In the FV method a computational field is divided into a number of non-overlapping control volumes (also known as cells) such that each control volume surrounds a grid point. The transport PDEs are integrated over each control volume, and the surface and volume integrals are approximated using suitable quadrature formulae. The resulting convection and diffusion fluxes across the volume's faces are approximated

by the piece-wise profiles expressing the variation of dependent variables between the grid points. The discretisation equations obtained in this manner represent the conservation principle for the dependent variables over the control volume.

The FV Method can be used for any type of grid, so it is suitable for complex geometries. The FV discretisation equations maintain a close link with the original PDEs because the method is conservative by construction. The conservative nature makes it simple to understand and to program. It is also easy to carry out model changes and to evaluate the modelling results while using FV method. The disadvantage of the FV method is the difficulties encountered in applying high-order schemes, as two levels of approximations (interpolation and integration) are used in derivation of discretisation equations (Ferziger & Peric, 1999).

- **Finite element method**

The use of finite element method in CFD has been well documented by Peyret & Taylor (1985), Fletcher (1988a), and Reddy & Gartling (1994). The finite element method (FEM) divides the calculation domain into a number of discrete volumes or finite elements that are generally unstructured. For two-dimensional domains, the finite elements are usually triangles or quadrilaterals, while for three-dimensional domains they are commonly tetrahedra or hexahedra. The solution of a PDE can be expressed approximately in terms of the variable values in the corners of each element and an interpolation function within the element. Piecewise polynomials of relatively low orders are used as the interpolation functions. Both the weighted-residual (Galerkin) and variational (Rayleigh-Ritz) approaches can be adopted to derive discretisation equations, but the former is far more popular in the area of CFD. In the weighted-residual method, the solution function is substituted into a weighted integral of conservation law, while the weight function is usually of the same form as the solution function. The algebraic equations to be solved are derived by requiring the derivative of the integral with respect to each nodal value to be zero.

The most important advantage of the finite element method is the ability to handle complex geometries and highly non-uniform grids. However, the finite element approach is significantly more intensive in computing requirements, and it can be cumbersome

while applying high-order schemes or changing model input data (Collins & Ciofalo, 1991).

2.3.3 Computational Grids

Jones & Whittle (1992) discussed the important aspects of computational grids. Small cells or elements and the resulting overall fine grid provide more details on the variation of the variables over a calculation domain, and also ensure greater accuracy of solution. Theoretically, grids should be fine enough to generate accurate results with an appropriate level of detail. However, computational costs would be prohibitive in order to generate so-called 'grid independent results', particularly for three-dimensional buoyant flows (Jones & Whittle, 1992). Fine grids should be applied in the areas where the solution variables have large space gradients, such as inlets, outlets and near-wall regions. The grids that are too coarse may lead to convergence difficulties and inaccuracy resulting from false diffusion, particularly when the local flow direction is inclined to the grid directions (Patankar, 1980; CHAM, 1995). The commonly used grids are structured, block-structured, and unstructured grids.

Regular or structured grids consist of families of grid lines with the property that members of a single family do not cross each other and cross each member of other families only once. The simplest structured grid is the rectilinear (Cartesian) one, in which the cells are formed by rectangles or cubes. Another type of structured grid is the curvilinear grid (body-fitted coordinates, BFC) that can be thought of as a distorted Cartesian grid. While defining a grid, the cell aspect ratios have to be kept as close to unity as possible. Aspect ratios greater than about 5:1 could affect the rate of convergence. The rate of expansion of cell size between adjacent grid lines also should be limited for the sake of accuracy (Jones & Whittle, 1992). The neighbour connectivity of the structured grids simplifies programming in grid generation, and the resulting matrix of algebraic equation system has a regular structure, which can benefit the solution of the algebraic equations. The disadvantages of the structured grids are: the limitation in representing complex geometries, and the difficulty in controlling the distribution of grid points (concentration of points in one region produces unnecessary small spacing in other parts of the solution domain) (Patankar, 1980; CHAM, 1995; Ferziger & Peric, 1999).

A block-structured grid is made up of a number of blocks, each of which is an individual structured mesh. This kind of grid is more flexible than the previous one, since it allows the use of finer grids in the regions where large spatial gradients of variables exist. The block interfaces can be treated in a fully conservative manner (Ferziger & Peric, 1999). A block-structured grid can correct badly distorted cells, and ensure satisfactory orthogonality to avoid the occurrence of severe false diffusion (Jones & Whittle, 1992). Block-structured grids with overlapping blocks are sometimes referred to as composite or Chimera grids, which are often used to represent moving bodies in fluid regions (Ferziger & Peric, 1999).

An unstructured mesh may contain triangular elements as well as four or six sided cells. Previously unstructured meshes are mainly used for finite-element methods, but newly-developed algorithms allow this type of mesh to be applied in the finite-volume formulation (Jones & Whittle, 1992). Unstructured grids are the most flexible grids that can fit any arbitrary solution domain boundary. Computer codes for unstructured grids are also more flexible, as they need not be altered when the grid is locally refined. However, the advantage of flexibility is offset by the disadvantage of irregularity of the data structure. Much more effort is required in grid generation and data pre-processing (Ferziger & Peric, 1999).

2.3.4 Solution Methods for Discretisation Equations

Discretisation produces a system of algebraic equations. The methods for solving the system of equations are closely related to the character of the problem posed by the original PDEs. Equilibrium problems (steady flows) result in systems of algebraic equations that must be solved simultaneously throughout the problem domain in conjunction with boundary conditions. For unsteady flows, the marching-in-time method has to be used, and at each time an elliptic problem has to be solved (Anderson *et al.*, 1984; Ferziger & Peric, 1999).

Most problems in CFD require the solution of coupled system of equations; for instance, velocity components appear in the energy equations. Furthermore, almost all systems of the discretisation equations are non-linear and very large, and this makes simultaneous solution very difficult and expensive. It is often preferable to treat each equation as if it

has only a single unknown, and temporarily to treat the other variables as known by using the best currently available values for them. Iterations are performed on each equation in turn, repeating the cycle until all equations are satisfied. Two or more levels of iteration may be used to improve computational efficiency (Ferziger & Peric, 1999).

2.3.5 Presentation and Verification of CFD Results

CFD results are usually examined in two ways. In the traditional method, the results data file provides all relevant information, including the spatial co-ordinates defining the computational mesh and the values of solved variables (velocity components, temperature, pressure and concentrations) for each cell or element. For a large CFD problem, it is obviously inconvenient to interpret the results from a huge amount of numerical data in the output file. The second method (often called post-processing) allows the user to visualise the calculated results. A post-processor is used to process the data in the output file and display them graphically on the computer screen. There are three commonly-used graphical presentation methods: vector plot, contour plot, and iso-surface plot (CHAM, 1995; Jones & Whittle, 1992; Scott & Richardson, 1997).

The validity of a CFD model has to be assessed by comparison with experiment results. Two types of experiments are often conducted to verify CFD predictions. One is experimental flow visualisation that can qualitatively verify the flow patterns predicted by the CFD models. Methods for visualisation of airflow include smoke-tube, helium-bubble, tufts and interferometer approaches (Bradshaw, 1970; Goldstein, 1983). The second type of experiment measures the values of variables in different positions of the flow field. The measured variables may be velocity, temperature, pressure, concentrations, and turbulence quantities. Air velocity can be measured by Pitot tube, chronophotograph, propeller and vane anemometer, thermal anemometer, ultrasonic anemometer, and laser Doppler anemometer (Bradshwa, 1970; Cheremisinoff & Cheremisinoff, 1988; Fingerson & Freymuth, 1983).

2.4 Porous Media Models

A porous medium is a material or a structure that contains interconnected spaces, so-called pores or voids, embedded in the solid or semi-solid matrix. The pores can be

occupied by single-phase or multiphase fluids. Comprehensive reviews on transport phenomena in porous media have been provided by Dullien (1979), Cheng (1985), Nield & Bejan (1992), and Kaviany (1995, 1998). This review focuses on the momentum and energy transport of single-phase flow in saturated and rigid porous media, corresponding to the situation in the cooling of fresh produce stored in containers, which may be treated as packed beds of particles.

2.4.1 Structural Properties of Packed Beds

The macroscopic and microscopic pore structure parameters of porous media have been well documented by Dullien (1979), while Haughey & Beveridge (1969) reviewed the structural properties of packed beds. The structure of a packed bed is determined by several factors that include the shape of the particles, the distribution of particle sizes, and whether the column is packed regularly or randomly. For any regular packing of particles, the resulting pore structure is anisotropic, while a randomly packed bed may be treated as isotropic if the particles have nearly uniform shapes and sizes.

- **Porosity**

Porosity is defined as the fraction of the bulk volume of the porous sample that is occupied by pore or void space. Table 2-1 shows the porosities of regularly packed beds of identical spheres for different packing arrangements (Dullien, 1979; Chauk & Fan, 1998). In the random packing of identical spheres, the range of mean porosity values is associated with particular methods of formation, which was described by Haughey & Beveridge (1969) as:

- Very loose random packing: for sedimentation of spheres and inversion of the bed container, porosity is about 0.44;
- Loose random packing: for rolling spheres individually into place, individual random hand-packing, and dropping the spheres into the container as a loose mass, porosity is between 0.40 and 0.41;
- Poured random packing: when spheres are poured into a container, mean porosity is from 0.375 to 0.391;

- Close random packing: when the bed is vibrated or shaken down vigorously, minimum porosities from 0.359 to 0.375 are obtained.

Table 2.1 Packed bed porosities for different packing arrangement

Packing arrangement	**Contact points of each particle with the others**	**Porosity**
Sphere-rhombohedral	12	0.2595
Sphere-tetragonal	10	0.3019
Sphere-orthorhombic	8	0.3954
Sphere-cubic	6	0.4764

Roblee *et al.* (1958) and Benenati & Brosilow (1962) reported that adjacent to an impermeable boundary there is a region of relatively high porosity due to the discrepancy between the radii of curvature of the wall and the particles. As a result, the velocity has its maximum values near the wall, and flow channelling and mal-distribution may take place (Schertz & Bischoff, 1969). The channelling effect may exert considerable influence on the heat and mass transfer characteristics of the system. The measurements show that the porosity of a packed-sphere bed increases from a value of 0.36-0.4 in the bulk of the bed to 0.8-1.0 at the wall. The variation of the porosity takes the form of a damped oscillatory function with the oscillations damped out at about 4-5 sphere diameters from the wall (Benenati & Brosilow, 1962). As the oscillation of the porosity is generally insignificant for heat and mass transfer, the porosity distribution in a pecked bed is usually modelled by an exponential decaying function of the distance to the wall:

$$\phi = \phi_{\infty}(1 + ae^{-\frac{by}{d_p}}) \tag{2.5}$$

where

ϕ = porosity.

ϕ_{∞} = free stream porosity.

d_p = particle diameter (m).

y = distance from wall(m).

a = empirical constant.

b = empirical constant.

Different researchers adopted various values for the empirical parameters a and b in association with different free stream porosity ε_∞, which were summarised in Table 2.2. The values were obtained by fitting experimental data.

Table 2.2 Values of parameter a and b in Equation (2.5).

a	b	ϕ_∞	References
1	2	0.4	Cheng & Hsu, 1985; Cheng & Zhu, 1987; Nithiarasu *et al.*, 1997
1 (d_P= 5mm) 0.9 (d_P= 8mm)	2	Not specified	Vafai *et al.*, 1985
0.35 (d_P= 3mm) 0.43 (d_P= 5mm)	3	0.37	Poulikakos & Renken, 1987
5	1	Not specified	Hsu & Cheng, 1990
1.7	6	0.37	Amiri & Vafai, 1994, 1997
0.8	6	0.4	Chen *et al.*, 1996
2.256	2	0.307	Fu *et al.*, 1996; Fu & Huang, 1997, 1999

- **Permeability**

Specific or intrinsic permeability is used to measure the conductivity of a porous medium with respect to permeation by a Newtonian flow. In the case of single-phase flow it can be abbreviated as permeability. The permeability is generally independent of the nature of the fluid, but uniquely determined by the pore structure. When the flow is sufficiently slow and steady, Darcy's law is employed to define the permeability (Nield & Bejan, 1992):

$$\langle \mathbf{v} \rangle = -\frac{K}{\mu} \nabla p \tag{2.6}$$

where:

$\langle \mathbf{v} \rangle$ = superficial velocity (m s^{-1}).

K = permeability of porous medium (m^2).

μ = dynamic viscosity of fluid (kg m^{-1} s^{-1}).

p = pressure (N m^{-2}).

Considering that the beds are packed with the particles of approximately spherical shape and the particle diameters fall within a narrow range, the permeability can be calculated as (Macdonald *et al.*, 1979):

$$K = \frac{d_{eq}\phi^3}{A(1-\phi)^2} \tag{2.7}$$

$$d_{eq} = 6\frac{V_p}{S_p} \tag{2.8}$$

where:

ϕ = porosity.

d_{eq} = equivalent mean sphere diameter (m).

A = empirical parameter.

V_p = mean particle volume (m^3).

S_p = mean particle surface (m^2).

For the value of parameter A in Equation (2.7), Ergun (1952) proposed 150, and MacDonald *et al.* (1979) suggested 180, while some researchers also used 175 (Poulikakos & Renken, 1987; Chang & Chang, 1996). If the beds are packed with non-spherical particles, other values for the parameter may be derived according to experimental results (Comiti & Renaud, 1989).

- **Specific Surface Area**

The specific surface area of a porous material is defined as the average interstitial surface area of the voids and pores per unit bulk volume of the porous material.

2.4.2 Modelling Transport Phenomena in Porous Media

- **Volume Averaging Method**

Transport in porous media involves complex flow patterns around a solid matrix. Due to the random orientations of the solid phase, exact solutions for the detailed local flow field are generally impossible. The volume averaging method is usually applied to integrate the pore-level microscopic governing equations over a representative elementary volume (REV) for deriving the macroscopic transport equations. Applications of the volume averaging method in modelling transport processes in porous media have been well documented by Carbonell & Whitaker (1984), Bear & Bacchmat (1984, 1990), Levec & Carbonell (1985a, 1985b), Hsu & Cheng (1990), and Whitaker (1997).

While spatially averaging the microscopic governing equations, therefore certain details of the information with respect to microscopic structure are lost, so some well-established empirical relations are required for closure of the macroscopic equations. The dimension of the REV is required to be large compared to the characteristic dimension of the void space in order to obtain a representative number of pores and particles, but small compared to the dimension of the entire domain (Carbonell & Whitaker, 1984; Bear & Bacchmat, 1990).

In the volume averaging method, one has to distinguish two average values, superficial average and intrinsic phase average (Carbonell & Whitaker, 1984; Bear & Bacchmat, 1990):

$$\langle \psi \rangle = \frac{1}{V} \int_{v_\beta} \psi dV \tag{2.9}$$

$$\langle \psi \rangle_\beta = \frac{1}{V_\beta} \int_{v_\beta} \psi dV \tag{2.10}$$

where

ψ = quantity ψ of β phase in porous medium.

$\langle \psi \rangle$ = superficial average of ψ.

$\langle\psi\rangle_\beta$ = intrinsic phase average of ψ.

V = volume of representative element volume (m^3).

V_β = volume of β phase in representative element volume (m^3).

The relationship between $\langle\psi\rangle$ and $\langle\psi\rangle_\beta$ is:

$$\langle\psi\rangle = \phi\langle\psi\rangle_\beta \tag{2.11}$$

where:

ϕ = porosity.

The quantity ψ can be decomposed into spatial average and spatial deviation:

$$\psi = \langle\psi\rangle_\beta + \psi' \tag{2.12}$$

where:

ψ' = spatial deviation of ψ.

The most important averaging rules are the averages of products and spatial derivatives (Bear & Bacchmat, 1990):

$$\langle\psi\varphi\rangle_\beta = \langle\psi\rangle_\beta\langle\varphi\rangle_\beta + \langle\psi'\varphi'\rangle \tag{2.13}$$

$$\langle\nabla\psi\rangle = \nabla\langle\psi\rangle + \frac{1}{V}\int_{A_{\beta\sigma}} \mathbf{n}_{\beta\sigma}\psi dA \tag{2.14}$$

where:

ψ = quantity ψ of β phase in porous medium.

ψ' = spatial deviation of ψ.

φ = quantity φ of β phase in porous medium.

φ' = spatial deviation of φ.

$A_{\beta\sigma}$ = interfacial area between β-phase and σ-phase contained within REV (m^2).

$\mathbf{n}_{\beta\sigma}$ = unit normal vector pointing from β-phase to σ-phase.

- **Macroscopic continuity equation**

Applying the volume averaging on the microscopic continuity equation for incompressible fluid, Equation (2.1), and using the no-slip boundary on solid-fluid interface, the macroscopic continuity equation can be derived (Bear & Bacchmat, 1990):

$$\nabla \cdot \langle \mathbf{v} \rangle = 0 \tag{2.15}$$

- **Macroscopic momentum equation**

Spatially averaging microscopic momentum equation for incompressible fluid, Equation (2.2), and using no-slip boundary on solid-fluid interface, the macroscopic momentum equation can be derived (subscripts f and s represent the fluid and solid phase in following equations) (Bear & Bacchmat, 1990; Hsu & Cheng, 1990):

$$\rho_f \frac{\partial}{\partial t}(\phi \langle \mathbf{v} \rangle_f) + \rho_f \nabla \cdot (\phi \langle \mathbf{v} \rangle_f \langle \mathbf{v} \rangle_f) + \rho_f \nabla \cdot (\phi \langle \mathbf{v}'\mathbf{v}' \rangle) = -\nabla(\phi \langle p \rangle_f) + \mu \nabla^2 (\phi \langle \mathbf{v} \rangle_f) + \phi \rho_f \mathbf{g} + \mathbf{B} \tag{2.16}$$

$$\mathbf{B} = -\frac{1}{V} \int_{A_{fs}} \mathbf{n}_{fs} P dA + \frac{1}{V} \int_{A_{fs}} \mathbf{n}_{fs} \cdot \mu \nabla \mathbf{v} dA \tag{2.17}$$

where:

$\mathbf{B}$ = body-force related to solid matrix ($N\ m^{-3}$).

$\mathbf{v}'$ = spatial deviation of fluid velocity ($m\ s^{-1}$).

ϕ = porosity.

A_{fs} = interfacial area between fluid phase and solid phase contained within REV (m^2).

$\mathbf{n}_{fs}$ = unit normal vector pointing from fruit phase to solid phase.

The third term in the left-hand side of Equation (2.16) is the hydrodynamic dispersion term, which is of higher order than the second term on the left-hand side, and can therefore be neglected. The body-force term **B** is a measure of the flow resistance due to the existence of the solid matrix. Vafai & Tien (1981) and Hsu & Cheng (1990) used the Ergun expression to relate **B** with the superficial velocity:

$$\mathbf{B} = -\frac{\mu\phi\langle\mathbf{v}\rangle}{K} - \frac{\rho_f F\phi|\langle\mathbf{v}\rangle|\langle\mathbf{v}\rangle}{\sqrt{K}} \tag{2.18}$$

where:

K = permeability (m^2).

F = Forcheimer coefficient.

Replacing **B** with the Ergun expression, the macroscopic momentum equation becomes (Hsu & Cheng, 1990):

$$\rho_f \frac{\partial}{\partial t}\langle\mathbf{v}\rangle + \rho_f \nabla\cdot\left(\frac{\langle\mathbf{v}\rangle\langle\mathbf{v}\rangle}{\phi}\right) = -\nabla\langle P\rangle + \mu_{eff}\nabla^2\langle\mathbf{v}\rangle - \frac{\mu\phi\langle\mathbf{v}\rangle}{K} - \frac{\rho_f F\phi|\langle\mathbf{v}\rangle|\langle\mathbf{v}\rangle}{\sqrt{K}} + \phi\rho_f\mathbf{g}$$

Transient term | macroscopic convection term | pressure gradient | Brinkman term | Darcy term | Forcheimer tem | gravitational body-force term

(2.19)

where:

μ_{eff} = effective viscosity of fluid in porous medium (kg m^{-1} s^{-1}).

The transient term is used for solving unsteady flow. The macroscopic convection term represents macroscopic inertia, which is responsible for the growth of the momentum boundary, and only significant over a length of the order of $K\rho u_c / \mu$ (u_c is characteristic velocity). The Brinkman term accounts for macroscopic or bulk viscous diffusion mainly caused by external bounding surface. The Darcy term describes the effect of microscopic viscous shear stress (surface drag) offered by the solid matrix. The Forcheimer term resembles the microscopic inertial force (form drag) due to solid obstacles (Vafai & Tien, 1981; Neild & Bejan, 1992; Kaviany, 1998). Equation (2.19) is often referred to as the generalised macroscopic momentum equation for porous media.

For most porous media, setting $\mu_{eff} = \mu$ provides good agreements with experimental data (Neale & Nader, 1974). It appears to be the established practice to identify μ_{eff} with μ for porous media in general.

The Forcheimer coefficient F may be expressed as follows for packed beds of particles:

$$F = \frac{B}{\sqrt{A\phi^3}} \tag{2.20}$$

where:

A = parameter in Equation (2.7).

B = empirical parameter.

Different values for the parameters A and B have been proposed. Ergun (1952) suggested A =150 and B=1.75 on the basis of 640 experiments on spheres of different diameters, sand and coke particles. Macdonald *et al.* (1979) recommended A=180 and B=1.8-4.0 depending on the surface roughness of the particles. Lee & Yang (1997) provided different correlations for permeability K and Forcheimer coefficient F after numerically solving the microscopic transport equations for fluid flow cross a bank of circular cylinders.

- **Macroscopic energy equations**

(a) General macroscopic energy equations

Applying volume averaging to the energy conservation equations for fluid and solid, Equation (2.3) & (2.4), and using no-slip boundary on solid-fluid interface, the macroscopic energy equations for incompressible fluid and solid phases can be derived:

$$\rho_f C_P \phi \frac{\partial \langle T_f \rangle_f}{\partial t} + \rho_f C_P \nabla \cdot (\langle \mathbf{v} \rangle \langle T_f \rangle_f) = \nabla \cdot (\phi K_f \nabla \langle T_f \rangle_f) + \nabla \cdot \left[\frac{1}{V} \int_{A_{fs}} \mathbf{n}_{fs} K_f T'_f dA \right] + \frac{1}{V} \int_{A_{fs}} \mathbf{n}_{fs} \cdot K_f \nabla T_f dA - \rho_f C_P \nabla \cdot (\phi \langle \mathbf{v}' T'_f \rangle) \tag{2.21}$$

where:

T_f = fluid temperature (T).

ρ_f = fluid density (kg m^{-3}).

C_P = fluid constant-pressure specific heat capacity (J K^{-1} kg^{-1}).

K_f = fluid thermal conductivity (W K^{-1} m^{-1}).

T_f' = spatial deviation of fluid temperature (K).

$\mathbf{v}'$ = spatial deviation of fluid velocity (m s^{-1}).

A_{fs} = interfacial area between fluid phase and solid phase contained within REV (m^2).

$\mathbf{n}_{fs}$ = unit normal vector pointing from fruit phase to solid phase.

ϕ = porosity.

$$\rho_s C_s (1-\phi)\frac{\partial \langle T_s \rangle_s}{\partial t} = \nabla \cdot [(1-\phi) K_s \nabla \langle T_s \rangle_s] - \nabla \cdot \left[\frac{1}{V} \int_{A_{fs}} \mathbf{n}_{fs} K_s T'_s dA \right] - \frac{1}{V} \int_{A_{fs}} \mathbf{n}_{fs} \cdot K_s \nabla T_s dA \tag{2.22}$$

where:

T_s = solid temperature (T).

ρ_s = solid density (kg m^{-3}).

C_s = solid specific heat capacity (J K^{-1} kg^{-1}).

K_s = solid thermal conductivity (W K^{-1} m^{-1}).

T_s' = spatial deviation of solid temperature (K).

While deriving above equations, the following relation is used (Bear & Bacchmat, 1990):

$$\nabla \phi = -\frac{1}{V} \int_{A_{fs}} \mathbf{n}_{fs} dA \tag{2.23}$$

The second terms on the right-hand side (RHS) of Equation (2.21) and (2.22) are called tortuosity terms involving the area integrals of the spatial deviations in temperature along the surface. The third terms on the RHS of the two equations represent heat exchange between fluid and solid phases. The fourth term on the RHS of Equation (2.21) is a thermal dispersion term that is the volume average of the product of spatial deviations in velocity and temperature (Levec & Carbonell, 1985).

(b) Thermal dispersion

Thermal dispersion is heat transfer caused by hydrodynamic mixing of the interstitial fluid at pore scale due to the nature of the porous structure (Neild & Bejan, 1992). The thermal dispersion term is usually related to the macroscopic temperature gradient and an empirical dispersion conductivity or diffusion tensor:

$$-\rho_f C_p \nabla \cdot (\varepsilon \langle \mathbf{v}' T_f' \rangle) = \nabla \cdot \mathbf{K}_d \cdot \nabla \langle T_f \rangle_f \tag{2.24}$$

where:

$\mathbf{K}_d$ = dispersion conductivity tensor (W K^{-1} m^{-1}).

For isotropic porous media, the longitudinal dispersion and transverse dispersion conductivities can be used to express the dispersion conductivity tensor (Kaviany, 1998):

$$\mathbf{K}_d = \mathbf{nn} K_{dl} + (\mathbf{I} - \mathbf{nn}) K_{dt} \tag{2.25}$$

where:

$\mathbf{n}$ = unit vector in direction of fluid superficial velocity.

$\mathbf{I}$ = second-order identity tensor.

K_{dl} = longitudinal dispersion conductivity (W K^{-1} m^{-1}).

K_{dt} = transverse dispersion conductivity (W K^{-1} m^{-1}).

Wakao & Kaguei (1982) suggested the longitudinal and transverse thermal conductivities as linear functions of Peclet number:

$$\frac{K_{dl}}{K_f} = C_l Pe_d \tag{2.26}$$

$$\frac{K_{dt}}{K_f} = C_t Pe_d \tag{2.27}$$

$$Pe_d = \frac{C_p \rho_f u d_p}{K_f} \tag{2.28}$$

where:

Pe_d = Peclet number based on particle dimension.

u = superficial fluid velocity component in main flow direction (m s^{-1}).

d_p = diameter of particles (m).

ρ_f = fluid density (kg m^{-3}).

C_P = fluid constant-pressure specific heat capacity (J K^{-1} kg^{-1}).

K_f = fluid thermal conductivity (W K^{-1} m^{-1}).

C_l = empirical parameter (~ 0.5).

C_t = empirical parameter (~ 0.1).

Amiri & Vafai (1994, 1998) applied the above relations for studying forced convective flows through 2D porous channels. The correlations were also used by various researchers to study natural convective flows in porous media, in which the ranges of the empirical parameters C_l and C_t were 1/7-1/3 (Hong & Tien, 1987, Hong *et al.*, 1987; Lai & Kulacki, 1989; Leu & Jang, 1995; Murthy & Singh, 1997).

Cheng and his co-workers related the local transverse dispersion conductivity with Peclect number and a dispersive length modelled by a Van Driest wall function (Cheng & Hsu, 1985; Cheng & Zhu, 1987; Cheng *et al.*, 1988):

$$\frac{K_{dt}}{K_f} = D_t Pe_d l \tag{2.29}$$

$$l = 1 - e^{-\frac{y}{wd_p}} \tag{2.30}$$

where:

D_t = empirical constant.

l = dimensionless dispersion length.

w = empirical constant.

y = distance from wall (m).

In the above equations, the empirical parameters w and D_t depend on the coefficients a and b in the equation for porosity Equation (2.5). The best match with experimental data are D_t = 1.2 and w = 1 if a = 5 and b = 1. Fu and his co-workers used this correlation to

formulate forced convection jet flow through porous blocks (Fu *et al.*, 1996; Fu & Huang, 1997, 1999).

Hsu & Cheng (1990) performed a theoretical analysis on velocity and temperature spatial deviations in a dilute array of spheres, and proposed the following expressions for the thermal dispersion conductivity tensor:

$$\mathbf{K_d} = \mathbf{D}K_f \frac{1-\phi}{\phi} Pe_d \qquad \text{(pore Reynolds number >> 10)} \qquad (2.31)$$

$$\mathbf{K_d} = \mathbf{D}^* K_f \frac{1-\phi}{\phi^2} Pe_d^2 \qquad \text{(pore Reynolds number << 10)} \qquad (2.32)$$

where:

D = constant tensor.

D* = constant tensor.

Kuwahara *et al.* (1996) obtained the following correlations for transverse thermal conductivity after solving the microscopic velocity and temperature fields for the flow passing a collection of square rods:

$$\frac{K_{dt}}{K_f} = 0.022 \frac{Pe_d^{1.7}}{(1-\phi)^{\frac{1}{4}}} \qquad (\mathrm{Pe_d} < 10) \qquad (2.33)$$

$$\frac{K_{dt}}{K_f} = 0.052(1-\phi)^{\frac{1}{2}} Pe_d \qquad (\mathrm{Pe_d} > 10) \qquad (2.34)$$

Other correlations for the thermal dispersion conductivity were summarised by Kaviany (1995, 1998), though many correlations are for the total diffusivity coefficient (including the effects of molecular thermal diffusion and thermal dispersion).

(c) Macroscopic energy equations under local thermal equilibrium

If the temperature difference between fluid and solid phases is negligible at all locations in the considered system, we can assume that the fluid and solid phases are at local thermal equilibrium, and following relation holds:

$$\langle T_f \rangle_f = \langle T_s \rangle_s = \langle T \rangle \tag{2.35}$$

By introducing an effective thermal conductivity tensor, $\mathbf{k_e}$, to account for the effects of the tortuosity terms, the Equation (2.21) and (2.22) can be combined into one energy equation (Kaviany, 1998):

$$[\phi \rho_f C_P + (1-\phi)\rho_s C_s]\frac{\partial \langle T \rangle}{\partial t} = \nabla \cdot \mathbf{K}_e \cdot \nabla \langle T \rangle + \nabla \cdot \mathbf{K}_d \cdot \nabla \langle T \rangle \tag{2.36}$$

where:

$\mathbf{K_e}$ = effective thermal conductivity tensor (W K^{-1} m^{-1}).

As only one energy equation is used, the above formulation is also called one-equation heat transfer model for porous media. The effective thermal conductivity for isotropic media K_e is defined by (Hsu & Cheng, 1990):

$$\nabla \cdot (K_e \nabla \langle T \rangle) = \nabla \cdot \{[(1-\phi)K_s + \phi K_f]\nabla \langle T \rangle\} + \nabla \cdot \left[\frac{1}{V}\int_{A_{fs}} \mathbf{n}_{fs}(K_f T'_f - K_s T'_s)dA\right] \tag{2.37}$$

The effective thermal conductivity depends on the thermal conductivity of each phase, the structure of the solid matrix (especially, the extent of the continuity of the solid phase), and contact resistance between particles (e.g. surface coatings). Kaviany (1995, 1998) reviewed several empirical correlations for isotopic effective thermal conductivity of packed beds, which are mainly derived based on experimental data or semi-analytical prediction.

(d) Macroscopic energy equations without assuming local thermal equilibrium

Local thermal equilibrium does not hold in many cases, which include large solid block surrounded by relatively narrow fluid pathways, significant heat generation occurring in either the fluid or solid phase, and large temperature variation at boundaries when the solid and fluid phases have significantly different heat capacities and thermal conductivities. Under these circumstances, two separate energy equations are needed for

the fluid and solid phases. This approach is usually referred to as two-equation model for heat transfer in porous media. Kaviany (1995, 1998) provided the solid and fluid energy equations derived directly from Equations (2.21) and (2.22). In these equations, a set of tensors were proposed for modelling turtuosity and dispersion terms, and an interfacial heat transfer coefficient was also employed to account for heat exchange between fluid and solid particles.

The following energy equations were applied by Vafai & Sozen (1990), Amiri & Vafai (1994), and Ichimiya *et al.* (1997) for modelling heat transfer for incompressible forced convective flows through packed beds:

$$\rho_f C_P \phi \frac{\partial \langle T_f \rangle_f}{\partial t} + \rho_f C_P \nabla \cdot (\langle \mathbf{v} \rangle \langle T_f \rangle_f) = \nabla \cdot (\phi K_f \nabla \langle T_f \rangle_f) + \nabla \cdot \mathbf{K}_d \cdot \nabla \langle T_f \rangle_f + h_{sf} a_{fs} (\langle T_s \rangle_s - \langle T_f \rangle_f) \tag{2.38}$$

$$\rho_s C_s (1-\phi) \frac{\partial \langle T_s \rangle_s}{\partial t} = \nabla \cdot [(1-\phi) K_f \nabla \langle T_f \rangle_f] - h_{sf} a_{fs} (\langle T_s \rangle_s - \langle T_f \rangle_f) \tag{2.39}$$

where:

a_{sf} = specific surface area (m^{-1}).

h_{sf} = interfacial heat transfer coefficient ($J\ K^{-1}\ m^{-2}$).

The above two-equation model was also used by Slimi *et al.* (1998) to study transient natural convection in a vertical cylinder filled with a porous medium. The value of interfacial heat transfer coefficient h_{sf} depends on the specific energy equations used. Kaviany (1995, 1998) summarised a number of relations for the interfacial heat transfer coefficient.

- **Boundary conditions**

For impermeable boundaries, if the momentum equation does not include the Brinkman term, a slip boundary condition has to be employed. Otherwise, the no-slip condition is applicable, as in a plain fluid (Neild & Bejan, 1992). The channelling effect is usually

taken into account by using variable porosity and permeability in the near-wall region, as discussed on Section 2.4.1.

At the interface between a porous medium and a fluid, the fluid flow and the temperature fields need to satisfy a set of continuity conditions, though there is a discontinuity of material properties at the interface. These conditions include continuity of normal and tangential velocities, pressure, stresses, temperature, and heat flux (Vafai & Thiyageeraja, 1987). When dealing with domains partially filled with a porous medium, Beckerman, *et al.* (1987), Hadim (1994), Fu *et al.* (1996), and Fu & Huang (1997, 1999) combined the volume-averaged momentum equation for porous media and the usual Navier-Stokes equation for fluids by introducing a binary parameter λ (λ=1 in porous region, λ=0 in fluid region). This approach simplified the numerical solution procedures.

However, the system of equations may be over-determined, if one just simply matches the momentum fluxes expressed by the volume-averaged velocity (porous medium side) and ordinary velocity (clear fluid side). A similar conclusion can be drawn for heat flux across the interface if local thermal equilibrium is not valid (Neild & Bejan, 1992). Sahraoui & Kaviany (1992, 1993, 1994) performed direct simulations on momentum and heat transfer across the interface between plain fluid and porous media made of cylindrical particles. Ochoa-Tapia & Whitaker (1995a, 1995b, 1997) derived a set of boundary conditions for the fluid and porous medium interface, in which the tangential stress and heat flux were specified in the form of jump conditions.

2.5 Modelling Airflow in Agricultural and Food Engineering

CFD has become a commonly-used tool for studying airflow in the agricultural and food engineering applications; for instance, CFD models have been used to simulate the airflow in ventilated buildings, refrigerated stores, food processing machines etc.

2.5.1 Modelling Airflow Patterns in Agricultural Buildings

A number of CFD models have been established to simulate air motions in agricultural buildings that are mainly greenhouses and livestock buildings (Mistriotis *et al.*, 1997b).

Gosman *et al.* (1980) applied a finite volume method to solve the 3D equations for air mass, momentum, energy, and turbulence quantities in the k-ε model. The effects of buoyancy were neglected in the model due to the low Archimedes number for air movement in the ventilated room. Acceptable agreement was obtained when measured and predicted velocity profiles in the room and velocity decay in the air jet were compared. Timmons *et al.* (1980) applied an inviscid two-dimensional model to simulate the airflow patterns in a slot-ventilated livestock facility. The model used the equations in stream function and vorticity form, combined with semi-empirical relationships for vorticity distribution. The accuracy was considered acceptable except in the near-wall region where the error was due to the inviscid assumption. Bottcher (1987) also used the vorticity stream-function approach to model the airflow driven by a ceiling fan. Three different wall boundary conditions were tried while applying a finite difference scheme to solve the model. Flow patterns obtained with both the zero-vorticity slip condition and the viscous sub-layer slip condition were found similar to those photographed in a cylindrical enclosure with a suspended fan.

Markatos & Malin (1982) developed a 2D finite-difference procedure for predicting velocity and temperature distributions in enclosures containing a fire. A heat source was used to represent the fire. Additional terms were added to the k-ε equations to prescribe the buoyant effects. The results were shown to be in reasonable agreement with experimental data. Markatos & Pericleous (1984) presented a computational method to obtain solutions of buoyancy-driven laminar and turbulent flows and heat transfer in a square cavity with differentially-heated sidewalls. The k-ε model was used for flows with Rayleigh numbers greater than 10^6. The results were compared with a published benchmark numerical solution, and the agreement was good. Reinartz & Renz (1984) investigated the behaviour of a jet emerging from a radial pallet and the resulting airflow in a rectangular room. A finite-volume scheme was applied to solve the 2D flow equations as well as the k-ε turbulence model. Acceptable accuracy of the numerical solution was found when it was compared with experimental data.

Choi *et al.* (1988) used a standard k-ε turbulence model to predict two-dimensional isothermal airflow patterns in a slot-ventilated enclosure of simple geometry. Air distribution patterns, velocities, jet growth and attachment, and entrainment predictions were found to agree well with published data. This model was further extended to model

a ventilated air space having an obstacle to flow (Choi *et al.*, 1990). Sufficiently refined grid spacing was used in simulating corner eddy motion near solid boundaries. Comparison of predictions with the measured data showed that air distribution patterns were well predicted, and calculated air velocities were reasonably accurate.

Awbi (1989) described a finite-volume method to predict the airflow and heat transfer in a 2D enclosure and the 3D flow of a wall jet over surface-mounted obstacles. The CFD solution produced good predictions of the air velocity and temperature distribution in a test room cooled by a ceiling jet. No experimental data were used to validate other predictions involving the heating and cooling of a room and flow of a wall jet over an obstacle. A Low-Reynolds-Number k-ε model was developed by Chen *et al.* (1990) for the prediction of natural convection flow in cavities with Rayleigh numbers of the order of 10^{10}. The buoyancy was represented according to the Boussinesq approximation, and the buoyancy production terms were added to the k-ε equations. Predicted velocity and temperature profiles were in good agreement with the measurements.

Hoff *et al.* (1992) applied a CFD model to investigate the effects of animal-generated buoyant forces on air temperature and speed distributions in a ceiling-slot, ventilated, swine-growing facility. The model incorporated the Lam-Bremhorst turbulence model (LBLR) for low Reynolds number airflow typical of slot-ventilated livestock facilities. Both numerical and experimental investigations were conducted using a 1/5 scale-model facility. The model predicted airflow patterns adequately for Archimedes number $Ar_c>40$ and inlet jet momentum number $J < 0.00053$. For $Ar_c<40$ and $J > 0.00053$, the discrepancy between predicted and measured airflow patterns was attributed to variations in inlet flow development assumptions. This model was further evaluated by Hoff *et al.* (1995). Overall, the LBLR model was found to adequately predict air speed and temperature profiles, however shortcomings were indicated by comparisons of specific profiles. The model had a tendency to under-predict the ceiling detachment location for flows with $Ar_c>40$, and to over-predict the detachment location for flows with $Ar_c < 40$. The model also under-predicted the overall spread of the inlet jet.

Hoff (1995) developed a simplified turbulence model for describing airflow in ceiling slot-ventilated enclosures. An effective viscosity was defined as a function of the inlet Reynolds number (Re_H) and normalised vertical height from the floor. The effective

viscosity was used to selectively augment the laminar viscosity in the Navier-Stokes equations. Predicted comparisons between the simplified and the LBLR models showed negligible differences for ventilation conditions with Re_H between 11,752 and 35,032.

Liu *et al.* (1996) numerically simulated a plane-free jet using the standard k-ε model and four non-uniform grid patterns. An adequate solution was reached with five grid points in the inlet for the jet studied. The solution was in good agreement with experimental results. A plane-wall jet was also simulated using five different grids and three k-ε models, which were the standard k-ε model (STD), Lam and Bremhorst low Reynolds number model (LB), and Lam and Bremhorst low Reynolds number model with wall functions (LBW). The LBW model was found better than the other two models. The LB model gave the worst performance for the grids tested, while the STD model did not always converge if all grid points were not in the fully turbulent region. Compared with published data, all three models predicted the velocity profile and velocity decay well, but significantly over-predicted the jet spread and entrainment ratio.

Maghirang & Manbeck (1993) and Maghirang *et al.* (1994) modelled the transport of buoyant bubbles and 5 μm particles in slot-inlet ventilated airspace under isothermal and fully turbulent flow conditions. Airflow was modelled using the standard k-ε turbulence model. Particle transport was formulated using the equation of motion of particles. The model was solved by a CFD code FLUENT. Comparison between the numerical solution and experimental results showed good agreement in velocity fields and bubble trajectories, fates, and residence times. Worley & Manbeck (1995) applied a similar approach to the modelling of airflow patterns and particle transport through a two-storey stack layer facility with mild weather conditions. The model was validated by experimental results obtained from a 1/5 scale physical model.

Hoff & Bundy (1996) compared a LBLR model and a multi-zoned model in describing the distribution of carbon dioxide in a simulated swine grower pen. The multi-zoned model, initially developed by Liao & Fedds (1992), assumed three general airflow regions. Both the LBLR and multi-zoned models predicted similar trends in normalised CO_2 levels in the region immediately affected by the ventilating air jet. The multi-zoned model, which required a prescribed airflow pattern and a detailed knowledge of entrainment ratio, had less predictive ability of overall contaminant dispersion.

Boulard *et al.* (1997) used the commercial CFD software PHOENICS to simulate airflow in a greenhouse. The predicted mean airflow pattern in a horizontal plane at the level of the ventilators was in close agreement with the measured one. Harral & Boon (1997) employed a k-ε turbulence model to predict the airflow pattern in a section of a ventilated livestock building. When compared with experimental data, the difference between the predicted and measured mean velocity was less than 5% in most areas. Twenty percent error was found in re-circulation zone at the edge of the incoming jet, and this level of error remained the same irrespective of the sizes of grids.

Mistriotis *et al.* (1997a) used a k-ε model to investigate the natural ventilation process in greenhouses at no-wind and low-wind speed conditions. The simulations were performed with two different CFD software packages, PHOENICS v2.1 and FLUENT v.4. The numerical solutions were checked by comparing the results with measured temperature and flow patterns obtained from the literature. Good agreement was reported. The Chen-Kim k-ε model was also adopted by Mistriotis *et al.* (1997b) to calculate the pressure coefficient along the roof of a seven-span greenhouse. Good agreement was observed between numerical and experimental data.

2.5.2 Modelling Airflow Patterns in Refrigerated Spaces

The application of CFD-based models for studying airflow patterns in refrigerated spaces is still at the development stage. Unlike an office or living room, a refrigerated space is almost fully occupied with produce and packaging, and the free space for the air circulation has a very complicated geometry. Therefore, either a very fine and complex grid or the porous media approach has often been used to deal with the irregular geometry of the refrigerated space while solving the transport equations.

Chau *et al.* (1985) measured air velocity and pressure drop in bulks and cartons of orange. While fitting the experimental data into the Ergun equations, the resulting empirical parameters A and B in permeability (Equation (2.7)) and Forcheimer constant (Equation (2.20)) were found to be significantly different for different fruit sizes and stacking patterns. As the fruit sizes were comparable with the dimension of containers (dimensional ratio less than 10), the channelling effect may be important, which the authors did not consider.

Wang & Touber (1990) described a distributed dynamic model of a refrigerated room. The modelling was carried out in two steps. The first step was to model the flow pattern without considering any heat and mass transfer. Because the airflow was treated as steady-state (the effect of buoyancy was also neglected), the three-dimensional Navier-Stokes equation was decoupled from the equations for energy and mass transfer. The air velocity and turbulence quantities in the k-ε model were solved using the commercial CFD package PHOENICS. The second step was to model the heat and mass transport based on the predicted flow pattern. Although such a strategy reduced the computational time significantly, the prediction of the airflow pattern in the room still required 100 hours of computing on a Sun 3/60 workstation. The produce in the refrigerated room was modelled as a porous medium. The model was tested against measured temperatures, and satisfactory results were obtained.

Van Gerwen *et al.* (1991) used the PHOENICS package to simulate stationary 3D airflow distribution in a carcass chiller. The carcass rows in the chiller were modelled as porous layers. The air velocity around a carcass, calculated by the CFD model, was used as input for calculating heat and mass transfer coefficients on the surface of a thermal carcass model. Their model was also validated by measured data, and good agreement was found. Mariotti *et al.* (1995) used a similar approach to model air distribution in a refrigerated room. The velocity field was firstly solved under a steady state assumption. Then using the calculated velocity distribution, the transient temperature field was solved. The solution procedure was based on the finite element method, which was claimed to provide the intrinsic flexibility to treat complex flow situations and irregular geometry conditions.

2.6 Modelling Heat Transfer during Product Cooling Operations

Product cooling involves several heat generation and transfer processes including:

- Heat generation due to respiration
- Convection on the surfaces of products and packaging materials;
- Conduction within products, between products, and between products and packaging materials
- Convection and conduction within the cooling medium

- Radiation between surfaces of products and packaging materials
- Evaporative cooling effect due to transpiration

The influences of the above processes on cooling efficiency differ with cooling conditions. For instance, the effects of transpiration and respiration may be negligible during product precooling due to high cooling rates. However, these two factors have been shown to play an important role in product thermal stability during long-term storage.

Based on the approaches in handling the cooling media, the relevant heat transfer models are divided into two categories. In the first category, only heat conduction within the product is modelled in detail; the temperature of cooling medium is assumed to be constant or a function of time, and no differential equation is derived for the energy conservation of cooling medium. The models in this category are usually used to simulate single product situations. The second category models take into account the energy conservation for both product and cooling medium, and generally two differential equations are needed to simulate the temperature variation within the product and cooling medium. Produce contained in packages is often modelled with this approach.

2.6.1 Product Heat Conduction Models

The product heat conduction model is usually made up of the heat conduction equation (Equation (2.4)) and the boundary and initial conditions. Cleland (1990) presented five types of boundary conditions defining the heat transfer from the solid object being cooled to the external cooling medium. The most commonly used one is the third kind that is known as Newton's cooling law, which equates the heat flow per unit area at the surface of the solid with the heat transfer to the ambient fluid.

$$h_e(T_{s-surface}-T_{am})=-K_s\left[\frac{\partial T_s}{\partial n}\right]_{surface} \tag{2.40}$$

where:

T_{am} = ambient temperature (K).

$T_{s\text{-}surface}$ = solid surface temperature (K).

h_e = surface heat transfer coefficient (W m^{-2} K^{-1}).

n = surface normal direction coordinate (m).

K_s = solid thermal conductivity (W m^{-1} K^{-1}).

Cleland (1990), Lin (1994), and Amos (1995) have given comprehensive reviews for product heat conduction models. According to the solution methods for the heat conduction equation, the models can be classified as analytical, empirical, or numerical.

- **Analytical models**

Analytical or exact solution can be derived for heat conduction in a regularly-shaped product if proper boundary and initial conditions are imposed, and the product thermal properties are constant. The regular shapes include infinite slab, infinite cylinder, sphere, infinite rectangular rod, rectangular brick and finite cylinder. The typical solutions for these shapes were well presented by Gaffney *et al.* (1985b), Cleland (1990), and Lin (1994).

- **Empirical models**

The basis for most empirical methods is that almost all chilling processes follow a similar trend: the temperature of the product decreases at an exponential rate after an initial 'lag' period. Instead of developing shape-specific empirical prediction methods, many efforts have been made to extend the analytical solutions for regular shapes in an empirical, but general fashion (Cleland, 1990).

Considerable theoretical and experimental work has been carried out to predict the cooling rate of irregular-shaped objects (Smith & Nelson, 1969; Smith *et al.*, 1967 &1968; Clary *et al.*, 1968 & 1971). A geometry index, G, was employed to account for the effect of geometry on product chilling rate. A set of time-dependent charts and graphs was presented for predicting chilling time under a wide range of conditions and geometries. A nomogram was used to find a so-called 'equivalent Biot number' (Bi) so that the G value derived for Bi $\rightarrow \infty$ could be applied in situations where Bi is finite.

Cleland & Earle (1982) presented a simple method for predicting rates of chilling solid food product. A Bi-dependent shape factor, E (equivalent heat transfer dimensionality), was developed. The empirical equations for calculating E for regular and irregular shapes were suggested. The method was restricted to chilling time prediction for the thermal centre position in an object. Lin (1994) and Lin *et al.* (1996a, 1996b) proposed an empirical method for chilling time prediction. This method involved the use of the first term of the analytical series solution for convective cooling of a sphere in conjunction with two shape-dependent parameters, E and L (lag factor). A set of algebraic equations was used to calculate the E and L based on several simple dimensional measurements and Bi. This approach can be applied to regular and irregular, 2D and 3D objects.

- **Numerical models**

The heat conduction equation is commonly solved by the finite-difference or finite-element methods. As previously mentioned, the finite difference schemes require less computational effort, but are difficult to implement for irregular shapes while compared with finite-element analysis (Cleland, 1990).

Hayakawa (1978) modelled heat transfer and moisture loss from fresh produce subjected to cooling process. Internal heat generation was included in the model. The produce was assumed to be an infinite slab. An implicit finite difference method was applied to solve the model. Later, Hayakawa & Succar (1982) applied finite element techniques to solve the model for cooling and moisture loss of spherically produce with time-varying respiratory heat generation and temperature-dependent density and thermal conductivity. The model predictions were in close agreement with experimental data obtained from cooling of potatoes and tomatoes.

Abdul Majeed *et al.* (1980) introduced a one-dimensional heat conduction model to analyse air-cooling characteristics of food products with the shapes of sphere, slab, and cylinder. The enthalpy potential concept was adopted to represent the cooling effect of evaporation. Using the same concept, Narayana & Murthy (1981) presented a finite difference model to predict unsteady heat transfer of slab-shaped product. A similar approach was also used by Ansari *et al.* (1984) for solving the one-dimensional transient heat conduction equation in spherical co-ordinates. The calculation was made with both

heat and water mass transfer from the product surface for up to half the cooling time, and thereafter only the heat transfer component was included. The surrounding temperature was set to vary with time. The predicted temperatures for apples and potatoes were compared with the measured data, and good agreements were observed.

Chau & Gaffney (1990) developed a finite-difference model for simulating heat and mass transfer in the products with respiration and transpiration. Besides conduction and convection, the model also accounted for evaporative cooling due to transpiration and radiation heat transfer. The solutions agreed with known analytical solutions and with experimental results.

Jiang *et al.* (1987) modelled the chilling of broccoli stalk. A two-dimensional axisymmetric finite-element grid was used to represent the three-dimensional object. Experimentally-determined thermal properties were employed to simplify the model. Temperature differences between the simulated and measured values were within 1.1 ^{0}C. Haghighi & Segerlind (1988) proposed a finite-element model to study the simultaneous heat and mass transfer within an isotropic sphere. The model was used to solve a sample problem of drying a soybean kernel. The predicted drying curve for the soybean model agreed with the experimental results in the literature. Pan & Bhowmik (1991) developed a finite-element model for predicting the temperature distribution in mature green tomatoes represented by axisymmetric shape. The vertical cross-section of one half of a tomato was divided into 104 elements and 70 node points. Excellent agreement was obtained between model predictions and experimental data.

2.6.2 Product Heat Conduction plus Cooling Media Models

The above heat conduction models are most suitable for modelling heat transfer for single product items. During cooling, most products are packed or bulk-stacked, and the temperature and velocity distribution within the cooling media may be significantly affected by packaging and stack patterns. In these cases, a simple conduction model may not be practical. A general procedure for dealing with such complex situations consists of the simultaneous solution of the mass, momentum and energy conservation equations for both the fluid and the solid region.

Bakker-Arkema & Bickert (1966) and Bakker-Arkema *et al.* (1967) used a numerical model to analyse heat and water mass transfer during cooling of a deep bed of biological produce. The temperature gradient within individual particles was considered negligible, and constant air velocity was also assumed. The model prediction showed good agreement with experimentally measured temperature and moisture content of air and produce. Misener & Shove (1976) presented a model to simulate the temperature and moisture loss during cooling of a deep bed of potatoes. Their solution assumed that the temperature gradient within the tubers is zero, and the respiratory heat generation is a linear function of temperature. Moisture loss rate was derived from experimentally determined cumulative moisture loss, which is a function of vapour difference and time. They reported satisfactory agreement between the predicted and measured temperature and total moisture loss.

Baird & Gaffney (1976) developed a numerical model to simulate temperature distribution within a bulk load of products. Heat transfer within individual products was described using the heat conduction equation with a connective boundary. Airflow was assumed to pass through the bulk load at a constant velocity. The change in energy of the air moving through a control volume was assumed to be equal to the change in energy of products in the control volume. The energy conservation equation was derived based on these assumptions, and finite-difference method was used to solve the model. Predicted temperature distributions within both individual products and the bed were in good agreement with data from experimental cooling tests on oranges and grapefruit. Holdrege & Wyse (1982) applied a finite difference model to describe unsteady heat and water mass transfer during forced-air cooling of stored sugar beets. The respiratory heat generation was modelled as a function of temperature and time. The model predictions agreed with experimental data.

Remero & Chau (1987) proposed a finite-difference model to simulate heat and mass transfer when oranges were stored in a bulk-refrigerated store in the absence of ventilation. The effects of respiratory heat generation and evaporative cooling due to transpiration were also accounted for. The bulk store was divided into several layers. For each layer a node was assigned to the air in the void volume and the products were discretised into elemental volumes. The air temperature and product (heat and mass transfer) characteristics were assumed not to vary within each layer. The airflow within

the bulk store was described as Darcy flow through a porous medium. The Boussinesq approximation was applied to describe natural convection. A similar approach was adopted by Bazan *et al.* (1989) to predict the three-dimensional temperature response during room cooling of a confined bin of spherical fruit. Close agreement between simulation and experimental results was obtained.

Reynoso & Michels (1988) proposed a simplified model to evaluate the performance of batch cryogenic freezers. It was assumed that the refrigerant medium in the freezer was perfectly mixed, and no internal temperature gradients exited in the products. An explicit finite-difference method was used to solve the model, and the model was validated by experimental results. Comini *et al.* (1995) modelled the conductive and convective heat transfer in refrigerated transport. Average air velocities and the convection coefficients were first evaluated and then specified as input data for the model. Energy conservation equations for the solid regions and fluid regions were solved using a finite-element approach.

In some of the models reviewed earlier in Section 2.5.2 (Wang & Touber, 1990; Van Gerwen *et al.*, 1991), steady-state airflow fields were firstly solved using a CFD package. Based on predicted airflow patterns, transient energy conservation equations for air, wall and products were solved using the finite-difference method. Products stored in bulk were modelled as a porous medium using a two-step approach. The produce packages were assumed to be impenetrable blocks in order to determine the macro velocity and pressure distributions around them, and then these parameters were used as input data to calculate the micro velocity through the product bed.

Amos (1995) and Tanner (1998) developed a multi-zone model for predicting apple temperature and weight loss with both position and time within a ventilated carton. In the model, airflow inside the carton was modelled by defining forced convection pathways with natural convection mixing to adjacent zones. The air in each zone was assumed perfectly mixed. Energy and water vapour mass balances were performed on each zone to determine air enthalpy and humidity ratio, as well as the temperature of apples and packaging materials. The model predictions fitted the measured temperature data satisfactorily. However, the airflow pattern was estimated from measured air velocity

data within the specified carton. The approach to airflow characterisation limits the application of the model under different package designs.

Zou (1998) developed a CFD model to simulate airflow patterns and heat transfer in a ventilated apple carton during precooling. The CFD package PHOENICS was used to solve the model. The flow equations were solved under steady-state condition for both laminar and turbulent situations. Based on the predicted airflow patterns, the energy equations were solved dynamically to obtain temperature profiles. The temperatures in the centres of apples in various positions were measured. Good agreement between model predictions and experimental data was obtained in most locations, but large errors were found in the apple temperatures near carton inlets and outlets.

Tassou & Xiang (1998) developed a 2D CFD model for simulating airflow pattern and heat and water vapour mass transfer in a wet air-cooled store. In their model, momentum transport was formulated using the turbulent Reynolds-average equation plus Darcy and Forchheimer terms, and local thermal equilibrium was also assumed. However, the transport equations for turbulent quantities were not specified. The temperature prediction was found to be in good agreement with experimental result.

Xu & Burfoot (1999) presented a 3D model of heat and mass transfer in porous bulks of particulate foodstuff. The generalised volume-averaged momentum equation was used for air velocity. Heat and moisture transfer was formulated by volume-averaged transfer equations plus energy and mass transport equations for a single particle. Generally, the predicted temperature for cooling of potato agreed well with experimental results. The difference between prediction and experimental results in the inlet of the column was attributed to the turbulent fluctuation.

2.7 Summary

In general three types of models have been developed for modelling airflow patterns, heat and water vapour mass transfer in horticultural produce packages or refrigerated spaces during produce cooling.

- **Zoned models**

In this type of model (e.g., Amos, 1995; Tanner, 1998), the domains considered were divided into a number of zones. Airflow was modelled by defining an airflow pathway according to experimental data. The air in each zone was usually assumed perfectly mixed. Energy and water vapour mass balances were performed on each zone to determine air temperature, air humidity ratio, and the temperature of products and packaging materials. Zoned models require much less computing effort, and it is easy to write computer codes for model solution. However, since the airflow patterns were estimated from measured data for certain packages or coolstores, this approach limits the application of the model under different package designs or coolstore arrangements.

- **Fully-distributed models**

This approach applies CFD methods (FD, FV, or FE) to solve 2D or 3D air momentum conversation (Navier-Stokes) equations, mass conservation (continuity) equation, heat transfer (energy) equations, and water vapour mass conservation equation to obtain air velocity, air temperature, air humidity ratio, and product temperature (e.g., Wang, 1990; Zou, 1998). As the airflow patterns are solved explicitly by the models, no experimental data are required to run the model. To achieve an accurate solution, a large amount of computing capacity is needed. The CFD programming is usually complicated, and may require specialised software. If the model is used for the transport processes within a produce package, a complex body-fitted grid system has to be generated to describe the complicated configurations inside the package, which could be a daunting task for most model users. The difficulties in grid generation for detailing the geometries of different types of packaging systems largely reduced the accessibility of this type of model.

- **Porous-medium models**

In the porous-medium models, products inside the packages are treated as saturated porous media. Macroscopic volume-averaged continuity, momentum, heat transfer and species mass transfer equations are solved to find the volume-averaged velocity, temperature, and species concentration. Since certain information with respect to microscopic structure is lost in the spatial averaging process, a set of empirical

parameters is required for the closure of the macroscopic equations. These parameters are found in the expressions for porosity, permeability, Forchheimer constant, thermal and mass dispersion, and interfacial heat and mass transfer coefficients. The volume-averaged approach eliminates the need to generate complicated meshes to describe the geometric details of the packaging systems commonly used in agriculture and horticulture. Since simple grids can be employed while solving the transport equations, the porous medium models usually require less computing capacity than the microscopic models. However, existing studies (Tassou & Xiang, 1998; Xu & Burfoot, 1999) only dealt with some specific cooling conditions and bulk containers, and thus are not readily applicable to a wide range of packaging systems and horticultural crops.

In conclusion, treating the packaged fresh produce as porous media is an efficient way for modelling heat and mass transfer in various cooling processes due to the simplification of domain geometries. Compared with the fully distributed models, the porous media models require much less user-input data for specifying and discretising the calculation domains. Therefore the porous media approach makes it possible to develop a generalised modelling system applicable for a range of products and packaging systems.

CHAPTER 3
INITIAL ANALYSIS AND RESEARCH OBJECTIVES

3.1 Introduction

This chapter discusses forced-air cooling systems for horticultural crops, and then defines the exact system that is to be modelled in this study. Based on the overall project aim and evidence from the literature review, the specific objectives of the research project are outlined.

3.2 Analysis of Forced-Air Cooling Systems for Horticultural Crops

3.2.1 Ventilated Packaging Systems

To apply forced-air cooling, ventilated containers are used. For most horticultural crops in New Zealand, the commonly-used packages are wood or plastic bulk bins and corrugated fibreboard cartons. Based on the way products are packed in the containers, these ventilated packages can be divided into two main types, as shown in Figure 3.1 and 3.2:

- *Bulk packages*, in which products are placed in a bin or carton without any other packaging materials (Figure 3.1).
- *Layered packages*, in which products are placed on several trays, and which are then stacked into a package (Figure 3.2).

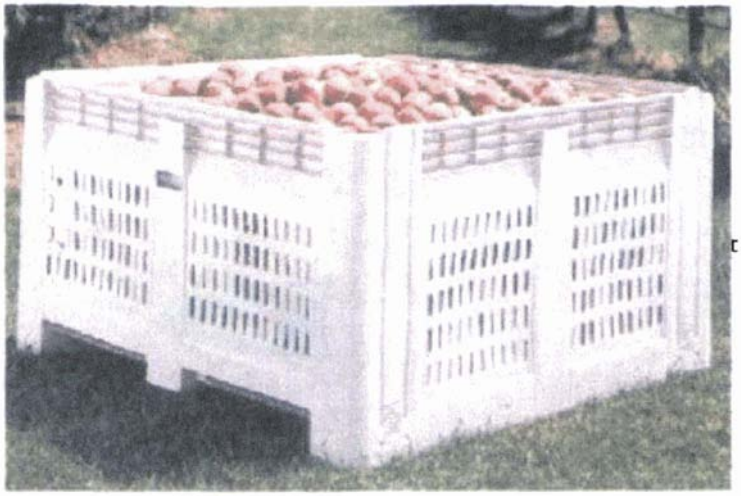

Figure 3.1 Example of bulk packages – ventilated apple bin (Tanner, 1998)

Figure 3.2 Example of layered packages – ventilated apple carton and tray

To facilitate unitised handling, individual cartons are usually grouped together as a pallet (Figure 3.3). During forced-air cooling, bulk bins and pallets are stacked in front of fans or plenums as shown in Figures 3.4-3.6. For secure palletisation, cross-stacked patterns may be used.

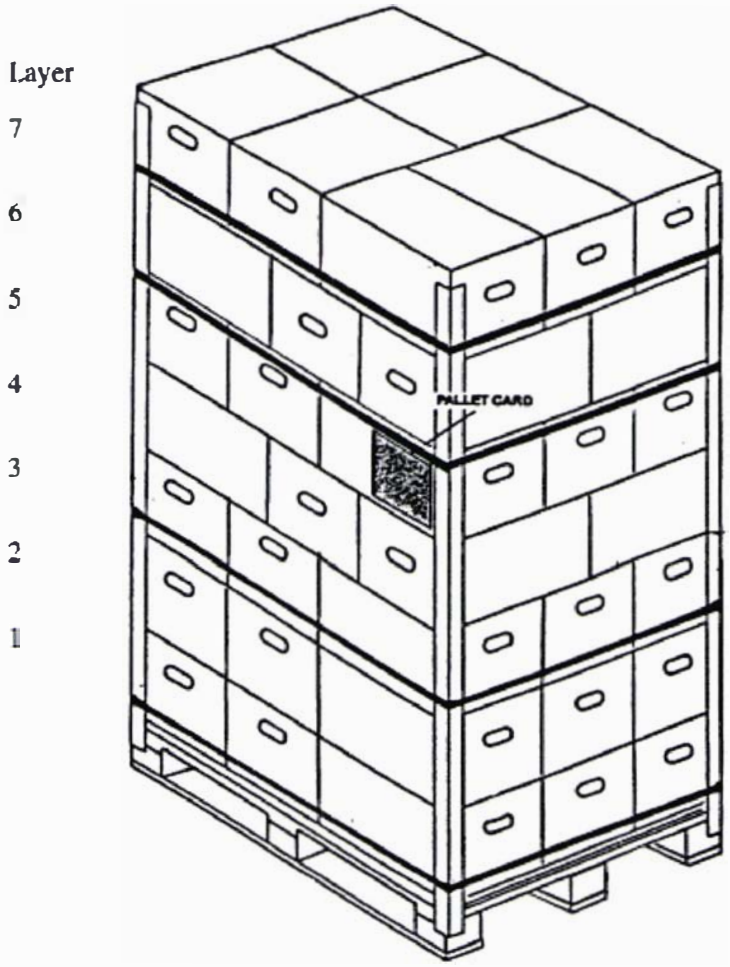

Figure 3.3 Pallet of fruit carton (ENZA, 1996)

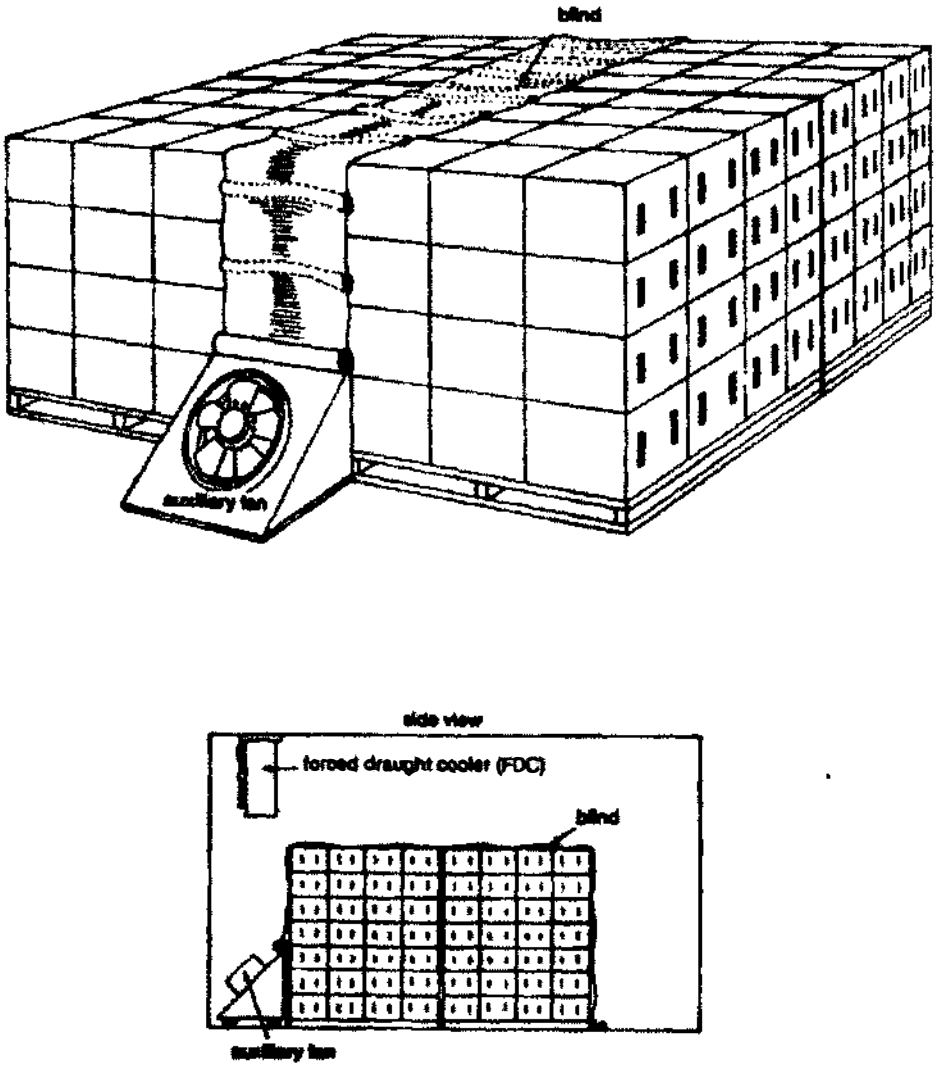

Figure 3.4 Types of forced-air cooling systems – tunnel cooling (Watkins, 1989)

To investigate the performance of a packaging system in terms of produce cooling efficiency, both the characteristics of individual package (configuration, dimensions, vents, and packaging materials, etc.) and the structure of the stack should be considered. Therefore this study took account of two domains of the packaging systems: *individual package* and *stack of packages*.

3.2.2 Forced Air Cooling Systems

Forced-air cooling commonly involves passing cold air along an induced pressure difference (gradient) through vented containers. The pressure difference is induced by fans that circulate cold air through produce and packaging, which constitute the

resistance to airflow (Wills *et al.*, 1998). The most commonly-used forced-air cooling methods are summarised as follows (Mitchel, 1992; Watkins, 1989).

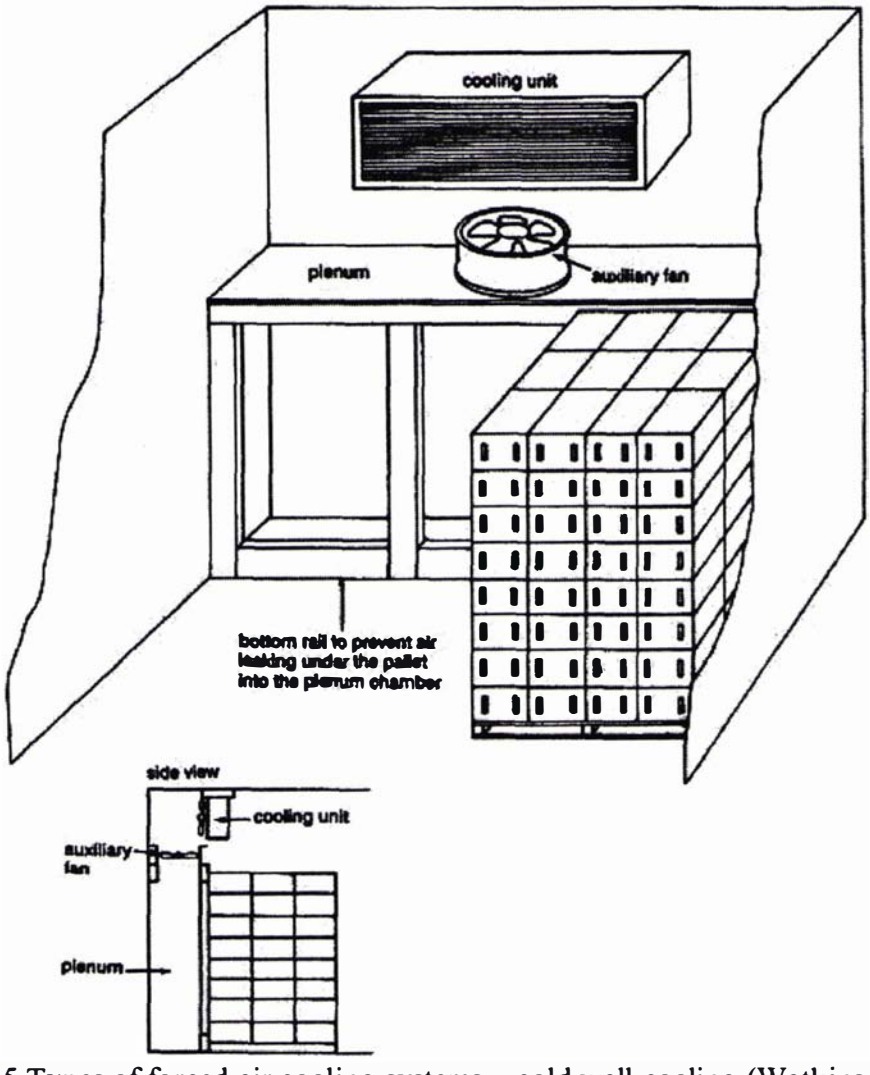

Figure 3.5 Types of forced-air cooling systems – cold wall cooling (Watkins, 1989)

- **Tunnel cooling**

As shown in Figure 3.4, two rows of pallets or bulk bins are placed against a fan to form an aisle between the rows. The aisle is covered to create an air tunnel. The fan creates negative air pressure within the tunnel. Cold air from the coolstore room is then sucked through the vents in the containers toward the low-pressure tunnel.

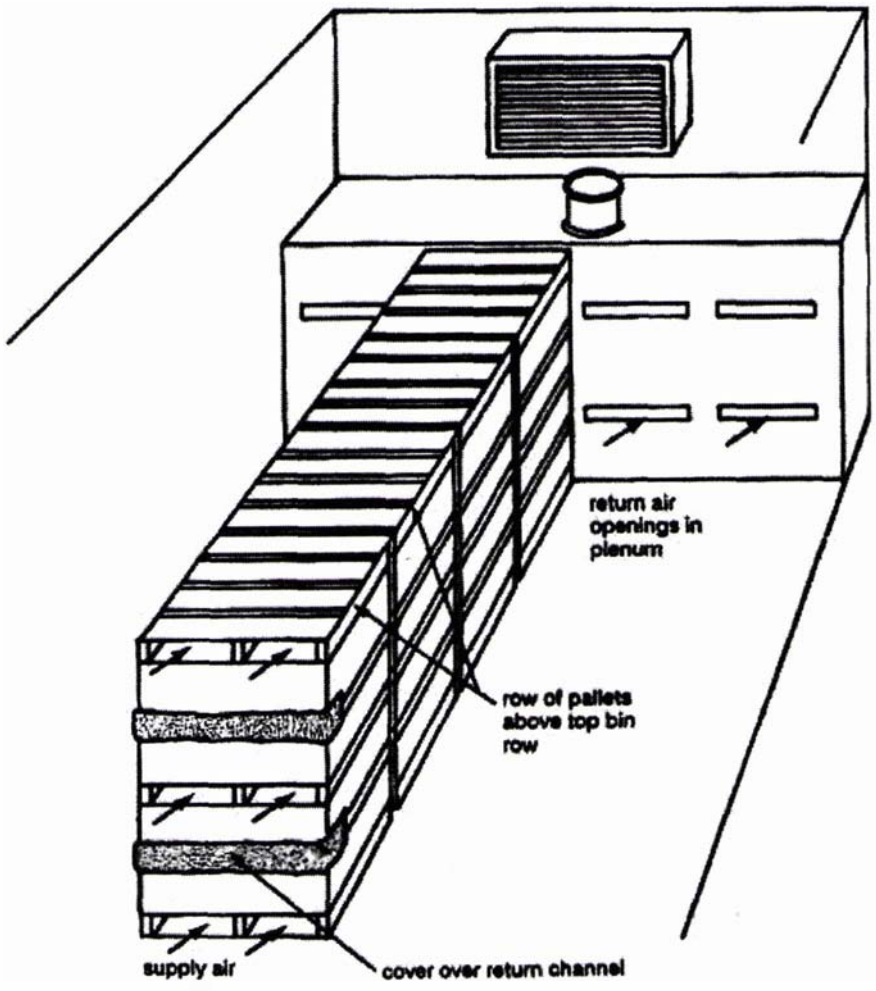

Figure 3.6 Types of forced-air cooling systems – serpentine cooling (Watkins, 1989)

- **Cold wall**

The cold wall cooling system employs an air plenum equipped with exhaust fans (Figure 3.5). The pallets or bulk bins are placed against the openings in the plenum. Air is pulled through the containers into the plenum and back through the auxiliary fans to the cooler.

- **Serpentine cooling**

The serpentine system usually employs a portable plenum similar to the cold wall, and is used for cooling produce in stacks of bins. The bins must have bottom ventilation slots or forklift openings. As shown in Figure 3.6, by blocking alternate forklift openings on the cold wall and room sides, air is forced to pass vertically through bins.

In the above cooling systems, the airflow conditions inside the package stack are very similar, and can be approximately described as follows.

- On the stack side close to the fans, airflow leaves the vents with an approximately constant flow rate.
- On the stack sides other than the one close to the fans, airflow pressure is approximately equal to the pressure of surrounding environment.
- If airflow enters a vent, it has the temperature and humidity ratio that are approximately equal to that of the air leaving the evaporator of the cooling system.

Due to the similar airflow conditions inside the package stacks in different forced-air cooling systems, this study focused on the transport processes taking place inside packaging systems during forced-air cooling, and therefore avoided dealing with minor details of these cooling systems.

3.2.3 Transport Processes

The transport processes taking place during forced-air cooling include air mass transfer, air momentum transfer, heat transfer, and moisture transfer. Moisture movement is caused by moisture concentration gradient between airflow and produce. Over the relatively short period of forced-air cooling, the moisture loss from produce to airflow is less than 0.1% of total produce mass, and the effects of moisture transfer on airflow and heat transfer are also negligible (Tanner, 1998). Therefore the moisture transfer and its effects on other transport processes were ignored, and only the air mass transfer, air momentum transfer, and heat transfer were considered in this study.

3.2.4 System to Be Modelled

Based on the above analyses, the key features of the system to be modelled are summarised in Table 3.1.

Table 3.1 Features of the packaging system to be modelled.

Features	**Descriptions**
Domains	• Individual package • Stack of packages
Package types	• Bulk package • Layered package
Transport processes	• Air mass transfer • Air momentum transfer • Heat transfer
Boundary conditions	• On one side of the stack or individual package, airflow leaves or enters vents with fixed velocity • On the other sides, airflow pressure on the vents is equal to that of the surrounding environment • If airflow enters a vent with constant temperature

3.3 Research Objectives

The overall aim of this project was to develop a modelling system for simulating airflow and heat transfer processes, and for predicting airflow patterns and temperature profiles inside ventilated packaging systems during the forced-air cooling of fresh produce. The modelling system envisaged should be useful for evaluating forced-air cooling operations and the cooling performance of different packaging designs for a variety of horticultural commodities. Taking account of this overall aim, and the techniques and methods for airflow and heat transfer modelling reviewed in the previous chapter, the following specific objectives were identified.

1) Develop *airflow models* for simulating air mass and momentum transfer in both bulk and layered packaging systems during forced-air cooling.

2) Develop *heat transfer models* for simulating heat transfer processes in both bulk and layered packaging systems during forced-air cooling.

3) Develop CFD methods for solving the airflow and heat transfer models.

4) Develop a computer program (*airflow solver*) to implement the CFD methods for solving the airflow models.

5) Develop a computer program (*heat transfer solver*) to implement the CFD methods for solving the heat transfer models.

6) Develop a computer user interaction program (*system designer*) to enable the model users to define the packaging systems and cooling conditions.

7) Develop a computer user interaction program (*visualization tool*) to enable the model users to visualise the airflow patterns and temperature profiles predicted by the models.

8) Incorporate the above computer programs into an integrated software package.

9) Validate the airflow and temperature predictions with experimental results.

A Conceptual framework of the interrelations between the project objectives is presented in Figure 3.7.

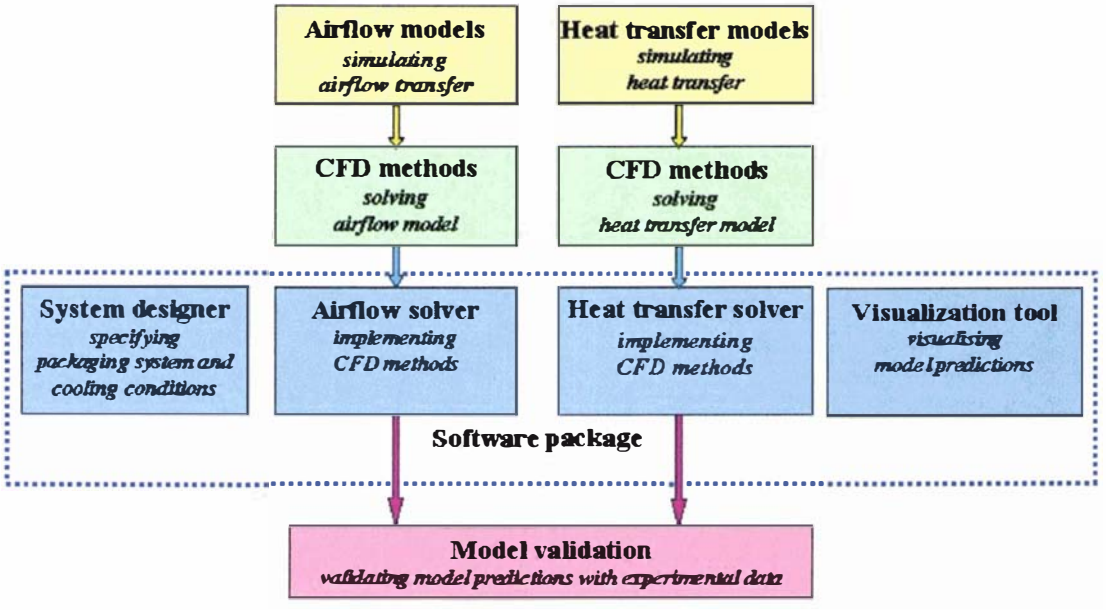

Figure 3.7 Research objectives and their interrelation

CHAPTER 4
DEVELOPMENT OF AIRFLOW MODELS

4.1 Introduction

This chapter first presents the conceptual models for airflow in the bulk and layered packaging systems. These conceptual models specify airflow transport processes and make assumptions to simplify the model formulation and solution. Following conceptualisation, the airflow models for the bulk and layered packages are developed and presented.

4.2 Conceptual Models

4.2.1 General Analysis of Airflow Transport Processes

Airflow patterns, i.e. the distributions of air velocity and pressure over the domain of interest, are obtained by solving a set of partial differential equations that describe air mass and conservation over the domain. To select and solve air mass and momentum conservation equations over ventilated packaging systems, it is essential to carry out a detailed analysis of the transport processes and associated domain.

- **Effects of heat transfer on air mass and momentum transfer**

Heat transfer between air, produce, and package results in air temperature change, which in turn alters air density. The variation in air density generates buoyancy forces that affect airflow momentum transfer. Since the air velocity is relatively large during forced-air cooling, the effect of buoyancy forces is considered negligible. By neglecting buoyancy forces, the heat transfer was assumed to have no effects on the airflow mass and momentum transfer. Therefore, airflow transport processes were treated as steady state, and the related airflow transport equations were decoupled from the heat transfer equations.

- **Geometric features of ventilated packaging systems**

For both layered and bulk packaging systems, the domain inside an individual package or stack of packages can be divided into three types of regions as shown in Figures 4.1 and 4.2.

1) *Produce-air regions* (the void spaces and produce inside bulk packages and the void spaces and produce between trays in layered packages).
2) *Plain air regions* (the spaces in the vents).
3) *Solid regions* (package walls and trays).

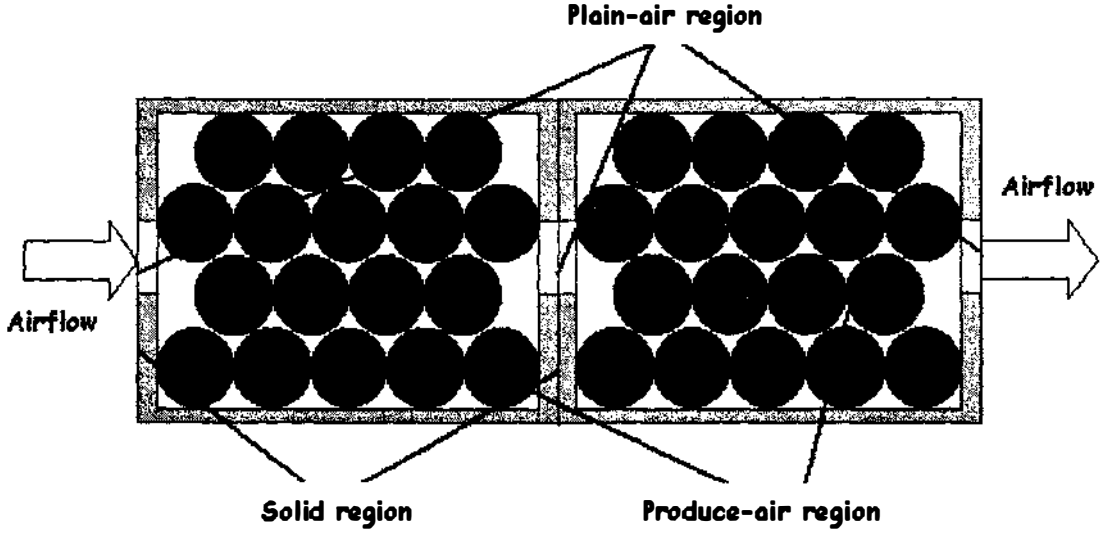

Figure 4.1 Regions in the bulk packaging systems.

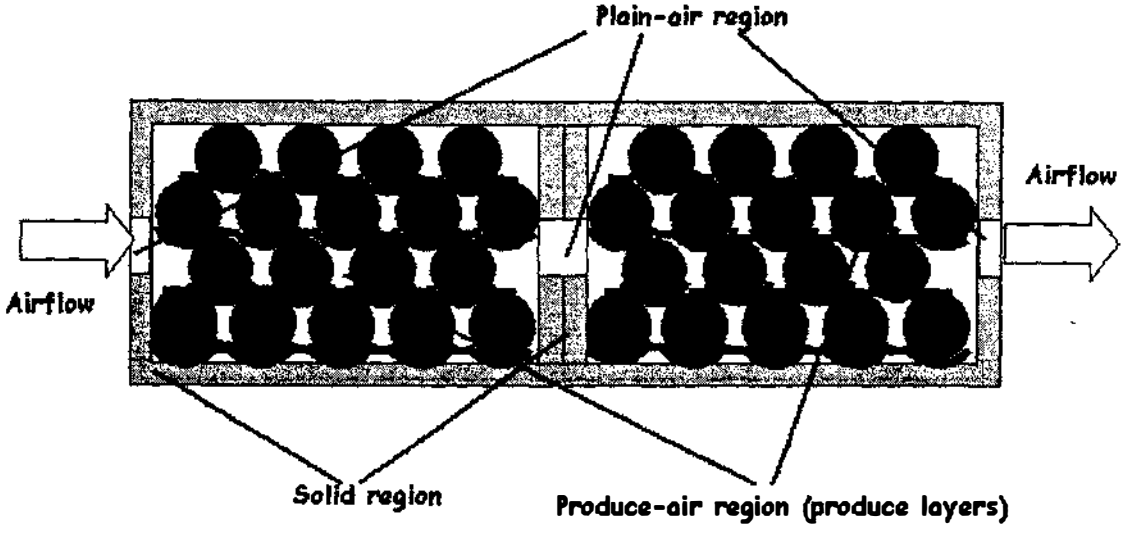

Figure 4.2 Regions in the layered packaging systems.

- **Airflow patterns in package layers of a stack**

For most ventilated packaging systems, the vents on the bottom and top surfaces of packages are either blocked or do not exist when the packages are stacked, which causes no air movement between different package layers in a stack. Hence, it is reasonable to assume that there is no air movement between the packages in different layers of a stack, and airflow pattern in each layer of packages is independent of the others.

- **Airflow in vents**

It was assumed that the airflow in the vents is one-dimensional, and perpendicular to the package walls containing the vents.

- **Air properties**

The ranges of air velocity (0.5 – 3.0 m/s) in forced-air cooling indicate that the possible changes in air temperature, pressure, and moisture content will not cause any significant changes in most air properties. Thus it was assumed that air density, specific heat capacity, thermal conductivity and viscosity are constant.

4.2.2 Analysis of Airflow Transport in the Bulk Packaging Systems

Items of produce are placed in the bulk packages without any packaging materials. Due to the complicated geometry inside the packages, it is very difficult to solve air transport equations in the domain. To avoid dealing with the geometric details inside the packages the porous media approach was adopted.

- **Porous media treatment of produce-air region**

Most fresh products are more or less sphere-shaped, and have relatively uniform sizes. The dimensions of bulk bins are generally at least one-order larger than the sizes of individual products. Therefore it was assumed that the produce-air regions inside bulk packages are isotropic, rigid, saturated porous media with uniform spherical particles as shown in Figure 4.3.

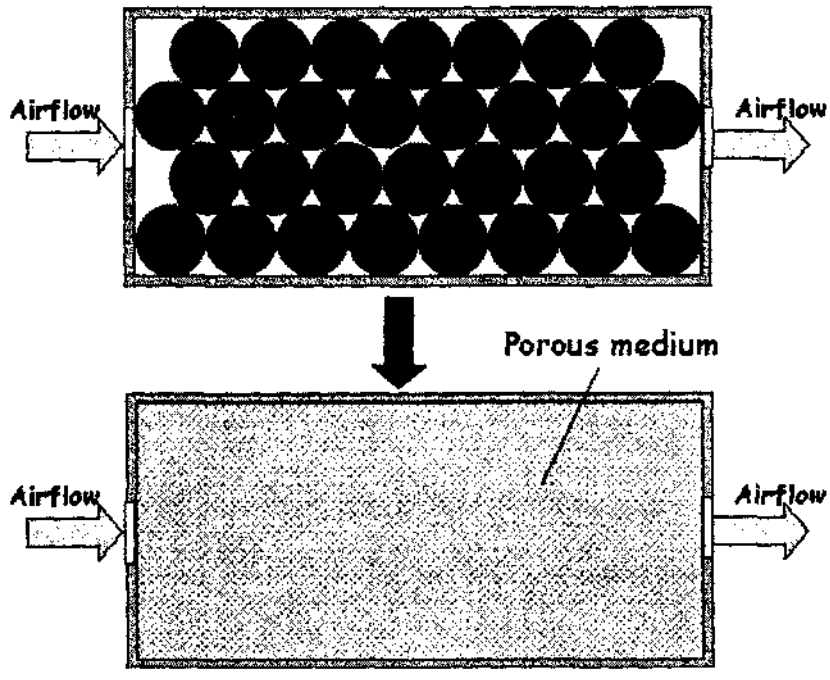

Figure 4.3 Illustration of porous media approach for bulk package.

Based on the above assumptions, the volume averaging method can be applied to integrate the pore-level microscopic governing equations over a representative elementary volume (REV) to derive the macroscopic transport equations as described in Section 2.4.2.

- **Geometric parameters needed to specify the bulk packaging system**

Due to application of the porous media approach, there is no need to specify the positions of every produce item. Table 4.1 summarises the geometric parameters needed to specify the bulk packaging systems. The structural properties of porous media such as porosity, permeability, specific surface area, and equivalent mean sphere diameter can be calculated from these geometric parameters.

4.2.3 Analysis of Airflow Transport in the Layered Packaging Systems

The geometry inside a layered package is more complex than that of bulk package. In general, the air-product region inside the layered package is divided into several produce layers by the trays, as shown in Figure 4.2. The distances between two neighbouring trays usually have the same order as the sizes of produce items, so the

strict porous media approach cannot be used. A pseudo-porous-media treatment was employed to deal with the geometries of layered packages.

Table 4.1 Geometric parameters of the bulk packaging systems.

Objects	**Geometric parameter**
Product	• Average volume • Average surface area
Individual package	• Number of products contained • Outside length • Outside width • Outside height • Side wall thickness • Top wall thickness • Bottom wall thickness
Stack of packages	• Stack patterns in each package layers • Number of packages in each package layers

- **Horizontal airflow in the produce layers between trays**

The air movement along the vertical direction in the produce layer is usually negligible when compared with the air movement at horizontal directions. Therefore it was assumed that the airflow in each produce layer between two trays has only horizontal movements.

- **Porous media treatment of produce layers between trays**

The thickness of a produce layer, i.e. the distance between two trays, is the same order as the sizes of produce items, so in theory the air-produce region in the produce layer cannot be treated as a porous medium. However, when examining the geometric characteristics of the layered packages carefully, it was found that the structure of the produce layer between two trays is very similar to that of a section cut from a packed bed since the trays are designed to tightly fit the shapes of produce. Hence the produce-air regions between trays were treated as isotropic, rigid, saturated porous media with uniform spherical particles, if package length and width are at least one-order larger than sizes of individual products.

As shown in Figures 4.4 and 4.5, the package interior geometric structure with four layers of product is transformed into five or six porous media layers. The additional bottom porous layer is used to represent the space between the package bottom wall and the bottom tray. If the top product layer is covered with a tray, an additional porous layer is needed as illustrated in Figure 4.5.

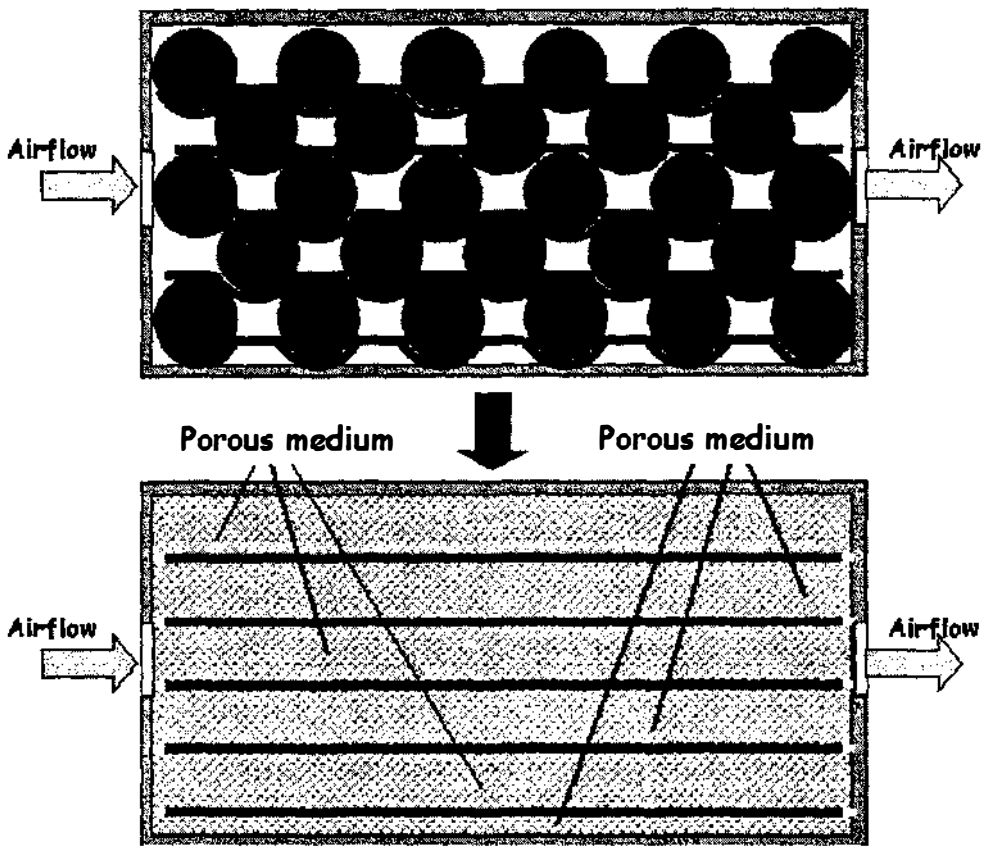

Figure 4.4 Illustration of the porous media approach for a layered package without a top- covering tray.

- **Vertical airflow between product layers**

Produce layers are separated by trays, and the air movement between these produce layers is mainly caused by pressure difference and the gaps between the tray edges and package walls. To simplify the treatment of air movement between produce layers, it was assumed that the air movement between produce layers is only along the direction of the package height.

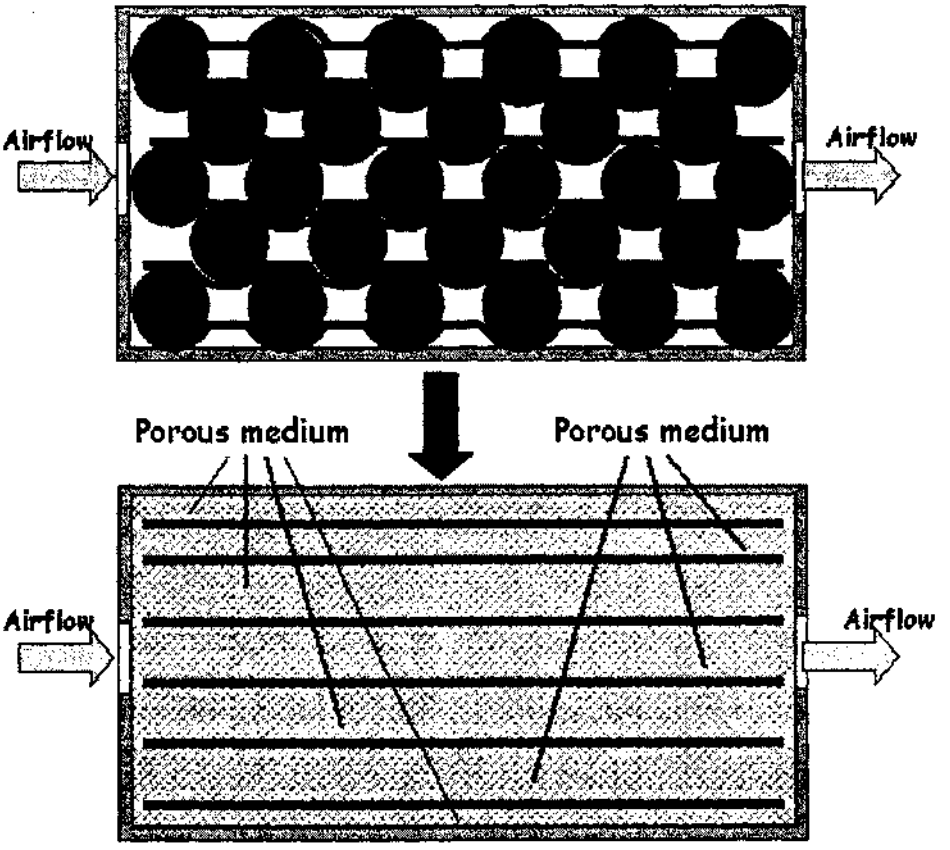

Figure 4.5 Illustration of the porous media approach for a layered package with a top-covering tray.

- **Vertical tunnel for airflow between produce layers**

As shown in Figure 4.6, the vertical airflow from one product layer to the others was assumed to pass through a narrow tunnel. Due to the complicated geometry in the near-package-wall regions in the tunnel, the resistance to airflow caused by produce items close to the packaging was estimated by the Darcy and Forchheimer terms in the generalised macroscopic momentum equation for porous media (Section 2.4.2). As it is difficult to calculate the porosity of the next-to-package-wall regions in the tunnel, a roughly- estimated value was used.

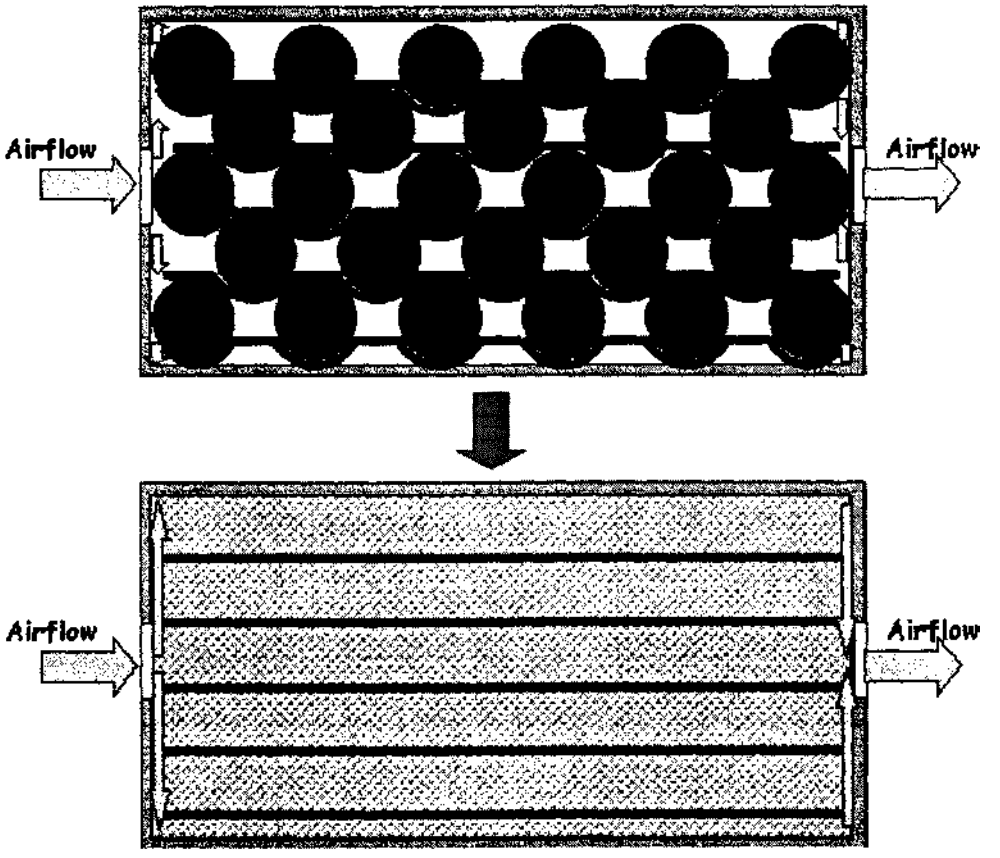

Figure 4.6 Illustration of airflow between produce layers in layered package.

- **Relations between the horizontal airflow within the produce layers and the vertical airflow between the produce layers**

As shown in Figure 4.6, parts of the near-package-region in the vertical tunnel overlap with the product layers. This indicates that the horizontal airflow within the produce layers is related to the vertical airflow between the product layers. The correlation is shown in the following two aspects:

1) The momentum conservation equations for airflow within the product layers share the pressure field with the momentum conservation equation for airflow between the product layers.
2) The velocity of the vertical airflow on the boundaries of the product layers should satisfy the mass conservation for each product layer.

Apart from the above relations, it was assumed that the horizontal airflow has no effect on the vertical airflow, and therefore the vertical airflow moves in the vertical narrow tunnels within the widths of the gaps between tray edges and package walls.

- **Geometric parameters needed to specify the bulk packaging system**

Table 4.2 summarises the geometric parameters needed to specify the layered packaging systems.

Table 4.2 Geometric parameters of the layered packaging systems.

Objects	**Geometric parameter**
Product	• Average volume • Average surface area
Individual package	• Number of products contained • Outside length • Outside width • Outside height • Side wall thickness • Top wall thickness • Bottom wall thickness • Number of product layers • Is the top product layer is covered with tray?
Tray	• Porosity of the space between the package bottom wall and the bottom tray • Tray thickness • Gaps between tray edges and package walls • Tray height
Stack of packages	• Stack patterns in each package layers • Number of packages in each package layers

4.2.4 Analysis of Domain Boundaries

As shown in Figures 4.7 and 4.8, the following types of boundaries in the ventilated packaging systems need to be specified.

- **Vents with fixed air velocities**

For the vents on the stack side near the auxiliary fans, assumptions were made as follows:

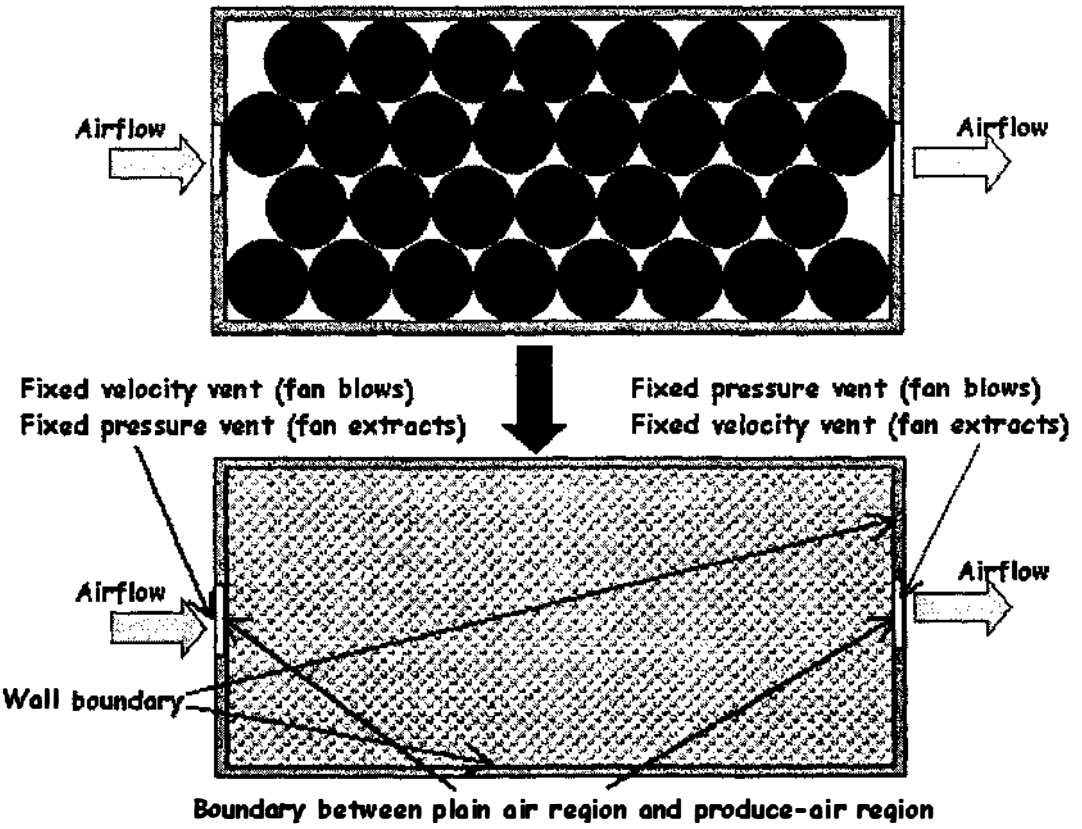

Figure 4.7 Illustration of boundaries in the domain of bulk package.

1) Airflow enters the vents with fixed velocities in the direction perpendicular to the vent if the fans blow air into the packages.
2) Airflow leaves the vents with fixed velocities in the direction perpendicular to the vent if the fans extract air out of the packages.

- **Vents with fixed pressures**

For the vents on the stack sides other than the one near the auxiliary fans, it was assumed that air pressure is equal to the pressure of the surrounding environment.

- **Wall boundaries**

Wall boundaries include inner surfaces of package walls, surfaces of trays, and surfaces around the perimeters of vents.

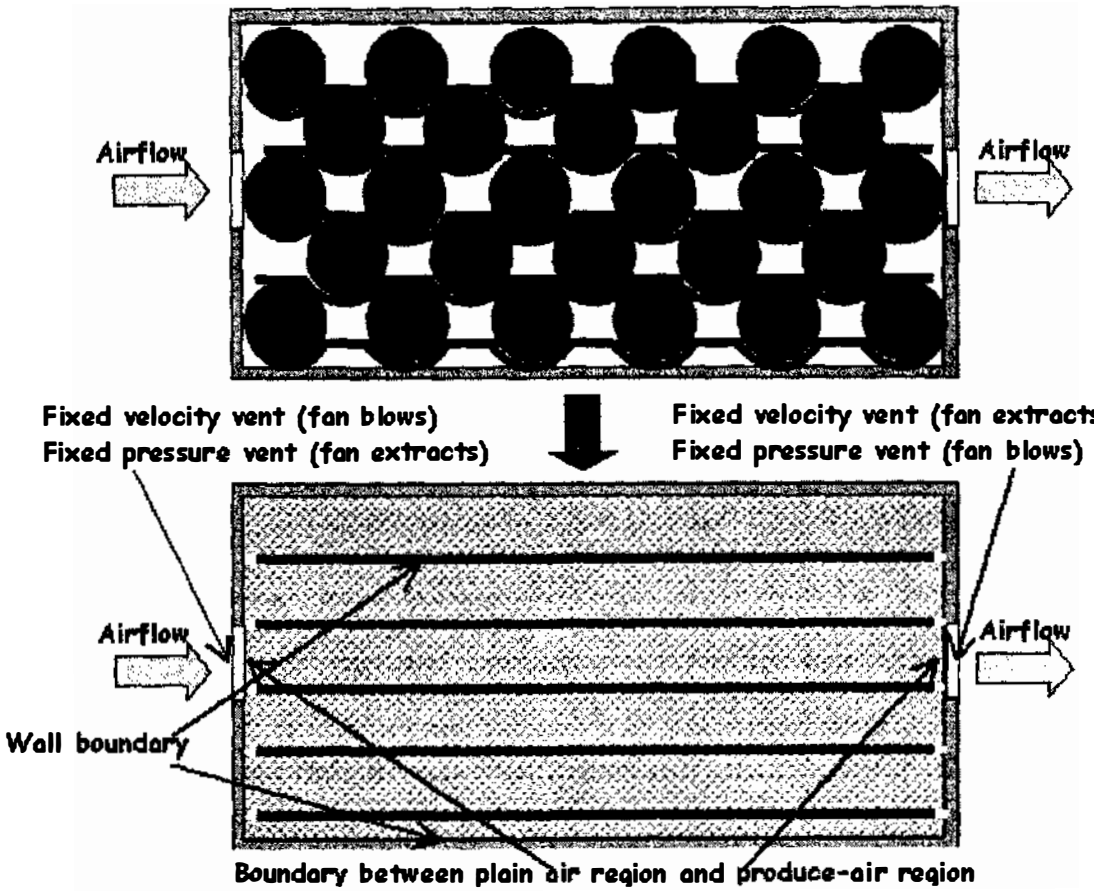

Figure 4.8 Illustration of boundaries in the domain of layered package.

- **Boundaries between plain air and produce-air regions**

Boundaries between the plain air and produce-air regions are the boundaries between the vents and the region inside package. As the airflow in the vents is one-dimensional, the airflow is perpendicular to the interfaces between the plain air and produce-air regions.

4.2.5 Summary of Conceptual Models

The conceptual models for the bulk and layered packaging systems are summarised in Tables 4.3 and 4.4.

Table 4.3 Conceptual model for airflow in the bulk packaging systems.

Model components	**Descriptions**
Domains of interest	• Individual bulk package • Stack of bulk packages
Conservation laws	• Conservation of air mass • Conservation of air momentum
Assumptions	• Unsteady state heat transfer processes have no effect on airflow transfer, and airflow transfer processes are steady state. • Airflow patterns in every layer of packages in a stack are independent of each other. • Airflow in the vents is one-dimensional. • Constant air properties. • Produce-air regions inside bulk packages are isotropic, rigid, saturated porous media.
Types of regions	• Plain air regions (vents) • Produce-air porous regions (within the packages) • Solid regions (package walls)
Boundaries	• Vents with fixed air velocities • Vents with fixed air pressure • Walls • Boundaries between plain air regions and produce-air regions

4.3 Model Formulation for Airflow in the Bulk Packaging Systems

The mathematical model for airflow in the bulk packaging systems consists of the following equations:

1) Continuity equation describing air mass conservation in the plain air regions.
2) Volume-averaged continuity equation describing air mass conservation in the produce-air regions.
3) Momentum equations for describing air momentum conservation in the plain air regions
4) Volume-averaged momentum equations for describing air momentum conservation in the produce-air regions.

Table 4.4 Conceptual model for airflow in the layered packaging systems.

Model components	**Descriptions**
Domains of interest	• Individual layered package • Stack of layered packages
Conservation laws	• Conservation of air mass • Conservation of air momentum
Assumptions	• Unsteady state heat transfer processes have no effect on airflow transfer, and airflow transfer processes are steady state. • Airflow patterns in every layer of packages are independent of each other. • Airflow in the vents is one-dimensional. • Constant air properties. • Airflow in each produce layer between two trays is 2-dimensional flow without vertical air movement. • Produce-air regions in produce layers between two trays are treated as isotropic, rigid, saturated porous medium. • Air movement between product layers is only along the direction of package height. • The vertical airflow from one product layer to the another passes through a narrow tunnel. • The resistance to the vertical airflow between produce layers caused by produce items close to packages was estimated by the Darcy term and Forchheimer term. • Apart from sharing pressure fields and maintaining mass conservation, the horizontal airflow within the produce layers has no effect on the vertical airflow between the produce layers.
Types of regions	• Plain air regions (vents) • Produce-air porous regions within produce layers • Vertical tunnel along package walls for the airflow between the produce layers. • Solid regions (package walls and trays)
Boundaries	• Vents with fixed air velocities • Vents with fixed air pressure • Walls • Boundaries between plain air regions and air-product regions

5) Auxiliary algebraic equations for calculating the porosity and permeability in the produce-air regions.
6) Auxiliary algebraic equations for describing the boundary conditions.

4.3.1 Conservation of air mass

- **Continuity equation for plain air regions**

The air mass conservation in vents is described by the one-dimensional continuity equation (Bird *et al.*, 1960):

$$\frac{du}{dx} = 0 \tag{4.1a}$$

$$\frac{dv}{dy} = 0 \tag{4.1b}$$

where:

u = component of air velocity in the direction of x-axis (m s^{-1}).

v = component of air velocity in the direction of y-axis (m s^{-1}).

- **Volume-averaged continuity equation for the produce-air regions**

The air mass conservation in the produce-air regions is described by the volume-averaged continuity equation (Hsu & Cheng, 1990; Kaviany, 1995):

$$\frac{\partial}{\partial x}\left(\phi\langle u\rangle_a\right)+\frac{\partial}{\partial y}\left(\phi\langle v\rangle_a\right)+\frac{\partial}{\partial z}\left(\phi\langle w\rangle_a\right)=0 \tag{4.2}$$

where:

ϕ = porosity.

$\langle u\rangle_a$ = intrinsic phase average of air velocity component in the direction of x-axis (m s^{-1}).

$\langle v\rangle_a$ = intrinsic phase average of air velocity component in the direction of y-axis (m s^{-1}).

$\langle w\rangle_a$ = intrinsic phase average of air velocity component in the direction of z-axis (m s^{-1}).

4.3.2 Conservation of Air Momentum

- **Momentum equation for plain air regions**

The air momentum conservation in vents is described by one-dimensional Navier-Stokes equations (Bird *et al.*, 1960):

$$\rho_a u \frac{du}{dx} - \frac{d}{dx}\left(\mu \frac{du}{dx}\right) = -\frac{dp}{dx} \tag{4.3a}$$

$$\rho_a v \frac{dv}{dy} - \frac{d}{dy}\left(\mu \frac{dv}{dy}\right) = -\frac{dp}{dy} \tag{4.3b}$$

where:

p = air pressure (N m^{-2}).

μ = air dynamic viscosity (N s m^{-2}).

ρ_a = air density (kg m^{-3}).

- **Generalised volume-averaged momentum equation for the produce-air regions**

The conservation of air momentum in the produce-air regions is described by the generalised volume-average momentum equation (Hsu & Cheng, 1990; Kaviany, 1995; Vafai & Tien, 1981):

$$\begin{aligned}&\frac{\partial}{\partial x}\left(\rho_a \phi \langle u\rangle_a \langle u\rangle_a\right) + \frac{\partial}{\partial y}\left(\rho_a \phi \langle v\rangle_a \langle u\rangle_a\right) + \frac{\partial}{\partial z}\left(\rho_a \phi \langle w\rangle_a \langle u\rangle_a\right) \\ &- \frac{\partial}{\partial x}\left(\mu\phi \frac{\partial \langle u\rangle_a}{\partial x}\right) - \frac{\partial}{\partial y}\left(\mu\phi \frac{\partial \langle u\rangle_a}{\partial y}\right) - \frac{\partial}{\partial z}\left(\mu\phi \frac{\partial \langle u\rangle_a}{\partial z}\right) = \\ &- \frac{\partial\left(\phi \langle p\rangle_a\right)}{\partial x} - \frac{\mu\phi^2 \langle u\rangle_a}{K} - \frac{F\phi^3 \rho_a}{\sqrt{K}} \left|\langle u\rangle_a\right| \langle u\rangle_a\end{aligned} \tag{4.4a}$$

$$\frac{\partial}{\partial x}\left(\rho_a\phi\langle u\rangle_a\langle v\rangle_a\right)+\frac{\partial}{\partial y}\left(\rho_a\phi\langle v\rangle_a\langle v\rangle_a\right)+\frac{\partial}{\partial z}\left(\rho_a\phi\langle w\rangle_a\langle v\rangle_a\right)$$
$$-\frac{\partial}{\partial x}\left(\mu\phi\frac{\partial\langle v\rangle_a}{\partial x}\right)-\frac{\partial}{\partial y}\left(\mu\phi\frac{\partial\langle v\rangle_a}{\partial y}\right)-\frac{\partial}{\partial z}\left(\mu\phi\frac{\partial\langle v\rangle_a}{\partial z}\right)= \tag{4.4b}$$
$$-\frac{\partial\left(\phi\langle p\rangle_a\right)}{\partial y}-\frac{\mu\phi^2\langle v\rangle_a}{K}-\frac{F\phi^3\rho_a}{\sqrt{K}}\left|\langle v\rangle_a\right|\langle v\rangle_a$$

$$\frac{\partial}{\partial x}\left(\rho_a\phi\langle u\rangle_a\langle w\rangle_a\right)+\frac{\partial}{\partial y}\left(\rho_a\phi\langle v\rangle_a\langle w\rangle_a\right)+\frac{\partial}{\partial z}\left(\rho_a\phi\langle w\rangle_a\langle w\rangle_a\right)$$
$$-\frac{\partial}{\partial x}\left(\mu\phi\frac{\partial\langle w\rangle_a}{\partial x}\right)-\frac{\partial}{\partial y}\left(\mu\phi\frac{\partial\langle w\rangle_a}{\partial y}\right)-\frac{\partial}{\partial z}\left(\mu\phi\frac{\partial\langle w\rangle_a}{\partial z}\right)= \tag{4.4c}$$
$$-\frac{\partial\left(\phi\langle p\rangle_a\right)}{\partial z}-\frac{\mu\phi^2\langle w\rangle_a}{K}-\frac{F\phi^3\rho_a}{\sqrt{K}}\left|\langle w\rangle_a\right|\langle w\rangle_a$$

where:

ϕ	=	porosity.
K	=	permeability (m^2).
F	=	Forcheimer coefficient.
$\langle u\rangle_a$	=	intrinsic phase average of air velocity component in the direction of x-axis ($m\ s^{-1}$).
$\langle v\rangle_a$	=	intrinsic phase average of air velocity component in the direction of y-axis ($m\ s^{-1}$).
$\langle w\rangle_a$	=	intrinsic phase average of air velocity component in the direction of z-axis ($m\ s^{-1}$).
$\langle p\rangle_a$	=	intrinsic phase average of air pressure ($N\ m^{-2}$).

4.3.3 Auxiliary Equations

- **Porosity**

The porosity distribution in a packed bed is usually modelled by an exponential decaying function of the distance to the nearest interface (Amiri & Vafai, 1994, 1998):

$$\phi = \phi_{\infty}(1 + ae^{-\frac{by}{d_{eq}}}) \tag{4.5}$$

where

ϕ = porosity.

ϕ_{∞} = free stream porosity.

y = distance from the nearest boundary (m).

a = empirical constant.

b = empirical constant.

The free stream porosity is calculated as (Dullien, 1979):

$$\phi_{\infty} = 1 - \frac{\rho_B}{\rho_p} \tag{4.6}$$

where

ρ_B = bulk density of container packed with products (kg m^{-3}).

ρ_p = density of product (kg m^{-3}).

The bulk density of packed products is

$$\rho_B = \frac{m_{product\_total}}{V_{package}} \tag{4.7}$$

where:

$m_{product\_total}$ = total mass of products in the package (kg).

$V_{package}$ = package volume (m^3).

- **Permeability and Forcheimer coefficient**

For packed beds of sphere-like particles, permeability K and Forcheimer coefficient F can be expressed as (Ergun, 1952):

$$K = \frac{d_{eq}^{\ 2}\phi^3}{A(1-\phi)^2} \tag{4.8}$$

$$F = \frac{B}{\sqrt{A\phi^3}} \tag{4.9}$$

where:

d_{eq} = equivalent mean sphere diameter (m).

A = empirical constant.

B = empirical constant.

- **Empirical constants**

The empirical constants used in Equations (4.5)-(4.9) are summarised in Table 4.5 (Amiri & Vafai, 1994, 1998).

Table 4.5 Empirical constant in porous media model.

Equations	**Constant**	**Value**
Permeability and Forcheimer coefficient (Equation 4.8-4.9)	A	180
Forcheimer coefficient (Equation 4.9)	B	1.8
Porosity distribution (Equation 4.5)	a	1.7
Porosity distribution (Equation 4.5)	b	6

4.3.4 Boundary Conditions

- **Fixed velocity vents**

The boundary conditions for a fixed velocity vent were specified as

$u_i = u_{fixed}$ (i is the direction perpendicular to the vent) (4.10a)

$u_j = 0$ (j is the direction parallel to the vent) (4.10b)

where:

u_{fixed} = value of air velocity at the vent (m s^{-1}).

- **Fixed pressure vents**

The boundary condition for a fixed pressure vent was specified as

$$p = p_{fixed} \tag{4.11}$$

where:

p_{fixed} = value of pressure at the vent (N m^{-2}).

- **Wall boundaries**

For the interfaces between plain air regions and solids, the boundary condition was specified by the no-slip condition :

$$u = 0 \tag{4.12a}$$
$$v = 0 \tag{4.12b}$$
$$w = 0 \tag{4.12c}$$

For the interfaces between produce-air regions and solids, the no-slip condition still applies, as the macroscopic viscous term is included in the momentum equation.

$$\langle u \rangle_a = 0 \tag{4.13a}$$
$$\langle v \rangle_a = 0 \tag{4.13b}$$
$$\langle w \rangle_a = 0 \tag{4.13c}$$

- **Boundaries between the plain air regions and the air-product porous regions**

As airflow is perpendicular to the interfaces between the plain air and the air-product porous regions, it is adequate to maintain the mass and momentum conservation on the boundaries. The detailed treatment is described in Appendix A.

4.4 Model formulation for Airflow in the Layered Packaging Systems

The mathematical model for airflow in the layered packaging systems consists of the following equations:

1) Continuity equation describing air mass conservation in the plain air regions.
2) Volume-averaged continuity equation describing air mass conservation in the produce-air regions between trays.
3) Continuity equation describing air mass conservation in the vertical tunnels (airflow between produce layers).
4) Momentum equations for describing air momentum conservation in the plain air regions.
5) Volume-averaged momentum equations for describing air momentum conservation in the produce-air regions between trays.
6) Momentum equations for describing air momentum conservation in the vertical tunnels (airflow between produce layers).
7) Auxiliary algebraic equations for calculating porosity and permeability in the air-product regions.
8) Auxiliary algebraic equations for describing the boundary conditions.

4.4.1 Conservation of air mass

- **Continuity equation for plain air regions**

The air mass conservation equation in the plain air regions of a layered packaging system is the same as that of the bulk packaging system (Equation 4.1).

- **Volume-averaged continuity equation for the produce-air regions between trays**

The two-dimensional volume-averaged continuity equation was employed (Hsu & Cheng, 1990; Kaviany, 1995):

$$\frac{\partial}{\partial x}\left(\phi\langle u\rangle_a\right)+\frac{\partial}{\partial y}\left(\phi\langle v\rangle_a\right)=0 \qquad (4.14)$$

where:

ϕ = porosity.

$\langle u \rangle_a$ = intrinsic phase average of air velocity component in the direction of x-axis (m s^{-1}).

$\langle v \rangle_a$ = intrinsic phase average of air velocity component in the direction of y-axis (m s^{-1}).

- **Continuity equation for vertical tunnels**

The air mass conservation in vertical tunnels is described by the one-dimensional continuity equation (Bird *et al.*, 1960):

$$\frac{dw}{dz} = 0 \tag{4.15}$$

where:

w = component of air velocity in the direction of z-axis (m s^{-1}).

4.4.2 Conservation of Air Momentum

- **Momentum equation for plain air regions**

The air momentum conservation equation in the plain air regions of the layered packaging system is the same as that of the bulk packaging system (Equation 4.3).

- **Generalised volume-averaged momentum equation for produce-air regions between trays**

The volume-averaged equations of motion for airflow with only horizontal movements were written as follows (Hsu & Cheng, 1990; Kaviany, 1995; Vafai & Tien, 1981):

$$\frac{\partial}{\partial x}\left(\rho_a \phi \langle u\rangle_a \langle u\rangle_a\right)+\frac{\partial}{\partial y}\left(\rho_a \phi \langle v\rangle_a \langle u\rangle_a\right)-\frac{\partial}{\partial x}\left(\mu\phi\frac{\partial\langle u\rangle_a}{\partial x}\right)-\frac{\partial}{\partial y}\left(\mu\phi\frac{\partial\langle u\rangle_a}{\partial y}\right)-\frac{\partial}{\partial z}\left(\mu\phi\frac{\partial\langle u\rangle_a}{\partial z}\right)=$$
$$-\frac{\partial\left(\phi\langle p\rangle_a\right)}{\partial x}-\frac{\mu\phi^2\langle u\rangle_a}{K}-\frac{F\phi^3\rho_a}{\sqrt{K}}\left|\langle u\rangle_a\right|\langle u\rangle_a$$

(4.16a)

$$\frac{\partial}{\partial x}\left(\rho_a \phi \langle u\rangle_a \langle v\rangle_a\right)+\frac{\partial}{\partial y}\left(\rho_a \phi \langle v\rangle_a \langle v\rangle_a\right)-\frac{\partial}{\partial x}\left(\mu\phi\frac{\partial\langle v\rangle_a}{\partial x}\right)-\frac{\partial}{\partial y}\left(\mu\phi\frac{\partial\langle v\rangle_a}{\partial y}\right)-\frac{\partial}{\partial z}\left(\mu\phi\frac{\partial\langle v\rangle_a}{\partial z}\right)=$$
$$-\frac{\partial\left(\phi\langle p\rangle_a\right)}{\partial y}-\frac{\mu\phi^2\langle v\rangle_a}{K}-\frac{F\phi^3\rho_a}{\sqrt{K}}\left|\langle v\rangle_a\right|\langle v\rangle_a$$

(4.16b)

where:

ϕ	=	porosity.
K	=	permeability (m^2).
F	=	Forcheimer coefficient.
$\langle u\rangle_a$	=	intrinsic phase average of air velocity component in the direction of x-axis ($m\ s^{-1}$).
$\langle v\rangle_a$	=	intrinsic phase average of air velocity component in the direction of y-axis ($m\ s^{-1}$).
$\langle p\rangle_a$	=	intrinsic phase average of air pressure ($N\ m^{-2}$).

- **Momentum equation for vertical tunnel**

The momentum conservation equation for one-directional flow was employed, and the Darcy and Forcheimer terms were used to account for the resistance caused by produce items next to the package walls. (Vafai and Tien, 1981):

$$\rho_a w\frac{\partial w}{\partial z}-\frac{\partial}{\partial x}\left(\mu\frac{\partial w}{\partial x}\right)-\frac{\partial}{\partial y}\left(\mu\frac{\partial w}{\partial y}\right)-\frac{\partial}{\partial z}\left(\mu\frac{\partial w}{\partial z}\right)=-\frac{\partial p}{\partial z}-\frac{\mu\phi_{gap}w}{K}-\frac{F\phi_{gap}^2\rho_a}{\sqrt{K}}|w|w$$

(4.17)

where:

ϕ_{gap}	=	estimated porosity of the vertical tunnel along package wall.
K	=	permeability (m^2).
F	=	Forcheimer coefficient.

w = air velocity component along package height(m s^{-1}).

p = air pressure (N m^{-2}).

4.4.3 Auxiliary Equations

- **Porosity**

As number and position of produce items on each tray is pre-defined for a layered package, the porosity at any position can be calculated accordingly.

- **Permeability and Forcheimer coefficient**

The same equations are used to compute permeability and Forcheimer coefficient F as for layered packages (Equations 4.8-4.9).

4.4.4 Boundary Conditions

For layered packaging systems, the same boundary conditions were used for the fixed velocity vents, fixed pressure vents, wall boundaries, and the interfaces between the plain air and air-product regions as for the bulk package systems.

4.5 Summary

This chapter outlined the conceptual and mathematical models for airflow in both bulk and layered packaging systems. In the conceptual models, the domains within the packaging systems were classified as several types of regions. The porous media approach was applied in order to avoid dealing with the complicated geometry inside packages. In the mathematical models, the partial differential equations for describing air mass and momentum conservation in these regions were presented. The solution of the mathematical models is discussed in Chapter 6 and Appendix A.

CHAPTER 5
DEVELOPMENT OF HEAT TRANSFER MODELS

5.1 Introduction

This chapter first presents the conceptual models for heat transfer in the bulk and layered packages. These conceptual models specify the important heat transfer processes, and make assumptions to simplify the model formulation or solution. Following conceptualisation, the heat transfer models for the bulk and layered packaging systems are developed.

5.2 Conceptual Models

5.2.1 General Analysis of Heat Transfer Processes

Temperature profiles, i.e. the air, produce, and package materials temperatures over the domain of interest are obtained by solving the partial differential equations that describe energy conservation over the domain. To select and solve the energy conservation equations over the domains of ventilated packaging systems, it is essential to carry out a detailed analysis of the heat transfer processes and associated domain.

- **Conceptualisation conducted for the airflow models**

The airflow patterns predicted by the airflow models are to be used as input data for heat transfer calculations, and the porous media approach is also employed for deriving the volume-averaged equations for air and produce energy conservation. Hence the conceptualisation conducted for the airflow models forms a basis for the heat transfer models. Conceptualisation for the airflow models is summarised in Tables 4.3and 4.4

- **Effects of radiative heat transfer**

As produce items are packaged in boxes or bins, the individual produce item would likely receive minimal net radiative heat transfer (Tanner, 1998). Hence, it was assumed that effects of radiative heat transfer were negligible.

- **Constant thermal properties**

Thermal properties of produce and package materials (package walls and trays) are affected mainly by moisture content. As discussed in Section 3.2.3, moisture content variation can be negligible during forced-air cooling. Hence it was assumed that produce and packaging materials have constant density, thermal conductivity, and specific heat capacity. In airflow models, constant air thermal properties were assumed, which is still valid for the heat transfer models.

- **Heat transfer in plain air regions**

In the airflow models, airflow in vents was assumed to be one-dimensional and perpendicular to the package walls containing the vents. Similarly it was assumed that heat transfer in the vents is one-dimensional and perpendicular to the package walls containing the vents.

- **Heat transfer in package layers of a stack**

In the airflow models, it was assumed that there was no air movement between the packages in different package layers, and airflow patterns in each layer of packages are independent of each other. The heat transfer between the package layers of a stack is achieved by heat conduction through the package surfaces, which is considered negligible compared with the heat transfer between airflow and products during forced-air cooling. Therefore it was assumed there is no heat transfer between the package layers, and heat transfer in the package layers are independent of each other.

5.2.2 Analysis of Heat Transfer in the Bulk Packaging Systems

The heat transfer processes in the bulk packages during produce cooling are shown in Figure 5.1 and Table 5.1

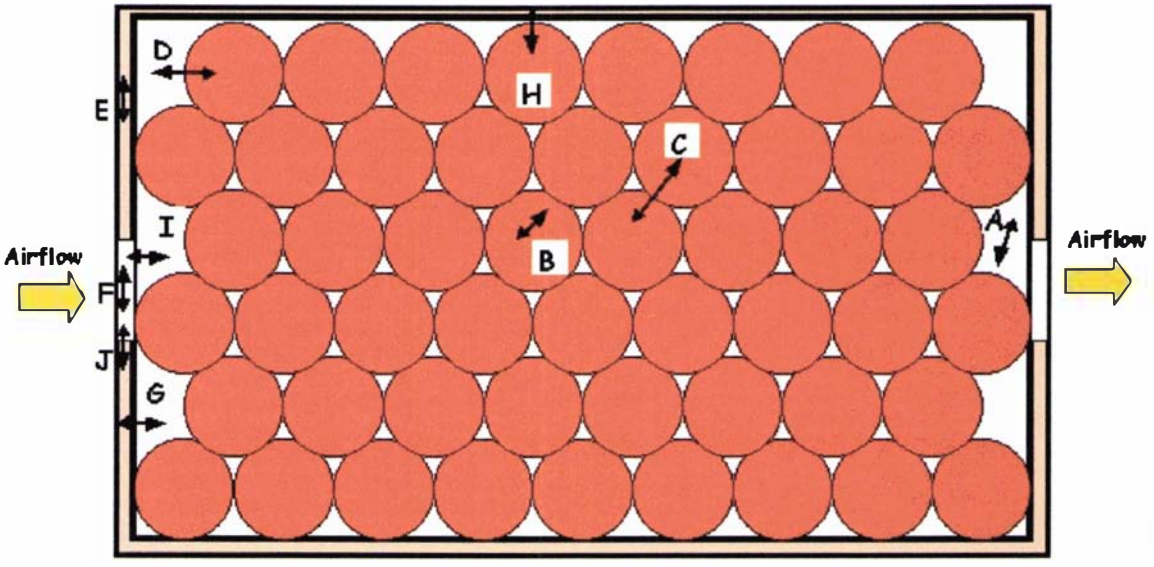

Figure 5.1 Illustration of heat transfer processes in a bulk package (the capital letters represent type of heat transfer processes, which are explained in Table 5.1)

- **Porous media approach for air and produce energy conservation**

In the heat transfer model for bulk packaging systems, the produce-air regions were treated as porous media, so the volume-averaged energy conservation equations for air and produce were used.

- **Heat transfer inside individual items of produce**

To model the heat transfer inside individual items of produce, the energy conservation equation for a solid was employed. To simplify the model solution, one-dimensional heat conduction equation in a representative spherical produce item was used.

The treatments of various heat transfer processes inside the bulk packages are summarised in Table 5.1.

Table 5.1 Heat transfer processes in the bulk packaging system.

Process	**Region**	**Classification**	**Modelling approach**
A. Heat transfer within the air in produce-air region	Produce-air regions	Conduction Convection	Volume-averaged energy conservation equation for incompressible fluid
B. Heat transfer within items of produce	Produce-air regions	Conduction	Energy conservation equation in spherical solid
C. Heat transfer between items of produce	Produce-air regions	Conduction	Volume-averaged equation for solid energy conservation
D. Heat transfer between air and produce	Produce-air regions	Convection	Newton's cooling law
E. Heat transfer within package walls	Solid regions	Conduction	Energy conservation for solid
F. Heat transfer within air in vents	Plain air regions	Convection Conduction	One-dimensional energy conservation for impressible fluid
G. Heat transfer between air in produce-air region and package walls	Interfaces between solid and produce-air regions	Convection	Newton's cooling law
H. Heat transfer between produce and package walls	Interfaces between solid and produce-air regions	Conduction	Assumed to be negligible, due to small contact areas and dominance of air cooling
I. Heat transfer between air in vents and air in produce-air regions	Interfaces between plain air and produce-air regions	Conduction Convection	Match energy flux on the interfaces
J. Heat transfer between air in vents and package walls	Interfaces between solid and plain air regions	Convection	Assumed to be negligible, due to small contact areas.

5.2.3 Analysis of Heat Transfer in the Layered Packaging Systems

The heat transfer processes in the layered packages during produce cooling are shown in Figure 5.2 and Table 5.2.

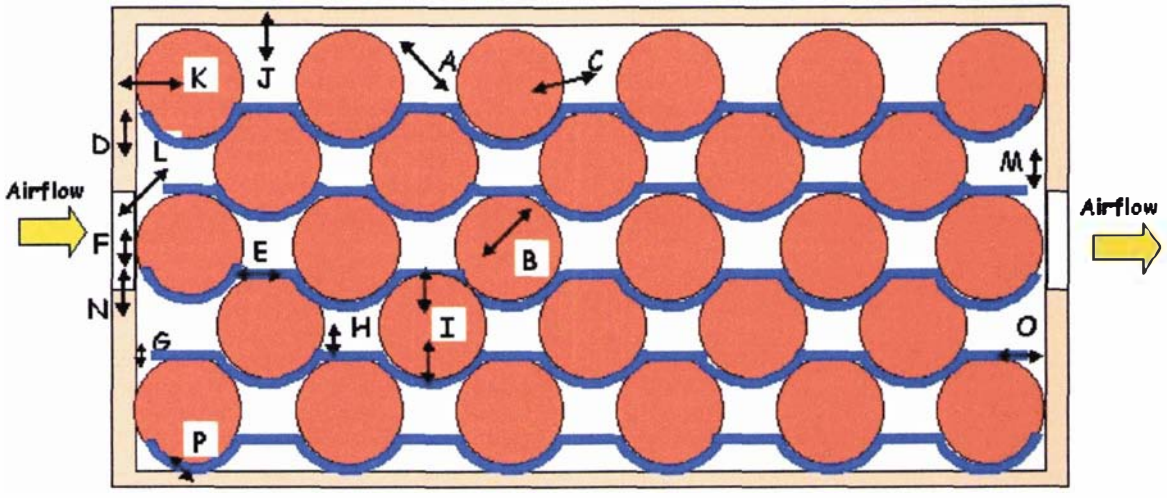

Figure 5.2 Illustration of heat transfer processes in a layered package (the meanings of letters are explained in Table 5.2)

Table 5.2 Heat transfer processes in the layered packaging system.

Process	**Region**	**Classification**	**Modelling approach**
A. Heat transfer within air	Produce-air regions	Conduction Convection	Volume-averaged energy conservation equation for incompressible fluid
B. Heat transfer within items of produce	Produce-air regions	Conduction	Energy conservation equation in spherical solid
C. Heat transfer between air and product	Produce-air regions	Convection	Newton's cooling law
D. Heat transfer within package walls	Solid regions	Conduction	Energy conservation for solid
E. Heat transfer within trays	Solid regions	Conduction	Energy conservation for solid
F. Heat transfer within air in vents	Plain air regions	Convection Conduction	One-dimensional energy conservation equation for impressible fluid
G. Heat transfer within air in gaps between tray edges and package walls	Plain air regions	Convection Conduction	One-dimensional energy conservation equation for impressible fluid
H. Heat transfer between air and trays	Interfaces between solid and produce-air regions	Convection	Newton's cooling law

Table 5.2 (continued) Heat transfer processes in the layered packaging system.

I. Heat transfer between trays and produce	Interfaces between solid and produce-air regions	Conduction	Energy conservation equation for solid
J. Heat transfer between air and package walls	Interfaces between solid and produce-air regions	Convection	Newton's cooling law
K. Heat transfer between produce and package walls	Interfaces between solid and produce-air regions	Conduction	Assumed to be negligible, due to small contact areas and dominance of air cooling
L. Heat transfer between air in vents and air in produce-air regions	Interfaces between plain air and produce-air regions	Conduction Convection	Match energy flux on the interfaces
M. Heat transfer between air in produce-air regions and air in gaps between package wall and trays	Interfaces between plain air and produce-air regions	Conduction Convection	Match energy flux on the interfaces
N. Heat transfer between air in vents and package walls	Interfaces between solid and plain air regions	Convection	Assumed to be negligible, due to small contact areas.
O. Heat transfer between trays (or package walls) and air in gaps between package wall and tray edges	Interfaces between plain air and solid regions	Conduction Convection	Assumed to be negligible, due to small contact areas.
P. Heat transfer between trays and package walls	Interfaces between solid and solid regions	Conduction	Assumed to be negligible, due to small contact areas and dominance of air cooling

- **Porous media approach for air energy conservation**

In the airflow model for the layered packaging systems, the produce-air regions between trays were treated as porous media, and the airflow in the produce layer was assumed to have only horizontal movements. Similarly the heat transfer within the

airflow in the produce-air region in the vertical direction were assumed to be negligible. The assumption of porous media is still valid for heat transfer within the air in produce-air region, and the volume-averaged equation for air energy conservation was used.

- **Gaps between tray edges and package walls**

In the airflow model for the layered packaging systems, air movements between produce layers were calculated by assuming vertical airflow in narrow tunnels. In the heat transfer model, air in the gaps was treated in the same way as air in the vents, so the gaps are plain air regions, and heat transfer in the gaps is one-dimensional and perpendicular to the trays.

- **No heat transfer between items of produce**

In the layered packages, items of produce are generally not allowed to be in contact with each other so as to reduce the incurrence of produce mechanical damage. It was therefore assumed that the items of produce in the layered packages do not contact each other. This assumption made it impossible to use the porous media approach for produce energy conservation. It is enough to model heat transfer within individual items of produce, which only requires an energy conservation equation for spherical solid.

The treatments of various heat transfer processes inside the layered packages are summarised in Table 5.2.

5.3 Model Formulation for Heat Transfer in the Bulk Packaging Systems

The mathematical model for heat transfer in the bulk packaging systems consists of the following equations:

1) Fluid energy equation describing air energy conservation in the plain air regions (vents).
2) Solid energy conservation equation describing energy conservation in the solid regions (package walls).

3) Volume-averaged fluid energy equation describing air energy conservation in the produce-air regions.
4) Volume-averaged solid energy equation describing produce energy conservation in the produce-air regions.
5) Solid energy conservation equation describing energy conservation in single items of produce.
6) Auxiliary algebraic equations for calculating heat transfer coefficients, dispersion conductivity, geometric properties, produce respiration rate, etc.
7) Auxiliary algebraic equations for describing boundaries.

5.3.1 Energy Conservation in Plain Air Region

- **Energy conservation equation for air in vents**

Air was treated as a viscous incompressible fluid, and the one-dimensional air energy equations were written (Bird *et al.*, 1960):

$$\frac{\partial(\rho_a C_a T_a)}{\partial t} + \frac{\partial(\rho_a u C_a T_a)}{\partial x} - \frac{\partial}{\partial x}\left(K_a \frac{\partial T_a}{\partial x}\right) = 0 \qquad (5.1a)$$

$$\frac{\partial(\rho_a C_a T_a)}{\partial t} + \frac{\partial(\rho_a v C_a T_a)}{\partial y} - \frac{\partial}{\partial y}\left(K_a \frac{\partial T_a}{\partial y}\right) = 0 \qquad (5.1b)$$

where:

u	=	air velocity component in the direction of x-axis (m s^{-1}).
v	=	air velocity component in the direction of y-axis (m s^{-1}).
C_a	=	air specific heat at constant pressure (J kg^{-1} K^{-1}).
ρ_a	=	air density (kg m^{-3}).
T_a	=	air temperature (K).
K_a	=	air thermal conductivity (W m^{-1} K^{-1}).

5.3.2 Energy Conservation in Solid Regions

- **Energy conservation equation for package walls**

The energy equation for package walls was written (Bird *et al.*, 1960):

$$\frac{\partial(\rho_{pack} C_{pack} T_{pack})}{\partial t} - \frac{\partial}{\partial x}(K_{pack} \frac{\partial T_{pack}}{\partial x}) - \frac{\partial}{\partial y}(K_{pack} \frac{\partial T_{pack}}{\partial y}) - \frac{\partial}{\partial z}(K_{pack} \frac{\partial T_{pack}}{\partial z}) = 0 \quad (5.2)$$

where:

ρ_{pack} = packaging material density (kg m^{-3}).

C_{pack} = packaging material specific heat capacity (J K^{-1} m^{-1})

T_{pack} = packaging material temperature (K).

K_{pack} = packaging material thermal conductivity (W K^{-1} m^{-1}).

5.3.3 Energy Conservation in Produce-air Regions

- **Volume-averaged energy conservation equation for air**

The volume-averaged energy conservation equation for the fluid phase in porous media was written for air energy conservation; the item on the RHS of the Equation (5.3) represents heat exchange between produce and air (Hsu & Cheng, 1990; Kaviany, 1995).

$$\frac{\partial(\rho_a \phi C_a \langle T_a \rangle_a)}{\partial t} + \frac{\partial(\rho_a \phi \langle u \rangle_a C_a \langle T_a \rangle_a)}{\partial x} + \frac{\partial(\rho_a \phi \langle v \rangle_a C_a \langle T_a \rangle_a)}{\partial y} + \frac{\partial(\rho_a \phi \langle w \rangle_a C_a \langle T_a \rangle_a)}{\partial x}$$
$$- \frac{\partial}{\partial x}\left((\phi K_a + K_{dis}) \frac{\partial \langle T_a \rangle_a}{\partial x} \right) - \frac{\partial}{\partial y}\left((\phi K_a + K_{dis}) \frac{\partial \langle T_a \rangle_a}{\partial y} \right) - \frac{\partial}{\partial z}\left((\phi K_a + K_{dis}) \frac{\partial \langle T_a \rangle_a}{\partial z} \right) =$$
$$h_t a_{aP} (T_{PSurface} - < T_a >_a) \quad (5.3)$$

where:

$\langle u \rangle_a$ = intrinsic phase average of air velocity component in the direction of x-axis (m s^{-1}).

$\langle v \rangle_a$ = intrinsic phase average of air velocity component in the direction of y-axis (m s^{-1}).

$\langle w \rangle_a$ = intrinsic phase average of air velocity component in the direction of z-axis (m s^{-1}).

$\langle T_a \rangle_a$ = intrinsic phase average of air temperature (K).

$T_{PSurface}$ = produce surface temperature (K).

ρ_a = air density (kg m^{-3}).

C_a = air specific heat at constant pressure (J kg^{-1} K^{-1}).

K_a = air thermal conductivity (W K^{-1} m^{-1}).

K_{dis} = dispersion conductivity (W K^{-1} m^{-1}).

ϕ = porosity.

a_{ap} = specific interstitial surface area (m^{-1}).

h_t = heat transfer coefficient between air and solid surface (W m^{-2} K^{-1}).

- **Volume-averaged energy conservation equation for produce**

The volume-averaged energy conservation equation for the solid phase in porous media was written for produce energy conservation; the first item on the RHS of Equation (5.4) represents heat exchange between produce and air (Hsu & Cheng, 1990; Kaviany, 1995).

$$\frac{\partial\left(\rho_p C_p (1-\phi)\langle T_p\rangle_p\right)}{\partial t} - \frac{\partial}{\partial x}\left((1-\phi)K_p \frac{\partial\langle T_p\rangle_p}{\partial x}\right) - \frac{\partial}{\partial y}\left((1-\phi)K_p \frac{\partial\langle T_p\rangle_p}{\partial y}\right) - \frac{\partial}{\partial z}\left((1-\phi)K_p \frac{\partial\langle T_p\rangle_p}{\partial z}\right)$$
$$= -a_{ap} h_t (T_{PSurface} - \langle T_a\rangle_a) + (1-\phi)\rho_p R_P \qquad (5.4)$$

where:

t = time(s).

ρ_p = product density ($kg \cdot m^{-3}$).

$\langle T_p\rangle_p$ = intrinsic phase average of product temperature (K).

K_p = product thermal conductivity ($W \cdot K^{-1} \cdot m^{-1}$).

C_p = product specific heat ($J \cdot kg^{-1} \cdot K^{-1}$).

R_p = product respiration heat (W kg^{-1}).

ϕ = porosity.

a_{ap} = specific interstitial surface area (m^{-1}).

h_t = heat transfer coefficient between air and solid surface (W m^{-2} K^{-1}).

- **Energy conservation equation for a single item of produce**

The energy conservation equation for a spherical solid was written for energy conservation of single items of produce (Bird *et al.*, 1960):

$$\frac{\partial(\rho_p C_p T_p)}{\partial t} - \frac{1}{r^2}\frac{\partial}{\partial r}(K_p r^2 \frac{\partial T_p}{\partial r}) = \rho_p R_p \tag{5.5}$$

where:

t	=	time(s).
r	=	spatial variable along sphere radius (m).
ρ_p	=	product density ($kg \cdot m^{-3}$).
T_p	=	produce temperature (K).
K_p	=	product thermal conductivity ($W \cdot K^{-1} \cdot m^{-1}$).
C_p	=	product specific heat ($J \cdot kg^{-1} \cdot K^{-1}$).
R_p	=	product respiration heat ($W\ kg^{-1}$).

5.3.4 Auxiliary Equations

- **Geometric parameters**

Porosity was computed as in Section 4.3.3.

The equivalent mean diameter of produce items is calculated as:

$$d_{eq} = 6\frac{V_p}{S_p} \tag{5.6}$$

where:

d_{eq}	=	equivalent mean diameter (m).
V_p	=	mean volume of produce item (m^3).
S_p	=	mean surface area of produce item (m^2).

The specific surface area of a porous material is defined as the surface area of the produce items per unit bulk volume of the porous medium. For a sphere-packed bed, specific surface area is (Dullien, 1979):

$$a_{aP} = \frac{6(1-\phi)}{d_{eq}} \tag{5.7}$$

where:

a_{ap} = specific interstitial surface area (m^{-1}).

- **Heat transfer coefficient for convection between air and solid surfaces**

Geankoplis (1993) presented a forced convection correlation for gas flow in a packed bed of spheres:

$$\frac{Nu_d}{Re_d Pr}\phi Pr^{0.66} = \frac{2.876}{Re_d} + \frac{0.3023}{Re_d^{0.35}} \tag{5.8}$$

$$Nu_d = \frac{h_t d_{eq}}{k_a} \tag{5.9}$$

$$Re_d = \frac{\phi(\langle u\rangle_a^2 + \langle v\rangle_a^2 + \langle w\rangle_a^2)^{\frac{1}{2}} d_{eq}}{\mu} \tag{5.10}$$

$$Pr = \frac{C_a \mu}{K_a} \tag{5.11}$$

where:

h_t = heat transfer coefficient between air and solid surface (W m^{-2} K^{-1}).

Nu_d = Nusselt number.

Re_d = Reynolds number.

Pr = Prandtl Number.

μ = air dynamic viscosity (N s m^{-2}).

ϕ = porosity.

d_{eq} = equivalent mean sphere diameter (m).

C_a = air specific heat at constant pressure (J kg^{-1} K^{-1}).

K_a = air thermal conductivity (W m^{-1} K^{-1}).

Typical heat transfer coefficient values range from 1 to 20 W m^{-2} K^{-1}.

- **Dispersion conductivity**

The dispersion conductivity is a tensor that is a function of Peclet number based on the superficial velocity in the main flow direction (Kaviany, 1995; Wakao & Kaguei, 1982). Since the main flow direction is difficult to define, the tensor is simplified as a scalar, and assumed to be a linear function of the Peclet number based on the local superficial velocity:

$$K_{dis} = C_{dis} Pe_d K_a \tag{5.12}$$

$$Pe_d = \frac{C_a \rho_a \phi \left(\langle u \rangle_a^{\,2} + \langle v \rangle_a^{\,2} + \langle w \rangle_a^{\,2} \right)^{\frac{1}{2}} d_{eq}}{K_a} \tag{5.13}$$

where:

Pe_d	=	Peclet number based on particle dimension.
$\langle u \rangle_a$	=	intrinsic phase average of air velocity component in the direction of x-axis (m s^{-1}).
$\langle v \rangle_a$	=	intrinsic phase average of air velocity component in the direction of y-axis (m s^{-1}).
$\langle w \rangle_a$	=	intrinsic phase average of air velocity component in the direction of z-axis (m s^{-1}).
d_{eq}	=	equivalent mean sphere diameter (m).
ρ_a	=	air density (kg m^{-3}).
C_a	=	air constant-pressure specific heat capacity (J K^{-1} kg^{-1}).
K_a	=	air thermal conductivity (W K^{-1} m^{-1}).
C_{dis}	=	empirical constant (~ 0.2).

- **Respiration heat**

Product respiration heat was calculated as follows (Tanner, 1998):

$$R_p = c\left(T_p - 255.35\right)^r \tag{5.14}$$

where:

R_p = product respiration heat (W kg^{-1}).

T_P = produce temperature (K).

c = constant.

d = constant.

The values of constant c and d are associated with specific crops, and were summarised by Tanner (1998).

- **Relation between produce temperature and its volume average**

The relation between produce temperature and its volume average is written as follow.

$$\langle T_p \rangle_P = \frac{2}{3d_{eq}^{\ 3}} \int_0^{\frac{d_{eq}}{2}} T_P r^2 dr \tag{5.15}$$

where:

d_{eq} = equivalent diameter of product (m).

T_p = produce temperature (K).

$\langle T_p \rangle_p$ = intrinsic phase average of air temperature (K).

5.3.5 Boundary Conditions

- **Vents with airflow entering packaging systems**

As a boundary condition for energy conservation equation in plain air regions, if cold air enters a vent, fixed temperature was assumed.

$$T_a = T_{a-enter} \tag{5.16}$$

where:

$T_{a\text{-}enter}$ = temperature of air entering a vent (K).

- **Vents with airflow leaving packaging systems**

As a boundary condition for energy conservation equation in plain air regions, if air leaves a vent, air temperature was assumed to be invariant along the direction normal to the vent.

$$\frac{\partial T_a}{\partial x_i} = 0 \qquad (x_i \text{ normal to vent}) \qquad (5.17)$$

- **Interfaces between package walls and surrounding environment**

If package walls are exposed to outside airflow, Newton's cooling law was used

$$q_{out-pack} = -h_{t-out}(T_{pack} - T_{a-out}) \qquad (5.18)$$

where:

$q_{out\text{-}pack}$	=	heat flux from outside airflow to packaging material (W m^{-2}).
T_{pack}	=	packaging material temperature (K).
$T_{a\text{-}out}$	=	outside airflow temperature (K).
$h_{t\text{-}out}$	=	heat transfer coefficient between outside airflow and package walls (W m^{-2} K^{-1}).

If the package top or bottom sides are adjacent to other packages, it was assumed that no heat transfer occurs.

- **Interfaces between produce-air regions and solid regions**

As stated in Section 5.2.2, heat transfer between produce and packaging walls was assumed to be negligible, and heat transfer between air and package walls was modelled with Newton's cooling law.

$$q_{air-pack} = -h_t(T_{pack} - < T_a >_a) \qquad (5.19)$$

where:

$q_{air\text{-}pack}$ = heat flux from air to packaging material (W m^{-2}).

T_{pack} = packaging material temperature (K).

h_t = heat transfer coefficient between air and solid surface (W m^{-2} K^{-1}).

The above equation was used as a boundary condition for both the volume-averaged air energy conservation equation in produce-air regions and the energy conservation equation for package walls.

- **Interfaces between air and produce in produce-air regions**

As a boundary condition for the energy equation for a single items of produce, convection heat transfer between air and produce was modelled according to Newton's cooling law.

$$q_{air-produce} = -h_t(T_{PSurface} - < T_a >_a) \tag{5.20}$$

where:

$q_{produce\text{-}air}$ = heat flux from air to produce item (W m^{-2}).

$T_{PSurface}$ = produce surface temperature (K).

h_t = heat transfer coefficient between air and solid surface (W m^{-2} K^{-1}).

- **Interface between plain air regions and produce-air regions**

As airflow is perpendicular to the interfaces between plain air and air-product porous regions, it is adequate to match energy flow from one region to another. The detailed treatment is described in Appendix A.

5.4 Model Formulation for Heat Transfer in the Layered Packaging Systems

The mathematical model for heat transfer in the layered packaging systems consists of following equations:

1) Fluid energy equation describing air energy conservation in the plain air regions (vents or gaps between tray edges and package walls).
2) Solid energy conservation equation describing energy conservation in the solid region (package walls and trays).
3) Volume-averaged fluid energy equation describing air energy conservation in the produce-air regions.
4) Solid energy conservation equation describing energy conservation in single items of produce.
5) Auxiliary algebraic equations for calculating heat transfer coefficients, dispersion conductivity, geometric properties, produce respiration rate, etc.
6) Auxiliary algebraic equations for describing boundaries.

5.4.1 Energy Conservation in Plain Air Region

- **Energy conservation equation for air in vents and in the gaps between package walls and tray edges**

The energy conservation equation in vents of the layered packaging system is the same as that of the bulk packaging system (Equation 5.1). For the gaps between tray edges and package walls, energy conservation equation along z-axis was written.

$$\frac{\partial(\rho_a C_a T_a)}{\partial t}+\frac{\partial(\rho_a w C_a T_a)}{\partial z}-\frac{\partial}{\partial z}\left(K_a\frac{\partial T_a}{\partial z}\right)=0 \qquad (5.21)$$

where:

w = air velocity component in the direction of y-axis (m s^{-1}).

5.4.2 Energy Conservation in Solid Regions

- **Energy conservation equation for package walls and trays**

The energy conservation equation in solid regions of the layered packaging system is the same as that of the bulk packaging system (Equation 5.2).

5.4.3 Energy Conservation in Produce-air Regions

- **Volume-averaged energy conservation equation for air**

The volume-averaged energy conservation equation for the fluid phase in porous media was written for the energy conservation of airflow with horizontal movements (Hsu & Cheng, 1990; Kaviany, 1995).

$$\frac{\partial(\rho_a \phi C_a \langle T_a \rangle_a)}{\partial t} + \frac{\partial(\rho_a \phi \langle u \rangle_a C_a \langle T_a \rangle_a)}{\partial x} + + \frac{\partial(\rho_a \phi \langle v \rangle_a C_a \langle T_a \rangle_a)}{\partial y}$$
$$- \frac{\partial}{\partial x}\left((\phi K_a + K_{dis}) \frac{\partial \langle T_a \rangle_a}{\partial x} \right) - \frac{\partial}{\partial y}\left((\phi K_a + K_{dis}) \frac{\partial \langle T_a \rangle_a}{\partial y} \right) - \frac{\partial}{\partial z}\left((\phi K_a + K_{dis}) \frac{\partial \langle T_a \rangle_a}{\partial z} \right) =$$
$$h_t a_{P-exposed} (T_{Psurface} - < T_a >_a)$$

(5.22)

where:

$\langle u \rangle_a$	=	intrinsic phase average of air velocity component in the direction of x-axis (m s^{-1}).
$\langle v \rangle_a$	=	intrinsic phase average of air velocity component in the direction of y-axis (m s^{-1}).
$\langle T_a \rangle_a$	=	intrinsic phase average of air temperature (K).
$T_{PSurface}$	=	produce surface temperature (K).
ρ_a	=	air density (kg m^{-3}).
C_a	=	air specific heat at constant pressure (J kg^{-1} K^{-1}).
K_a	=	air thermal conductivity (W m^{-1} K^{-1}).
K_{dis}	=	dispersion conductivity (W K^{-1} m^{-1}).
ϕ	=	porosity.
$a_{p\text{-}exposed}$	=	exposed-to-air produce surface area per unit volume of air-produce region (m^{-1}).
h_t	=	heat transfer coefficient between air and solid surface (W m^{-2} K^{-1}).

- **Energy conservation equation for single item of produce**

The energy conservation of single items of produce in the layered packaging system is the same as that of the bulk packaging system (Equation 5.5).

5.4.4 Auxiliary Equations

All auxiliary equations in heat transfer model for the bulk packaging systems were the same as for the layered packaging systems.

5.4.5 Boundary Conditions

The boundary conditions defined for heat transfer model in the bulk packaging systems are equally valid in the layered packaging system. Additional boundary conditions are defined as follow.

- **Interfaces between the air in produce-air regions and trays**

Convection heat transfer between the air in produce-air regions and trays was modelled according to Newton's cooling law.

$$q_{air-tray} = -h_t (T_{traySurface} - < T_a >_a) \tag{5.23}$$

where:

$q_{air-tray}$ = heat flux from air to tray (W m^{-2}).

$T_{traySurface}$ = tray surface temperature (K).

h_t = heat transfer coefficient between solid surface and air (W $m^{-2} K^{-1}$).

The above equations were used as a boundary condition for both the volume-averaged air energy conservation equation in produce-air regions and the energy conservation equation for trays.

- **Interfaces between produce items and trays**

An item of produce generally contacts trays at both bottom and top. The heat transfer between the produce items and trays is conduction. The detailed treatment is described in Appendix A.

- **Interfaces between the air in air–produce regions and the air in gaps between package wall and tray edges**

The boundary condition was specified via matching energy flow from one region to another. The detailed treatment is described in Appendix A.

5.5 Summary

This chapter outlined the conceptual and mathematical models for heat transfer in both bulk and layered packaging systems. In the conceptual models, the heat transfer processes within the packaging systems were analysed. In the mathematical models, the partial differential equations for describing these heat transfer processes were presented. The solution of the heat transfer models is presented in Chapter 6 and Appendix A.

CHAPTER 6
SOLUTION OF AIRFLOW AND HEAT TRANSFER MODELS

6.1 Introduction

The airflow and heat transfer models presented in Chapters 4 and 5 are made up of groups of partial differential equations (PDEs) and auxiliary equations. It was impossible to solve these PDEs analytically on complex domains inside produce packages, so numerical solutions were sought as approximations.

The process of obtaining the numerical solutions consisted of two stages. The first stage was discretisation that employed the finite-volume method to convert the continuous transport equations into discrete systems of algebraic equations. The second stage was to solve these systems of algebraic equations.

The finite volume method divides the calculation domain into a number of non-overlapping control volumes (cells) such that every cell surrounds a grid point. The differential equations of solved-for variables, for example, momentum equations for velocity components, are then integrated over each control volume. Piecewise profiles expressing the variation of the corresponding variables between the grid points are used to evaluate the required integrals. For each solved-for variable in each cell, an algebraic discretisation equation is generated, which contains the values of the variable in the grid node of the current cell and the grid points of its neighbouring cells as unknowns (Patankar, 1982; Ferziger & Peric, 1999).

This chapter first deals with the process of grid generation, i.e. how the calculation domain (individual package or a layer of packages) is divided into a collection of cells. Then it describes the numerical schemes for converting the PDEs in the airflow and heat transfer models to the systems of algebraic equations; the details on derivations of the discretisation equations are presented in Appendix A. Finally the solution methods for the systems of discretisation equations are discussed.

6.2 Grid Generation

Since only cubic packages were considered in the models, and the application of the porous-media treatment meant that the meshes did not have to describe the complicated geometries inside the packages, a Cartesian coordinate system was adopted.

As shown in Figure 3.3, the orientations of individual bins or cartons in a layer of packages in a stack are usually different from each other. This structural feature makes it necessary to use a very fine mesh to represent the package details such as the thickness of package walls or trays. However, the use of extremely fine grids not only requires large computing capacity, but it also produces physically meaningless cell size (the smallest cell should contain approximately one single product). To overcome this problem, a block-structured grid was applied, in which each individual package constitutes one mesh block. The block-structured grid system was specified with a global grid and two local grids. The global grid system specifies the location of individual packages in a layer of packages. The local grid systems describe the package structural details, and the local cells are used to derive the discretisation equations.

6.2.1 Coordinates and Cell Index Convention

The location of each cell is specified by the cell indices (I, J, K) that are the count numbers of the cell in x, y, z directions. Each cell has six faces named as south (s), north (n), west (w), east (e), low (l), and high (h) faces. The conventions for coordinates and positions in calculation domains are shown in Figures 6.1 and 6.2. Attention was focused on the current grid node P in the centre of a cell, which had the grid nodes E, W, N, S, H, L, etc, as its neighbours. The subscript e, w, n, s, h, l denote the surfaces of the current cell.

6.2.2 Global Grid System

The global grid system divides an individual package or a layer of packages into a number of cells as shown in Figures 6.3 and 6.4. In a layer of packages, the positions of individual packages are specified by the cell index in the left-bottom corners of the

packages. Along each horizontal axis (x-axis or y-axis), the global grid is equally spaced. The dimensions of global cells are decided according to the types of calculation domains (single package or a layer of packages) and types of packaging systems (layered or bulk packaging system).

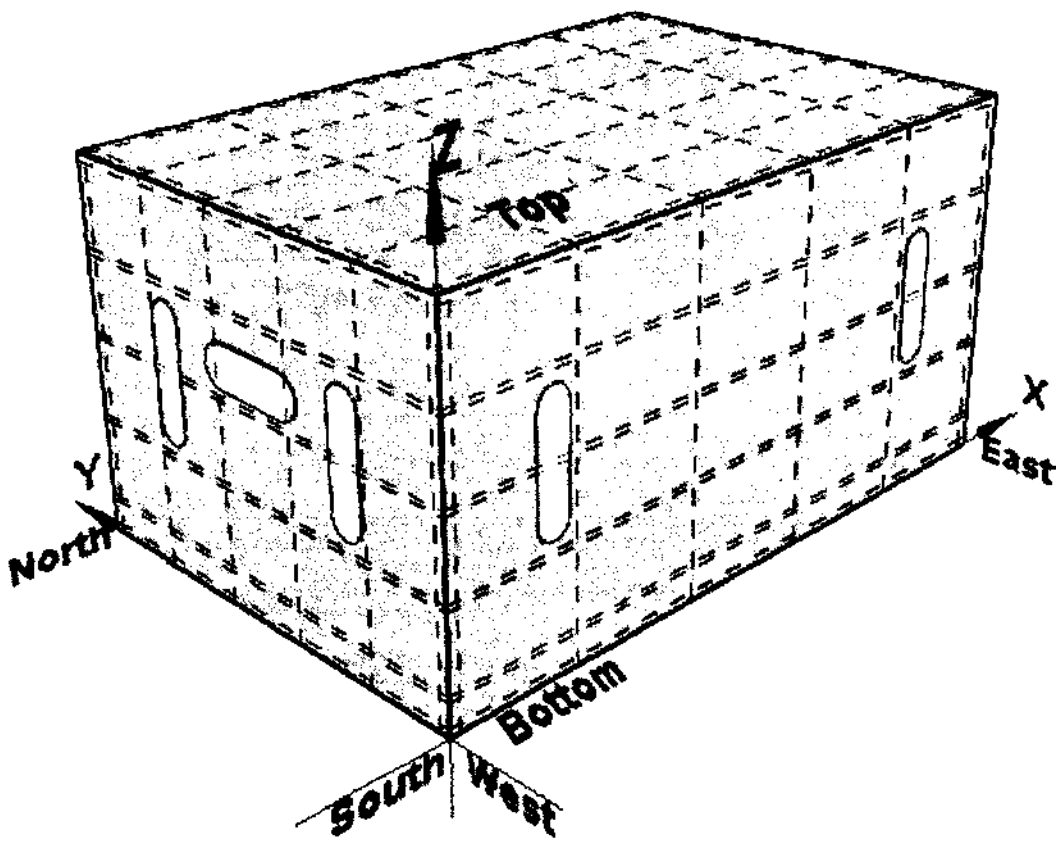

Figure 6.1 Coordinate systems used in this study and local grid system of a single package with its length along x-axis.

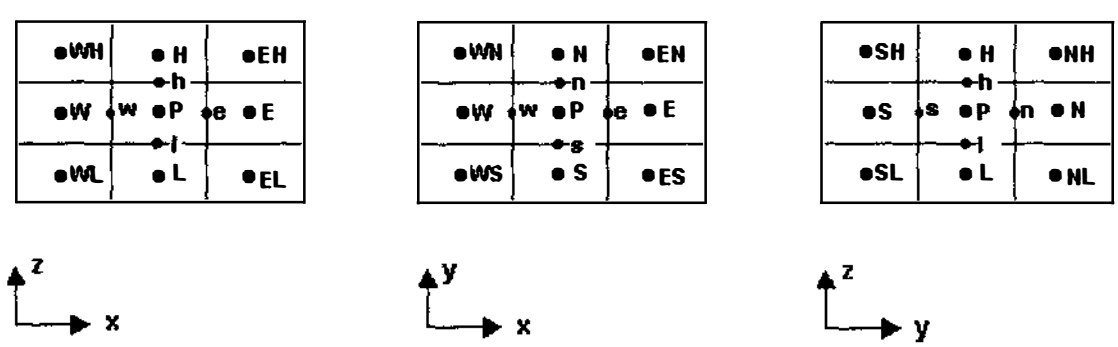

Figure 6.2 Conventions for specifying the positions in calculation domains.

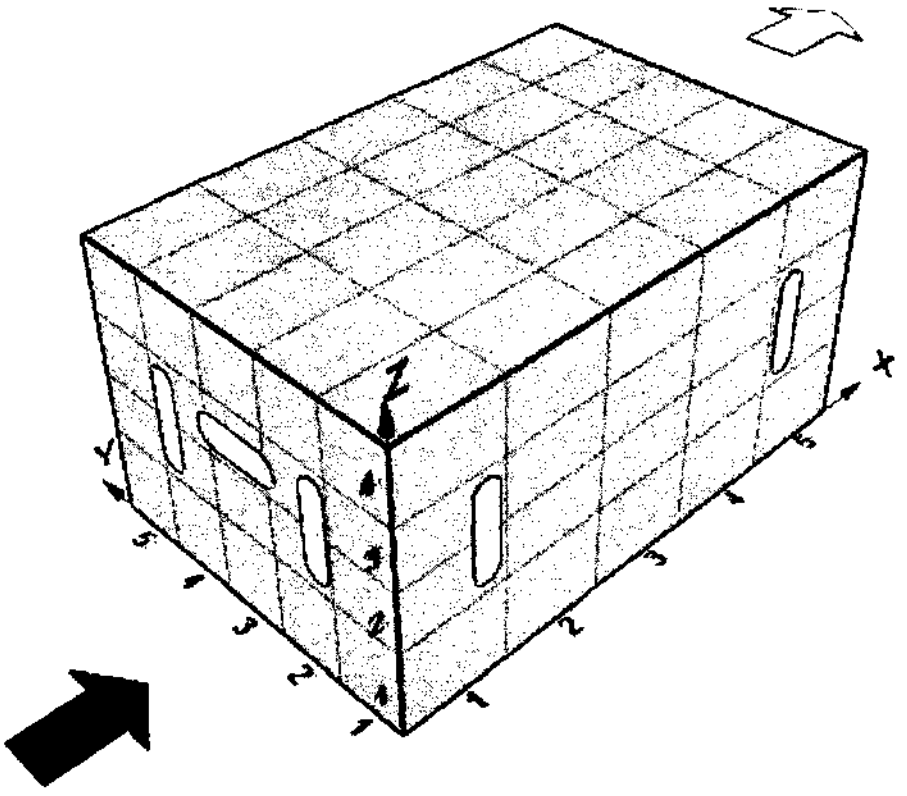

Figure 6.3 Global grid system of the domain of individual package.

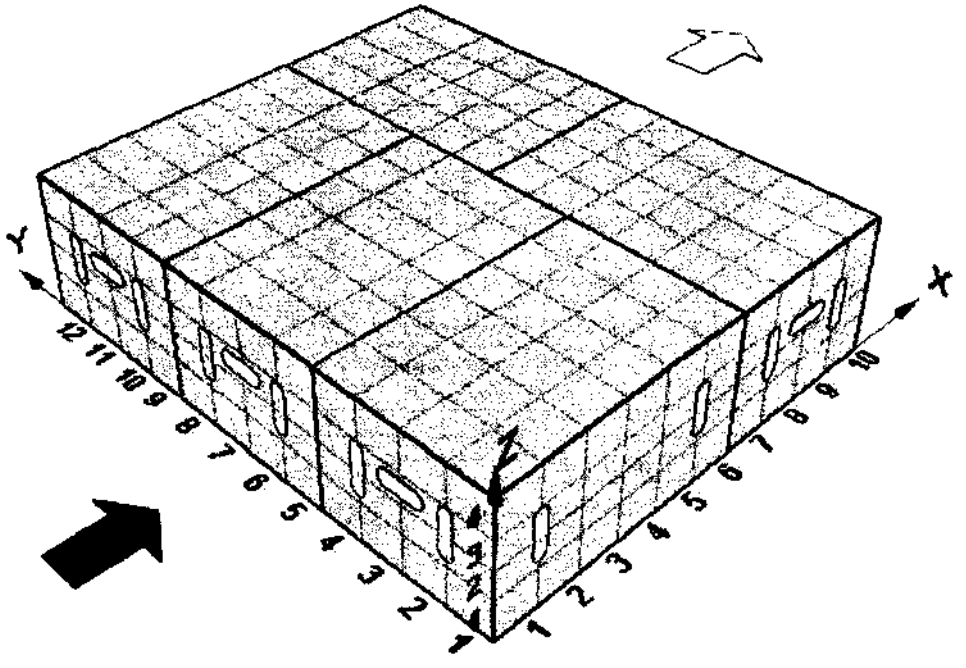

Figure 6.4 Global grid system of the domain of a layer of packages.

- **Global cells for the domain of a single package**

When a single package is considered in the model, the length and width of global cells (the dimensions along x and y axes) are calculated using the number of cells in each of the two horizontal directions.

$$L_{cell} = \frac{L_{pack}}{n_x} \tag{6.1}$$

$$W_{cell} = \frac{W_{pack}}{n_y} \tag{6.2}$$

where:

L_{cell}	=	length of global cell (dimension of cell along x-axis) (m).
W_{cell}	=	width of global cell (dimension of cell along y-axis) (m).
L_{pack}	=	length of package (dimension of package along x-axis) (m).
W_{pack}	=	width of package (dimension of package along y-axis) (m).
n_x	=	number of global cells along x-axis.
n_y	=	number of global cells along y-axis.

For a domain of a single layered package, the heights of global cells (dimension along z-axis) are determined according to the position of trays, as shown in Figure 6.5.

For a domain of a single bulk package, the global grid along the z-axis is equally spaced. The height of global cells is calculated as follows:

$$n_z = ceil\left(\frac{H_{pack}}{\min(W_{cell}, L_{cell})}\right) \tag{6.3}$$

$$H_{cell} = \frac{H_{pack}}{n_z} \tag{6.4}$$

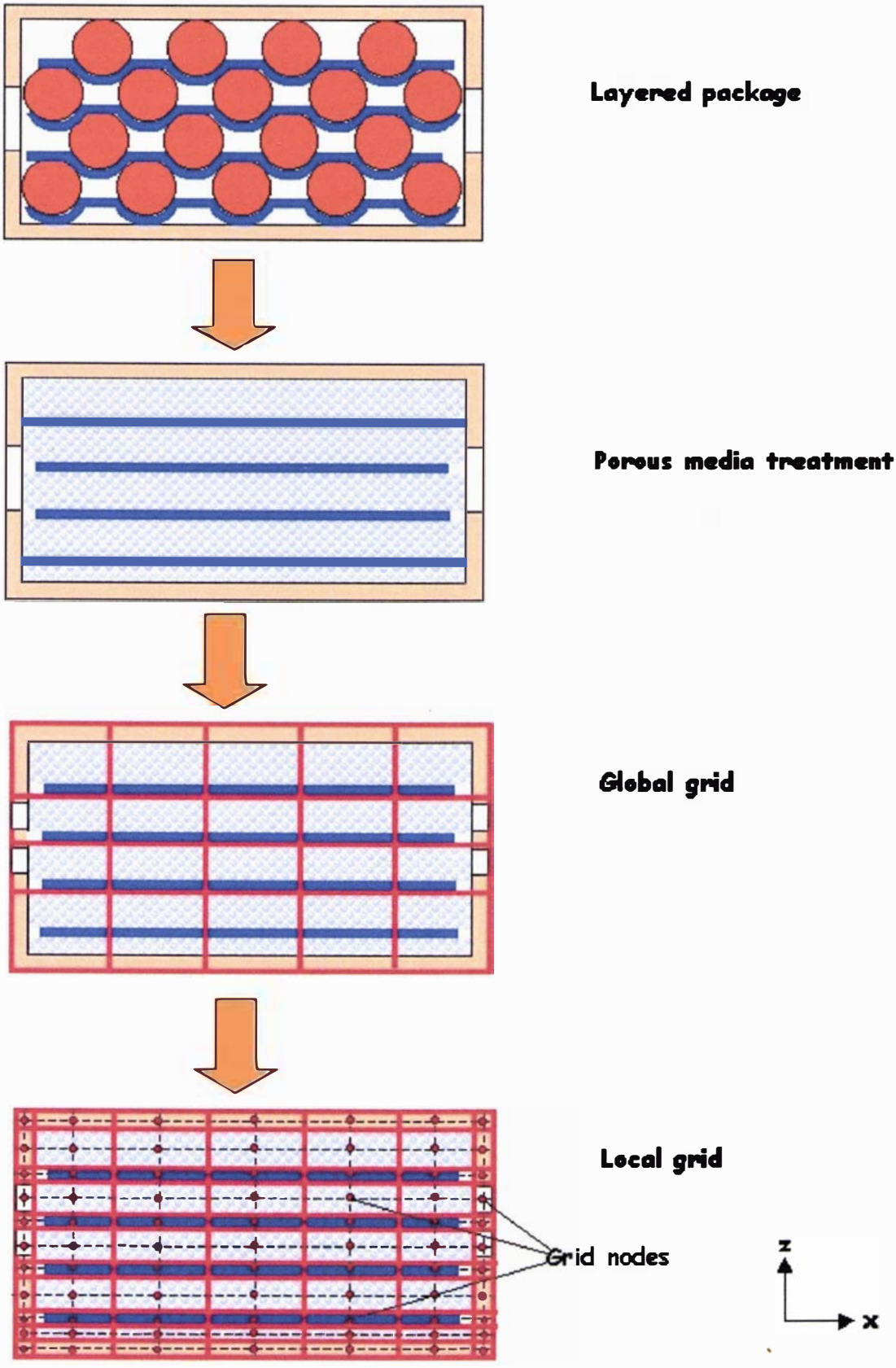

Figure 6.5 Illustration of grid generation processes for layered packages (grid generation for x-z plane of a layered package).

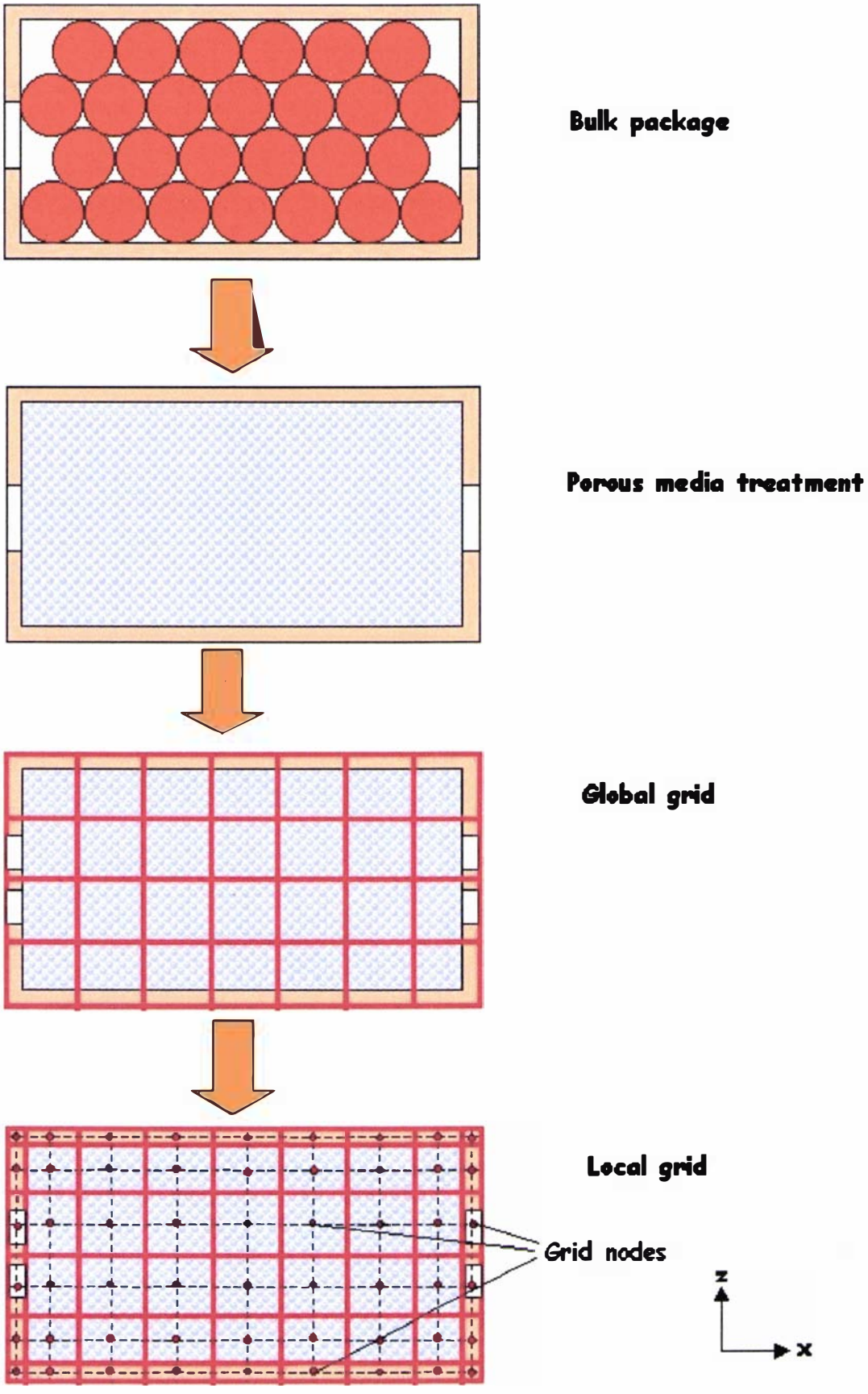

Figure 6.6 Illustration of grid generation processes for bulk package (grid generation for x-z plane of a bulk package).

where:

H_{cell} = height of global cell (dimension of cell along z-axis) (m).

L_{cell} = length of global cell (dimension of cell along x-axis) (m).

W_{cell} = width of global cell (dimension of cell along y-axis) (m).

H_{pack} = height of package (dimension of package along z-axis) (m).

n_z = number of global cells along z-axis.

ceil = function that rounds a number toward plus infinity.

min = function that finds the minimum among several variabels.

- **Global cells for the domain of a layer of packages**

As shown in Figure 6.4, packages may be cross-stacked. To form a cubic stack, the ratio of package length and width was assumed to be a ratio of two integers:

$$\frac{L_{pack}}{W_{pack}} = \frac{n_1}{n_2} \tag{6.5}$$

where:

L_{pack} = length of package (dimension of package along x-axis) (m).

W_{pack} = width of package (dimension of package along y-axis) (m).

n_1 = integer.

n_2 = integer.

The global grids for a package layer are set to be equally spaced along x-axis and y-axis. The horizontal dimension of global cells is calculated according to the ratio between product equivalent diameter and cell size:

$$D_{cell-est} = d_{eq} R_{cell-produce} \tag{6.6}$$

$$L_{cell} = W_{cell} = \frac{W_{pack}}{ceil\left[\frac{\left(ceil\left(\frac{W_{pack}}{D_{cell-est}}\right)\right)}{n_2}\right] n_2} \tag{6.7}$$

where:

L_{cell}	=	length of global cell (dimension of package along x-axis) (m).
W_{cell}	=	width of global cell (dimension of package along y-axis) (m).
$D_{cell\text{-}est}$	=	estimated cell width (m).
d_{eq}	=	equivalent mean diameter (m).
$R_{cell\text{-}produce}$	=	ratio between global cell horizontal dimension and produce equivalent diameter (m).
W_{pack}	=	width of package (dimension of package along y-axis) (m).
n_1	=	integer in Equation 6.5.
n_2	=	integer in Equation 6.5.
$ceil$	=	function that rounds a number toward plus infinity.

Heights of global cells for the domain of a package layer are calculated in the same way as for the single package domain.

6.2.3 Local Grid Systems

The global grid system discussed in the proceeding section separates the calculation domain into a group of global cells with the same horizontal dimensions. In each block (an individual package), the global cells next to container walls or trays were further divided so as to include the cells for walls or trays as shown in Figures 6.5 and 6.6. Hence the local grid systems are generated by adding structural details to global cells for individual packages. The discretisation equations were derived by integrating the relevant PDEs over the local cells.

For a layer of packages, only two local grid systems need to be specified, corresponding to two possible orientations of individual packages (package length in the x-axis direction or in the y-axis direction), as shown in Figures 6.1 and 6.7. The position of any local cell can be determined by its position in one of the local grid systems and the package position in the global grid system.

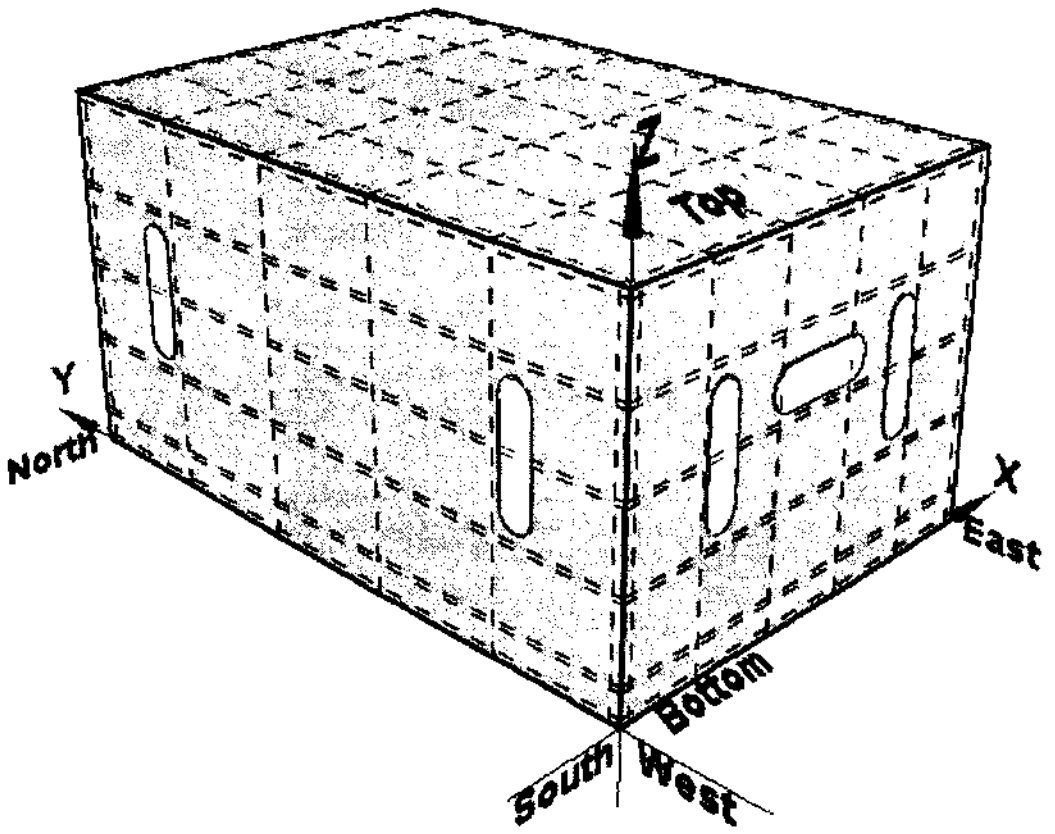

Figure 6.7 Local grid system of a single package with its length along y-axis.

6.2.4 Vents across More than One Local Cell

A vent on a package wall may cross several cells as show in Figure 6.8. To simplify the calculation, a vent that cuts across several cells is treated as a group of small vents located in the cells, and the area of the vent in the narrow cells corresponding to package walls or trays were ignored. As shown in Figure 6.8, a vent occupying six cells is divided into four vents located in four larger cells, and the remaining two narrow cells are blocked. The resulting small vents are represented by the porosities of the cells in package wall:

$$\phi = \frac{A_{vent}}{A_{cell}} \tag{6.8}$$

where

ϕ = porosity.

A_{vent} = area of the vent portion in a cell (m^2).

A_{cell} = area of the cell (m^2).

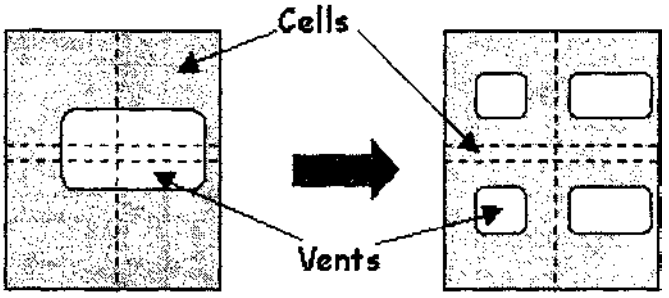

Figure 6.8 – Illustration of the treatment of the vents across several cells.

Since the airflow and heat transfer in vents were assumed to be one-dimensional, the shapes of vents have no effect on transport processes in vents, and the sizes of vents, which are represented by the porosities of cells on package walls, are enough for derivation of discretisation equations.

6.2.5 Treatments of Boundaries between Packages

Due to the way in which the global and local grid systems are constructed, the global cells in two adjacent package walls match with each other, but the local cells may not. Moreover the vents in two adjacent walls may not have the same sizes. To simplify the calculation and indexing in the boundaries of package walls, the following treatments were applied as shown in Figure 6.9:

- If two adjacent local cells have vents with different sizes, the size of the larger vent is set to that of the smaller vent.
- A local cell is contained in global cell A in one package wall that is adjacent to global cell B in other package wall. Then the local cell in global cell A was assumed to have a imaginary matching neighbouring local cell, which takes the properties of the local cell having the largest area among all the local cells in global cell B. This enables us to treat local cells as continuous over the whole package layer.

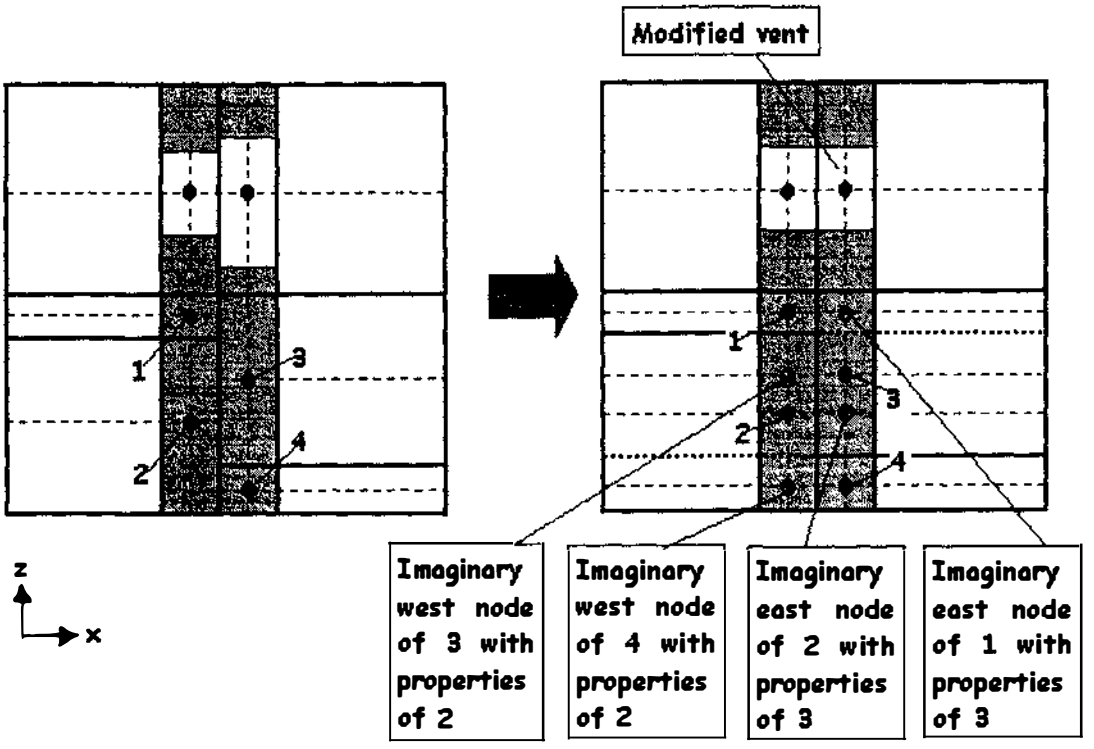

Figure 6.9 Illustration of the treatments of the boundaries between packages

6.3 Discretisation Equations for PDEs in the Airflow and Heat Transfer Models

6.3.1 Numerical Schemes

Discretisation of the airflow transport equations were based on the SIMPLER (Semi-Implicit Method for Pressure-Linked equations Revised) method proposed by Patankar (1980).

- **Staggered grids**

To avoid occurrence of wavy velocity and pressure fields, a staggered grid was used. The scalars including temperature, pressure, and pressure correction are stored at the centre points of local cells (scalar cells). The velocity vector components are stored at the centre points of the six faces of scalar cells. Vector quantities are computed by reference to vector cells that are staggered with respect to the scalar cells. There are three types of vector cells: x-momentum cells (Figure 6.10), y-momentum cells (Figure 6.11), and z-momentum cells (Figure 6.12).

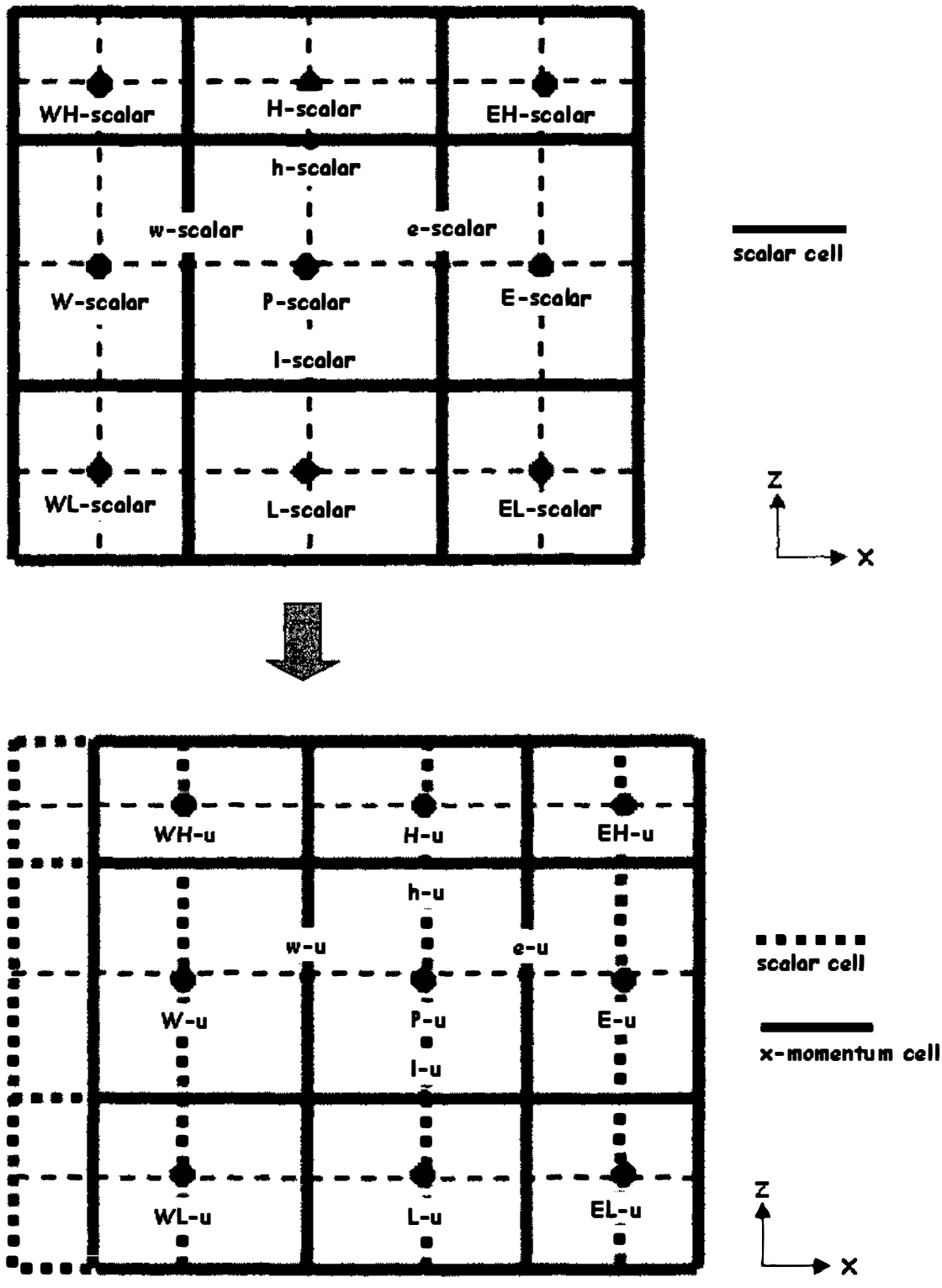

Figure 6.10 Conventions for the positions in the calculation domain referenced by scalar cells and x-momentum cells

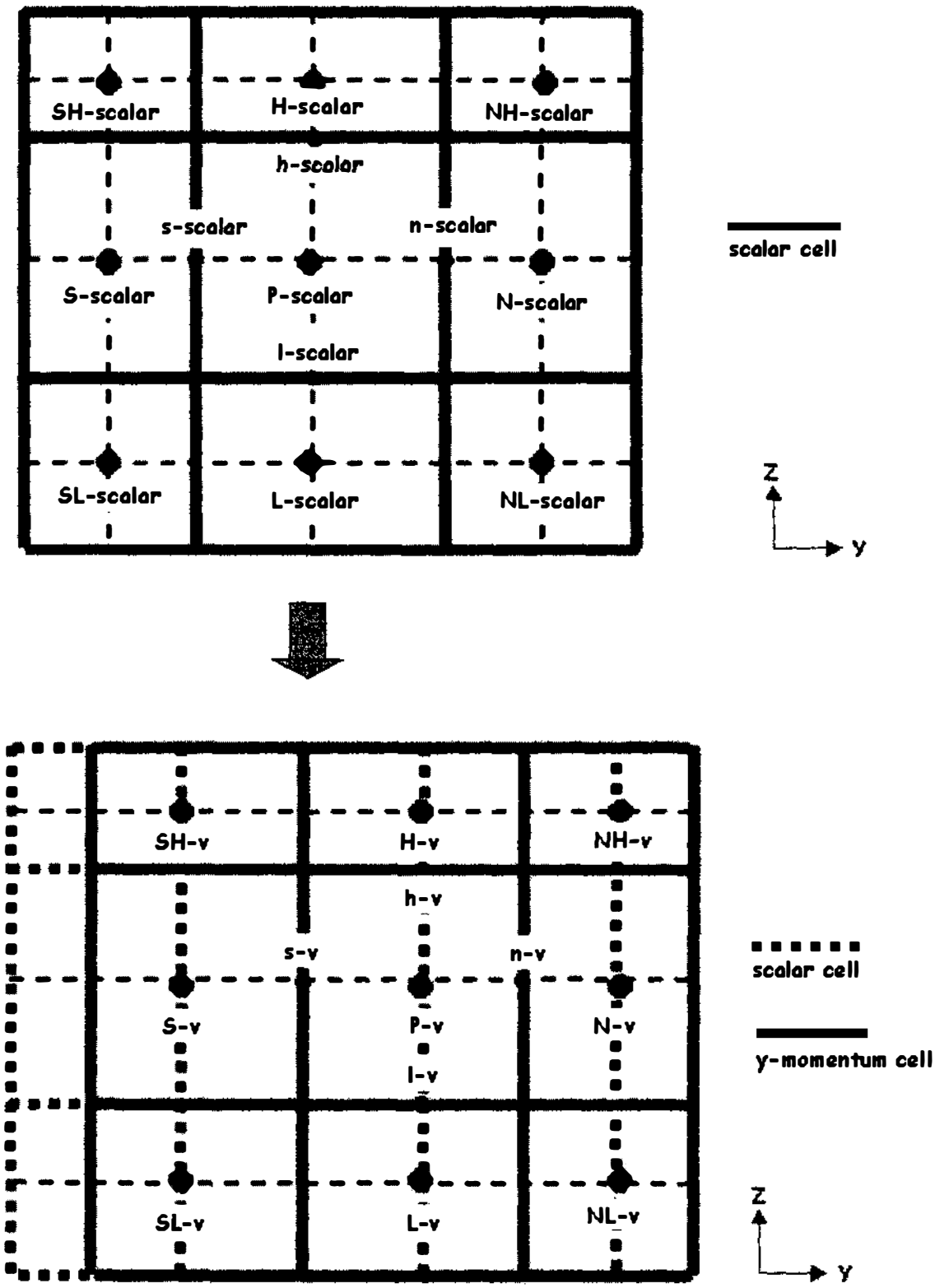

Figure 6.11 Conventions for the positions in the calculation domain referenced by scalar cells and y-momentum cells

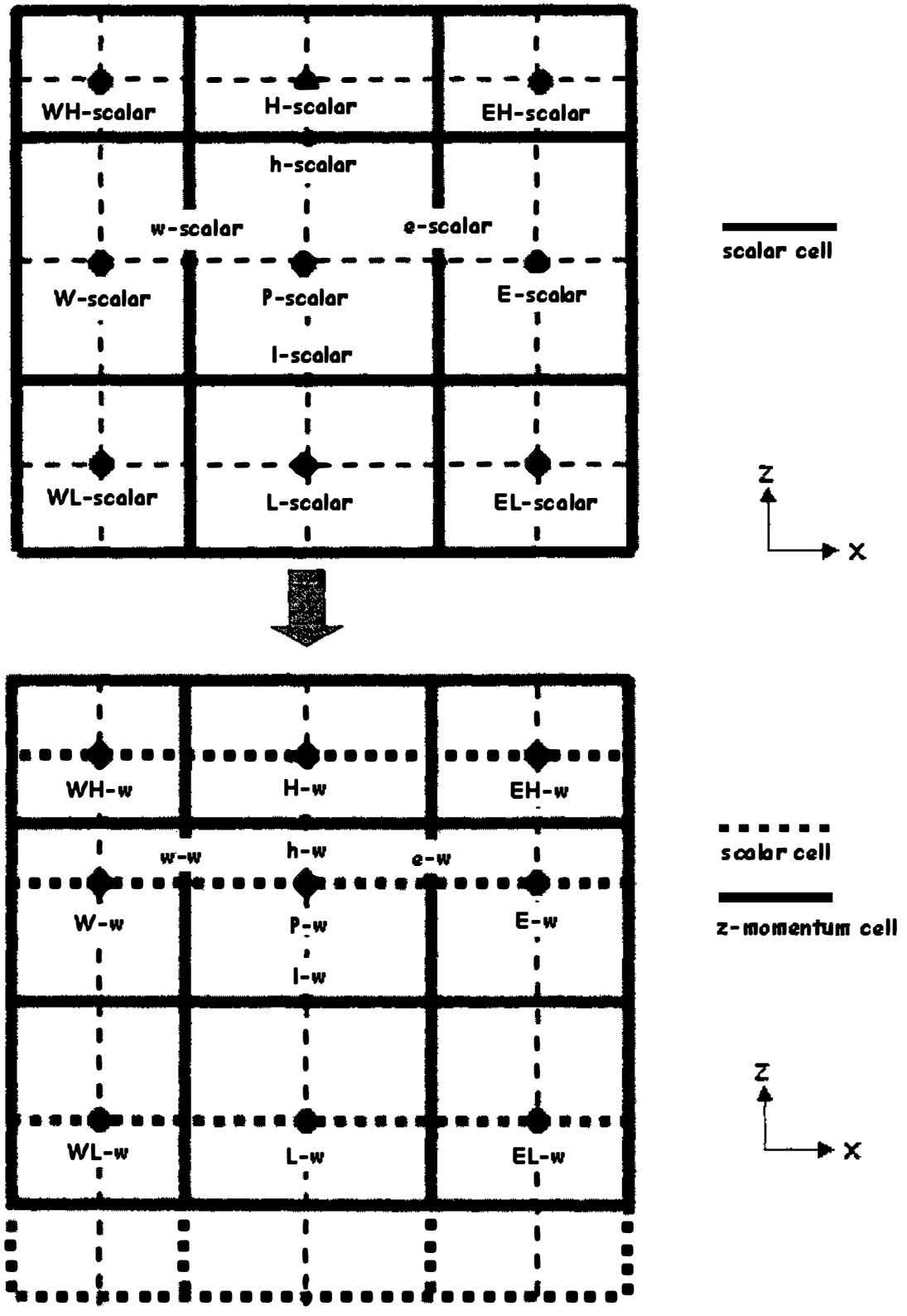

Figure 6.12 Conventions for the positions in the calculation domain referenced by scalar cells and z-momentum cells

6.3.2 Discretisation equations for PDEs in the Airflow Model for Bulk Packaging Systems

Using the SIMPLER method, five types of discretisation equations are derived from the PDEs in the airflow model for bulk packaging systems:

1) For each x-momentum cell, an x-momentum discretisation equation was derived by integrating the momentum equation in the direction of x-axis (Equation 4.3a or 4.4a) over the cell

2) For each y-momentum cell, a y-momentum discretisation equation was derived by integrating the momentum equation in the direction of y-axis (Equation 4.3b or 4.4b) over the cell

3) For each z-momentum cell, a z-momentum discretisation equation was derived by integrating the momentum equation in the direction of z-axis (Equation 4.4c) over the cell

4) For each scalar cell, a pressure correction discretisation equations was derived by enforcing mass conservation (Equation 4.1a or 4.1b or 4.2) over the cell with velocity corrections obtained from the momentum discretisation equations

5) For each scalar cell, a pressure discretisation equation was derived by enforcing mass conservation (Equation 4.1a or 4.1b or 4.2) over the cell with velocity components obtained from the momentum discretisation equations. The pressure discretisation equation has the same coefficients as its corresponding pressure correction equation.

The details on derivation of the above discretisation equations are presented in Section A.1 of Appendix A.

6.3.3 Discretisation equations for PDEs in the Airflow Model for Layered Packaging Systems

Using the SIMPLER method, five types of discretisation equations are derived from the PDEs in the airflow model for layered packaging systems:

1) For each x-momentum cell, an x-momentum discretisation equation was derived by integrating the momentum equation in the direction of x-axis (Equation 4.3a or 4.16a) over the cell

2) For each y-momentum cell, a y-momentum discretisation equation was derived by integrating the momentum equation in the direction of y-axis (Equation 4.3b or 4.16b) over the cell

3) For each z-momentum cell, a z-momentum discretisation equation was derived by integrating the momentum equation in the direction of z-axis (Equation 4.17) over the cell

4) For each scalar cell, a pressure correction discretisation equations was derived by enforcing mass conservation (Equation 4.1a or 4.1b or 4.14 or 4.15) over the cell with velocity corrections obtained from the momentum discretisation equations

5) For each scalar cell, a pressure discretisation equation was derived by enforcing mass conservation (Equation 4.1a or 4.1b or 4.14 or 4.15) over the cell with velocity components obtained from the momentum discretisation equations. The pressure discretisation equation has the same coefficients as its corresponding pressure correction equation.

The details on derivation of the above discretisation equations are presented in Section A.2 of Appendix A.

6.3.4 Discretisation equations for PDEs in the Heat Transfer Model for Bulk Packaging Systems

Using the SIMPLER method, for each scalar cell in a bulk package two discretisation equations are derived from the PDEs in the heat transfer model:

1) A solid energy discretisation equation was derived by integrating the energy conservation equation for package walls in solid region (Equation 5.2) or the volume- averaged energy conservation equation for produce in produce-air region (Equation 5.4) over the cell

2) Air energy discretisation equation was derived by integrating the energy conservation equation for air in vents (Equation 5.1a or 5.1b) or the volume-averaged energy conservation equation for air in produce-air region (Equation 5.3) over the cell

For each scalar cell in produce-air region, as shown in Figure 6.13, a representative produce item was divided into four sub-cells. For each sub-cell, a discretisation equation was derived from the energy equation for produce item (Equation 5.5).

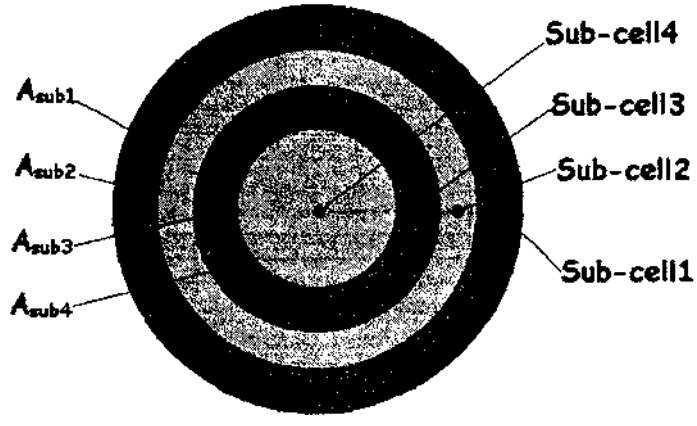

Figure 6.13 Discretisation of single produce item

The details on derivation of the above discretisation equations are presented in Section A.3 of Appendix A.

6.3.5 Discretisation equations for PDEs in the Heat Transfer Model for Layered Packaging Systems

Using the SIMPLER method, for each scalar cell in a layered package two discretisation equations are derived from the PDEs in the heat transfer model:

1) A solid energy discretisation equation was derived by integrating the energy conservation equation for package walls in solid region (Equation 5.2) over the cell

2) Air energy discretisation equation that was derived by the energy conservation equation for air in vents (Equation 5.1a or 5.1b) or the volume-averaged energy conservation equation for air in produce-air region (Equation 5.22)

Similar to bulk packages, for each scalar cell in produce-air region, a representative produce item was divided into four sub-cells. For each sub-cell, a discretisation equation was derived from the energy equation for produce item (Equation 5.5)

The details on derivation of the above discretisation equations are presented in Section A.4 of Appendix A.

For the scalar cells in produce-air regions, no actual solid energy discretisation equation is needed. To maintain the structure of the system of discretisation equations, the discretisation equations for this type of cells are set as follows:

- Coefficient for current grid node set to one
- Other coefficients and source term were set as zero

The above treatment ensures that the solid temperatures in these cells are zeros, and the discretisation equations for their neighbouring cells are not affected. The same treatment is applied to the air energy discretisation equations for the cells on the package walls without vent.

6.4 Solution of Systems of Discretisation Equations

6.4.1 Solution of Systems of Discretisation Equations in Airflow Models

- **Solution procedure**

Since the discretisation equations derived from the airflow model for the bulk packaging system have the same form as those for the layered packaging system, the same solution procedure was employed to solve the airflow models for both packaging systems. The discretisation process for the PDEs in the airflow models generated five systems of algebraic equations:

- System of x-momentum discretisation equations
- System of y-momentum discretisation equations
- System of z-momentum discretisation equations
- System of pressure correction discretisation equations
- System of pressure discretisation equations

The above systems of algebraic equations are coupled. For instance, the coefficients in x-momentum discretisation equations are calculated from the solutions of other discretisation equations. Thus iterative methods were applied to solve these equations. The iterative solution started from a guessed field of solved-for variables to compute the coefficients in the discretisation equations, and then the resulting systems of linear algebraic equations were used to obtain the improved solution for the solved-for variables. Successive repetitions of the algorithm finally lead to a solution that was sufficiently close to the correct solution of the algebraic equations. The solution procedure followed the SIMPLER procedure (Patankar, 1980), as summarised in Figure 6.14.

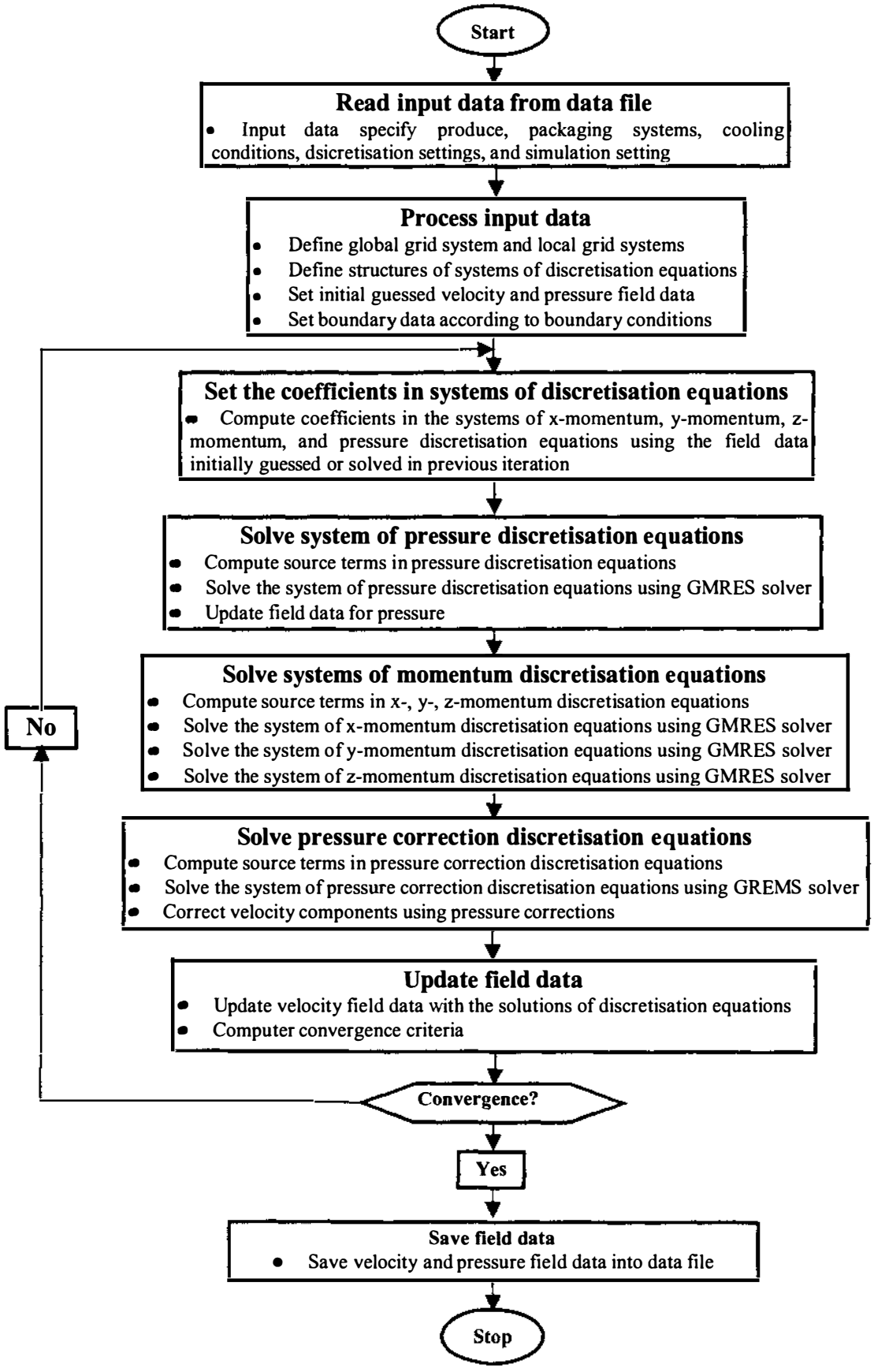

Figure 6.14 Solution procedure of systems of discretisation equations in airflow models

- **Convergence criteria**

The residuals were the most convenient quantities used to monitor the convergence of an iterative procedure. The residuals of the x (y, z) –momentum, pressure correction, and pressure equations over a cell are defined in Section A.5 of Appendix A.

The whole field residual is defined as the norm of residuals in all cells (see section A.5 of Appendix A for the definition). Convergence is achieved if the whole field residuals have reduced more than three or four orders of magnitude below the initial levels. The norm of difference between two successive iterations (see Section A.5 of Appendix A for the definition) was also monitored to represent the change of whole field error.

- **GMRES solver for system of algebraic equations**

As summarised in Figure 6.14, GMRES (Generalised Minimum Residual) iterative method was employed to solve the systems of algebraic equations in every iteration (Kelley, 1995). The 'gmres' function in Matlab was directly adopted as the solver (Mathworks, 2000).

6.4.2 Solution of Systems of Discretisation Equations in Heat Transfer Models

Since the discretisation equations derived from the heat transfer model for the bulk packaging systems have the same form as that for the layered packaging systems, the same solution procedure was employed to solve the heat transfer models for both packaging systems. The discretisation process for PDEs in heat transfer models generated two systems of algebraic equations:

- System of air energy discretisation equations
- System of solid energy discretisation equations

For each scalar cell in produce-air regions, a system of four produce item energy discretisation equations was also generated. Since all systems of produce item energy discretisation equations have the same coefficient matrix that is only related to predefined produce properties, the systems of produce item energy equations can be

solved by multiplying the pre-computed inverse of coefficient matrix and the vector of source terms. Therefore only the vectors of source terms need to be updated during iteration.

Since the systems of air energy, solid energy, and produce item energy discretisation equations are coupled, the iterative solution procedure was applied to achieve convergent solutions at each time step. Similar to the solution of airflow models, GMRES solver was used to solve the systems of algebraic equations in each iteration, and the whole-filed residuals and the normalised difference between two successive iterations were employed as the convergence criteria. The model solution procedure is summarise in Figure 6.15.

6.5 Summary

This chapter presented the solution methods for solving the airflow and heat transfer models in both bulk and layered packaging systems. In space discretisation, the packaging systems were divided into a collection of cells that are referenced by global and local grid systems.

The discretisation method for the airflow models was based on the SIMPLER schemes (Patankar, 1980). Over each x (y, z) -momentum momentum cell, an x (y, z) -momentum discretisation equation was derived from the momentum equations in the airflow models. Over each scalar cell, a pressure correction discretisation equation and a pressure discretisation equation were derived from continuity equations. The solid and air energy discretisation equations for the heat transfer models were derived over scalar cells in the same way as those in airflow models. For each scalar cell in produce-air region, four additional produce item energy discretisation equations were derived for the sections within the produce item.

Iterative methods were applied to solve the systems of discretisation equations for airflow and heat transfer models. The whole-field residuals and the normalised difference between two successive iterations were employed as the convergence criteria.

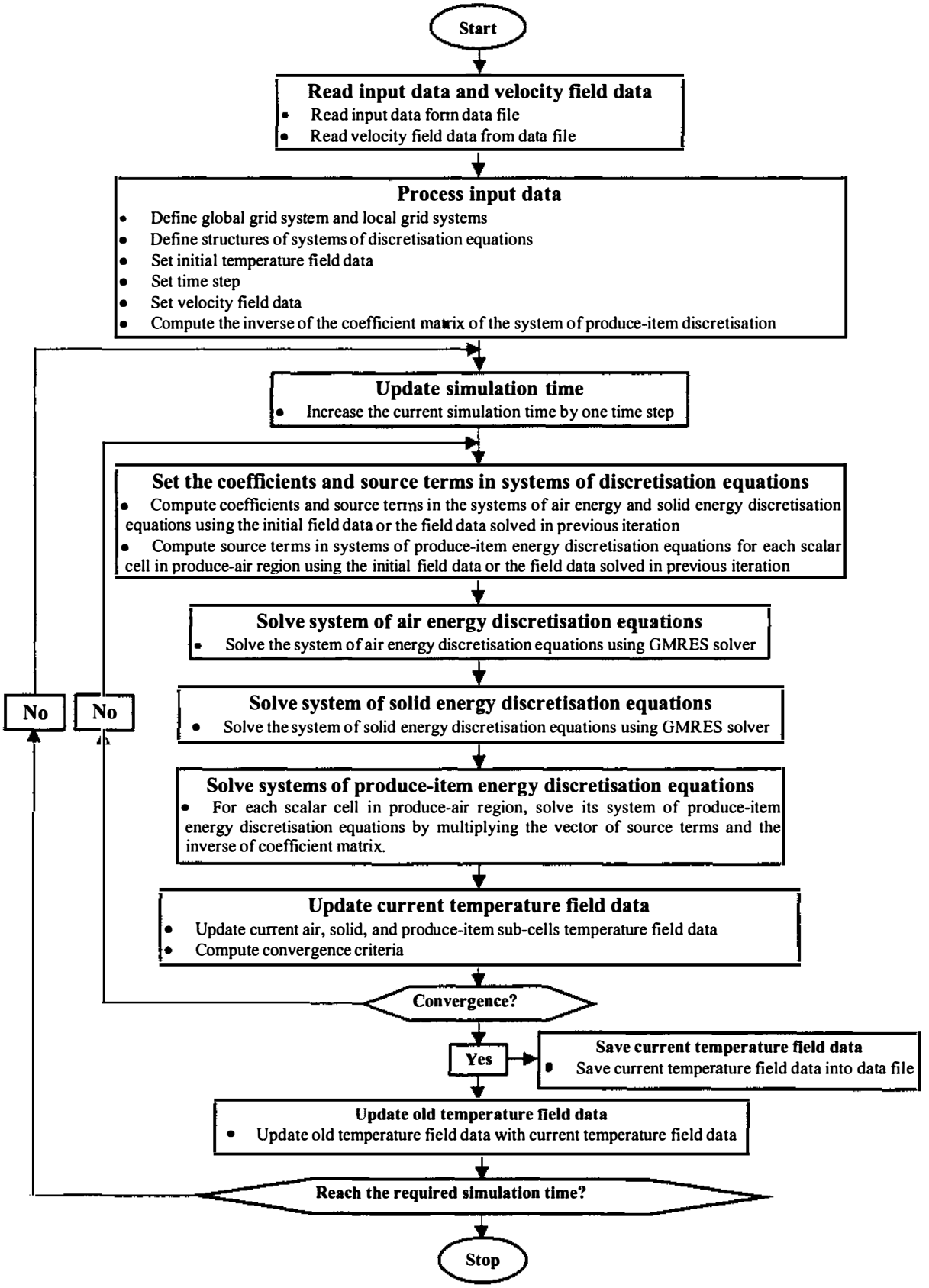

Figure 6.15 Solution procedure of systems of discretisation equations in heat transfer models

CHAPTER 7
MODEL IMPLEMENTATION and SOFTWARE 'CoolSimu' DEVELOPMENT

7.1 Introduction

A user-friendly software package called 'CoolSimu' was developed to implement the solution procedures of the airflow and heat transfer models. CoolSimu was designed to allow users without any knowledge of CFD and heat transfer principles to easily simulate airflow and heat transfer processes in layered and bulk packaging systems. This chapter firstly outlines the structure of CoolSimu, and then briefly introduces the functions of the components in software.

7.2 CoolSimu Overview

CoolSimu was constructed with the following components, as shown in Figure 7.1:

- System Designer for users to specify the product properties, packaging system, and airflow conditions
- Airflow Solver for solving the airflow models for the bulk and layered packaging systems
- Heat Solver for solving the heat transfer models for the bulk and layered packaging systems
- Solution Monitor for users to monitor and control the solution processes of the airflow and heat transfer model
- Visualization Tool for user to visualize the predicted airflow patterns and temperature profiles
- Database (files) for storing input data and simulation results

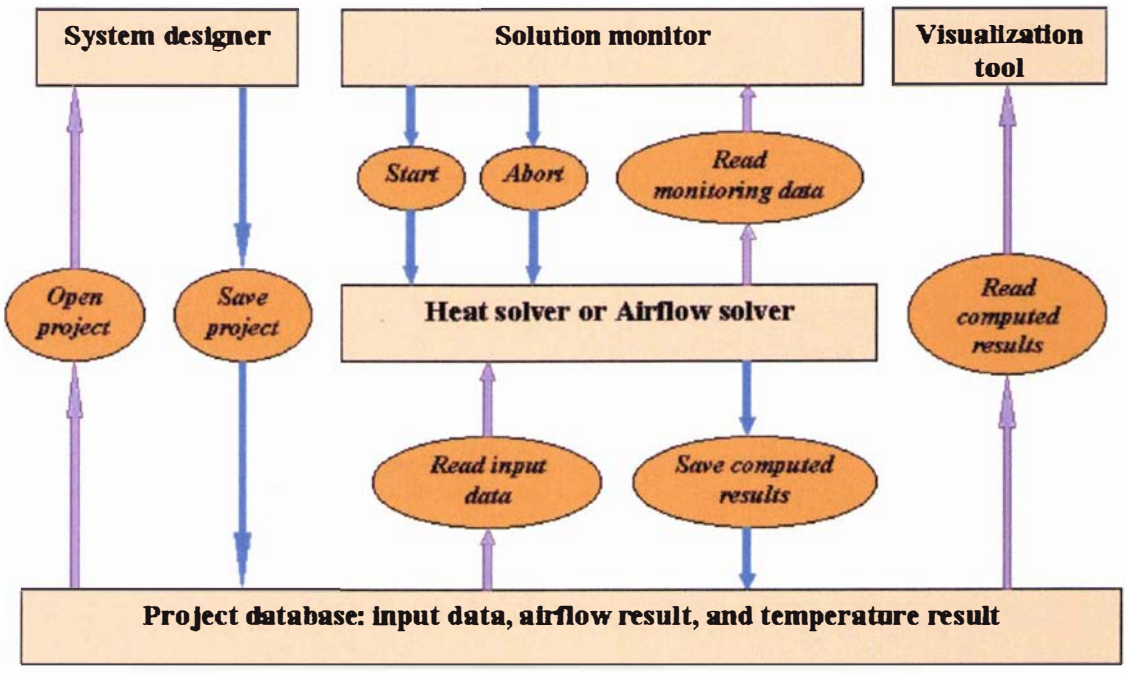

Figure 7.1 Components of simulation software package - CoolSimu.

Airflow and heat solvers are core components of CoolSimu. To improve computing efficiency, the solvers are written in C language. The Java native interface was employed to integrate the solvers with the other components, which are written in Java. Users interact with the software via three components: System Designer, Solution Monitor, and Visualization Tool. These components are integrated in the simulation environment as shown in Figure 7.2.

7.3 System Designer

The 'System Designer' component of the software is used to define and store the product properties, packaging system, and airflow conditions.

- **Defining product properties**

Product geometric and physical properties can be defined by entering proper values in the text fields in the data input panel as shown in Figure 7.2.

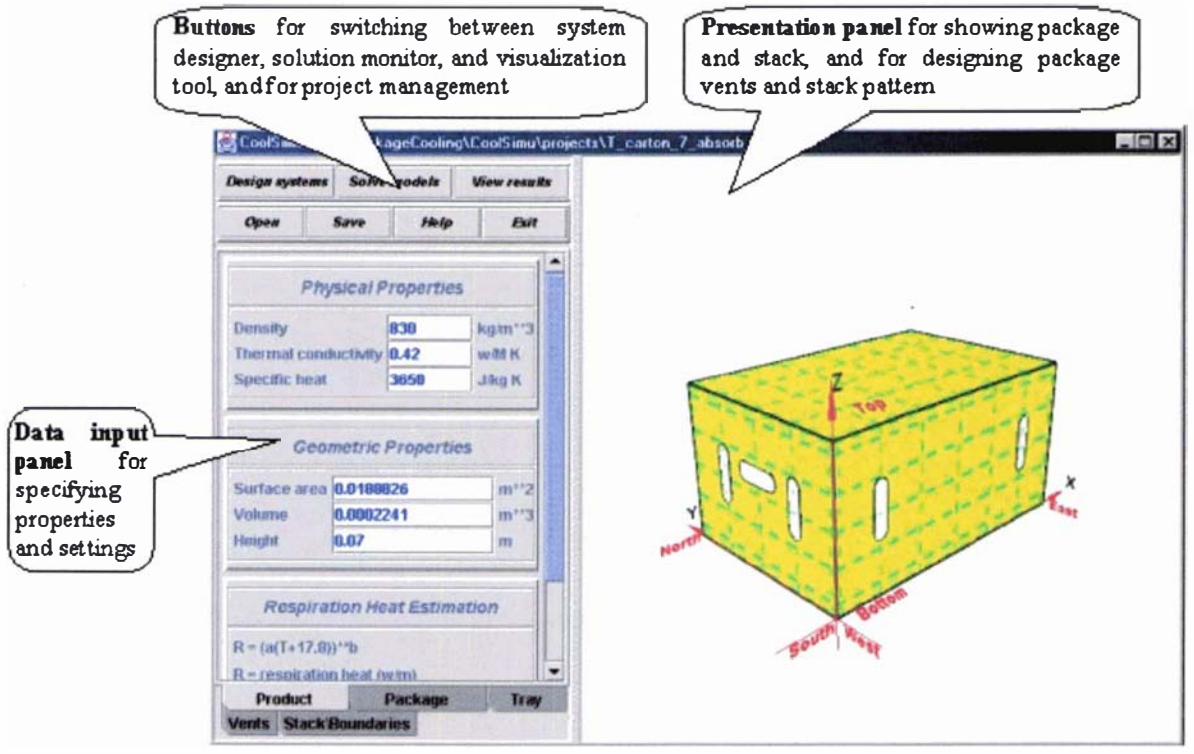

Figure 7.2 Interface structure of simulation software package CoolSimu.

- **Defining packaging systems**

The geometric and physical properties of individual package can be specified in the corresponding data input panel. With adequate geometric data, the package shape and orientation will be rendered in the presentation panel with a Java 3D component as shown in Figure 7.3.

- **Defining vents on package surfaces**

Users can define a vent by specifying its dimension, location, and shape. The defined vent can be added onto a package surface by clicking the 'Add' button. The vents on a package surface may be dragged, cut, copied, and pasted. Users can copy the vents on one package surface to another surface as shown in Figure 7.4.

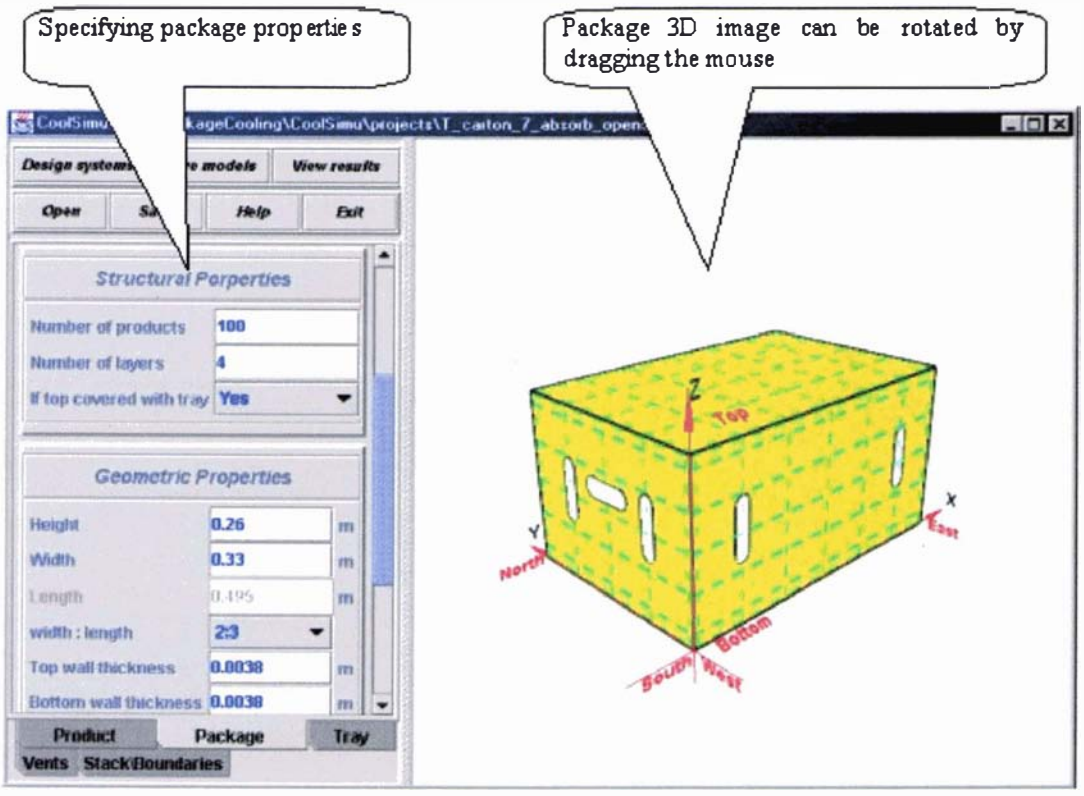

Figure 7.3 Definition of individual package in simulation software package CoolSimu.

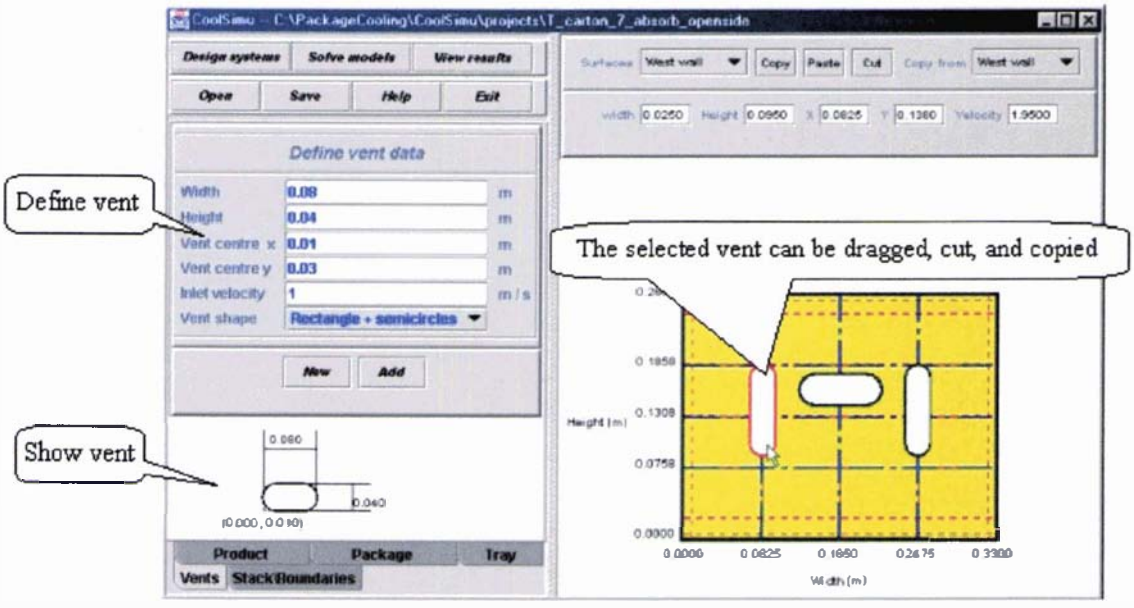

Figure 7.4 Definition of vents on package surface in simulation software package CoolSimu.

- **Arranging packages in a stack**

As shown in Figure 7.5, users can add package to a stack in two possible orientations, and place the package at any location by dragging the package with mouse. A package may be removed from the stack.

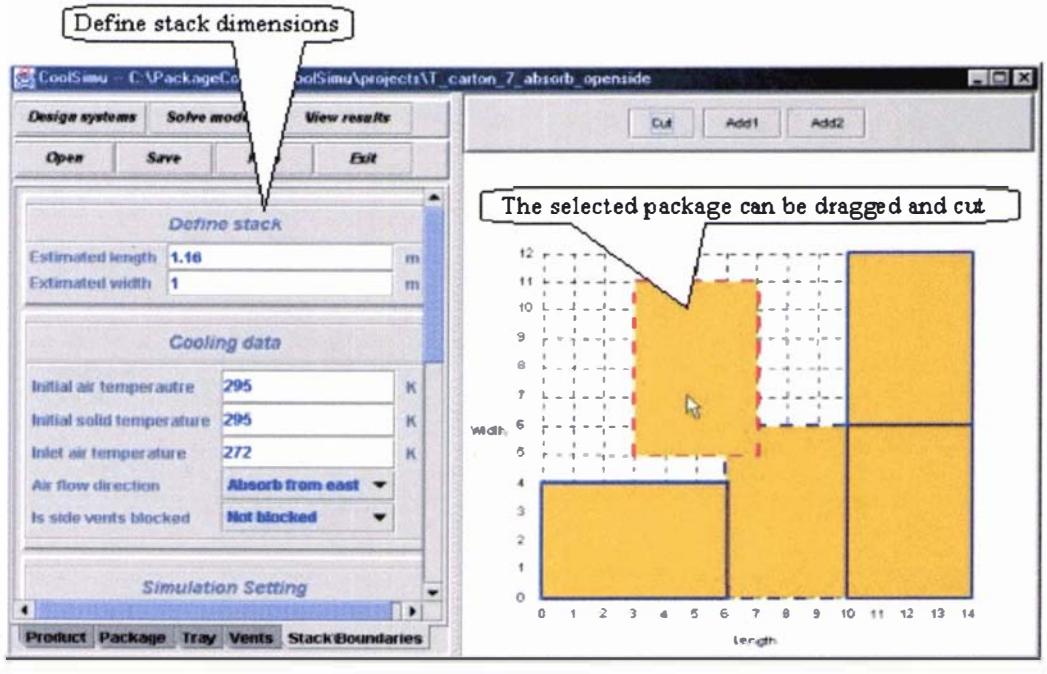

Figure 7.5 Definition of a package in a stack in simulation software package CoolSimu.

- **Defining cooling data and simulation setting**

Users can specify cooling conditions in the corresponding data input panel. The stack pattern and airflow directions are presented on the right panel, thereby enabling users to specify the location index of monitoring cell as shown in Figure 7.6.

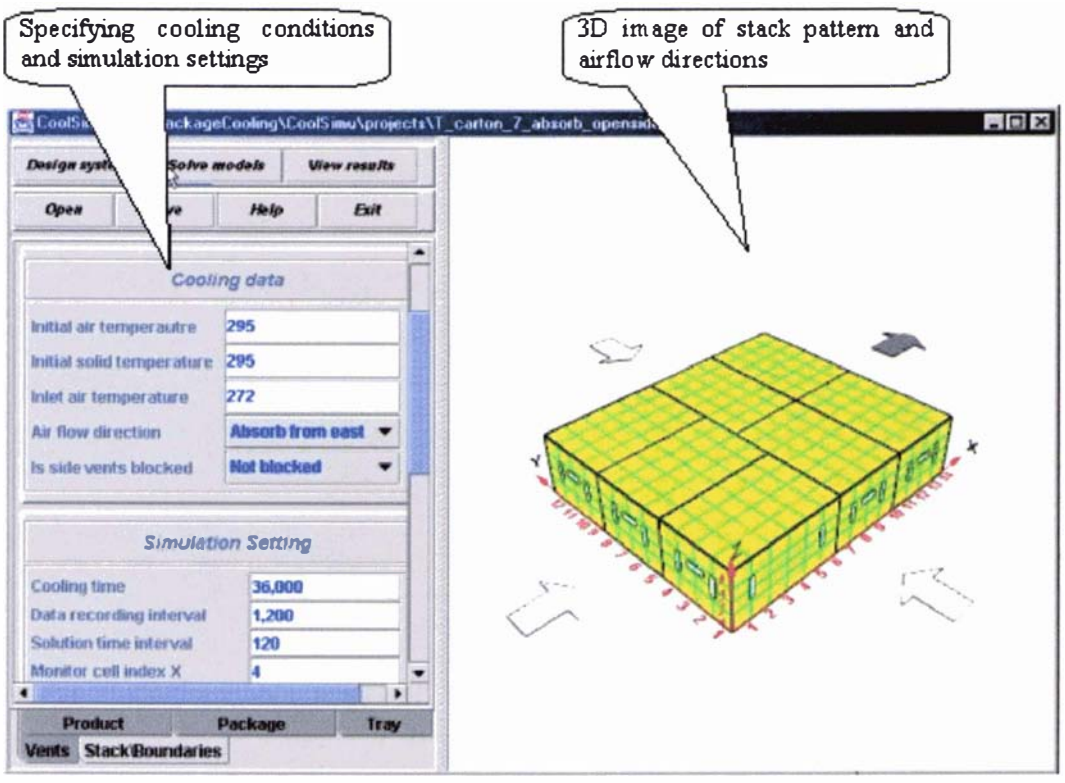

Figure 7.6 Definition of cooling conditions and simulation settings in simulation software package CoolSimu.

7.4 Airflow and Heat Transfer Solvers

The airflow and heat transfer solvers are core components of CoolSimu. The airflow solver implements the solution procedure described in Section 6.4.1 for solving the systems of discretisation equations derived from the airflow models for the bulk and layered packaging systems. The heat transfer solver implements the solution procedure described in Section 6.4.2 for solving the systems of discretisation equations derived from the heat transfer models of bulk and layered packaging systems. Both airflow and heat transfer solvers were first written as collections of MATLAB functions, and then translated into dynamically-linked C libraries after debugging and testing. The solvers were hidden behind the user interaction components, and thus the software user does not need to know the mathematical and thermodynamic principles underpinning the software.

7.5 Solution Monitor

The "Solution Monitor' component of the software is used to specify the solution settings, start the airflow or heat solvers, monitor the solution progress, and to abort the solution process (Figure 7.7).

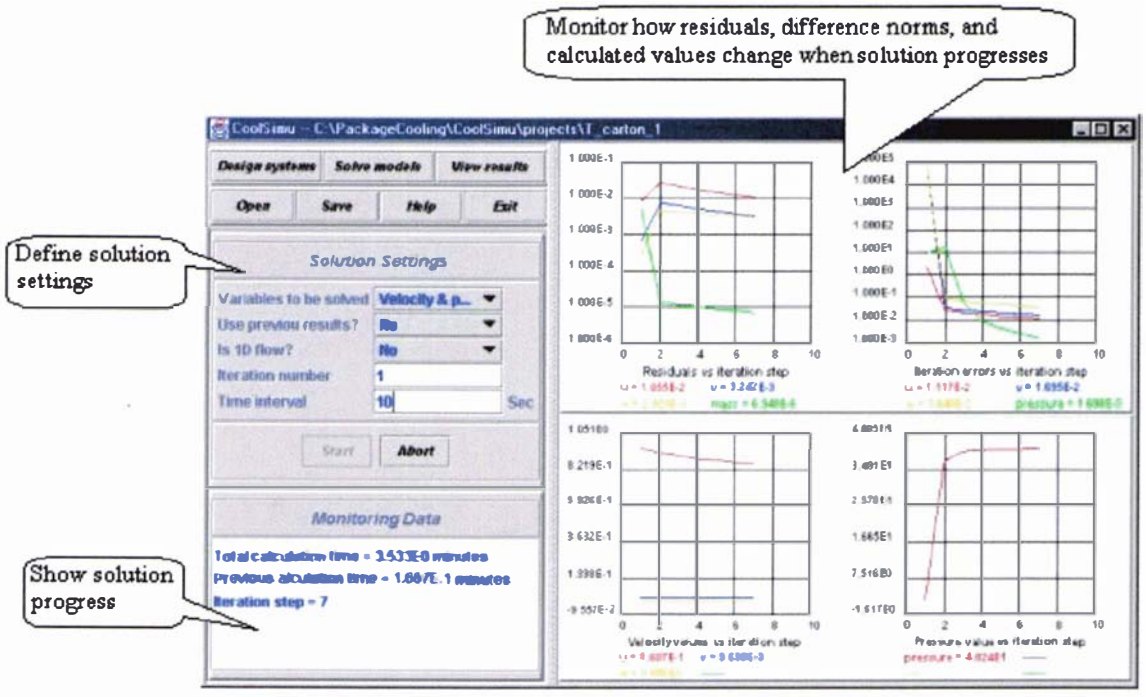

Figure 7.7 Control and monitoring of solution processes in simulation software package CoolSimu.

7.6 Visualization Tool

The Visualization Tool is used to visualize predicted velocity, pressure, and temperature results as shown in Figure 7.8. When a user first enters the visualization interface, a velocity result file and one of temperature result files are loaded.

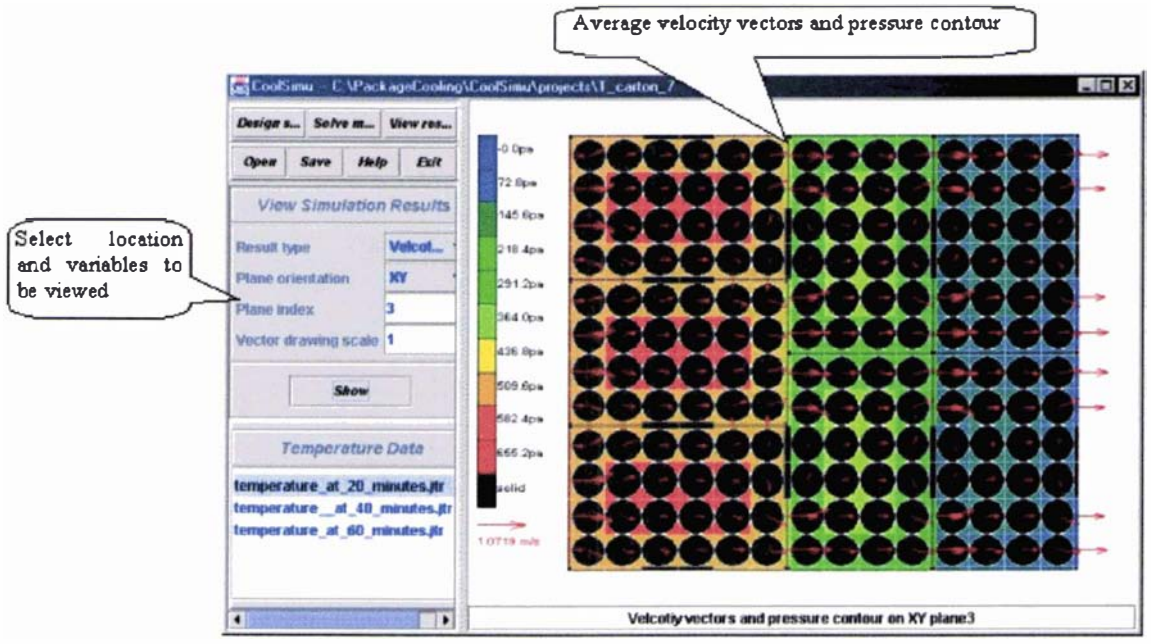

Figure 7.8 Visualization of predicted velocity and pressure field in simulation software package CoolSimu

7.7 Summary

This chapter introduced the simulation software package CoolSimu, which integrates the overall modeling system that has been developed. The airflow and heat transfer solvers are the core components for solving the airflow and heat transfer models. The user interaction components in software allow potential users to define package systems and cooling conditions, to control solution processes, and to visualize the simulation results. This user friendliness enables the software to have wider applicability in the fields of research, development, and training.

CHAPTER 8
SIMULATION RESULTS AND MODEL VALIDATION

8.1 Introduction

This chapter presents the predicted airflow patterns and temperature profiles during forced-air cooling of produce in several layered and bulk packaging systems. The predicted temperature profiles were compared with experimental data for model validation.

8.2 Simulation Results for Layered Packaging Systems

8.2.1 Sensitivity Analysis

Prior to the simulation studies conducted in the real world packages, analysis was carried out to assess the sensitivity of the model predictions to variations or inaccuracy in the model input data. A single layered package (Figure 8.1) was used as case study for the analysis. Figures 8.2 shows the dimensions and positions of vents on package surfaces. Table 8.1 summarises the data for defining the packaging system and cooling conditions.

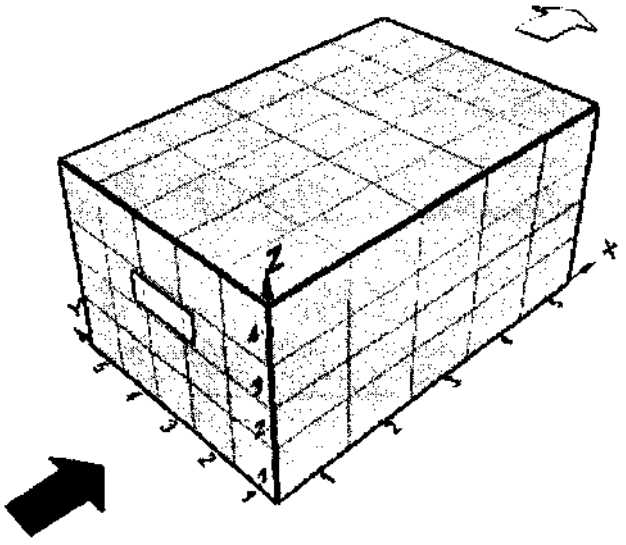

Figure 8.1 Forced-air cooling of apples in the layered package used for sensitivity analysis.

Table 8.1 Data of packaging system and cooling conditions for forced-air cooling of apple in the layered package used for sensitivity analysis.

Variable	**Value**
Produce item	
Density (kg m^{-3})	830
Thermal conductivity (W m^{-1} K^{-1})	0.42
Specific heat capacity (J kg^{-1} K^{-1})	3650
Volume (m^3)	0.0002241
Surface are (m^2)	0.0188826
Height when placed on tray (m)	0.007
Individual package	
Length (m)	0.5
Width (m)	0.33
Height (m)	0.26
Number of produce item	100
Number of produce layers	4
Is top layer covered with tray?	Yes
Package walls	
Density (kg m^{-3})	220
Thermal conductivity (W m^{-1} K^{-1})	0.048
Specific heat capacity (J kg^{-1} K^{-1})	1700
Thickness of side walls (m)	0.0076
Thickness of top wall (m)	0.0038
Thickness of bottom wall (m)	0.0038
Tray	
Density (kg m^{-3})	260
Thermal conductivity (W m^{-1} K^{-1})	0.048
Specific heat capacity (J kg^{-1} K^{-1})	1700
Thickness (m)	0.002
Height (m)	0.017
Gaps between tray edges and front and back walls (m)	0.004
Gaps between tray edges and sidewalls (m)	0.003
Contact area with produce item above (m^2)	0.003
Contact area with produce item under (m^2)	0.001
Cooling conditions	
Inlet air velocity (m s^{-1})	1.0
Inlet air temperature (K)	273
Initial air temperature (K)	293
Initial produce temperature (K)	293
External air velocity (m s^{-1})	1.0

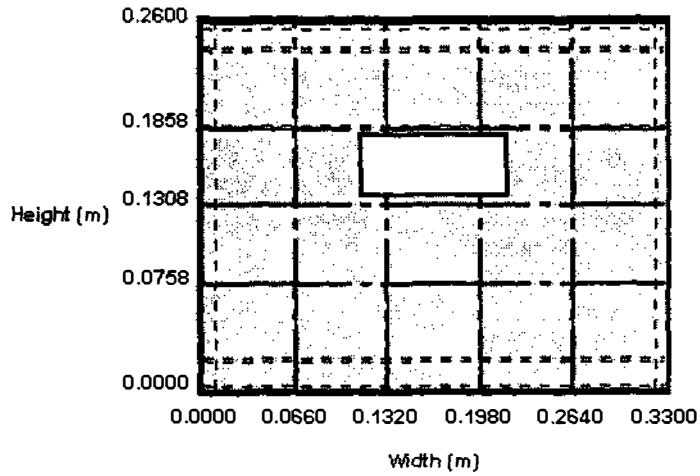

Figure 8.2 Dimensions and positions of vents on the front and back surfaces of the layered package used for sensitivity analysis.

Inlet air velocity, air velocity along the outside package walls, vent areas, vent position, and the width of the gaps between trays and package walls are altered separately to examine the effect of data variability on the reliability of the predicted temperature in product centres.

- **Sensitivity to variation in the inlet air velocity**

The sensitivity analysis was performed by using ± 10% changes in the inlet air velocity of 1.0 m/s. As shown in Table 8.2, the inaccuracy in the measurement of inlet air velocity has a small, but noticeable effect on the prediction accuracy. This model input variable is actually the average air velocity over the inlet vent, and is usually approximated by the average of several velocity measurements in the vent centre. Therefore it is likely that inaccurate input value of the inlet air velocity within 10% will contributes to inaccuracy of about 0.5 °K in the model predictions. This level of error is within the measurement error of most temperature measuring devices used in the postharvest industry. However, varying the input air velocity from 0.9 to 1.1 m/s resulted in a difference of 1.06 °K in predicted product centre temperature.

Table 8.2 Predicted product centre temperature after four hours of cooling for different inlet air velocities

Positions	Predicted product centre temperature (K) for the specified inlet air velocities			Temperature differences (K)		
	1 m/s	0.9 m/s	1.1 m/s	0.9 -1 m/s	1.1 -1 m/s	0.9-1.1 m/s
Cell (1, 3, 1)	276.65	277.17	276.22	0.52	-0.43	0.95
Cell (3, 3, 1)	284.66	285.39	283.97	0.73	-0.69	1.42
Cell (3, 1, 1)	281.22	281.88	280.61	0.66	-0.61	1.27
Cell (5, 3, 1)	287.19	287.66	286.73	0.47	-0.46	0.93
Cell (1, 3, 2)	274.36	274.61	274.16	0.25	-0.20	0.45
Cell (3, 3, 2)	281.47	282.28	280.76	0.81	-0.71	1.52
Cell (3, 1, 2)	279.34	280.06	278.71	0.72	-0.63	1.35
Cell (5, 3, 2)	286.50	287.17	285.84	0.67	-0.66	1.33
Cell (1, 3, 3)	273.04	273.04	273.03	0.00	-0.01	0.01
Cell (3, 3, 3)	276.45	277.00	276.02	0.55	-0.43	0.98
Cell (3, 1, 3)	276.94	277.63	276.36	0.69	-0.58	1.27
Cell (5, 3, 3)	281.90	282.68	281.18	0.78	-0.72	1.50
Cell (1, 3, 4)	274.08	274.25	273.94	0.17	-0.14	0.31
Cell (3, 3, 4)	279.08	279.77	278.50	0.69	-0.58	1.27
Cell (3, 1, 4)	278.09	278.72	277.55	0.63	-0.54	1.17
Cell (5, 3, 4)	282.92	283.64	282.26	0.72	-0.66	1.38
Average	279.62	280.18	279.12	0.57	-0.50	1.06

- **Sensitivity to variation in the air velocity along the outside package walls**

The sensitivity analysis was performed by using ± 20% changes in the outside air velocity of 1.0 m/s. As shown in Table 8.3, the predicted product temperatures are insensitive to the variation in the air velocity along the outside package walls. The insensitivity may be caused by the model assumption of no heat transfer between the package walls and produce items (Table 5.2), so the heat transfer between outside airflow and package walls does not have direct effect on product temperature.

- **Sensitivity to variation in the vent areas**

The sensitivity analysis was performed by using ± 20% changes in the areas of vents on both back and front walls. As shown in Table 8.4, the variation in the vent areas did not have significant effect on the model predictions in the near-inlet regions, but had noticeable influence in the package centre and near-outlet regions. Although the analysis on the vent areas has implication for the design of package systems, it is unlikely that the

Table 8.3 Predicted product centre temperature after four hours of cooling for different air velocities along the outside package walls

Positions	**Predicted product centre temperature (K) for the specified outside air velocities**			**Temperature differences (K)**	
	1 m/s	**0.8 m/s**	**1.2 m/s**	**0.8 -1 m/s**	**1.2 -1 m/s**
Cell (1, 3, 1)	276.65	276.65	276.65	0.00	0.00
Cell (3, 3, 1)	284.66	284.70	284.62	0.04	-0.04
Cell (3, 1, 1)	281.22	281.33	281.13	0.11	-0.09
Cell (5, 3, 1)	287.19	287.28	287.12	0.09	-0.07
Cell (1, 3, 2)	274.36	274.36	274.36	0.00	0.00
Cell (3, 3, 2)	281.47	281.50	281.44	0.03	-0.03
Cell (3, 1, 2)	279.34	279.41	279.28	0.07	-0.06
Cell (5, 3, 2)	286.50	286.55	286.45	0.05	-0.05
Cell (1, 3, 3)	273.04	273.04	273.03	0.00	-0.01
Cell (3, 3, 3)	276.45	276.49	276.41	0.04	-0.04
Cell (3, 1, 3)	276.94	276.95	276.92	0.01	-0.02
Cell (5, 3, 3)	281.90	281.98	281.83	0.08	-0.07
Cell (1, 3, 4)	274.08	274.08	274.08	0.00	0.00
Cell (3, 3, 4)	279.08	279.11	279.05	0.03	-0.03
Cell (3, 1, 4)	278.09	278.15	278.04	0.06	-0.05
Cell (5, 3, 4)	282.92	282.99	282.87	0.07	-0.05
Average	279.62	279.66	279.58	0.04	-0.04

Table 8.4 Predicted product centre temperature after four hours of cooling for different vent areas

Positions	**Predicted product centre temperature (K) for the specified vent areas**			**Temperature differences (K)**	
	400 mm^2	**320 mm^2**	**480 mm^2**	**320-400 mm^2**	**480-400 mm^2**
Cell (1, 3, 1)	276.65	277.35	276.00	0.70	-0.65
Cell (3, 3, 1)	284.66	286.06	283.34	1.40	-1.32
Cell (3, 1, 1)	281.22	282.71	280.26	1.49	-0.96
Cell (5, 3, 1)	287.19	288.07	286.28	0.88	-0.91
Cell (1, 3, 2)	274.36	274.69	274.07	0.33	-0.29
Cell (3, 3, 2)	281.47	282.33	280.20	0.86	-1.27
Cell (3, 1, 2)	279.34	280.92	278.36	1.58	-0.98
Cell (5, 3, 2)	286.50	287.60	285.23	1.10	-1.27
Cell (1, 3, 3)	273.04	273.05	273.03	0.01	-0.01
Cell (3, 3, 3)	276.45	277.00	275.89	0.55	-0.56
Cell (3, 1, 3)	276.94	278.45	276.18	1.51	-0.76
Cell (5, 3, 3)	281.90	283.19	280.56	1.29	-1.34
Cell (1, 3, 4)	274.08	274.30	273.87	0.22	-0.21
Cell (3, 3, 4)	279.08	280.24	278.08	1.16	-1.00
Cell (3, 1, 4)	278.09	279.57	277.29	1.48	-0.80
Cell (5, 3, 4)	282.92	284.24	281.66	1.32	-1.26
Average	279.62	280.61	278.77	0.99	-0.85

errors in model predictions are related to the input data for vent areas, as the areas can be easily measured to the required accuracy.

- **Sensitivity to variation in the vent positions**

The sensitivity analysis was performed by lowering the positions of the vents on both back and front walls by 30mm. As shown in Table 8.5, the variation in the vent positions affected the model predictions, as it alters the distribution of airflow among the produce layers, and consequently affects the heat transfer between air and produce items. The vent position relative to the produce layers may change as the produce items and trays may fit closer after handling operations. Therefore it is likely that inaccurate input values are used for the vent positions, and contribute to the inaccuracy in the model predictions.

Table 8.5 Predicted product centre temperature after four hours of cooling for different vent positions

Positions	**Predicted product centre temperature (K) for the specified vent positions**		**Temperature differences (K)**
	Base case	**30mm lower**	**30 mm lower – base case**
Cell (1, 3, 1)	276.65	275.66	-0.99
Cell (3, 3, 1)	284.66	281.67	-2.99
Cell (3, 1, 1)	281.22	279.89	-1.33
Cell (5, 3, 1)	287.19	285.26	-1.93
Cell (1, 3, 2)	274.36	273.10	-1.26
Cell (3, 3, 2)	281.47	277.40	-4.07
Cell (3, 1, 2)	279.34	278.11	-1.23
Cell (5, 3, 2)	286.50	282.90	-3.60
Cell (1, 3, 3)	273.04	273.12	0.08
Cell (3, 3, 3)	276.45	277.64	1.19
Cell (3, 1, 3)	276.94	278.19	1.25
Cell (5, 3, 3)	281.90	283.14	1.24
Cell (1, 3, 4)	274.08	275.57	1.49
Cell (3, 3, 4)	279.08	281.81	2.73
Cell (3, 1, 4)	278.09	280.17	2.08
Cell (5, 3, 4)	282.92	285.11	2.19
Average	279.62	279.30	-0.32

- **Sensitivity to variation in the width of the gaps between trays and package walls**

The sensitivity analysis was performed by changing the width of the gaps between trays and package walls by ± 2mm. As shown in Table 8.6, the model predictions are very sensitive to variations in the width of the gaps between trays and package walls, particularly for the predictions in the product layer that is far away from the airflow inlet. The trays may move slightly within the package during handling operations, which consequently alters the widths of the gaps between trays and package walls. Therefore it is likely that inaccurate input values for the gap widths will contribute to inaccuracy in the model predictions.

Table 8.6 Predicted product centre temperature after four hours of cooling for different widths of the gaps between trays and package walls

Positions	**Predicted product centre temperature (K) for the specified gap widths**			**Temperature differences (K)**	
	3 mm	**1mm**	**5 mm**	**1mm - 3mm**	**5 mm - 3mm**
Cell (1, 3, 1)	276.65	283.94	275.34	7.29	-1.31
Cell (3, 3, 1)	284.66	288.62	283.47	3.96	-1.19
Cell (3, 1, 1)	281.22	284.60	280.96	3.38	-0.26
Cell (5, 3, 1)	287.19	290.14	285.81	2.95	-1.38
Cell (1, 3, 2)	274.36	277.34	273.87	2.98	-0.49
Cell (3, 3, 2)	281.47	283.33	281.41	1.86	-0.06
Cell (3, 1, 2)	279.34	280.01	280.14	0.67	0.80
Cell (5, 3, 2)	286.50	287.38	285.89	0.88	-0.61
Cell (1, 3, 3)	273.04	273.14	273.02	0.10	-0.02
Cell (3, 3, 3)	276.45	276.55	276.58	0.10	0.13
Cell (3, 1, 3)	276.94	275.34	278.80	-1.60	1.86
Cell (5, 3, 3)	281.90	280.24	282.18	-1.66	0.28
Cell (1, 3, 4)	274.08	275.87	273.73	1.79	-0.35
Cell (3, 3, 4)	279.08	280.51	279.01	1.43	-0.07
Cell (3, 1, 4)	278.09	278.03	279.71	-0.06	1.62
Cell (5, 3, 4)	282.92	284.05	282.06	1.13	-0.86
Average	279.62	281.19	279.50	1.58	-1.69

8.2.2 Forced-Air Cooling in a Single Z-Pack Apple Carton

•• Packaging system and cooling conditions

Zou (1998) conducted an experiment on forced-air cooling of apples in a single Z-Pack (count-100) carton (Figure 8.3) used by ENZAFruit (International) in New Zealand. Figures 8.4 and 8.5 show the dimensions and positions of vents on package surfaces. Data used for defining the packaging system and cooling conditions are summarised in Table 8.7.

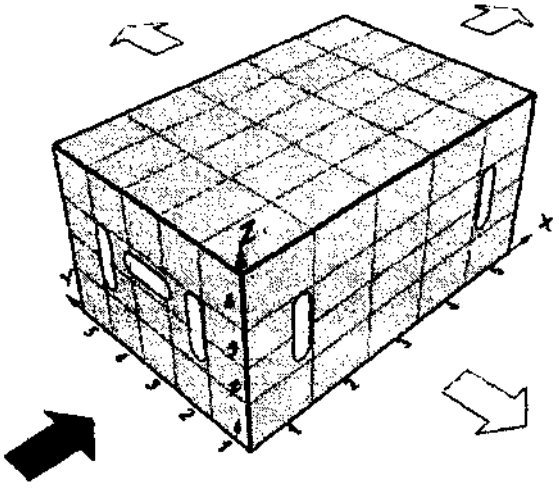

Figure 8.3 Forced-air cooling of apples in a single Z-Pack, count-100 carton.

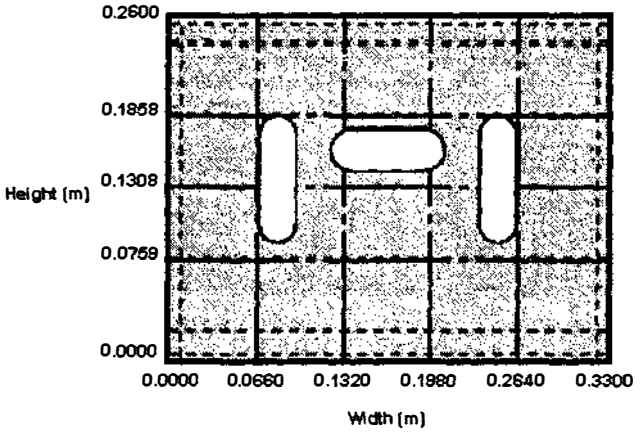

Figure 8.4 Dimensions and positions of vents on the front and back surfaces of Z-Pack, count-100 carton.

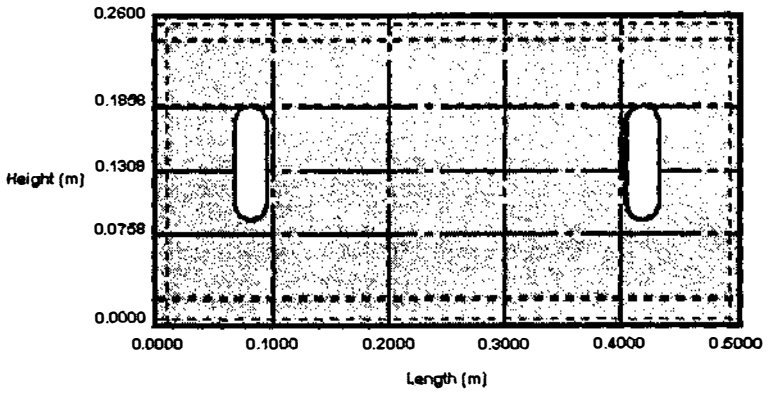

Figure 8.5 Dimensions and positions of vents on the side surfaces of Z-Pack, count-100 carton.

- **Predicted airflow patterns**

The predicted airflow patterns and pressure distributions in various planes of the Z-Pack apple carton are presented in Figures 8.6-8.12. The positions of these planes were referenced by the indexes shown in Figure 8.3. The airflow patterns were expressed with a collection of vector arrows, which were drawn in the centres of scalar local cells. The magnitude of a vector arrow in one direction (x, y, or z) represents the average volume flow rate in the axis direction per unit area of the cell surface perpendicular to the axis direction. Each figure has its unique scale for the vectors, which are displayed under the colour bars.

The pressure distributions are represented with collections of colours, and the meanings of these colours are explained with the vertical colour bars in the figures. The white circular areas in cells only illustrate the existence of produce items, which do not correspond to the real shape or size of produce items.

Table 8.7 Data of packaging system and cooling conditions for forced-air cooling of apples in a single Z-Pack carton (Zou, 1998).

Variable	**Value**
Produce item	
Density (kg m^{-3})	830
Thermal conductivity (W m^{-1} K^{-1})	0.42
Specific heat capacity (J kg^{-1} K^{-1})	3650
Volume (m^3)	0.0002241
Surface are (m^2)	0.0188826
Height when placed on tray (m)	0.007
Individual package	
Length (m)	0.5
Width (m)	0.33
Height (m)	0.26
Number of produce item	100
Number of produce layers	4
Is top layer covered with tray?	Yes
Package walls	
Density (kg m^{-3})	220
Thermal conductivity (W m^{-1} K^{-1})	0.048
Specific heat capacity (J kg^{-1} K^{-1})	1700
Thickness of side walls (m)	0.0076
Thickness of top wall (m)	0.0038
Thickness of bottom wall (m)	0.0038
Tray	
Density (kg m^{-3})	260
Thermal conductivity (W m^{-1} K^{-1})	0.048
Specific heat capacity (J kg^{-1} K^{-1})	1700
Thickness (m)	0.002
Height (m)	0.017
Gaps between tray edges and front and back walls (m)	0.004
Gaps between tray edges and side walls (m)	0.003
Contact area with produce item above (m^2)	0.003
Contact area with produce item under (m^2)	0.001
Cooling conditions	
Inlet air velocity (m s^{-1})	0.9
Inlet air temperature (K)	273.8
Initial air temperature (K)	292
Initial produce temperature (K)	292
External air velocity (m s^{-1})	2.8

Prediction results in Figure 8.6 show that the airflow entered the vents in the central areas of the front (west) package wall, and spread to four produce layers through the gaps between trays edges and the package wall. Since the cells containing the vents on sidewalls (south and north walls) were included in the ZY plane (X=1), Figure 8.6 also displays the airflow leaving the side vents.

Figure 8.7 shows that the airflow converged to the vents in the central areas of the back (east) package wall from the produce layers. Similar to Figure 8.6, Figure 8.7 also displays the airflow leaving the vents on the back parts of the sidewalls. As a portion of airflow left the carton from the side vents, the airflow rates in front gaps (Figure 8.6) were larger than those in back gaps (Figure 8.7).

Figure 8.8 illustrates the predicted airflow patterns and pressure distributions in the gaps between tray edges and side package walls. In the front portions of the side gaps, the airflow spread to bottom and top produce layers and the spaces between trays and top/bottom package walls. In the back portions of the side gaps, the airflow converged in the middle produce layers where the outlet vents are located.

Figures 8.9-8.12 display airflow patterns and pressure distributions in four produce layers.

Comparing the airflow rates in these produce layers, the middle layers that are directly connected to the package inlets and outlets had much larger airflow rates than the top and bottom layers, into which airflow got via the narrow gaps. In each produce layer, the airflow rates along the walls were larger than those in the middle (apart from the near-to-vents regions) due to the wall effect (porosities along the wall are bigger than that in the middle).

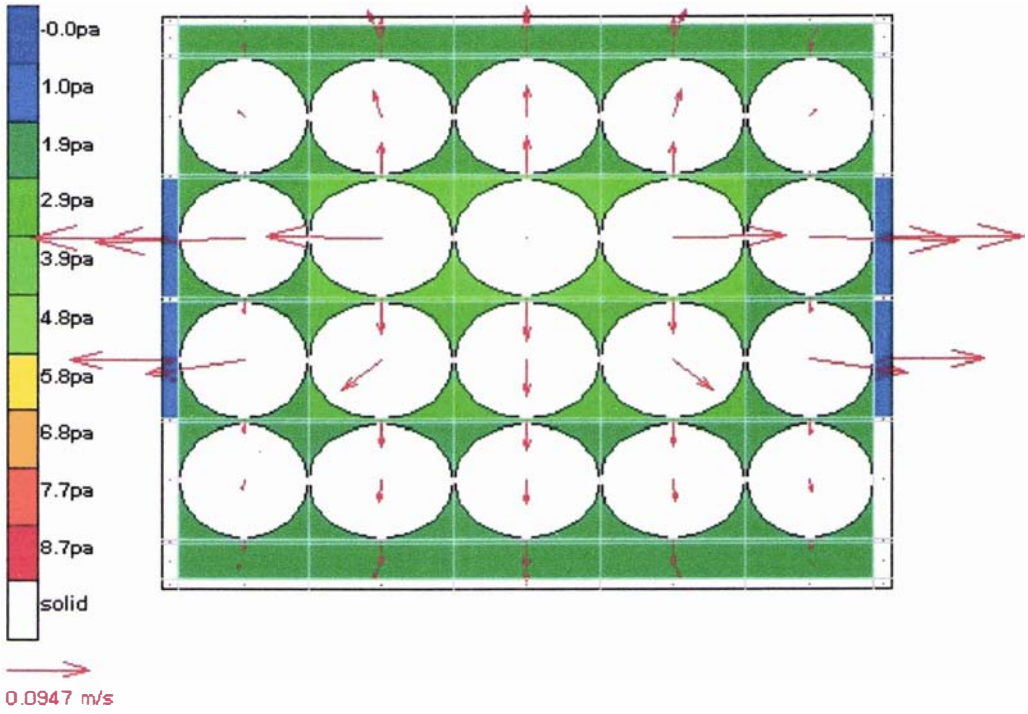

Figure 8.6 Predicted airflow pattern and pressure distribution in the gaps between front package wall and tray edges (YZ surface, X=1) in a single Z-Pack carton.

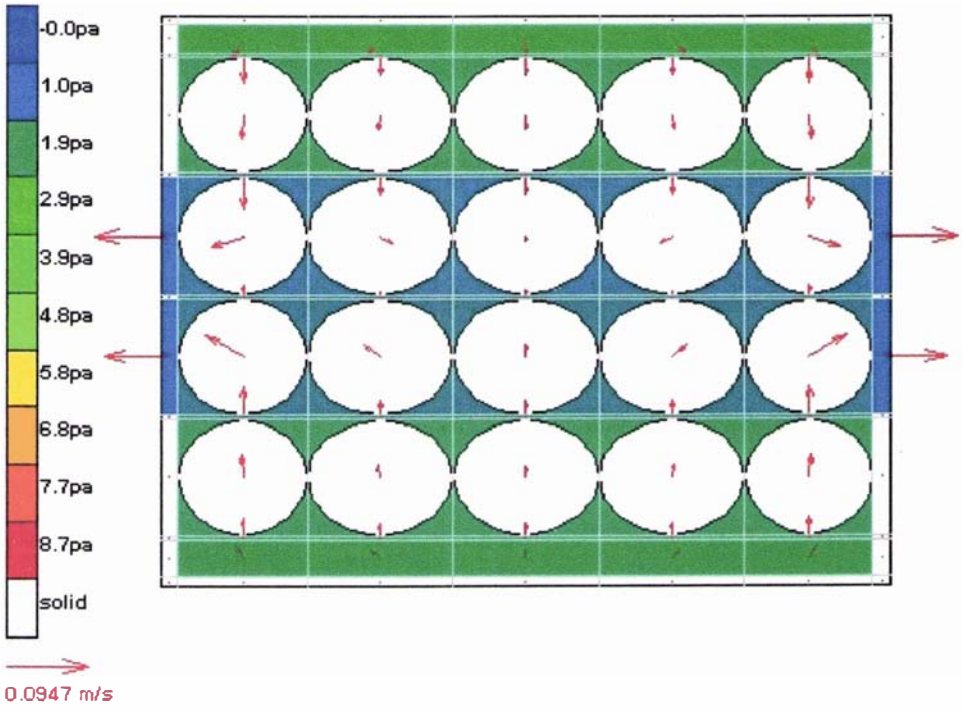

Figure 8.7 Predicted airflow pattern and pressure distribution in the gaps between back package wall and tray edges (YZ surface, X=5) in a single Z-Pack carton.

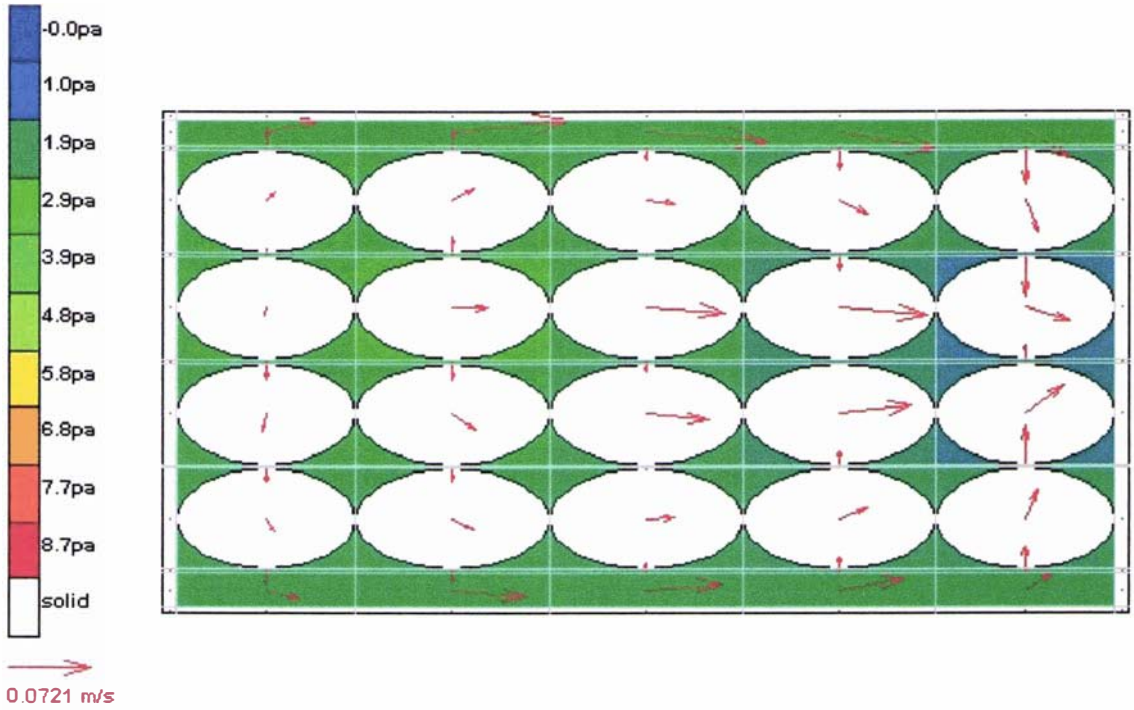

Figure 8.8 Predicted airflow pattern and pressure distribution in the gaps between side package walls and tray edges (XZ surface, Y=1 or Y=5) in a single Z-Pack carton.

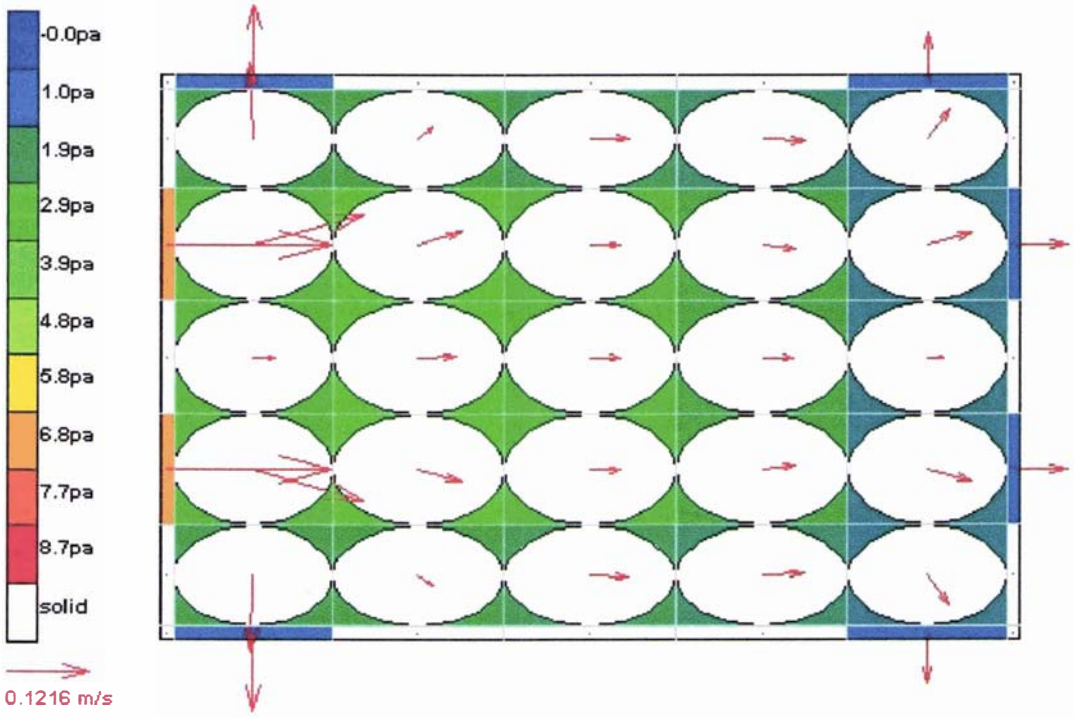

Figure 8.9 Predicted airflow pattern and pressure distribution in the bottom produce layer (XY surface, Z=1) in a single Z-Pack carton.

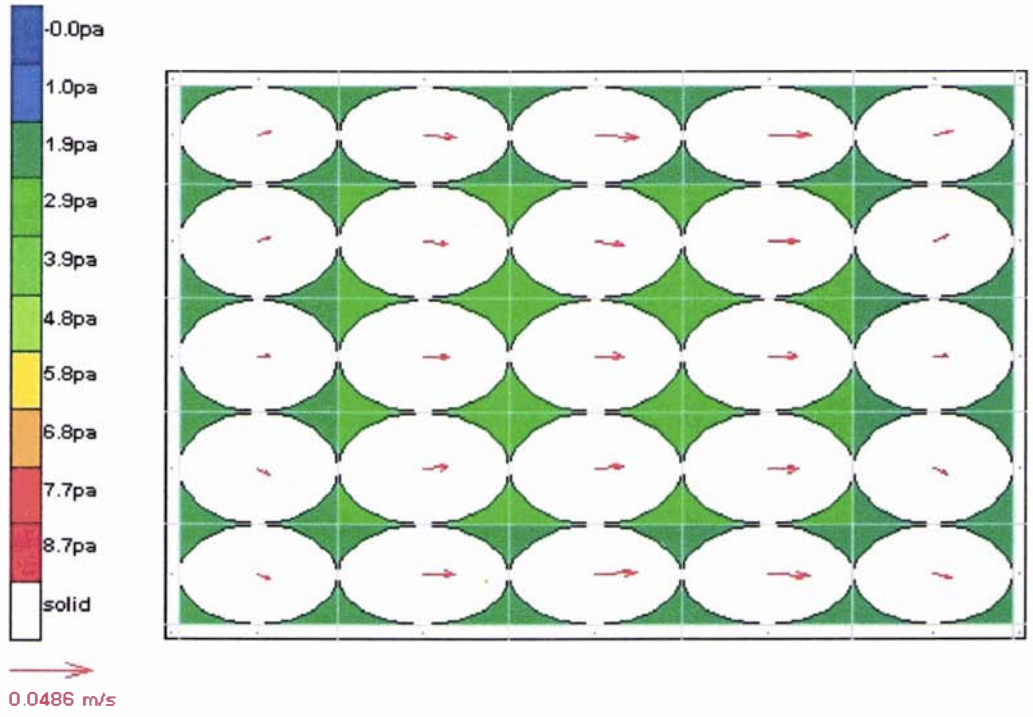

Figure 8.10 Predicted airflow pattern and pressure distribution in the lower middle produce layer (XY surface, Z=2) in a single Z-Pack carton.

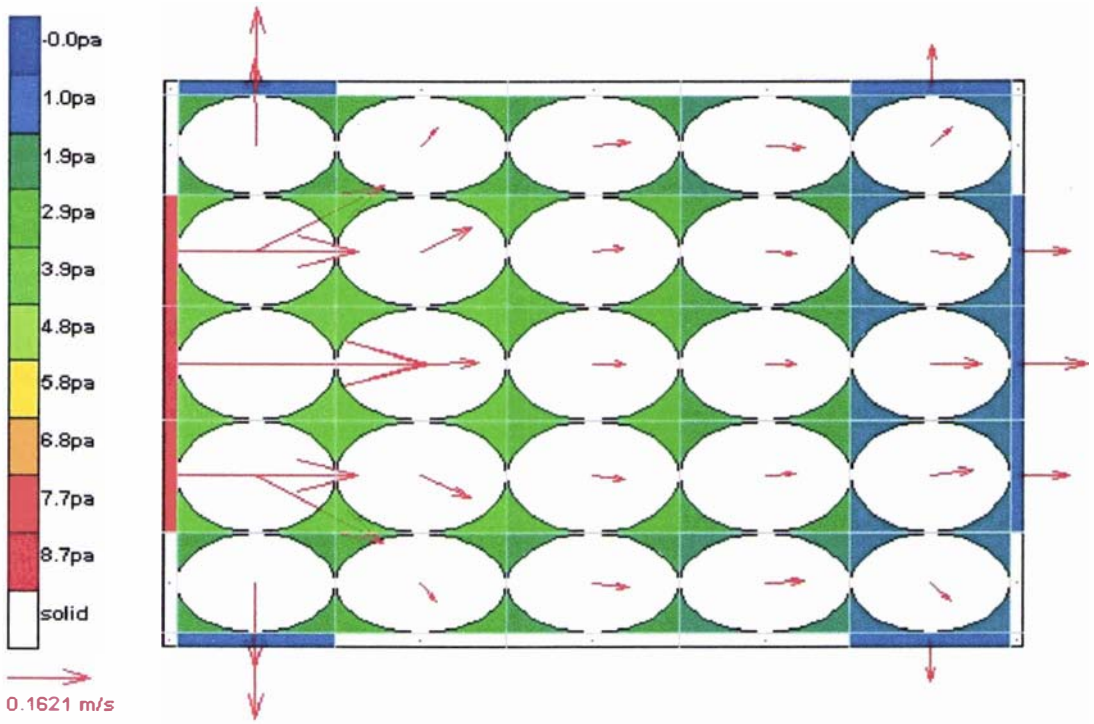

Figure 8.11 Predicted airflow pattern and pressure distribution in the upper middle produce layer (XY surface, Z=3) in a single Z-Pack carton.

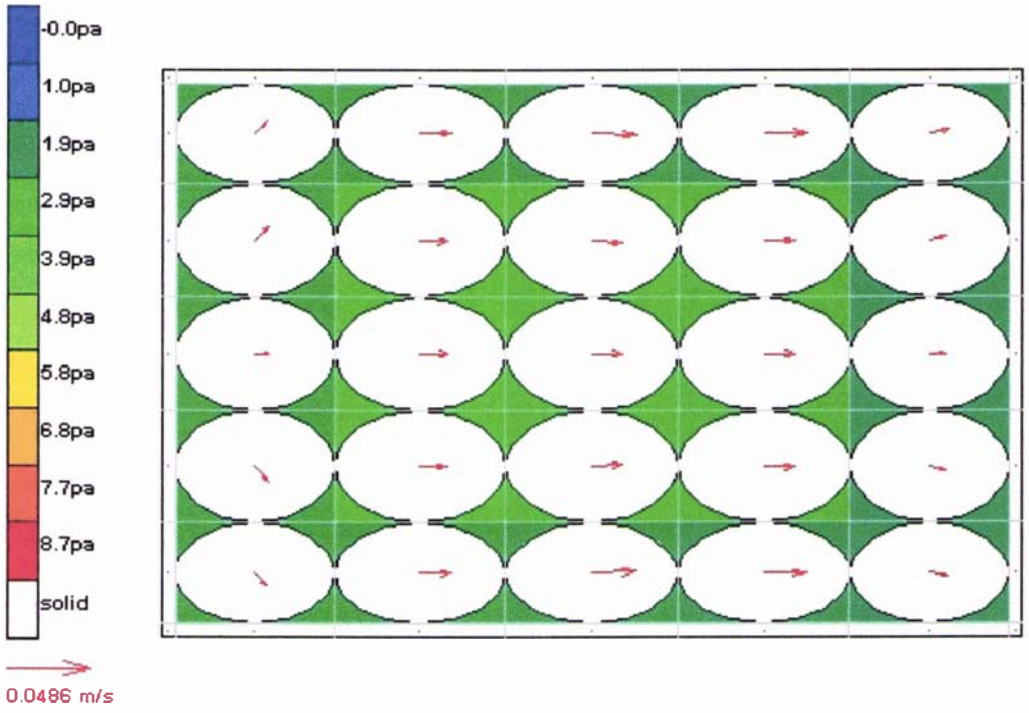

Figure 8.12 Predicted airflow pattern and pressure distribution in the top produce layer (XY surface, Z=4) in a single Z-Pack carton.

- **Predicted temperature profiles**

Figures 8.13-8.16 show the predicted air and produce temperature profiles of four produce layers after one hour of forced-air cooling. The temperature profiles were expressed with collection of colours, and the meanings of these colours were explained with the colour bars on the figures. The coloured circular areas in cells illustrate the temperature distributions inside produce items.

Comparing the produce cooling rates in these produce layers, the produce items in the middle layers were cooled much faster than those in the top and bottom layers. This result was consistent with the distribution of cooling media (air) in these layers (Figures 8.9-8.12).

The produce items near the inlets had the fastest cooling rates due to the biggest airflow rates around these items. The produce items along the package walls were generally cooled more rapidly than those in the middle because of the relatively large airflow rates caused by the high porosities in the near-wall regions (wall effects), as described in Section 2.4.1.

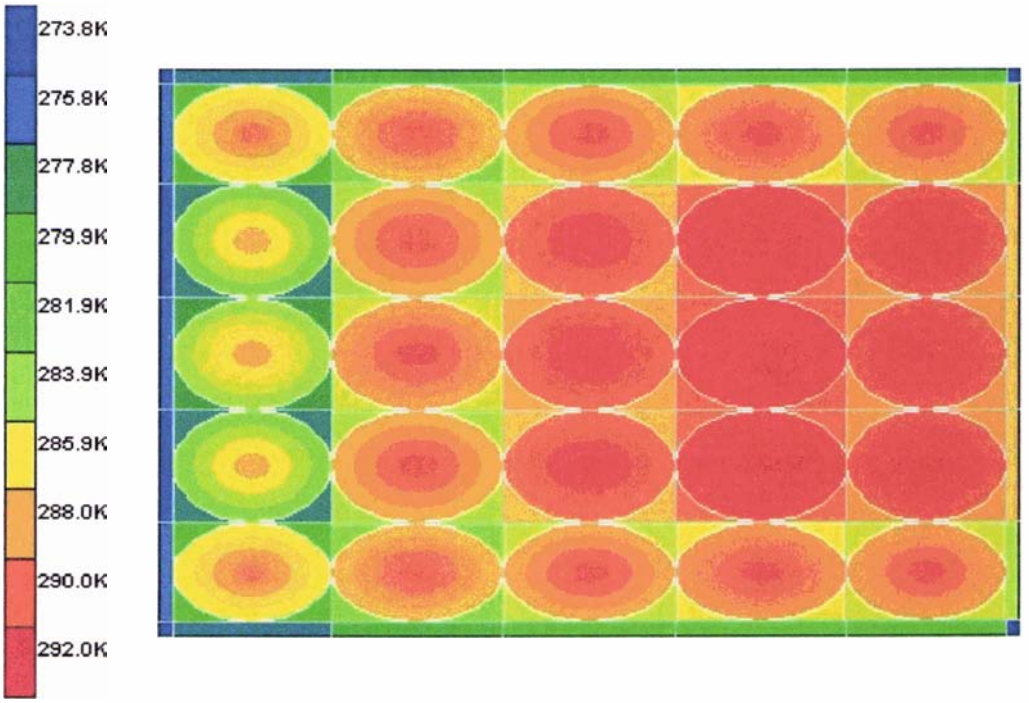

Figure 8.13 Predicted temperature profile in the bottom produce layer (XY surface, Z=1) in a single Z-Pack carton after 1 hour of cooling.

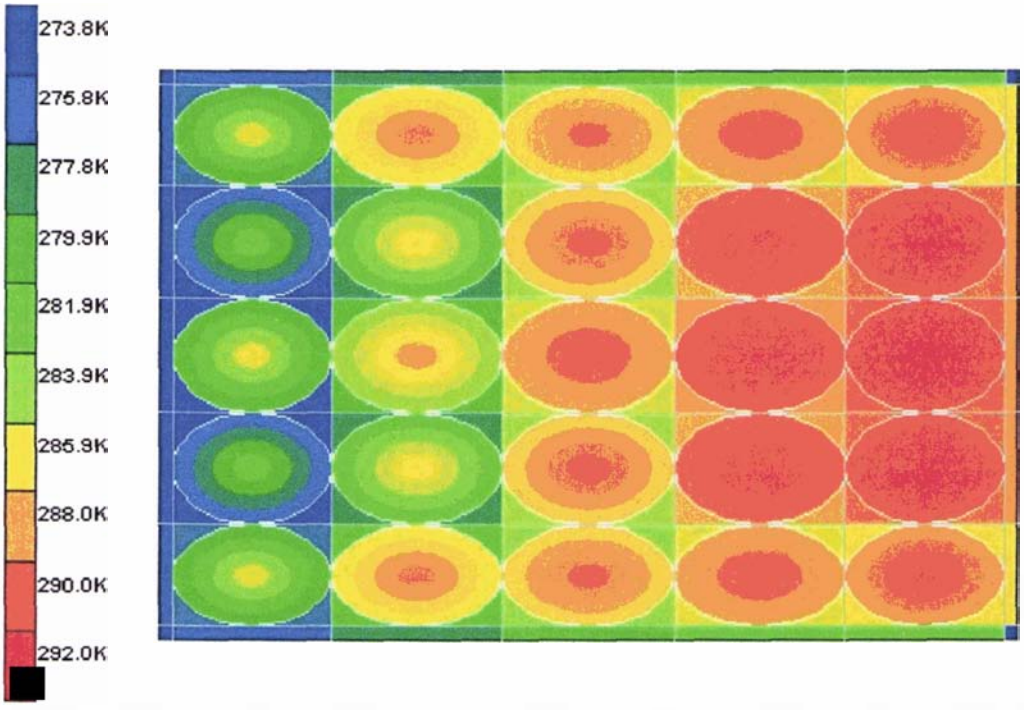

Figure 8.14 Predicted temperature profile in the lower middle produce layer (XY surface, Z=2) in a single Z-Pack carton after 1 hour of cooling.

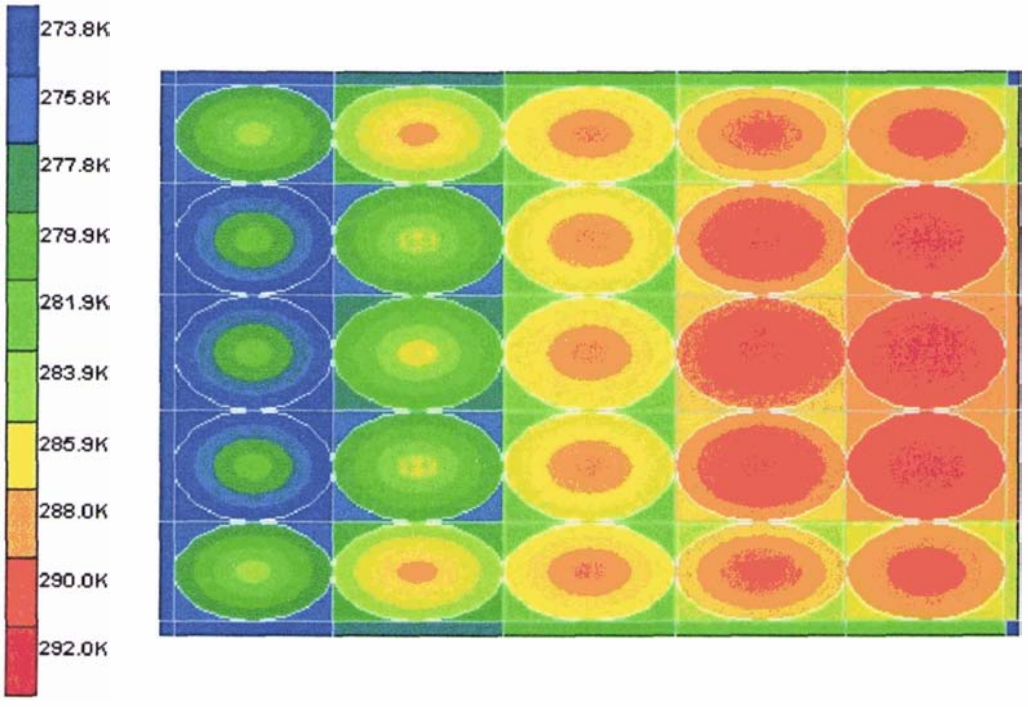

Figure 8.15 Predicted temperature profile in the upper middle produce layer (XY surface, Z=3) in a single Z-Pack carton after 1 hour of cooling.

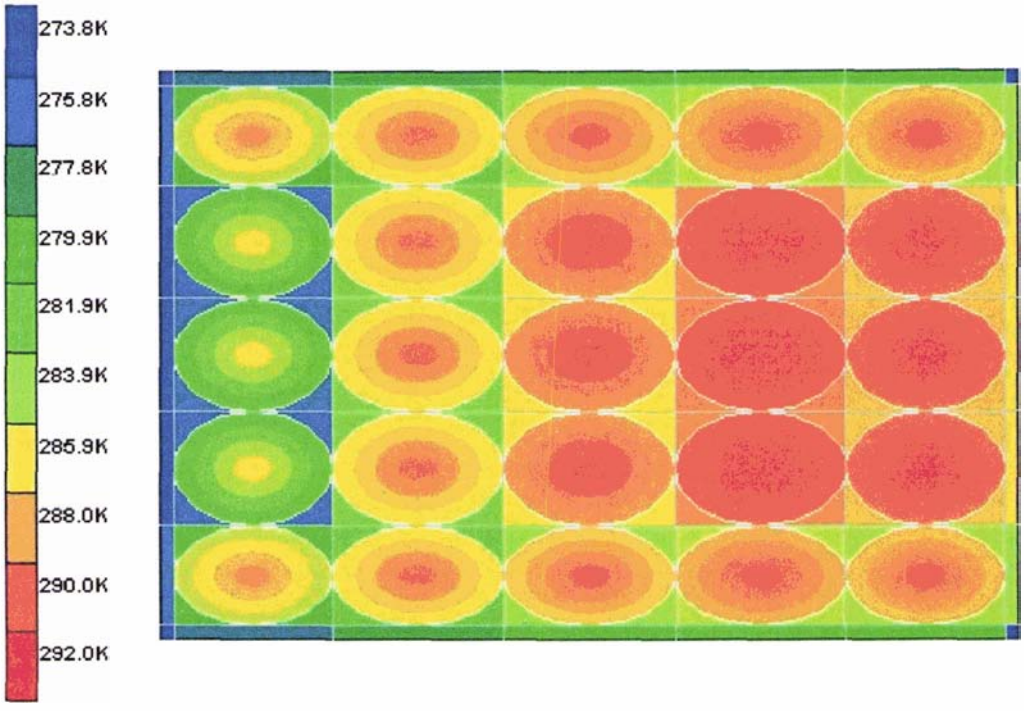

Figure 8.16 Predicted temperature profile in the top produce layer (XY surface, Z=4) in a single Z-Pack carton after 1 hour of cooling.

- **Comparisons between predicted and measured produce cooling rates**

Figures 8.17-8.20 show a comparison between the predicted cooling rates in the centres of produce items with the experimental data measured by Zou (1998). The positions of the indexed cells in the figures were shown in Figure 8.3. Errors in the measured temperature were obvious at the beginning of cooling, and this was due to the time needed for the temperature of datalogger to reach steady state (Zou, 1998).

Good agreements between model predictions and experimental data were obtained. In most positions the predicted product central temperatures fitted well with the measurements, where the temperature differences after 4 hours of cooling are less than 2K. The relatively big temperature differences (3–4K after 4 hours of cooling) occurred in the near inlet region of bottom layer (cell 1, 3, 1), the near outlet region of top layer (cell 5, 3, 4), and the centre of 2nd layer (cell 3, 3, 2). Lack of fit may be explained by inaccurate positioning of thermocouples and inaccurate model input values.

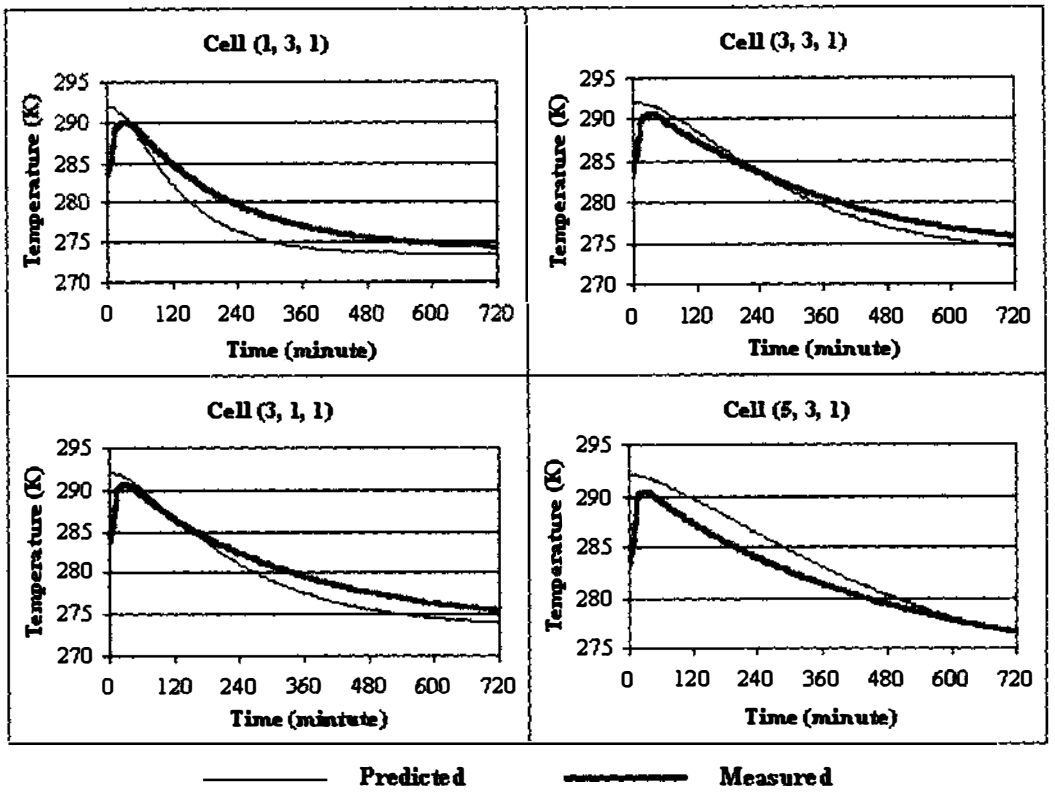

Figure 8.17 Predicted and measured temperature profiles in the centres of produce items in bottom layer of Z-Pack apple carton during forced-air cooling.

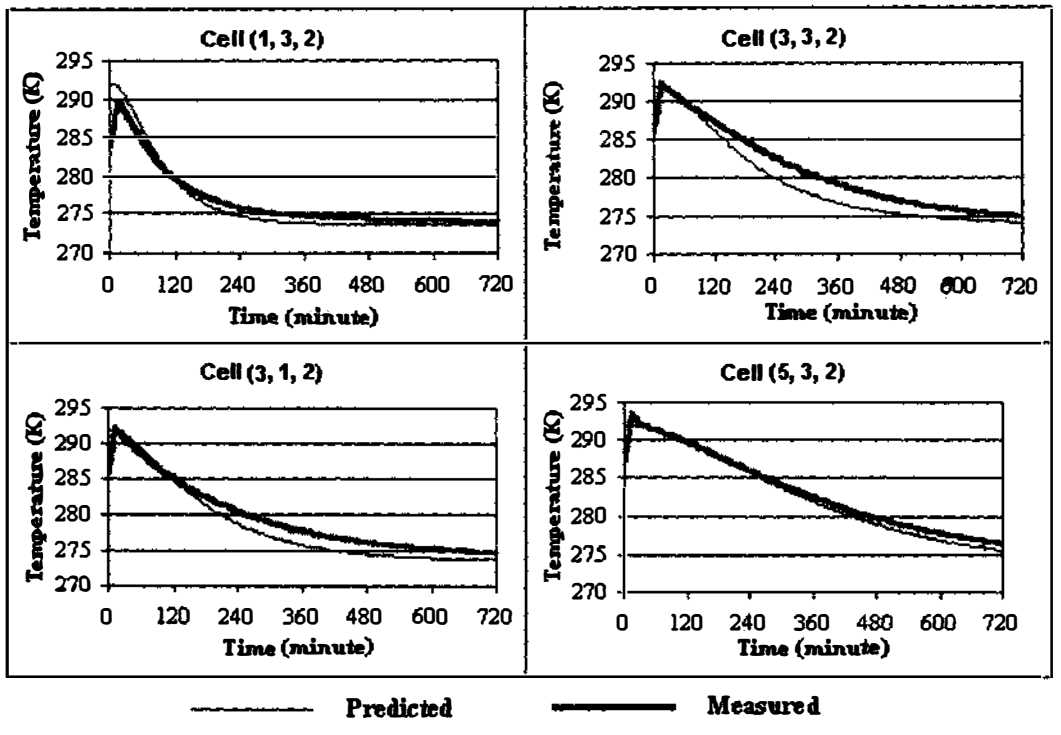

Figure 8.18 Predicted and measured temperature profiles in the centres of produce items in lower middle layer of Z-Pack apple carton during forced-air cooling.

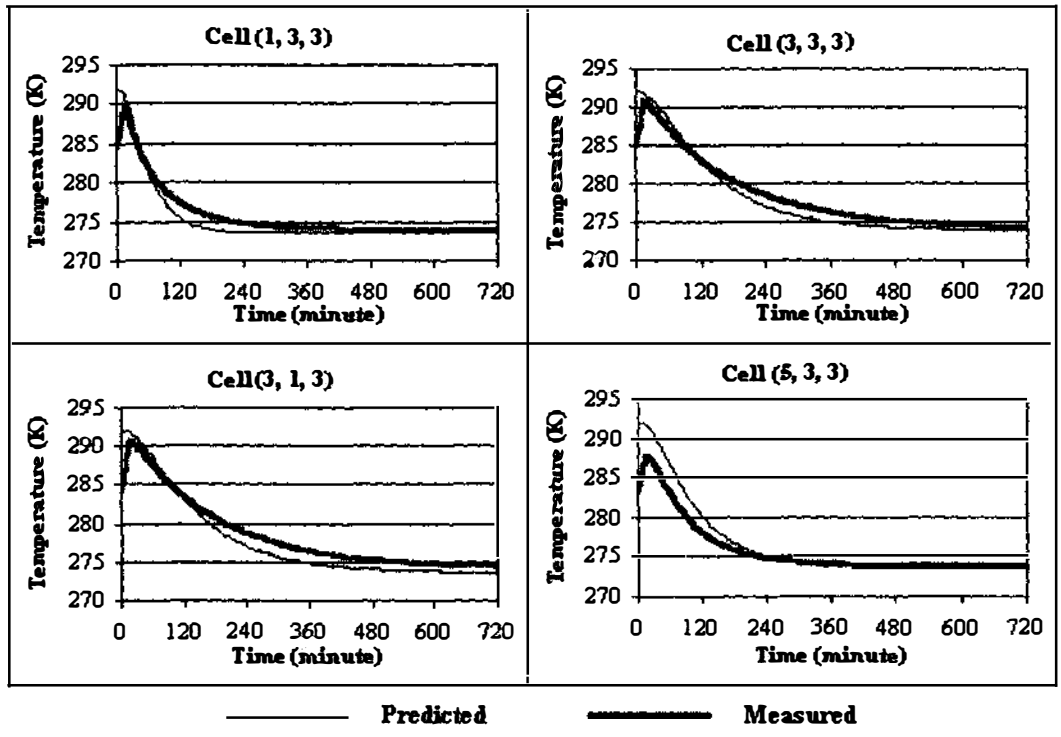

Figure 8.19 Predicted and measured temperature profiles in the centres of produce items in upper middle layer of Z-Pack apple carton during forced-air cooling.

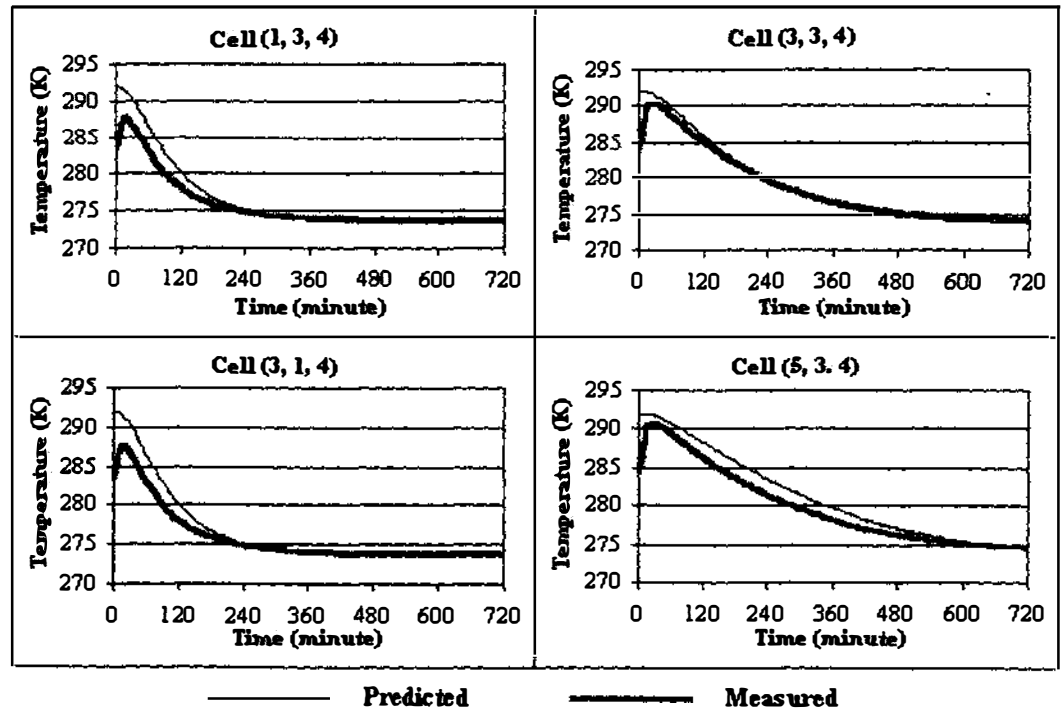

Figure 8.20 Predicted and measured temperature profiles in the centres of produce items in top layer of Z-Pack apple carton during forced-air cooling.

8.2.3 Forced-Air Cooling in Single Pre-1996 'Standard' 6-Layer Apple Carton

- **Packaging system and cooling conditions**

Amos (1995) conducted experiments on forced-air cooling of apples in a single Pre-1996 'Standard' 6-layer carton (Figure 8.21). Figure 8.22 shows the dimensions and position of vents on the front and back package surfaces. Table 8.8 summarises the data used to define the packaging system and cooling conditions.

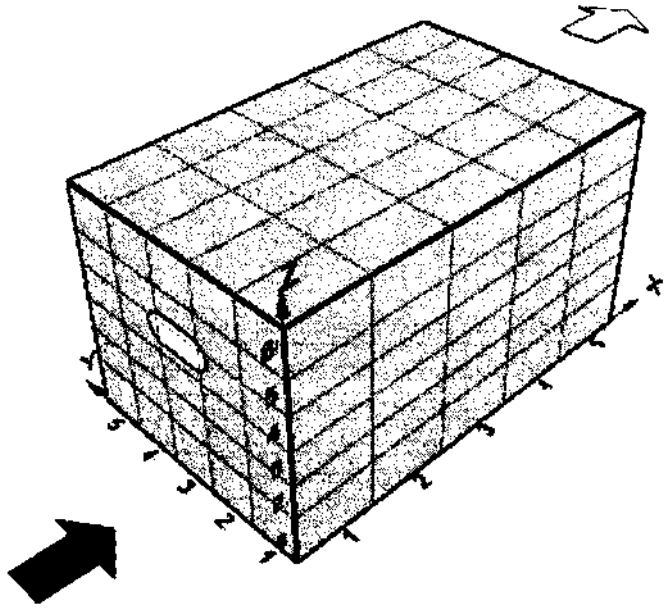

Figure 8.21 Forced-air cooling of apple in a Pre-1996 'Standard' 6-layer apple carton.

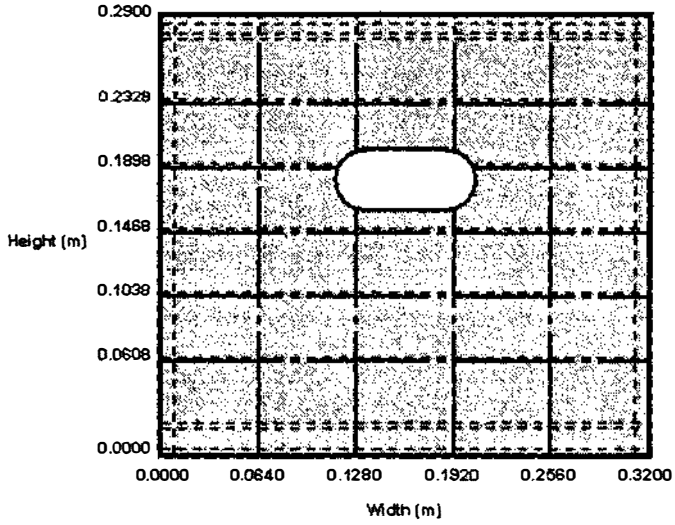

Figure 8.22 Dimensions and positions of vents on the front and back surfaces of in Pre-1996 'Standard' 6-layer apple carton.

Table 8.8 Data of packaging system and cooling conditions for forced-air cooling of apple in a Pre-1996 'Standard' 6-layer apple carton (Amos, 1995).

Variable	Value
Produce item	
Density (kg m^{-3})	830
Thermal conductivity (W m^{-1} K^{-1})	0.42
Specific heat capacity (J kg^{-1} K^{-1})	3650
Volume (m^3)	0.0001494
Surface are (m^2)	0.014444
Height when placed on tray (m)	0.0054
Individual package	
Length (m)	0.515
Width (m)	0.32
Height (m)	0.29
Number of produce item	150
Number of produce layers	6
Is top layer covered with tray?	Yes
Package walls	
Density (kg m^{-3})	220
Thermal conductivity (W m^{-1} K^{-1})	0.048
Specific heat capacity (J kg^{-1} K^{-1})	1700
Thickness of side walls (m)	0.0076
Thickness of top wall (m)	0.0038
Thickness of bottom wall (m)	0.0038
Tray	
Density (kg m^{-3})	260
Thermal conductivity (W m^{-1} K^{-1})	0.048
Specific heat capacity (J kg^{-1} K^{-1})	1700
Thickness (m)	0.002
Height (m)	0.014
Gaps between tray edges and front and back walls (m)	0.004
Gaps between tray edges and side walls (m)	0.003
Contact area with produce item above (m^2)	0.0024
Contact area with produce item under (m^2)	0.0008
Cooling conditions	
Inlet air velocity (m s^{-1})	1.4
Inlet air temperature (K)	273.4
Initial air temperature (K)	295.5
Initial produce temperature (K)	295.5
External air velocity (m s^{-1})	1.4

- **Predicted airflow patterns**

Figures 8.23-8.31 show the predicted airflow patterns and pressure distributions in various planes of the 6-layer apple carton. The position of these planes was referenced by the indexes shown in Figure 8.21. Similar to the airflow patterns presented in the previous section, the vector arrows represent the average volume flow rates per unit area of the cell surfaces.

Prediction results in Figure 8.23 show that the airflow entered the vent in the central area of the front (west) package wall, and spread to the six produce layers through the gaps between trays edges and the package walls. Figure 8.24 shows that the airflow converged to the vent in the central area of the back (east) package wall from the produce layers. Figure 8.25 illustrates the predicted airflow patterns and pressure distributions in the gaps between tray edges and side package walls. In the front portions of the side gaps, the airflow spread to the bottom and top from the middle of the carton. In the back portions of the side gaps, the airflow converged to middle produce layers (fourth and fifth produce layer) where the outlet vent are located.

Figures 8.26-8.31 display the airflow patterns and pressure distributions in six produce layers. Comparing the airflow rates in these produce layers, the middle layers ($Z = 4$ or 5) that are directly connected to the package inlet and outlet had much larger airflow rates than the produce layers near the top and bottom, where airflow entered via the narrow gaps. Similarly the wall effect caused the larger airflow rates along the walls than those in the middle because of the high porosities in the near-wall regions.

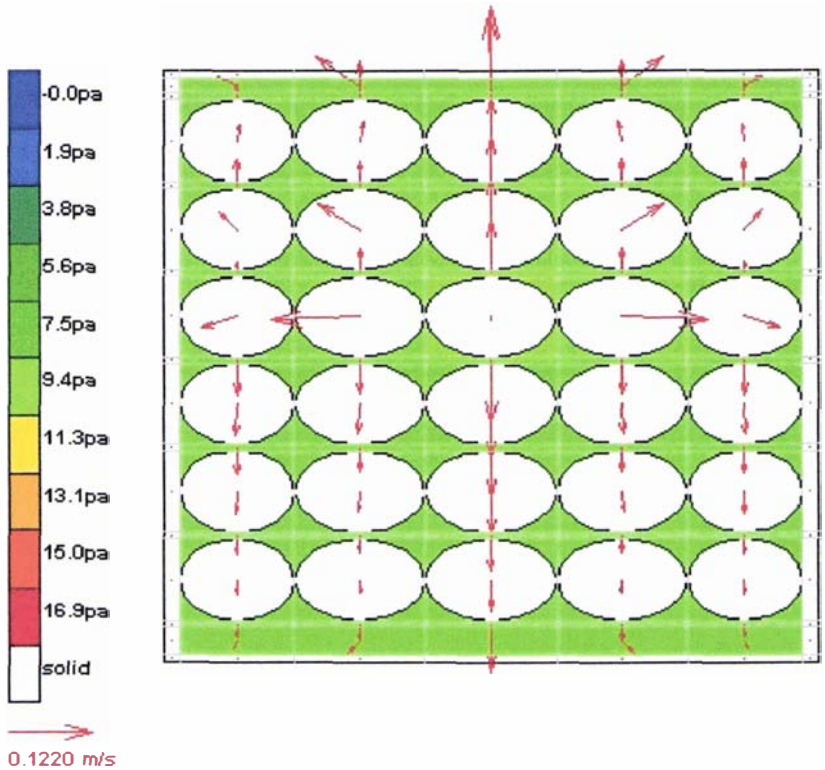

Figure 8.23 Predicted airflow pattern and pressure distribution in the gaps between front package wall and tray edges (YZ surface, X=1) in a 'Standard' 6-layer apple carton.

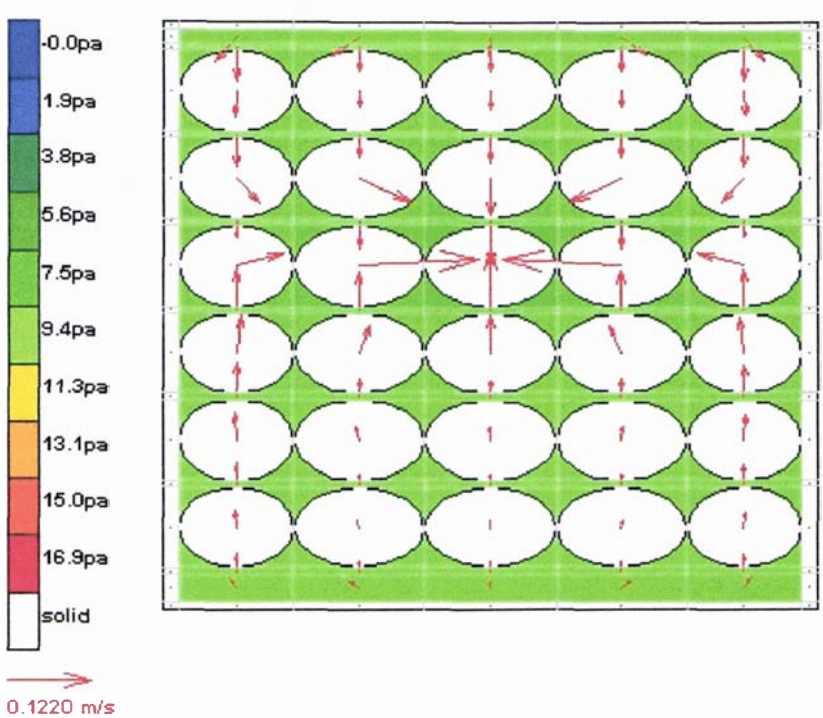

Figure 8.24 Predicted airflow pattern and pressure distribution in the gaps between back package wall and tray edges (YZ surface, X=5) in a 'Standard' 6-layer apple carton.

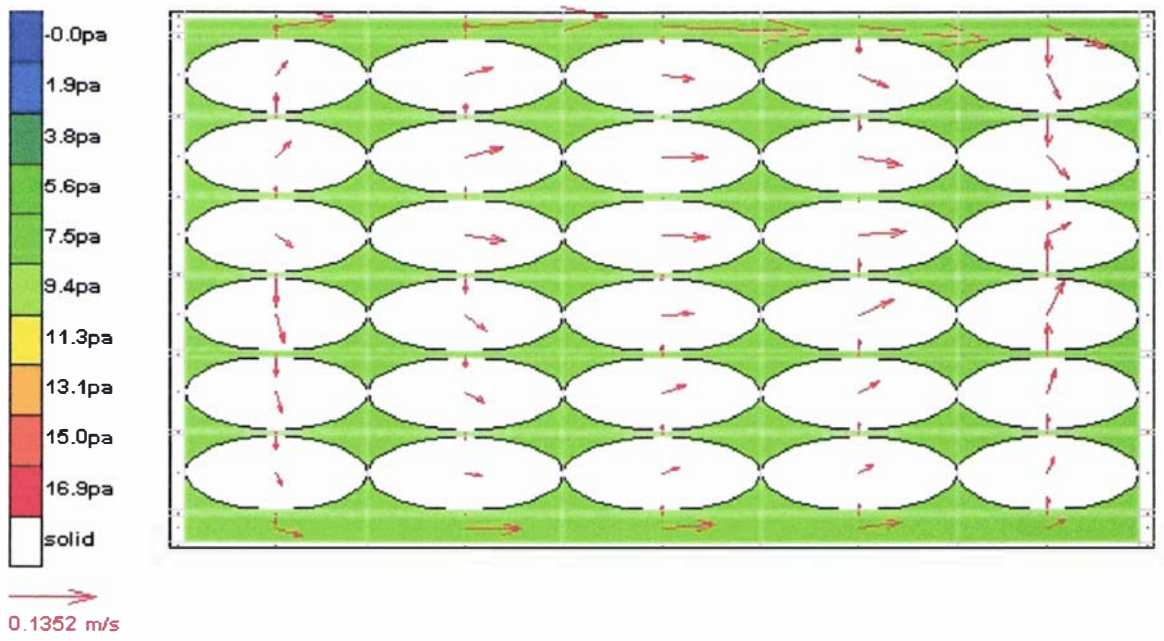

Figure 8.25 Predicted airflow pattern and pressure distribution in the gaps between side package walls and tray edges (XZ surface, Y=1 or Y=5) in a Pre-1996 'Standard' 6-layer apple carton.

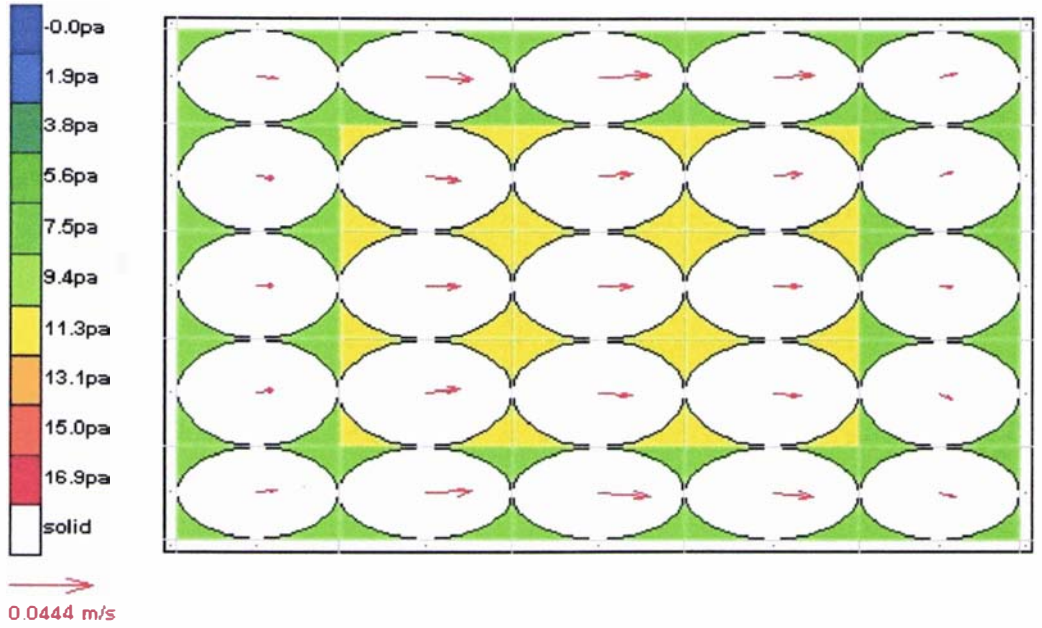

Figure 8.26 Predicted airflow pattern and pressure distribution in the bottom produce layer (XY surface, Z=1) in a Pre-1996 'Standard' 6-layer apple carton.

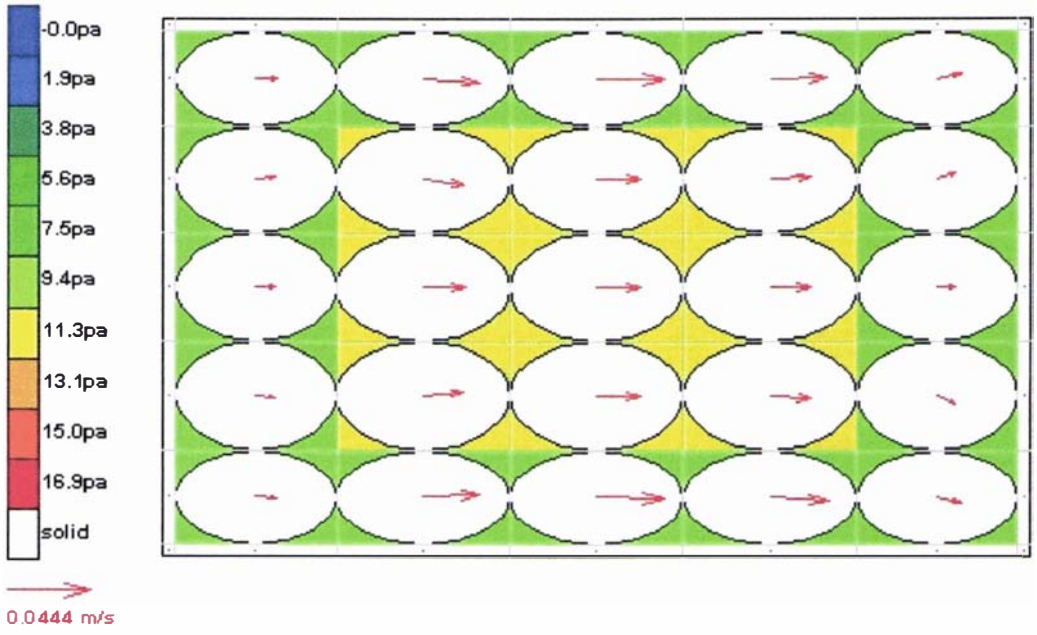

Figure 8.27 Predicted airflow pattern and pressure distribution in the 2nd produce layer (XY surface, Z=2) in a Pre-1996 'Standard' 6-layer apple carton.

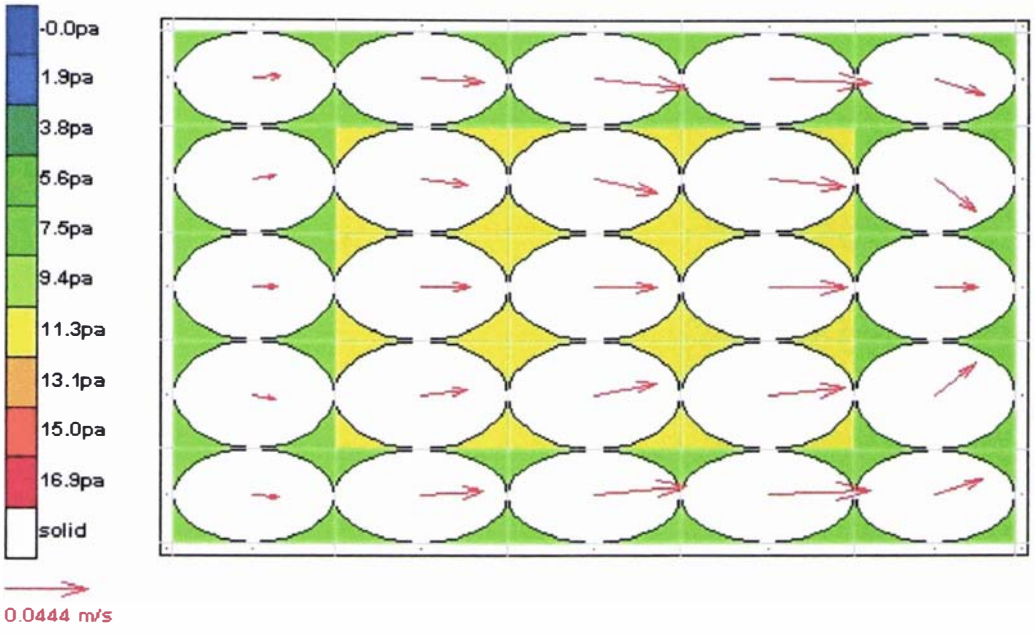

Figure 8.28 Predicted airflow pattern and pressure distribution in the 3rd produce layer (XY surface, Z=3) in a Pre-1996 'Standard' 6-layer apple carton.

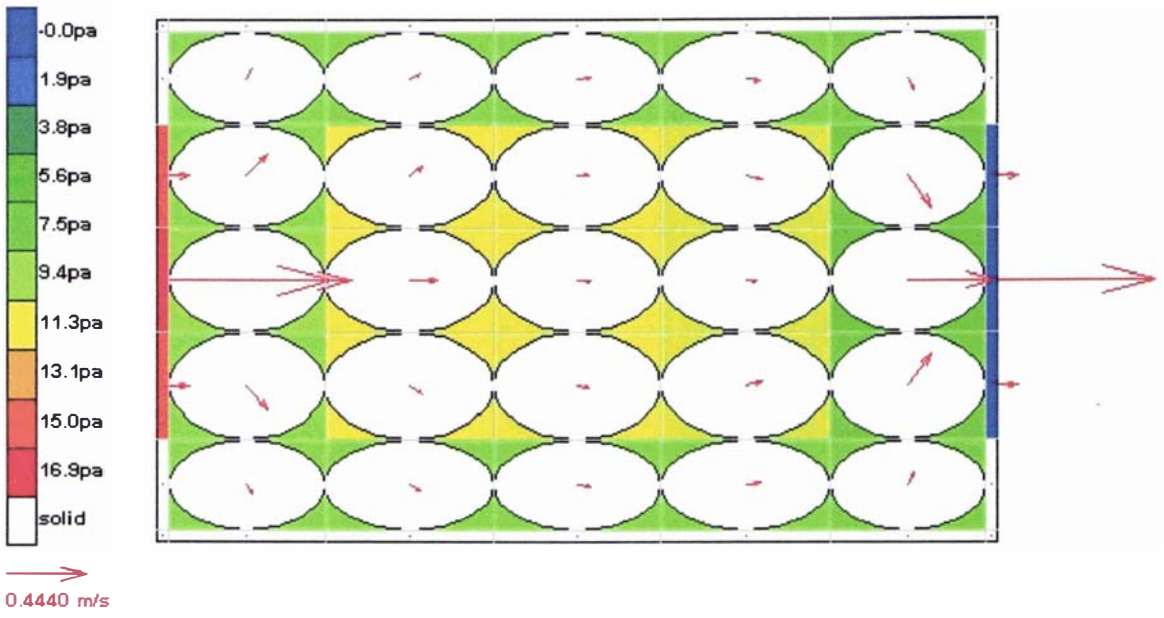

Figure 8.29 Predicted airflow pattern and pressure distribution in the 4th produce layer (XY surface, Z=4) in a Pre-1996 'Standard' 6-layer apple carton.

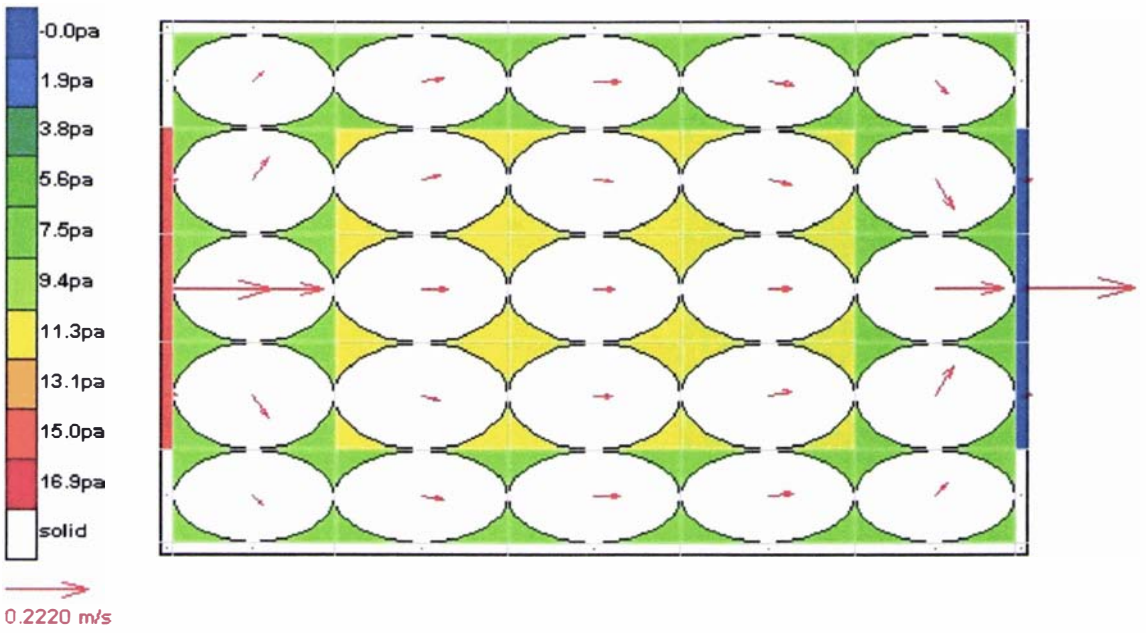

Figure 8.30 Predicted airflow pattern and pressure distribution in the 5th produce layer (XY surface, Z=5) in a Pre-1996 'Standard' 6-layer apple carton.

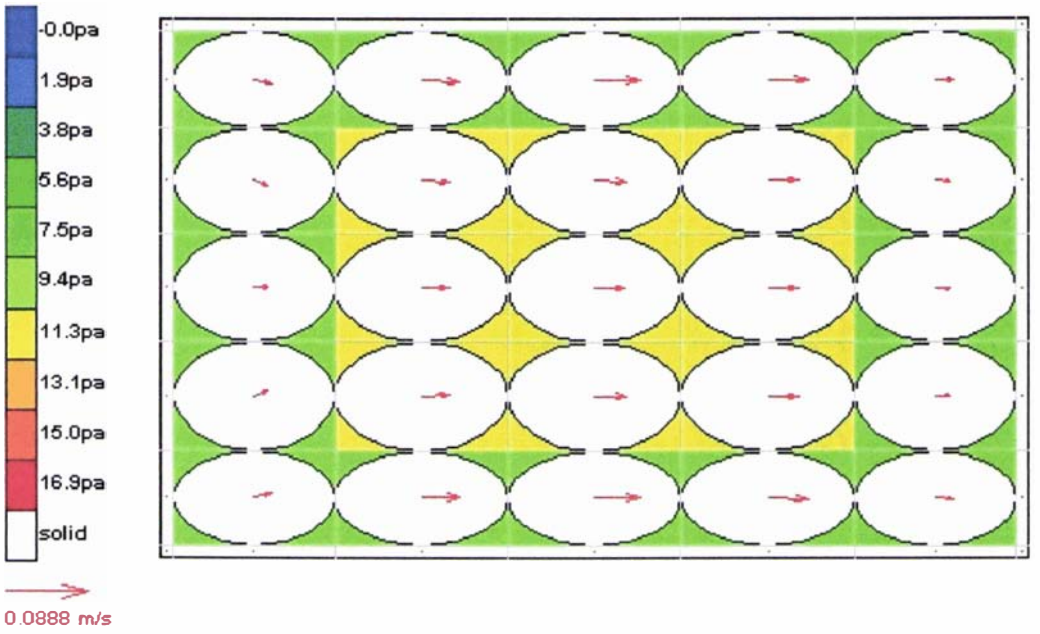

Figure 8.31 Predicted airflow pattern and pressure distribution in the top produce layer (XY surface, Z=6).

- **Predicted temperature profiles**

Figures 8.32-8.37 show the predicted air and produce temperature profiles of six produce layers after one hour of forced-air cooling. Comparing the produce cooling rates in these produce layers, the further a produce layer was away from the vent, the slower the produce items in the produce layer were cooled, which was consistent with the distribution of cooling media (air) in these layers (Figures 8.26-8.31). The produce items near to the inlet had the fastest cooling rates. The produce items along the package walls were generally cooled more rapidly that those in the middle because of because of the relatively large airflow rates caused by the high porosities in the near-wall regions.

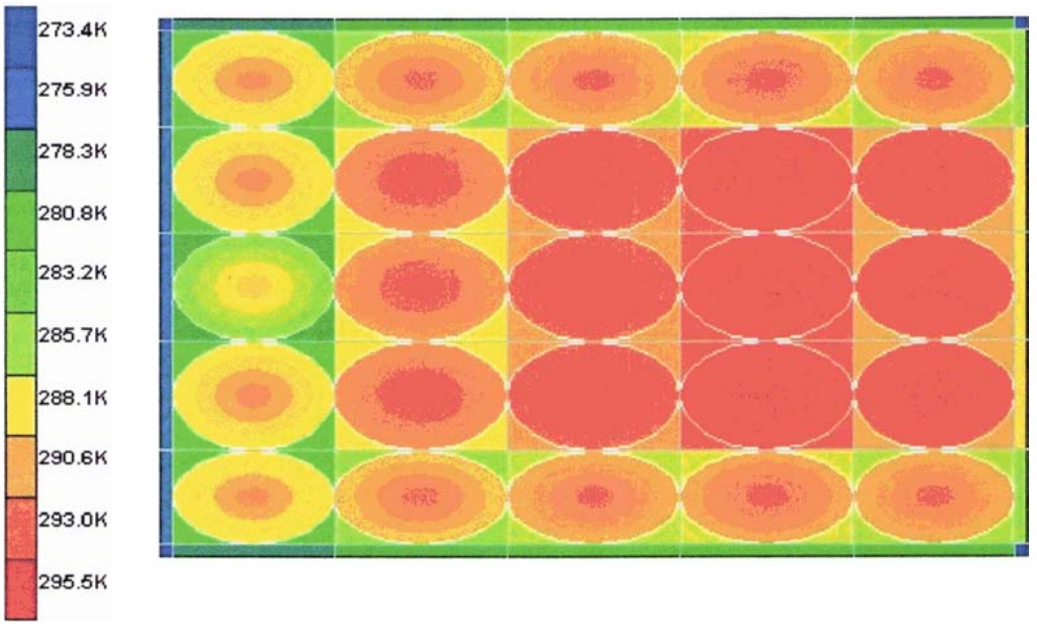

Figure 8.32 Predicted air and produce temperature profile in the bottom produce layer (XY surface, Z=1) in a Pre-1996 'Standard' 6-layer apple carton after 1-hour cooling.

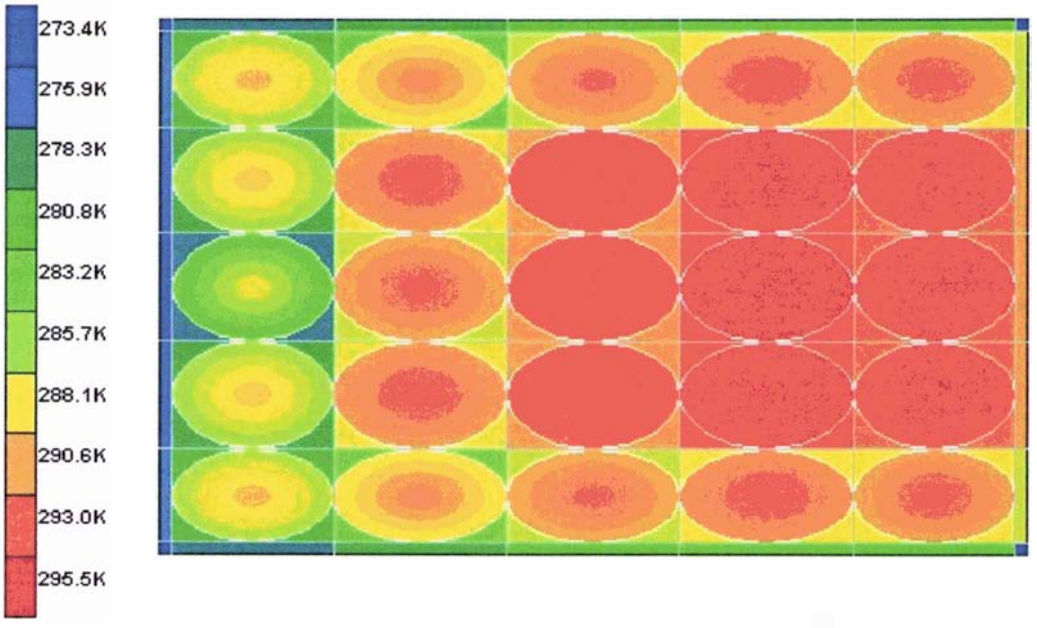

Figure 8.33 Predicted air and produce temperature profile in the 2nd produce layer (XY surface, Z=2) in a Pre-1996 'Standard' 6-layer apple carton after 1 hour of cooling.

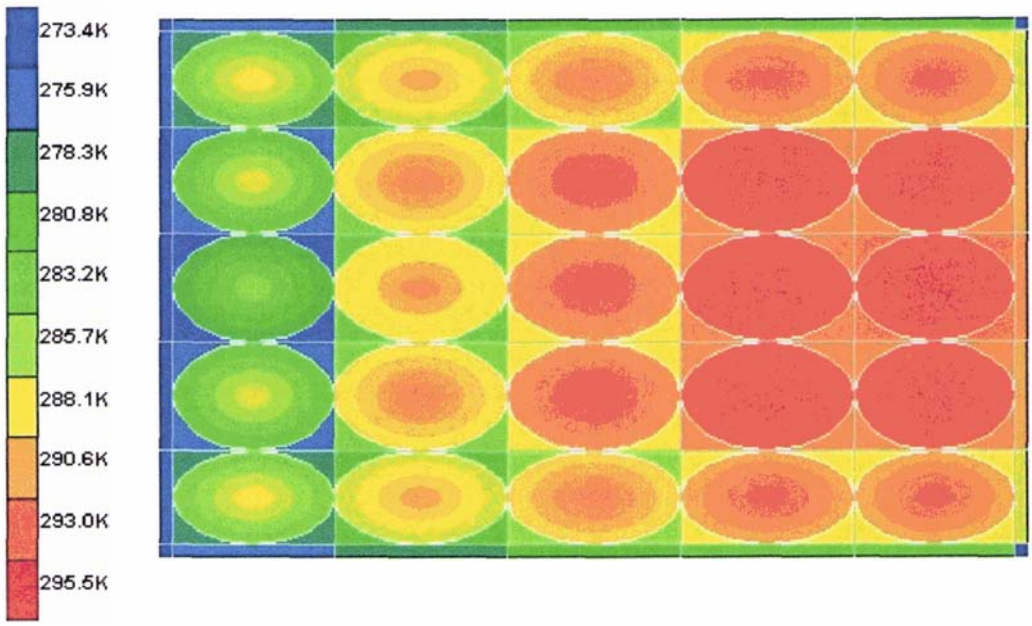

Figure 8.34 Predicted air and produce temperature profile in the 3rd produce layer (XY surface, Z=3) in a Pre-1996 'Standard' 6-layer apple carton after 1 hour of cooling.

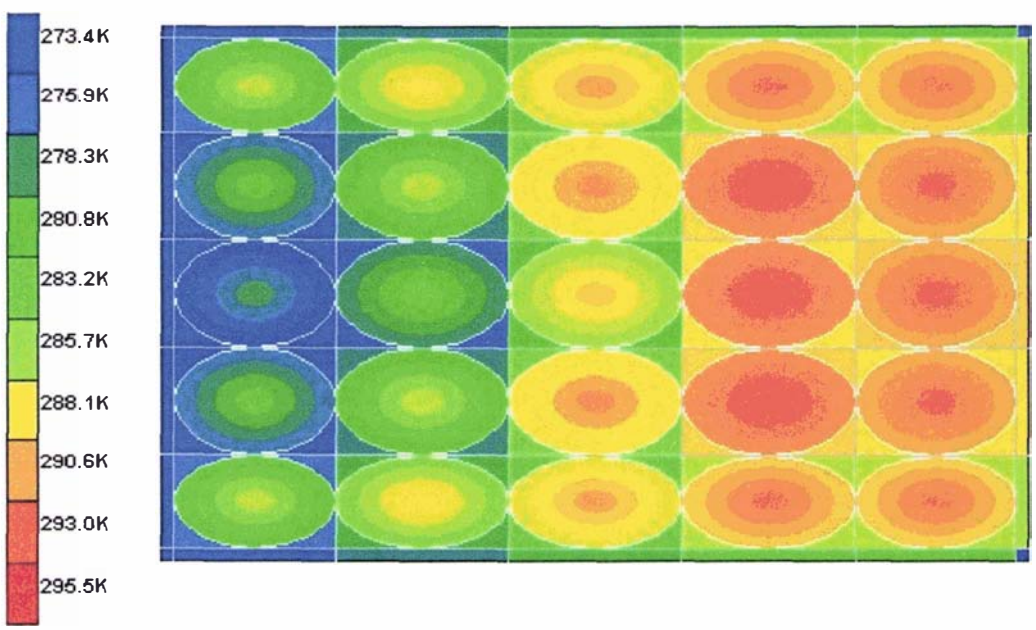

Figure 8.35 Predicted air and produce temperature profile in the 4th produce layer (XY surface, Z=4) in a Pre-1996 'Standard' 6-layer apple carton after 1 hour of cooling.

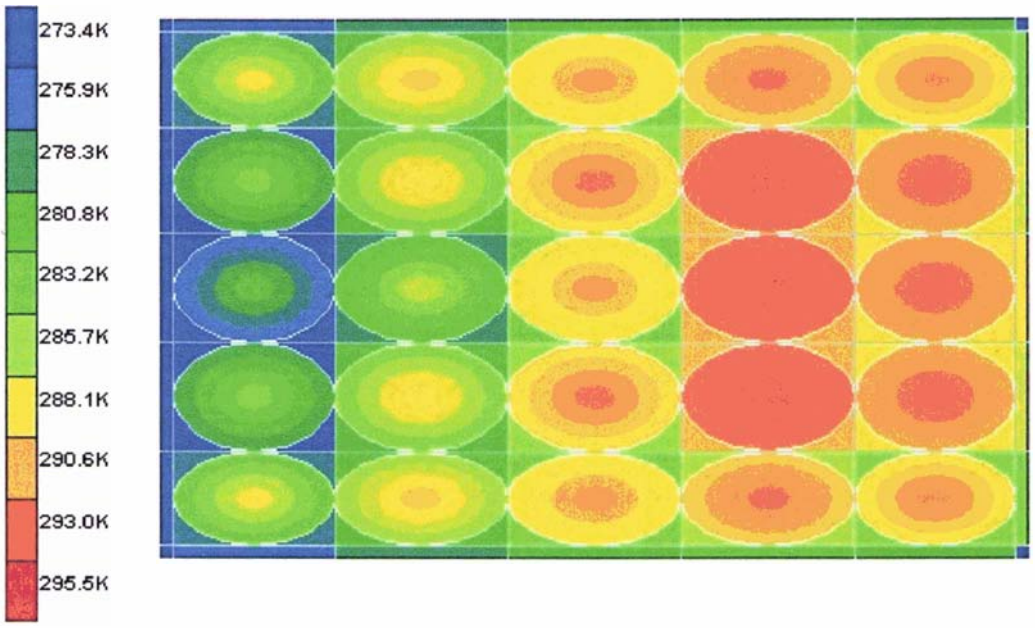

Figure 8.36 Predicted air and produce temperature profile in the 5th produce layer (XY surface, Z=5) in a Pre-1996 'Standard' 6-layer apple carton after 1 hour of cooling.

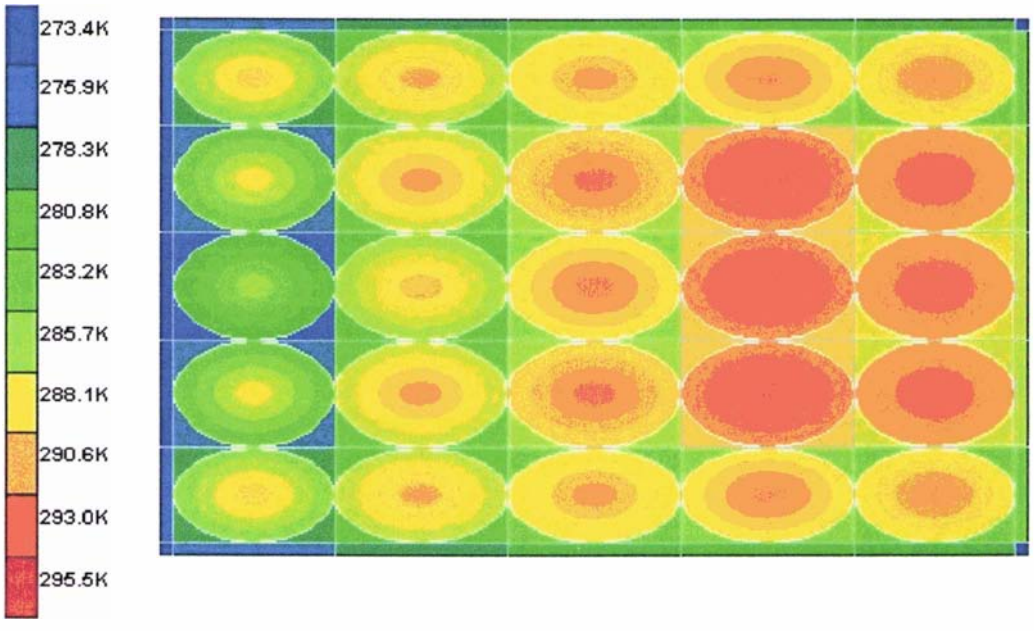

Figure 8.37 Predicted air and produce temperature profile in the top produce layer (XY surface, Z=6) in a Pre-1996 'Standard' 6-layer apple carton after 1 hour of cooling.

- **Comparisons between predicted and measured produce cooling rates**

Figures 8.38-8.43 compare the predicted cooling rates in the centres of produce items in various positions of the package with the experimental data measured by Amos (1995). The positions of the indexed cells in the figures were shown in Figure 8.21.

In general, good agreements between model predictions and experimental data were obtained. In most positions the predicted product central temperatures fitted well with the measurements, where the temperature differences after 4 hours of cooling were less than 2K. However, in all the produce layers, the model under-predicted the cooling rates of the produce items located along package sidewalls and in the middle of the carton (cells 3, 1, 1-6), where the temperature differences after 4 hours of cooling were 2.5 – 4.5 k. Lack of fit for the produce items along the package walls may be attributed to the assumption of no heat conduction between the product items and the package wall (Table 5.2). Compared with the example presented in Section 8.2.2, the size of a produce item is small, and the contact area between the product item and package wall relative to the total product surface area is large, so heat conduction may not be negligible.

Other bigger temperature differences (3 – 4K after 4 hours of cooling) occurred in the near outlet region of 2nd layer (cell 5, 3, 2), the near inlet region and centre of 3rd layer (cells 1, 3, 3 & 3, 3, 3), and the centre of 4th layer (cell 3, 3, 4). These differences may be attributed to inaccurate positioning of thermocouples or/and inaccurate model input values as discussed in Section 8.2.1.

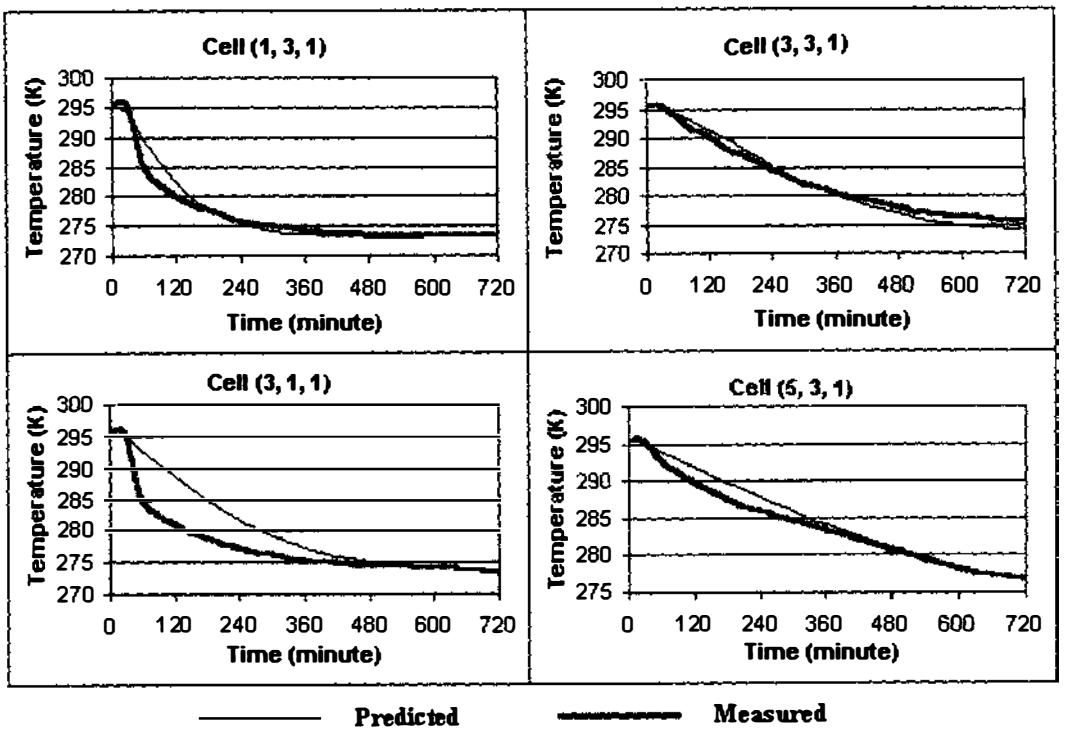

Figure 8.38 Predicted and measured temperature profiles in the centres of produce items in the bottom layer of Pre-1996 'Standard' 6-layer apple carton during forced-air cooling.

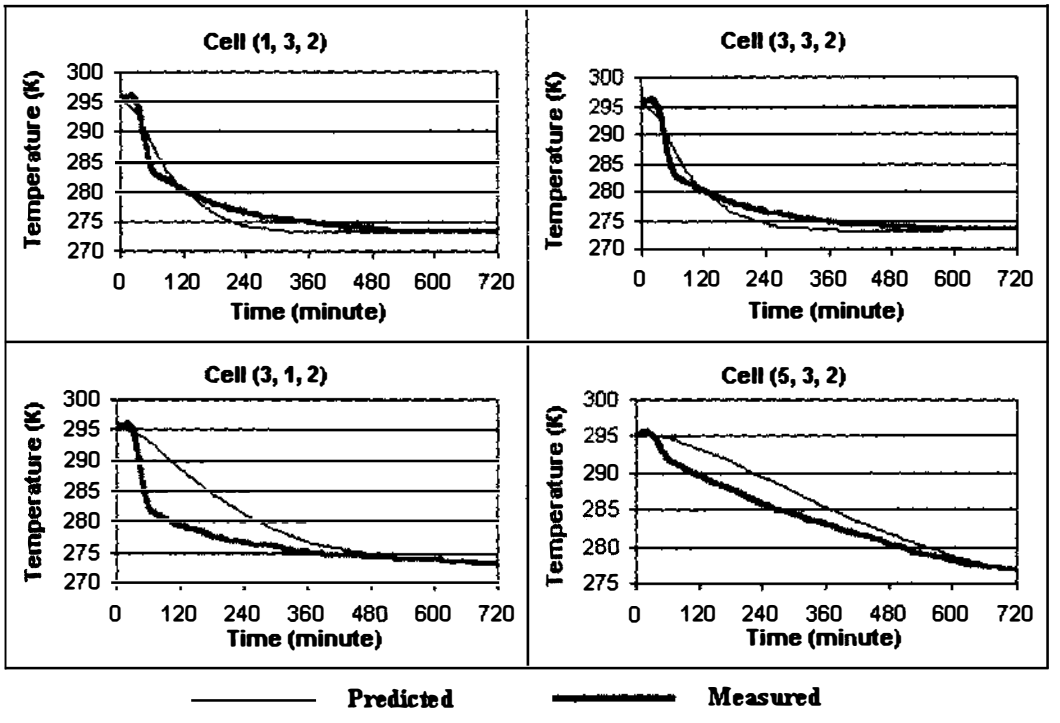

Figure 8.39 Predicted and measured temperature profiles in the centres of produce items in the 2nd layer of Pre-1996 'Standard' 6-layer apple carton during forced-air cooling.

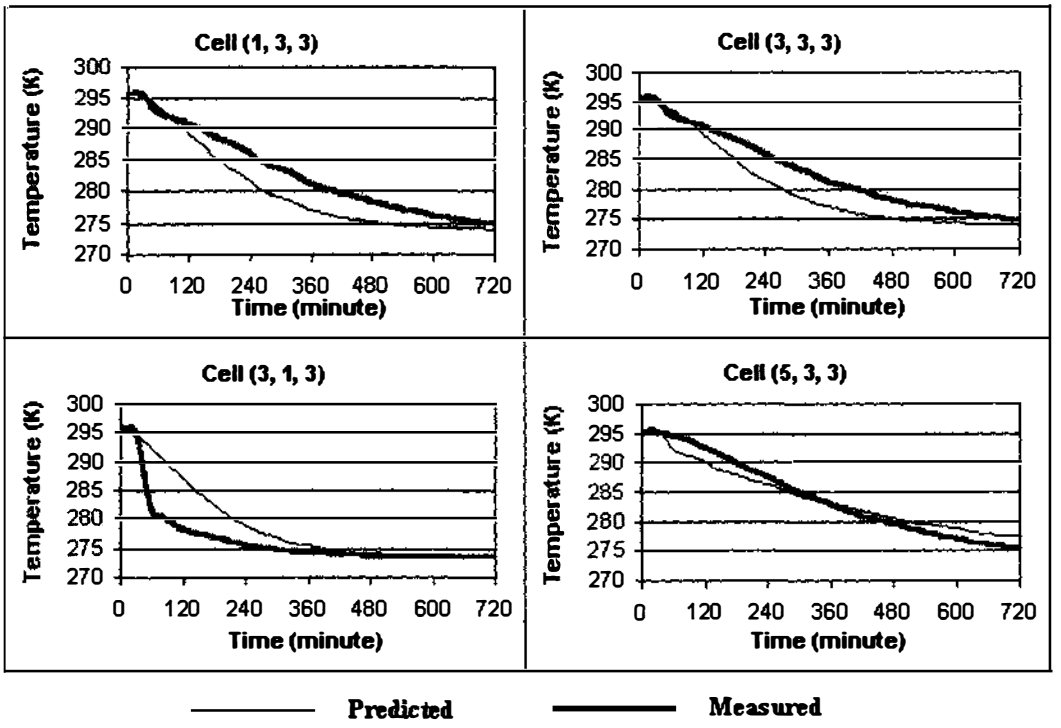

Figure 8.40 Predicted and measured temperature profiles in the centres of produce items in the 3rd layer of Pre-1996 'Standard' 6-layer apple carton during forced-air cooling.

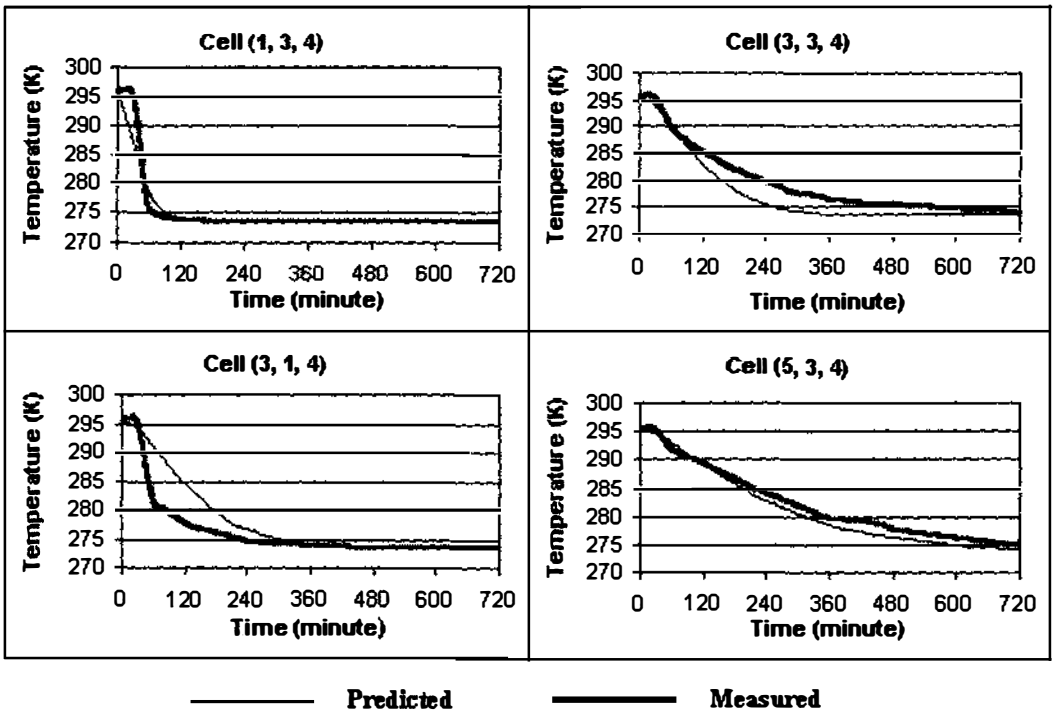

Figure 8.41 Predicted and measured temperature profiles in the centres of produce items in the 4th layer of Pre-1996 'Standard' 6-layer apple carton during forced-air cooling.

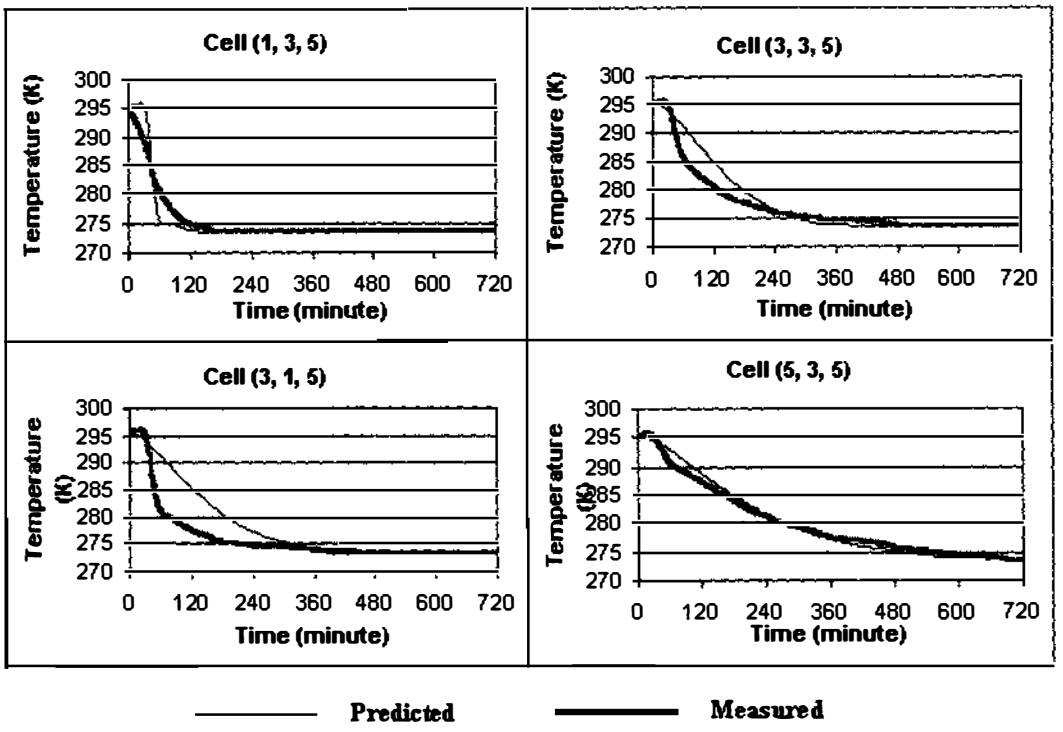

Figure 8.42 Predicted and measured temperature profiles in the centres of produce items in the 5th layer of Pre-1996 'Standard' 6-layer apple carton during forced-air cooling.

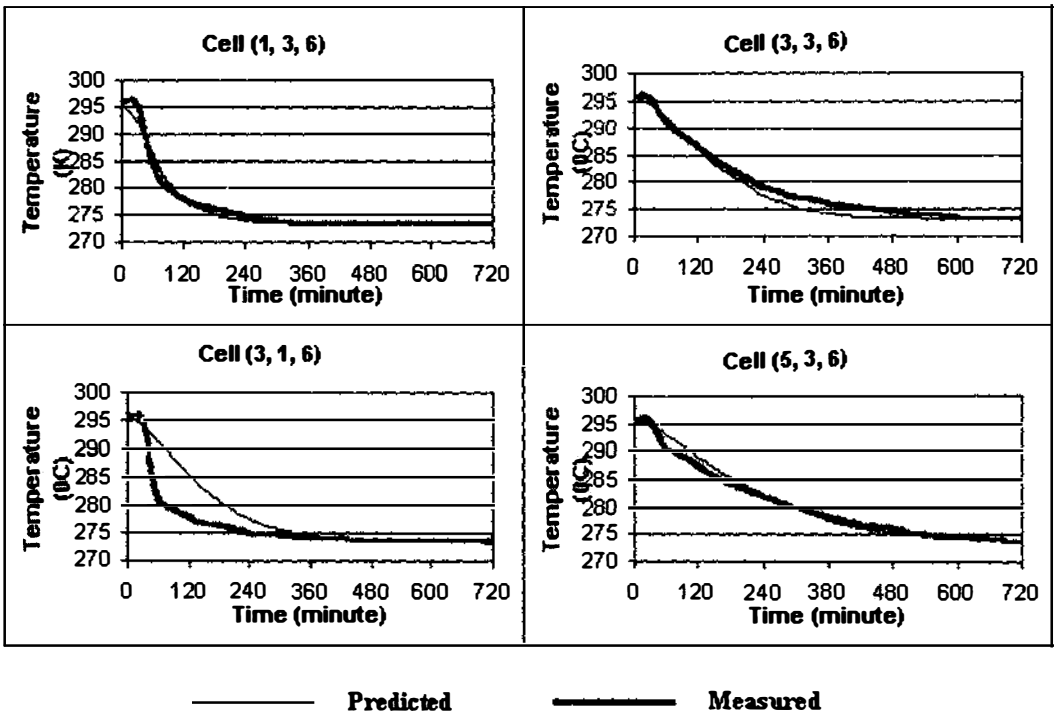

Figure 8.43 Predicted and measured temperature profiles in the centres of produce items in the top layer of Pre-1996 'Standard' 6-layer apple carton during forced-air cooling.

8.2.4 Forced-Air Cooling in A Pallet Layer of Z-Pack apple cartons

- **Packaging system and cooling conditions**

Falconer (Tanner, 1998) conducted experiments on forced-air cooling of apples in a pallet layer of Z-Pack cartons (Figure 8.44). The data for defining the individual package and produce were provided in Table 8.7. Table 8.9 summarises the data for cooling conditions.

Table 8.9 Data of cooling conditions for forced-air cooling of apples in a pallet layer of Z-Pack cartons

Variable	Value
Inlet air velocity (m s^{-1})	1.95
Inlet air temperature (K)	272
Initial air temperature (K)	295
Initial produce temperature (K)	295
External air velocity (m s^{-1})	1.95
Were the vents on two sides of package layer blocked?	Yes

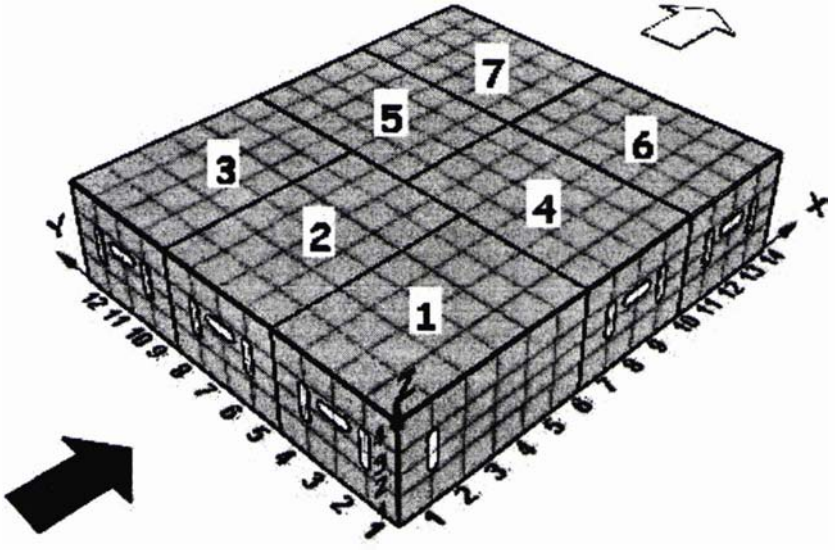

Figure 8.44 Forced-air cooling of apple in a layer of Z-Pack apple cartons.

- **Predicted airflow patterns**

Figures 8.45-8.48 display the airflow patterns and pressure distributions of four produce layers in a pallet layer. The position of these layers was referenced by the indexes shown in Figure 8.44. Similar to the airflow patterns presented in previous sections, the vector arrows represent the average volume flow rates per unit area of the cell surfaces, and different figures used different scales for the vectors.

Comparing the airflow rates in these produce layers, the middle layers that are directly connected to the package inlets and outlets had much larger airflow rates than the top and bottom layers, into which airflow got via the narrow gaps. Similarly the wall effect caused larger airflow rates along the walls than those in the middle.

By comparing pressure distributions among packages, three levels of pressure were found in three rows of packages: ~550 pa for cartons 1-3, ~350 pa for cartons 4-5, and ~150 pa for cartons 6-7. The reason for this pressure distribution pattern is that the main pressure drops occurred in package vents, and the pressure drops within individual packages were less significant.

- **Predicted temperature profiles**

Figures 8.49-8.52 show the predicted air and produce temperature profiles of four produce layers of the pallet layer after 1-hour forced-air cooling. Similar to the forced-air cooling in single package, the produce items in the middle produce layers of the pallet layer were cooled much faster than that in the top and bottom produce layers due to the larger airflow rates, and wall effects caused faster cooling rates along package walls.

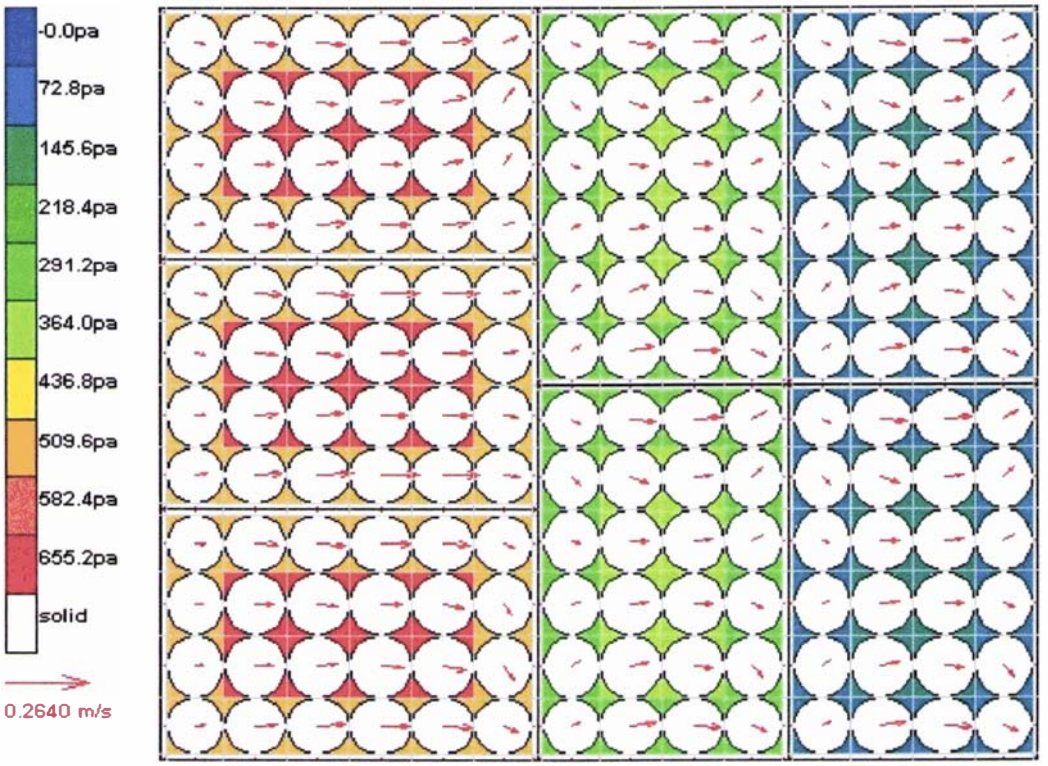

Figure 8.45 Predicted airflow pattern and pressure distribution in the bottom produce layer (XY surface, Z=1) in a pallet layer of Z-Pack apple cartons.

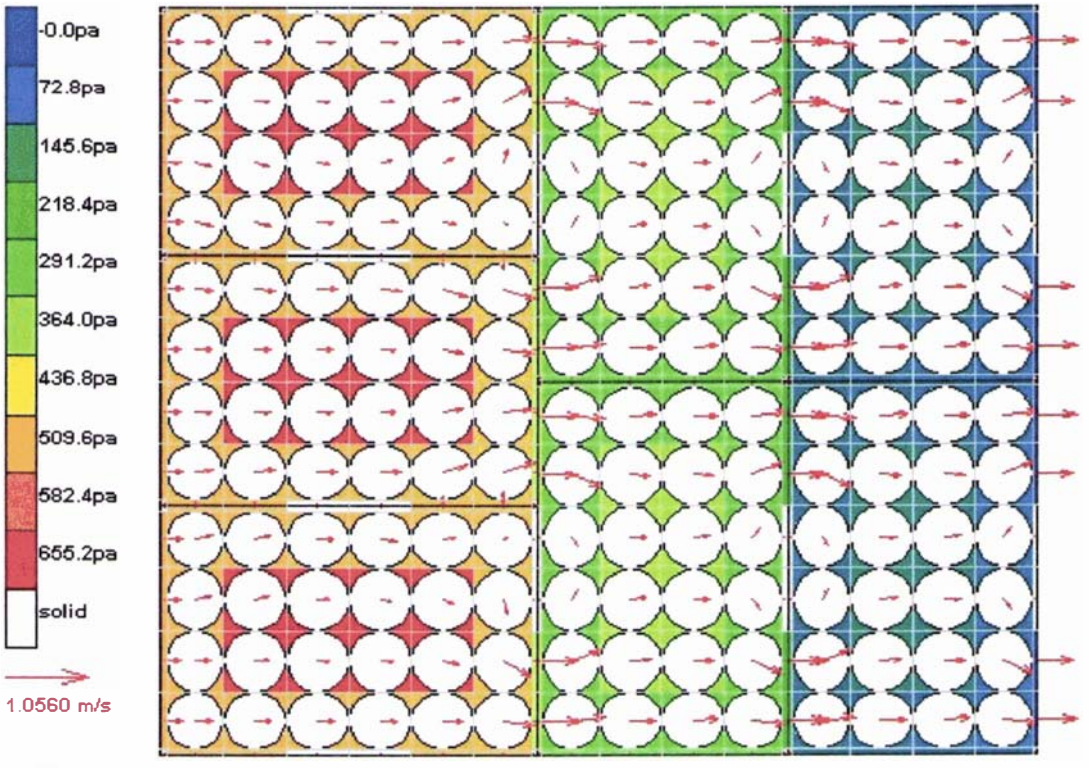

Figure 8.46 Predicted airflow pattern and pressure distribution in the lower middle produce layer (XY surface, Z=2) in a pallet layer of Z-Pack apple cartons.

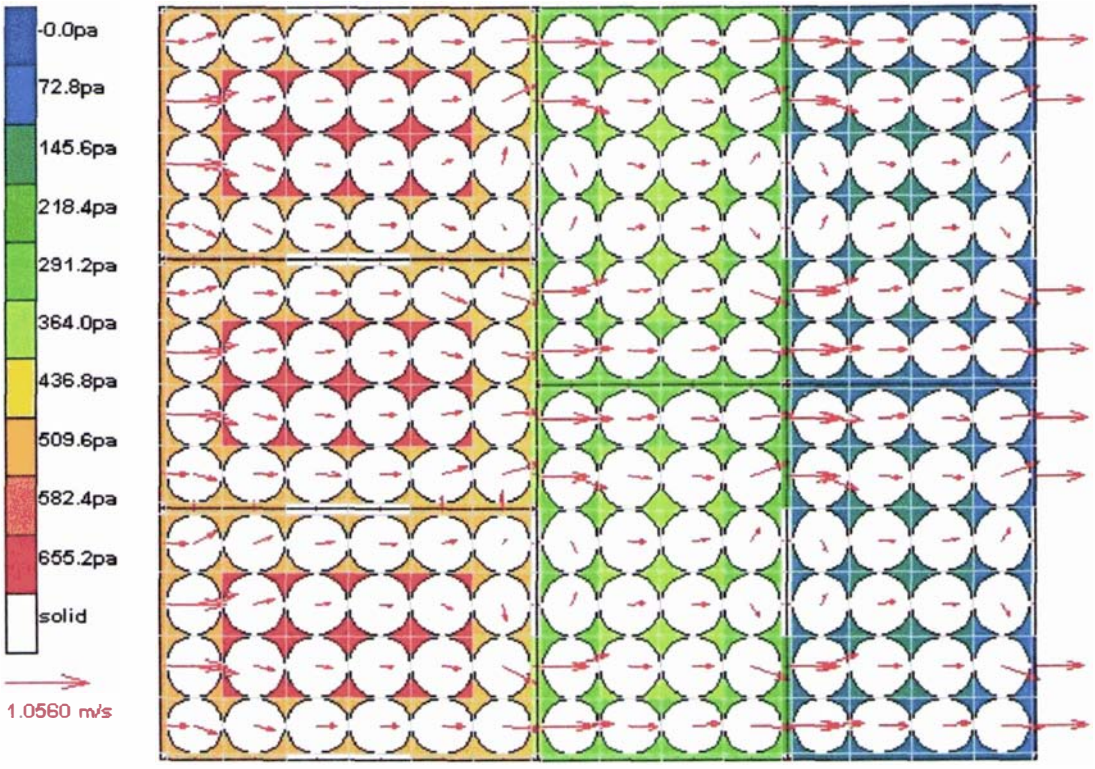

Figure 8.47 Predicted airflow pattern and pressure distribution in the upper middle produce layer (XY surface, Z=3) in a pallet layer of Z-Pack apple cartons.

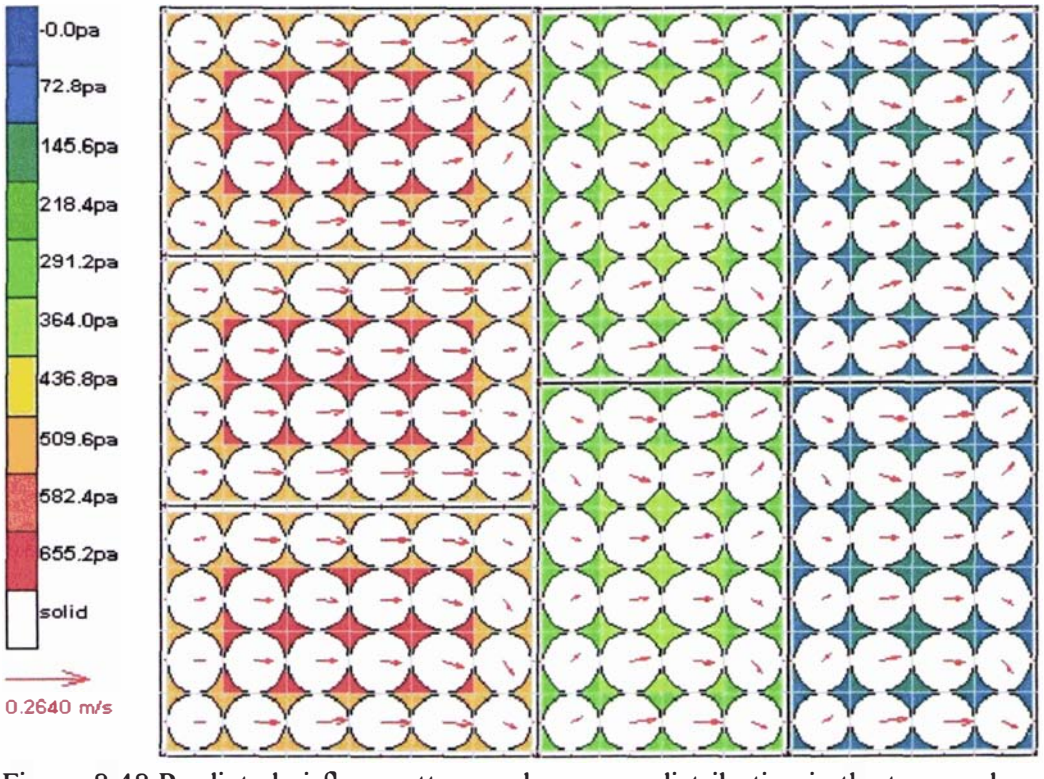

Figure 8.48 Predicted airflow pattern and pressure distribution in the top produce layer (XY surface, Z=4) in a pallet layer of Z-Pack apple cartons.

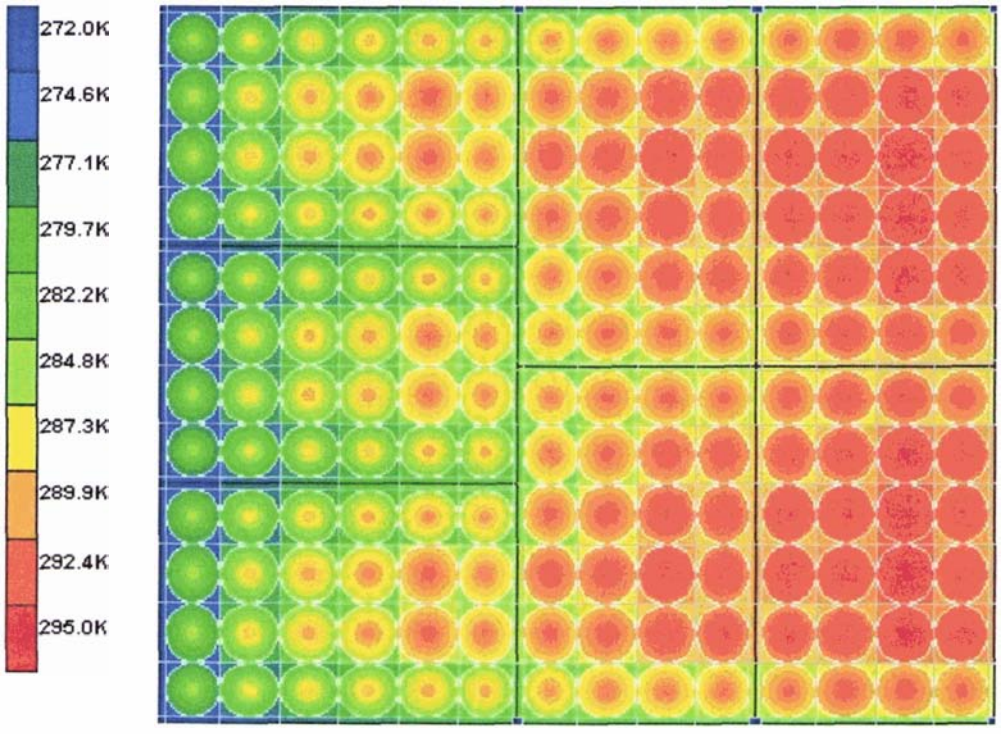

Figure 8.49 Predicted air and produce temperature profile in the bottom produce layer (XY surface, Z=1) in a pallet layer of Z-Pack apple cartons after 1 hour of cooling.

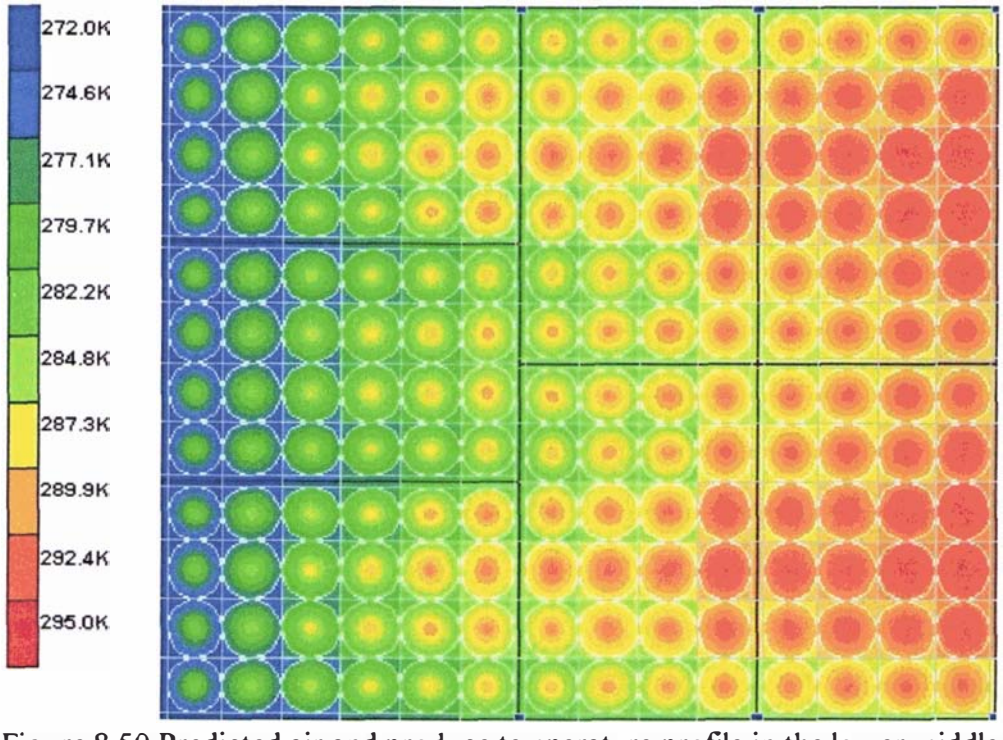

Figure 8.50 Predicted air and produce temperature profile in the lower middle produce layer (XY surface, Z=2) in a pallet layer of Z-Pack apple cartons after 1 hour of cooling.

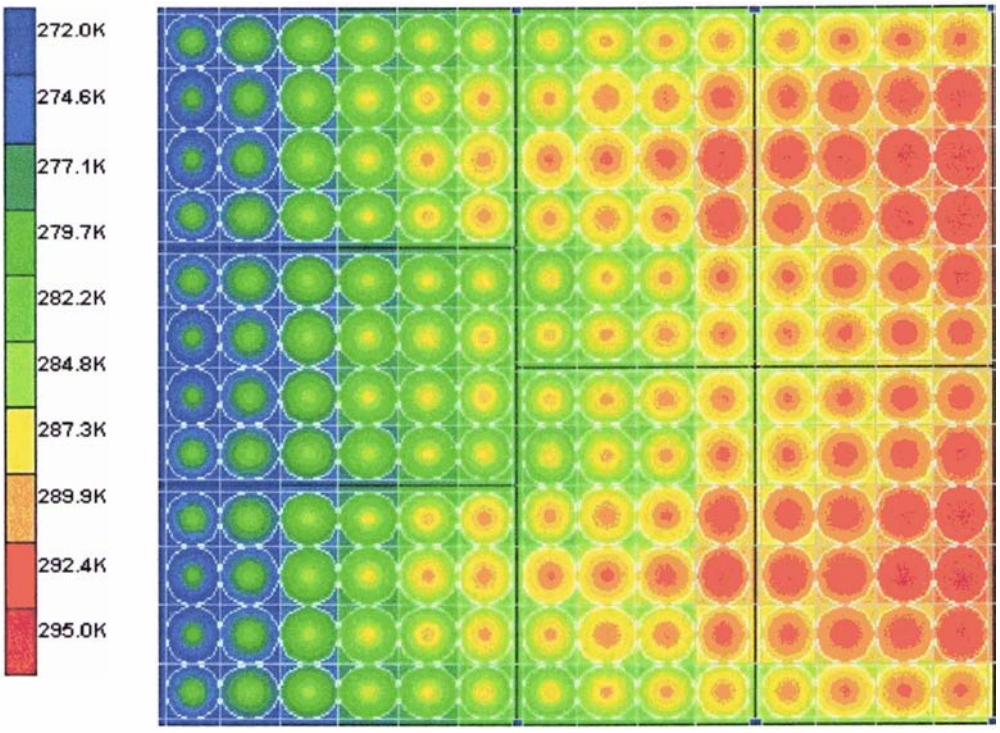

Figure 8.51 Predicted air and produce temperature profile in the upper middle produce layer (XY surface, Z=3) in a pallet layer of Z-Pack apple cartons after 1 hour of cooling.

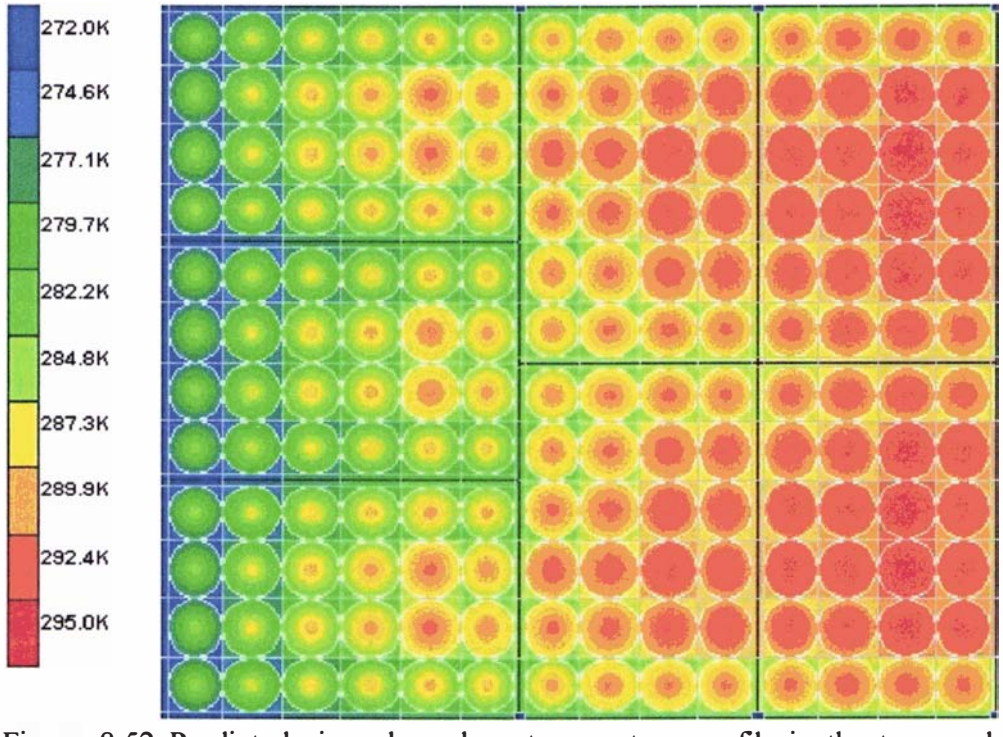

Figure 8.52 Predicted air and produce temperature profile in the top produce layer (XY surface, Z=4) in a pallet layer of Z-Pack apple cartons after 1 hour of cooling.

- **Comparisons between predicted and measured produce cooling rates**

Figures 8.53-8.56 compare the predicted and measured product central temperature in the centres of produce layers in each package of the pallet layer. The measured data were based on Tanner (1998). Due to the symmetric structure of the pallet layer, only the data from four cartons were needed. In general, good agreement between model predictions and experimental data were obtained. In all the positions the differences between the predicted and measured product central temperatures after four hours of cooling are less than 2.5 K. The model accurately predicted the produce cooling rates in the back row of packages, where the differences between the predicted and measured temperature after four hours of cooling were less than 1 K except for cell (12, 3, 2) with a difference of 1.8 K. The model slightly over-predicted the produce cooling rates in the front row of packages, where the predicted temperatures were 1.5-2.5 K lower than the measured ones after four hours of cooling. Lack of fit may be explained by inaccurate positioning of thermocouples or/and inaccurate model input values as discussed in Section 8.2.1.

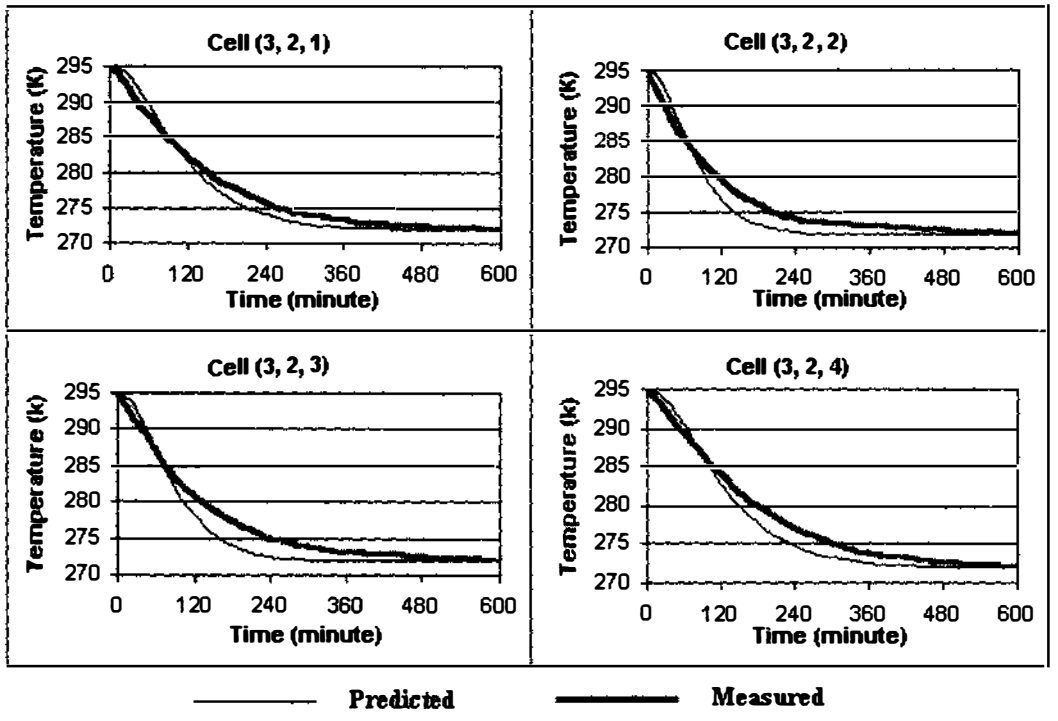

Figure 8.53 Predicted and measured temperature profiles in the centres of produce items in carton 1 of the pallet layer during forced-air cooling.

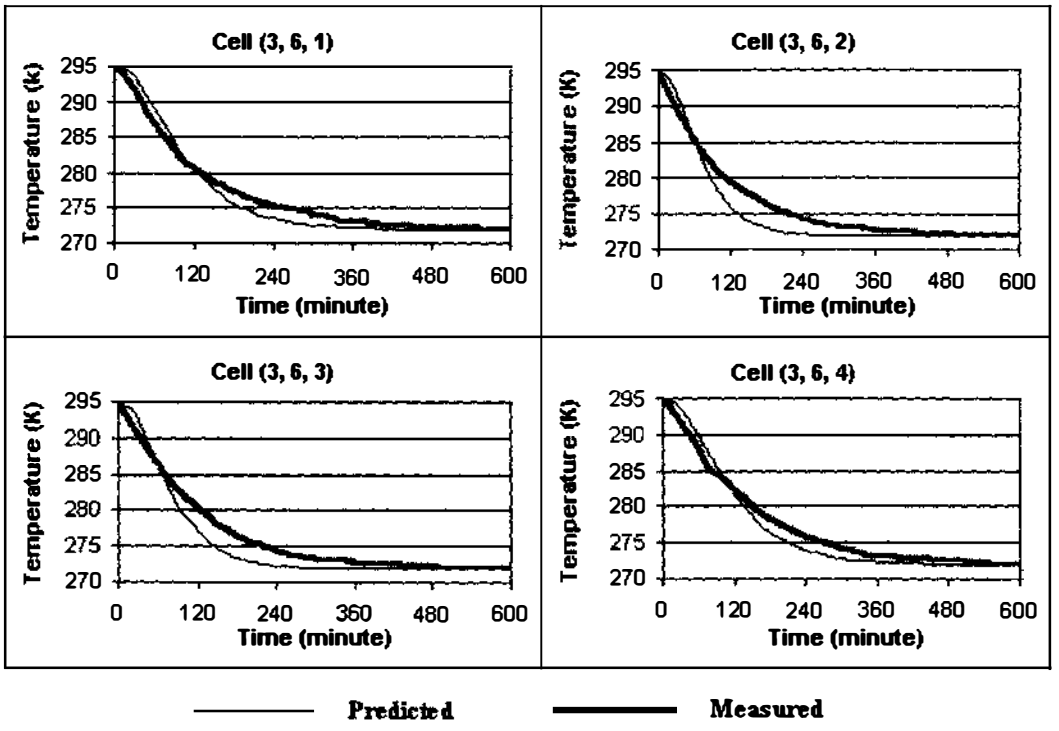

Figure 8.54 Predicted and measured temperature profiles in the centres of produce items in carton 2 the pallet layer during forced-air cooling.

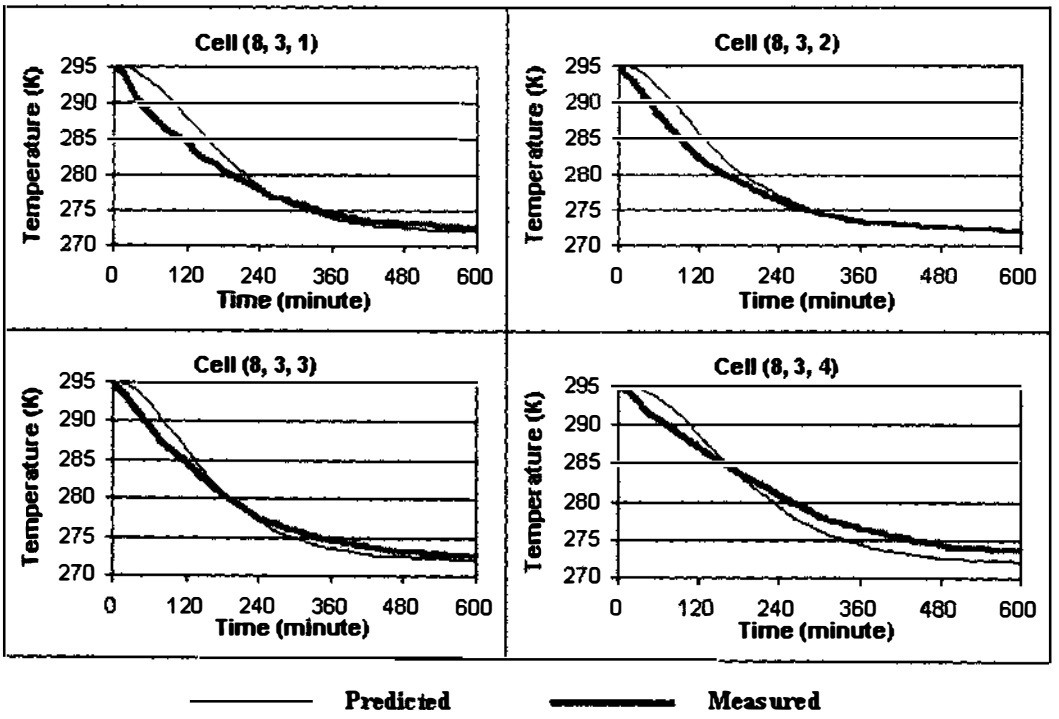

Figure 8.55 Predicted and measured temperature profiles in the centres of produce items in carton 4 of the pallet layer during forced-air cooling.

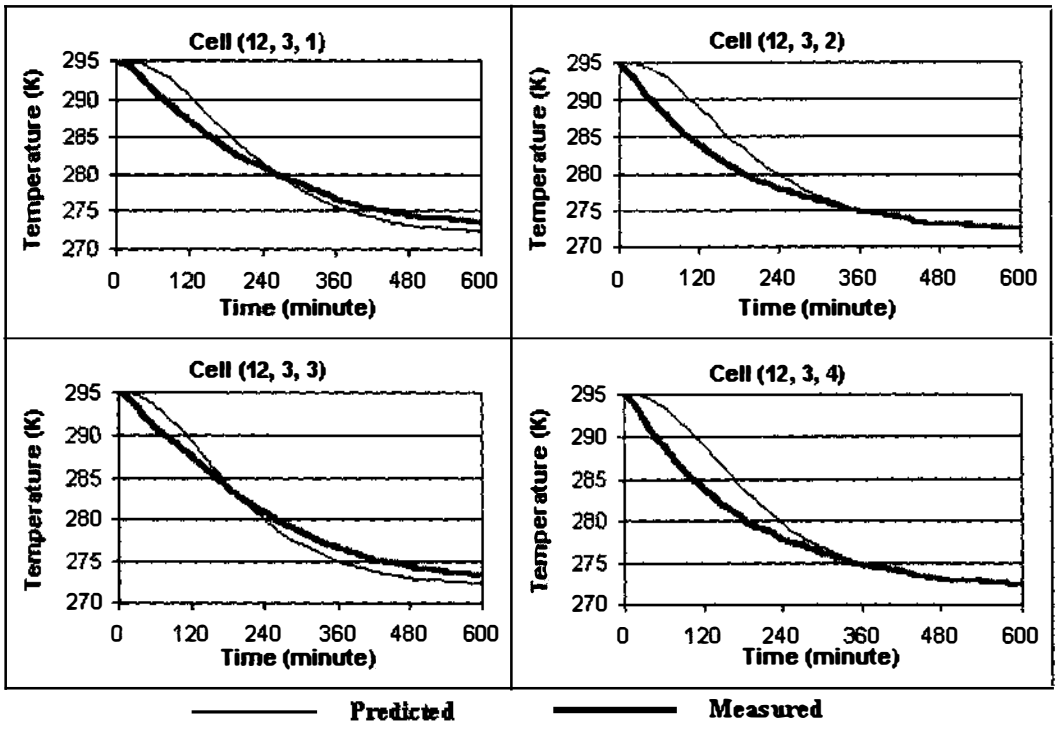

Figure 8.56 Predicted and measured temperature profiles in the centres of produce items in carton 6 of the pallet layer during forced-air cooling.

8.3 Simulation Results of Bulk Packaging System

8.3.1 Forced-Air Cooling in a Pack Bed

- **Packaging system and cooling conditions**

Tanner (1998) conducted experiments on forced-air cooling of apple in a plastic packed bed (Figure 8.57). The package was constructed with plastic materials for sidewalls and coarse wire mesh for front and back walls. 'BraeBurn' variety apples were randomly packed in the package. Table 8.10 summarises the data for defining the packaging system and cooling conditions.

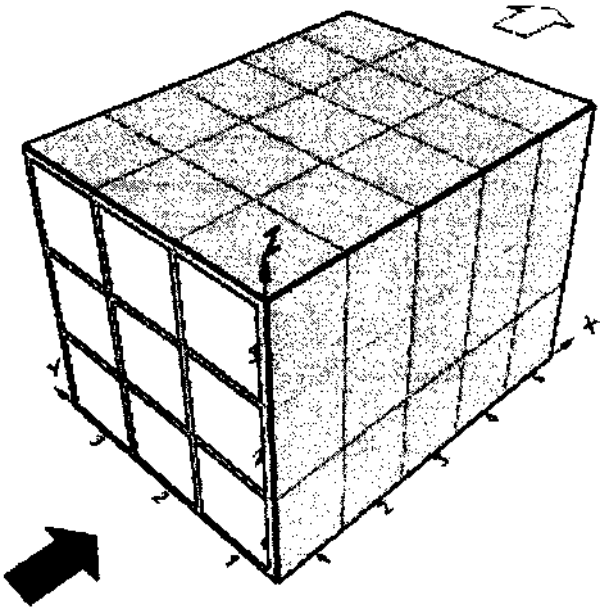

Figure 8.57 Forced-air cooling of apple in a package bed.

- **Predicted airflow patterns**

Figures 8.58-59 show the predicted airflow patterns and pressure distributions in the top, bottom, and middle layers of the package bed. The positions of these layers were referenced by the indexes shown in Figure 8.57. Due to the symmetric structure of the airflow, only two figures were needed. The predicted airflow was very close to one-dimensional uniform flow, and the airflow rates along the package walls were only slightly higher that those in the middle because of the wall effect.

- **Predicted temperature profiles**

Figures 8.60-8.61 show the predicted air and produce temperature in the top, bottom, and middle layers of the package bed after 40-minutes forced-air cooling. Corresponding to the predicted near-to-uniform airflow pattern, the temperature distributions along the plane normal to the flow direction were almost identical.

Table 8.10 Data of packaging system and cooling conditions for force-air cooling of apple in a packed bed.

Variable	**Value**
Produce item	
Density (kg m^{-3})	830
Thermal conductivity (W m^{-1} K^{-1})	0.42
Specific heat capacity (J kg^{-1} K^{-1})	3650
Volume (m^3)	0.0002241
Surface are (m^2)	0.0188826
Individual package	
Length (m)	0.32
Width (m)	0.24
Height (m)	0.24
Number of produce item	47
Package walls	
Density (kg m^{-3})	540
Thermal conductivity (W m^{-1} K^{-1})	0.12
Specific heat capacity(J kg^{-1} K^{-1})	1800
Thickness of side walls (m)	0.004
Thickness of top wall (m)	0.004
Thickness of bottom wall (m)	0.0038
Cooling conditions	
Inlet air velocity (m s^{-1})	0.5
Inlet air temperature (K)	272
Initial air temperature (K)	300
Initial produce temperature (K)	300
External air velocity (m s^{-1})	0.5

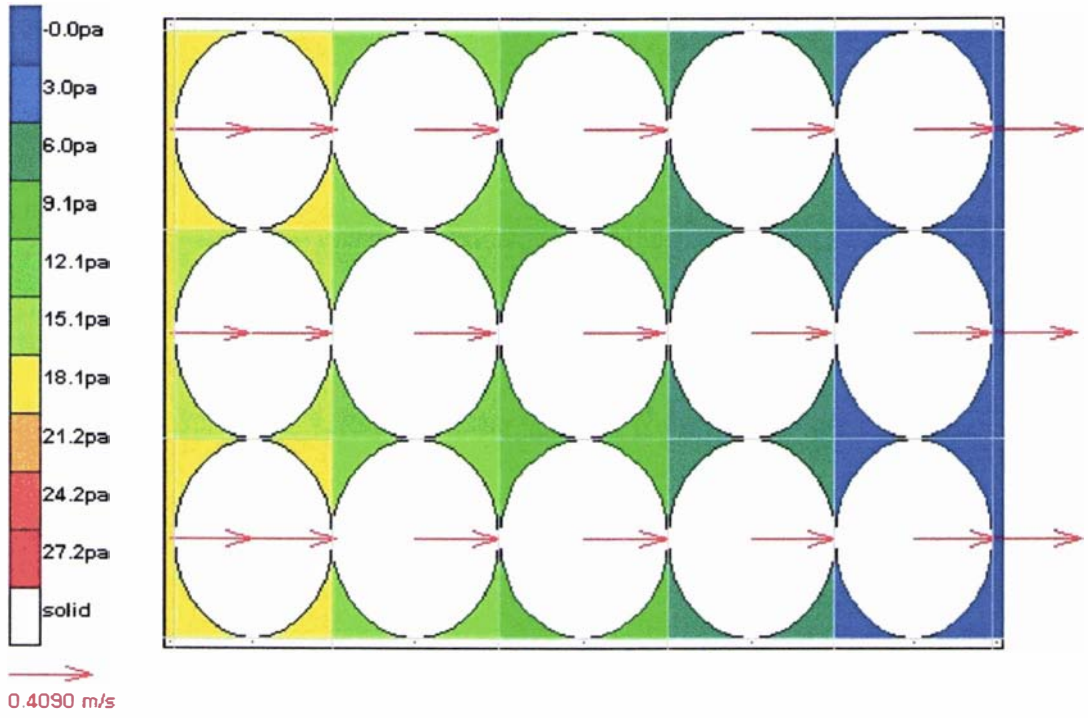

Figure 8.58 Predicted airflow pattern and pressure distribution in the top or bottom layer of a packed apple bed (XY surface, Z=1 or 3)

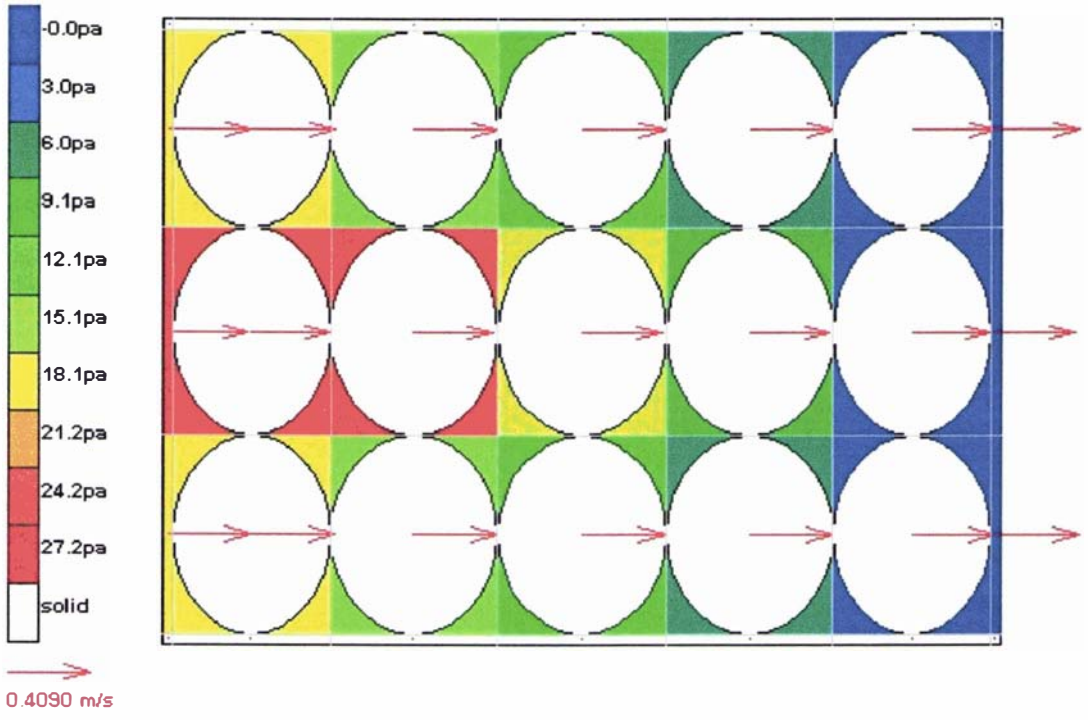

Figure 8.59 Predicted airflow pattern and pressure distribution in the middle layer of a packed apple bed (XY surface, Z=2)

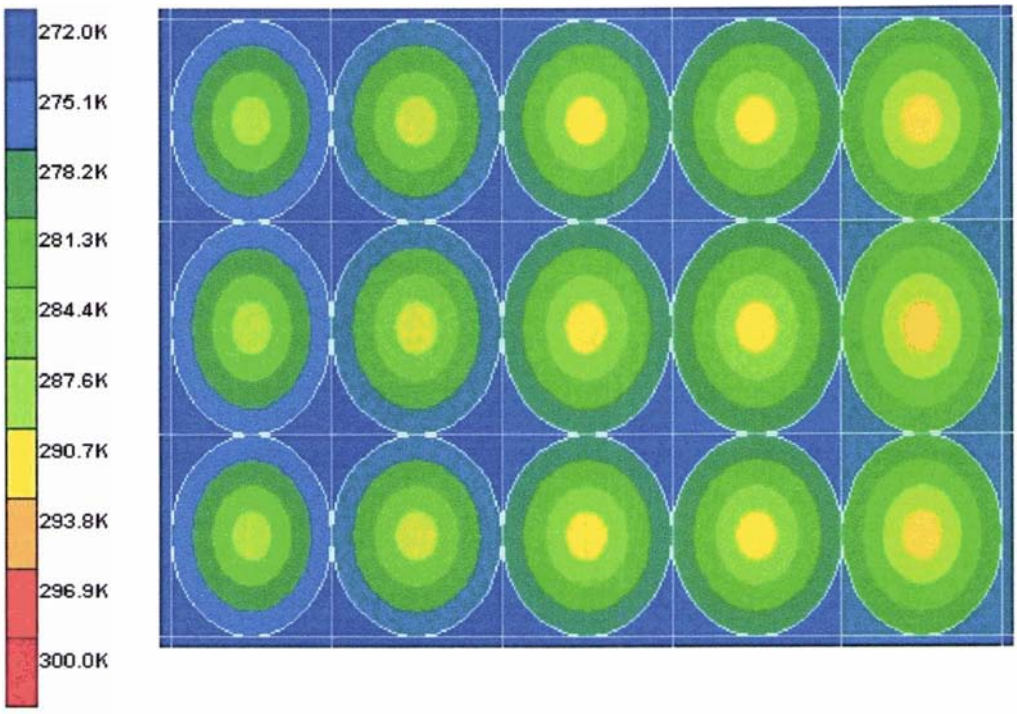

Figure 8.60 Predicted air and produce temperature profile in the bottom or top layer of a packed apple bed (XY surface, Z=1 or 3) after 40 minutes of cooling

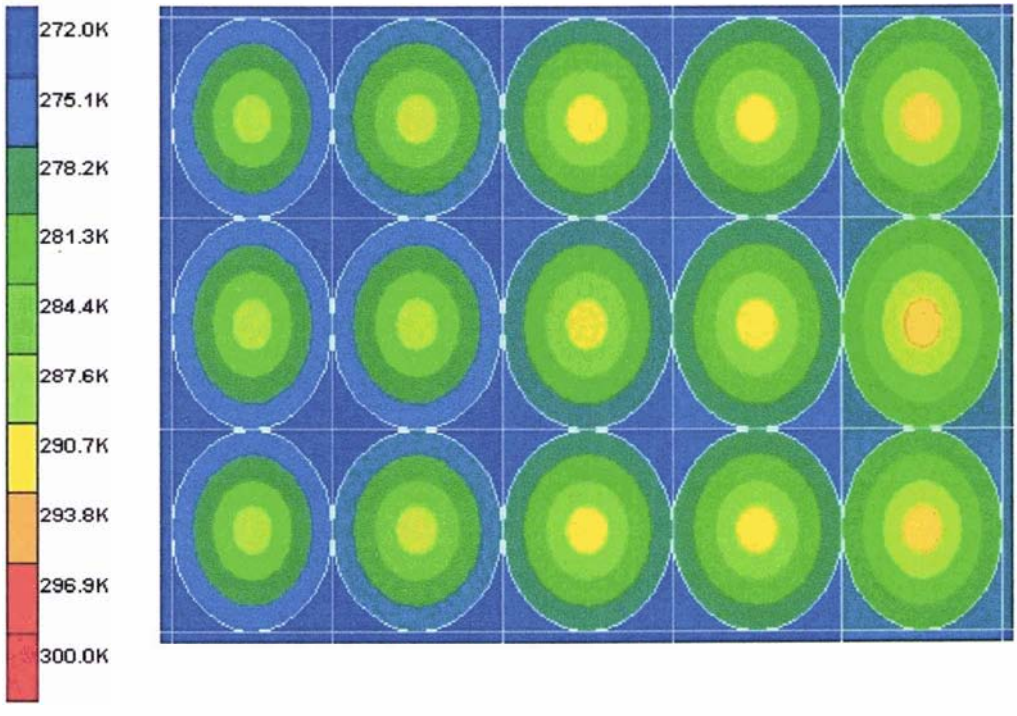

Figure 8.61 Predicted air and produce temperature profile in the middle layer of a packed apple bed (XY surface, Z=2) after 40 minutes of cooling

- **Comparisons between predicted and measured produce cooling rates**

Figure 8.62 compares the predicted product central cooling rate in the centre of the packed bed with the experimental data reported by Tanner (1998). In the initial and middle cooling stages the model under-predicted the cooling rate in produce item centre, and in the late cooling stage the predicted and measured temperature variations agreed well. The lack of fit in the initial and middle cooling stages may be attributed to ~~the~~ experimental errors. For instance, the thermocouple might not be positioned in the centre of produce item.

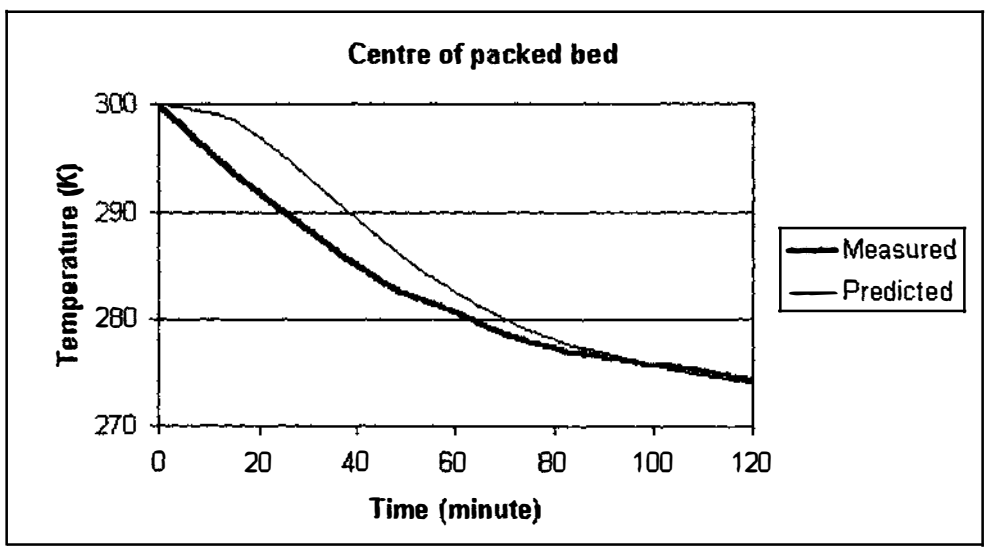

Figure 8.62 Predicted and measured temperature profile of produce item centre in the centre of the packed bed during forced-air cooling.

8.4 Summary

This chapter presented the predictions generated by the airflow and heat transfer models for the forced-air cooling of produce in several layered and bulk packaging systems. The simulation results were visualised in forms of vector graphs and coloured contours. In general the predicted cooling rates at produce centres agreed well with the experimental data extracted from literature, and the differences between model predictions and measured data may be attributed to inaccurate temperature measurement and model input data.

CHAPTER 9
CONCLUSION

9.1 Conclusion

Airflow and heat transfer models in bulk and layered packaging systems have been developed based on a porous media approach. The areas inside the packaging systems were categorised as solid, plain air, and produce-air regions. The produce-air regions inside the bulk packages or between trays in the layered packages were treated as porous media, in which volume-averaged transport equations were employed. This approach avoids dealing with the situation-specific and complex geometries inside the packaging systems, and therefore facilitates the development of a general modelling system suitable for a wide range of packaging designs, produce types and stacking arrangement inside coolstores.

The calculation domains were discretised with a block-structured meshing system that was referenced by both global and local grid systems. The global grid system specifies the positions of individual packages in a stack, and the local grid system describes the structural details inside individual packages. The block-structured meshing system is able to use a relatively coarse mesh to represent the geometric details of the packaging systems. The solution methods for airflow models were based on the SIMPLER schemes (Patankar, 1980). Staggered grid systems were adopted. Each scalar or momentum cell was classified according to which region it belongs to and which region it is adjacent to. Over each type of momentum cell, a momentum discretisation equation was derived. Over each type of scalar cell, a pressure correction discretisation equation and pressure discretisation equation were obtained. The solid and air energy discretisation equations for the heat transfer models were derived over scalar cells in the same way as that for the airflow models. The systems of discretisation equations were solved by iteration, and in each iteration the systems of linear algebraic equations were solved using GMRES method.

Based on the solution methods of the airflow and heat transfer models, a software package 'CoolSimu' was developed. The software package hid the core components (airflow and heat solvers) from the user, so that users without any knowledge of CFD

and heat transfer modelling can utilise the software to study cooling operations and thermal performance of package designs. The user interaction components in CoolSimu enable the software user to specify packaging systems and cooling conditions, control the simulation processes, and visualise the predicted airflow patterns and temperature profiles.

Model validation was carried out by comparing the predicted and measured product centre temperatures during the forced-air cooling of produce in several layered and bulk packaging systems. In general, good agreements between the model predictions and experimental data were obtained, and the lack of fit in certain locations of the packaging systems may be attributed to inaccurate temperature measurement and uncertainties in model input data.

Overall, the developed CFD modelling system is able to simulate airflow and heat transfer processes, and therefore predict airflow patterns and temperature profiles with satisfactory accuracy in the layered and bulk packaging systems during the forced-air cooling of various fresh produce.

9.2 Future Research

The modelling system may be improved further by undertaking the following research activities:

- Test and validate airflow models with measured airflow rates or velocities. In this study the airflow models were indirectly validated based on temperature measurements. By directly comparing the predicted and measured airflow data, the airflow models may be improved by modifying certain empirical constants in the volume-averaged transport equations.

- Test and debug the software package 'CoolSimu' using a larger number of packaging designs and under a wide range of cooling conditions. This will facilitate the adoption of the software for industrial applications and as an extension tool in postharvest horticulture.

REFERENCES

Abdul Majeed, P.M., Murthy, S.S. & Murthy, M.V. (1980). Prediction of air cooling characteristics of moist food products. *Transactions of the ASEA,* **23:** 788-792.

Abrams, C.F. & Fish, J.D. (1982). Airflow resistance characteristics of bulk piled sweet potatoes. *Transactions of the ASAE*, **25:** 1103-1106.

Amiri, A. & Vafai, K. (1994). Analysis of dispersion effects and non-thermal equilibrium, non-Darcian, variable porosity incompressible flow through porous media. *International Journal of Heat and Mass Transfer*, **37:** 939-954.

Amiri, A. & Vafai, K. (1998). Transient analysis of incompressible flow through a pecked bed. *International Journal of Heat and Mass Transfer*, **41:** 4259-4279.

Amos, N.D. (1995). *Mathematical modelling of heat transfer and water vapour transport in apple coolstore.* PhD Thesis, Massey University, Palmerston North, New Zealand.

Anderson, D.A., Tannehill, J.C. & Pletcher, R.H. (1984). *Computational Fluid Mechanics and Heat Transfer*. Hemisphere, New York.

Anotohe, B.V. & Lage, J.L. (1997). A general two-equation macroscopic turbulence model for incompressible flow in porous media. *International Journal of Heat and Mass Transfer*, **40:** 3013-3024.

Ansari, F.A., Charan, V. & Varma, H.K. (1984). Heat and mass transfer analysis in air-cooling of spherical food products. *International Journal of Refrigeration,* **7:** 194-197.

Arthur, J.F. & Rumsey, T.R. (1991). Two-dimensional drying model for stationary bin walnut dryers. *Transactions of the ASAE,* **34:** 193-200.

ASHRAE. (1993). *ASHRAE handbook - fundamentals*. American Society of Refrigeration and Air Conditioning Engineers Publishers, Atlanta, Ga.

ASHRAE. (1994). *ASHRAE handbook - Refrigeration.* American Society of Refrigeration and Air Conditioning Engineers Publishers, Atlanta, Ga.

Awbi, H.B. (1989). Application of computational fluid dynamics in room ventilation. *Building and Environment*, **24:** 73-84.

Baird, C.D. & Gaffney, J.J. (1976). A numerical procedure for calculating heat transfer in bulk loads of fruits and vegetables. *ASHRAE Transactions,* **82:** 525-540.

Baird, C.D., Chau, K.V. & Gaffney, J.J. (1985). Engineering/economic model for evaluating forced-air cooling systems for fruit and vegetables. *Refrigeration. Science & Technology*, **1985-5:** 259-266.

Bakker-Arkema, F.W. & Bickert, W.G. (1966). A deep-bed computational cooling produce for biological products. *Transactions of the ASAE,* **9:** 834-836, 845.

Bakker-Arkema, F.W., Bickert, W.G. & Patterso, R.J. (1966). Simultaneous heat and mass transfer during the cooling of a deep bed of biological products under varying inlet air conditions. *Journal of Agricultural Engineering Research,* **12:** 297-307.

Bazan, T., Chau, K.V. & Baird, C.D. (1989). Heat transfer simulation of the bulk cooling of fruits. *ASAE Paper No. 89559.*

Bear, J. & Bachmat, Y. (1984). Transport phenomena in porous media – basic equation. In *Fundamental of Transport Phenomena in Porous Media*, Bear, J. & Corapcioglu, M.Y., eds. Martinus Nijhoff Publishers, Dordrecht.

Bear, J. & Bachmat, Y. (1990). *Introduction to Modelling Transport Phenomena in Porous Media*. Kluwer Academic, Dordrecht, the Nerthlands.

Beckermann, C., Ramadhyani, S. & Viskanta, R. (1987). Natural convection flow and heat transfer between a fluid layer and a porous layer inside a rectangular enclosure. *ASEM Journal of Heat Transfer*, **109:** 363-370.

Benenati, R.F. & Brosilow, C.B. (1962). Void fraction distribution in beds of spheres. *A.I.Ch.E. Journal*, **8:** 359-361.

Bird, R.B., Stewart, W.Z. & Lightfoot, Z.N. (1960). *Transport Phenomena.* Wiley, New York.

Bottcher, R.W. (1987). Numerical calculation of flow driven by a ceiling fan. *Transaction of the ASAE,* **30:** 476-484.

Bourlard, T., Papadakis, G., Kittas, C. & Mermier, M. (1997). Air flow and associated sensible heat exchanges in a naturally ventilated greenhouse. *Agricultural and Forest Meteorology,* **88:** 111-119.

Bradshaw, P. (1970). *Experimental Fluid Mechanics* (2nd Ed.). Pergaman Press, Oxford.

Brooker, D.B. (1969). Computing air pressure and velocity distribution when air flows through a porous medium and non-linear velocity-pressure relationships exist. *Transactions of the ASAE*, **12:** 118-120.

Brooker, D.B., Bakker-Arkema, F.W. & Hall, C.W. (1992). *Drying and Storage of Grains and Oilseeds.* Van Nostrand Reinhold, New York.

Cardonell, R.G. & Whitaker, S. (1984). Heat and mass transfer in porous media. In *Fundamental of Transport Phenomena in Porous Media*, Bear, J. & Corapcioglu, M.Y., eds. Martinus Nijhoff Publishers, Dordrecht.

CHAM. (1995). *PHOENICS On-line Information System. PHOENICS 2.2.* CHAM Ltd., London.

Chang, W. & Chang, W. (1996). Mixed convection in a vertical parallel-plate channel partially filled with porous media of high permeability. *International Journal of Heat and Mass Transfer*, **39:** 1331-1342.

Chapman, J.E., Vance Morey, R., Cloud, H.A. & J.L., Nieber. (1989). Airflow patterns in flat storage aeration systems. *Transactions of the ASAE,* **32:** 1368-1376.

Chau, K.V. & Gaffney, J.J. (1990). A finite-difference model for heat and mass transfer in products with internal heat generation and transpiration. *Transactions of the ASAE*, **33:** 484-487.

Chau, K.V., Gaffney, J.J. & Romero, R.A. (1988a). A mathematical model for the transpiration from fruits and vegetables. *ASHRAE Transactions,* **94:** 1541-1552.

Chau, K.V., Gaffney, J.J., Baird, C.D. & Church, G.A. (1985). Resistance of airflow of oranges in bulk and in cartons. *Transaction of the ASAE*, **28:** 2083-2088.

Chau, K.V., Romero, R.A., Baird, C.D. & Gaffney, J.J., & (1988b). Transpiration coefficients from certain fruits and vegetables. *ASHRAE Transactions,* **94:** 1553-1563.

Chauk, S.S. & Fan, L. (1998). Heat transfer in packed and fluidized beds. In *Handbook of Heat Transfer*, Rohsenow, W.M., Hartnett, J.P. & Cho, Y.I., eds. McGraw-Hill, New York.

Chen, C., Chen, T.S. & Chen, C. (1996). Non-Darcy Mixed convection along nonisothermal vertical surfaces in porous media. *International Journal of Heat and Mass Transfer*, **39:** 1157-1164.

Chen, Q., Moser, A. & Huber, A. (1990). Prediction of bounce, turbulent flow by a low-Reynolds-number k-ε model. *ASHRAE Transactions*, **96:** 564-573.

Cheng, P. (1985). Geothermal heat transfer. In *Handbook of Heat Transfer Applications* (2nd Ed), Rohsenow, W.M., Hartnett, J.P., and Ganic, E.N., eds. McGraw-Hill, New York.

Cheng, P. & Hsu, C.T. (1985). Fully-developed, forced convective flow through an annular packed-sphere bed with wall effects. *International Journal of Heat and Mass Transfer*, **29:** 1843-1853.

Cheng, P. & Zhu, H. (1987). Effects of radial thermal dispersion on f-developed, forced convection in cylindrical packed tubes. *International Journal of Heat and Mass Transfer*, **31:** 2373-2383.

Cheng, P., Hsu, C.T. & Chowdhury, A. (1988). Forced convection in the entrance region of a packed channel with asymmetric heating. *ASME Journal of Heat Transfer*, **110:** 946-954.

Cheremisinoff, N.P & Cheremissionoff, P.N. (1988). *Flow Measurement for Engineers and Scientists*. Marcel Dekker., New York.

Choi, H.L., Albright, L.D. & Timmons, M.B. (1990). An application of the K-ε turbulence model to predict how a rectangular obstacle in a slot-ventilated enclosure affects airflow. *Transactions of the ASAE*, **33:** 274-281.

Choi, H.L., Albright, L.D., Timmons, M.B. & Warhaft, Z. (1988). An application of the K-Epsilon turbulence model to predict air distribution in a slot-ventilated enclosure. *Transactions of the ASAE*, **31:** 1804-1814.

Chow, W.K. & Fung, W.Y. (1996). Numerical studies on the indoor air flow in the occupied zone of ventilated and air-conditioned space. *Building and Environment,* **3:** 319-344.

Clary, B.L., Nelson, G.L. & Smith, R.E. (1968). Heat transfer from hams during freezing by low temperature air. *Transactions of the ASAE,* **11:** 496-499.

Clary, B.L., Nelson, G.L. & Smith, R.E. (1971). Application of geometry analysis technique in determining the heat transfer rate from biological materials. *Transactions of the ASAE,* **14:** 586-589.

Clayton, M., Amos, N.D., Banks, N.H. & Morton, R.H. (1995). Estimation of apple fruit area. *New Zealand Journal of Crop and Horticultural Science*, **23**: 345-349.

Cleland, A.C. (1983). Simulation of industrial refrigeration plants under variable load conditions, *International Journal of Refrigeration,* **6:** 11-19.

Cleland, A.C. (1985a). Experimental verification of a mathematical model for simulation of industrial refrigeration plants, *International Journal of Refrigeration,* **8:** 275-282.

Cleland, A.C. (1985b). RADS- a computer package for refrigeration analysis, design and simulation, *International Journal of Refrigeration,* **8:** 372-374.

Cleland, A.C. (1990*). Food Refrigeration Processes - Analysis, Design and Simulation.* Elsevier Science Publishers, London.

Cleland, A.C. & Earle, R.L. (1982). A simple method for prediction of heating and cooling rates in solids of various shapes. *International Journal of Refrigeration*, **5:** 98-106.

Cleland, D.J. & Cleland, A.C. (1989). Appropriate level of model complexity in dynamic simulation of refrigeration systems. *Refrigeration. Science. & Technology*, **1989-1:** 261-268.

Cleland, D.J., Boyd, N.S. & Cleland, A.C. (1982). A model for fish freezing and storage on aboard small New Zealand fishing vessels, *Refrigeration. Science. & Technology*, **1982-1:** 147-156.

Collins, M.W. & Ciofalo, M. (1991). Computational fluid dynamics and its application to transport processes. *Journal of Chemical Technology and Biotechnology,* **52**: 5-47.

Comini, G., Cortella, G. & Saro, O. (1995). Finite element analysis of coupled conduction and convection in refrigerated transport. *International Journal of Refrigeration*, **18:** 123-131.

Comiti, J. & Renaud, M. (1989). A new model for determining mean structure parameters of fixed beds from pressure drop measurements: application to beds packed with parallelepipedal particles. *Chemical Engineering Since*, **44:** 1539-1545.

Conner, J.J. & Brebbia, C.A. (1976). *Finite element techniques for fluid flow.* Newnes-Butterworths, London.

Dossat, R.J. (1980). *Principles of refrigeration* (2nd Ed). Wiley, New York.

Dullien, F.A.L. (1979). *Porous Media: Fluid Transport and Pore Structure.* Academic Press, New York.

Dybbs, A. & Edward, R.E. (1984). A new look at porous media Fluid Mechanics – Darcy to Turbulent. In *Fundamental of Transport Phenomena in Porous Media*, Bear, J. & Corapcioglu, M.Y., eds Martinus Nijhoff Publishers, Dordrecht.

Enterprise New Zealand Trust. (1993). *The New Zealand Apple and Pear Industry.* Wellington, New Zealand.

ENZA New Zealand (International). (1996). *Palletised Packaging System Information Pack.* Wellington, New Zealand.

Ergun, S. (1952). Fluid flow through packed columns. *Chemical Engineering Progresses*, **48:** 89-94.

Fand, R.M., Steinberger, T.E. & Cheng, P. (1986). Natural convection heat transfer from a horizontal cylinder embedded in a porous medium. *International Journal of Heat and Mass Transfer*, **29:** 119-133.

Ferziger, J.H. (1998). *Numerical Methods For Engineering Application* (2nd Ed). John Wiley & Sons, New York.

Ferziger, J.H. & Peric, M. (1999). *Computational Methods for Fluid Dynamics.* Springer-Verlag, New York.

Feustel, H.E. & Dieris, J. (1992). A survey of airflow models for multi-zone structures. *Energy and Buildings,* **18:** 79-100.

Fingerson, L.M. & Freymuth, P. (1983). Thermal anemometer. In *Fluid Mechanics measurement,* Goldstein, R.J., ed. Hemisphere Publishing Corporation, Washington.

Fletcher, C.A.J. (1988a). *Computational Techniques for Fluid Dynamics. Volume I, Fundamental and General Techniques.* Springer-Verlag New York.

Fletcher, C.A.J. (1988b). *Computational Techniques for Fluid Dynamics. Volume II, Specific Techniques for Different Flow Categories.* Springer-Verlag, New York.

Focken, F.H. & Meffert, H.F.T. (1972). Biophysical properties of horticultural products as related to loss of moisture during cooling down. *Journal of Science of Food and Agriculture,* **23:** 285-298.

Fu, W. & Huang, H. (1997). Thermal performances of different shape porous blocks under an impinging jet. *International Journal of Heat and Mass Transfer*, **40:** 2261-2272.

Fu, W. & Huang, H. (1999). Effects of a random porosity model on heat transfer performance of porous media. *International Journal of Heat and Mass Transfer*, **42:** 13-25.

Fu, W., Huang, H. & Liou, W. (1996). Thermal enhancement in laminar channel flow with a porous block. *International Journal of Heat and Mass Transfer*, **39:** 2165-2175.

Gaffney, J.J., Baird, C.D. & Chau, K.V. (1985a). Influence of airflow rate, respiration, evaporative cooling, and other factors affecting weight loss calculations for fruits and vegetables. *ASHRAE transactions,* **91(1B):** 690-707.

Gaffney, J.J., Baird, C.D. & Chau, K.V. (1985b). Methods for calculating heat and mass transfer in fruits and vegetables individually and in bulk. *ASHRAE transactions,* **91(1B):** 333-352.

Gan, G. & Woods, J.L. (1989). A deep bed simulation of vegetable cooling. *Proceedings of the Eleventh International Congress of Agricultural Engineering,* Dublin. Rotterdam, Netherlands. pp. 2301-2308.

Geankoplis, C.J. (1993). *Transport processes and unit operations* (3rd Ed.) Allyn & Bacon, Boston.

Goldstein, R.J. (1983). Optical systems for flow measurement: shadowgraph, schlieren, and interferometric techniques. In *Fluid Mechanics measurement*, Goldstein, R.J., ed. Hemisphere Publishing Corporation, Washington.

Gosman, A.D., Nielsen, P.V., Restivo, A. & Whitelaw, J.H. (1980). The flow properties of rooms with small ventilation openings. *Journal of Fluid Engineering,* **102**: 316-323.

Green, S.R. (1992). Modelling turbulent air flow in a stand of widely-spaced trees. *The PHOENICS Journal,* **5:** 294-312.

Hadim, A. (1994). Forced convection in a porous channel with localized heat sources. *ASME Journal of Heat Transfer*, **116:** 465-472.

Haghighi, K. & Sergerlind, L.J. (1988). Modelling simultaneous heat and mass transfer in an isotropic sphere-a finite element approach. *Transaction of the ASAE*, **31:** 629-637.

Harper, J.M. & Wanninger, L.A. (1969). Process modelling and optimisation 1. experimental design. *Food Technology*, **23**: 1153-1155.

Harper, J.M. & Wanninger, L.A. (1970a). Process modelling and optimisation 2. modelling. *Food Technology*, **24**: 267-268.

Harper, J.M. & Wanninger, L.A. (1970b). Process modelling and optimisation 3. optimisation. *Food Technology*, **24**: 590-595.

Harral, B.B. & Boon, C.R. (1997). Comparison of predicted and measured air flow patterns in a mechanically ventilated livestock building without animals. *Journal of agricultural Engineering Research,* **66:** 221-228.

Harris, S.D., Ingham, D.B. & Pop, I. (1999). Unsteady mixed convection boundary-layer flow on a vertical surface in a porous medium. *International Journal of Heat and Mass Transfer*, **42:** 357-372.

Haughey, D.P. & Beveridge, G.S.G. (1969). Structural properties of packed beds – a review. *Canadian Journal of Chemical Engineering*, **47:** 130-140.

Hayakawa, K. (1978). Computerised simulation for heat transfer and moisture loss from an idealised fresh produce. *Transactions of the ASAE,* **21:** 1015-1024.

Hayakawa, K. & Succar, J. (1982). Heat transfer and moisture loss of spheric fresh produce. *Journal of Food Sciences*, **47:** 596-605

Hoff, S.J. (1995). A simplified turbulence model for describing airflow in ceiling slot-ventilated enclosures. *Transactions of the ASAE*, **38:** 1853-1862.

Hoff, S.J. & Bundy, D.S. (1996). Comparison of contaminant dispersion modelling approaches for swine housing. *Transactions of the ASAE*, **39:** 1151-1157.

Hoff, S.J., Janni, K.A. & Jacobson, L.D. (1992). Three dimensional buoyant turbulent flows in a scaled model, slot-ventilated livestock confinement facility. *Transactions of the ASAE*, **35:** 671-686.

Hoff, S.J., Janni, K.A. & Jacobson, L.D. (1995). Evaluating the performance of a low Reynolds number turbulence model for describing mixed-flow airspace and temperature distributions. *Transactions of the ASAE*, **38:** 1533-1541.

Holdredge, R.M. & Wyse, R.E. (1982). Computer simulation of the forced convection cooling of sugarbeets. *Transactions of the ASAE,* **25:** 1425-1439.

Hong, J.T. & Tien, C.L. (1987). Analysis of thermal dispersion effect on the vertical-plate natural convection in porous media. *International Journal of Heat and Mass Transfer*, **30:** 143-150.

Hong, J.T., Yamada, Y. & Tien, C.L. (1987). Effects of non-Darcian and non-uniform porosity on vertical-plate natural convection in porous media. *ASME Journal of Heat Transfer,* **109:** 356-362.

Hsu, C.T. & Cheng, P. (1990). Thermal dispersion in a porous medium. *International Journal of Heat and Mass Transfer*, **33:** 1585-1597.

Ichimiya, K., Matsuda, T. & Kawai, Y. (1997). Effects of a porous medium on local heat transfer and fluid flow in a forced convection filed. *International Journal of Heat and Mass Transfer,* **40:** 1567-1576.

Irvine, D.A., Jayas, D.S. & Mazza, G. (1993). Resistance to airflow through clean and solid potatoes. *Transactions of the ASAE*, **36:** 1405-1410.

James, R.W. (1980). Refrigeration and air conditioning systems. *Modelling of Dynamic Systems,* Vol.1. Peter Peregrinus, Stevenage, UK. pp 62-69,

Jiang, H., Thompson, D.R. & Morey, R.V. (1987). Finite element model of temperature distribution in broccoli stalks during forced-air precooling. *Transactions of the ASAE*, **30:** 1473-1477.

Jones, P.J. & Whittle, G.E. (1992). Computational fluid dynamics for building air flow prediction-current status and capabilities. *Building and Environment*, **27:** 321-338.

Jones, W.P. & Launder, B.E. (1972). The prediction of laminarization with a 2-equation model of turbulence, *International Journal of Heat and Mass Transfer*, **15:** 301-314.

Kaviany, M. (1995). *Principle of Heat Transport in Porous Media.* (2nd Ed.) Springer, New York.

Kaviany, M. (1998). Heat transport in porous media. In *Handbook of Heat Transfer*, Rohsenow, W.M., Hartnett, J.P. & Cho, Y.I., eds. McGraw-Hill, New York.

Kays, S.J. (1993). *Postharvest physiology of perishable plant products.* Van Norstrand Reinhold, New York.

Kelley, C.T. (1995). *Iterative method for linear and nonlinear equations.* Society for Industrial and Applied Mathematics, Philadelphia.

Khankari, K.K, Patanker, S.V. & Morey, R.V. (1995). A mathematical model for natural convection moisture migration in stored grain. *Transactions of the ASAE*, **38:** 1777-1787.

Khelifi, M., Robert, J. L. & Lague, C. (1996a). Modelling airflow inside and around hoods used for pneumatic control of pest insects. Part I: development of a finite element model. *Canadian Agricultural Engineering*, **38:** 265-271.

Khelifi, M., Robert, J. L. & Lague, C. (1996b). Modelling airflow inside and around hoods used for pneumatic control of pest insects. Part II: application and validation of the model. *Canadian Agricultural Engineering*, **38 :** 272-281.

Kieviet, F.G., Van Raaij, J., De Moor, P.P.E. & Kerkhof, P.J.A.M. (1997). Measurement and modelling of the air flow patterns in a pilot-plant spray dryer. *Transaction of Institution of Chemical Engineers,* **75(A):** 321-329.

Kleinstreuer, C. (1997). *Engineering Fluid Dynamics, An Interdisciplinary Systems Approach.* Cambridge University Press, Cambridge.

Kotake. S, Hijikata. K. & Fusegi, T. (1993). *Numerical Simulation of Heat Transfer and Fluid Flow on a Personal Computer.* ELSEVIER Science Publishers, The Netherlands.

Kothandranaman C.P. & Subramanyan, S. (1977). *Heat and Mass Transfer Data Book.* John Wiley & Sons, New York.

Kuwahara, F., Nakayama, A. & Koyama, H. (1996). A numerical study of thermal dispersion in porous media. *ASME Journal of Heat Transfer,* **118:** 756-761.

Lai, F.C. & Kulacki, F.A. (1989). Thermal dispersion effects on non-Darcian convection over horizontal surfaces in saturated porous media. *International Journal of Heat and Mass Transfer*, **32:** 971-976.

Lam, C.K.G. & Bremhorst, K. (1981). A modified form of the k-ε model for predicting wall turbulence. *Transaction of the ASME, Journal of Fluids Engineering*, **103:** 456-460.

Launder, B.E. & Spalding, D.B. (1972). *Mathematical Models of Turbulence.* Academic Press. London.

Launder, B.E. & Spalding, D.B. (1974). The numerical computation of turbulent flows. *Computational Methods in Applied Mechanics and Engineering*, **3**: 269-289.

Lee, S.L. & Yang, H. (1997). Modelling of Darcy-Forchheimer drag of fluid flow across a bank of circular cylinders. *International Journal of Heat and Mass Transfer*, **40:** 3149-3155.

Lentz, C.P. & Rooke, E.A. (1964). Rates of moisture loss of apples under refrigerated storage conditions. *Food Technology,* **18:** 119-121.

Leschziner, M.A. (1990). Modelling engineering flows with Reynolds stress turbulence closure. *Journal of Wind Engineering and Industrial Aerodynamics*, **35**: 21-47

Leu, J. & Jang, J. (1995). The natural convection from a point heat source embedded in a non-Darcian porous medium. *International Journal of Heat and Mass Transfer*, **38:** 1097-1104.

Levec, J. & Carbonell, R.G. (1985a). Longitudinal and lateral thermal dispersion in Packed Beds, part I: theory. *A.I.Ch.E. Journal*, **31:** 581-590.

Levec, J. & Carbonell, R.G. (1985b). Longitudinal and lateral thermal dispersion in Packed Beds, part II: comparison between theory and experiment. *A.I.Ch.E. Journal*, **31:** 591-602.

Levine, L. (1997). Food process development and scale up using modelling and simulation. *Chemistry and Industry*, **5**: 346-349.

Liao, C.M. & Feddes, J.J.R. (1992). A lumped-parameter model for describing the airborne dust concentration in a ventilated airspace. *Transaction of the ASAE*, **35:** 1973-1978.

Lin, Z. (1994). *Prediction of Chilling Times of Foods.* PhD Thesis, Massey University, Palmerston North, New Zealand.

Lin, Z., Cleland, A.C., Cleland, D.J. & Serrallach, G.F. (1996a). A simple method for prediction of chilling times for objects of two-dimensional irregular shapes. *International Journal of Refrigeration,* **19:** 95-106.

Lin, Z., Cleland, A.C., Cleland, D.J. & Serrallach, G.F. (1996b). A simple method for prediction of chilling times for objects of three-dimensional irregular shapes. *International Journal of Refrigeration,* **19:** 107-114.

Liu, Q., Hoff, S.J., Maxwell, G.M. & Bundy, D.S. (1996). Comparison of three k-ε turbulence models for predicting ventilated air jets. *Transactions of the ASAE*, **39:** 689-698.

Lovatt,S.J. (1992). *A Dynamic Modelling Methodology for the Simulation of Industrial Refrigeration Systems.* PhD Thesis, Massey University, Palmerston North, New Zealand.

Lundgren, T.S. (1972). Slow flow through stationary random beds and suspensions of spheres. *Journal of Fluid Mechanics*, **51:** 273-299

Macdonald, I.F., EI-Sayed, M.S., Mow, K. & Dullien, F.A.L. (1979). Flow through porous media- the Ergun equation revisited. *Industrial and Engineering Chemistry Fundamental*, **18:** 199-208.

Maghirang, R.G. & Manbeck, H.B. (1993). Modelling particle transport in slot-inlet ventilated airspaces. *Transactions of the ASAE*, **36:** 1449-1459.

Maghirang, R.G., Manbeck, H.B. & Puri, V.M. (1994). Numerical simulation of particle transport in slot-inlet ventilated airspaces. *Transactions of the ASAE*, **37:** 1607-1612.

Marchant, J.A. (1976). The prediction of air flows in crop drying systems by finite element method. *Journal of Agricultural Engineering Research*, **21:** 417-429.

Mariotti, M., Rech, G. & Romagnoni, P. (1995). Numerical study of air distribution in a refrigerated room. *19th International Congress of Refrigeration 1995*, **2:** 98-105.

Markatos, N.C. & Malin, M.R. (1982). Mathematical modelling of buoyancy-induced smoke flow in enclosures. *International Journal of Heat and Mass Transfer*, **25:** 63-75.

Markatos, N.C. & Pericleous, K.A. (1984). Laminar and turbulent natural convection in an enclosed cavity. *International Journal of Heat and Mass Transfer*, **27:** 755-722.

Masuoka, T. & Takatsu, Y. (1996). Turbulence model for flow through porous media. *International Journal of Heat and Mass Transfer*, **39:** 2803-2809

Mathioulakis, E., Karathanos, V.T. & Belessiotis, V.G. (1998). Simulation of air movement in a dryer by computational fluid dynamics: application for the drying of fruits. *Journal of Food Engineering,* **36:** 183-200.

Mathworks, (2000). MATLAB Version 6.0. http://www.mathworks.com/

Meerschaert, M.M. (1993). *Mathematical modelling.* Academic Press, Boston.

Misener, G.C. & Shove, G.C. (1976). Simulated cooling of potato. *Transactions of the ASAE,* **19:** 954-061.

Ministry of Agriculture and Forest. (2000). *Horticulture Monitoring Report, A Short Term Financial and Physical Forecast Reflecting Grower, Consultant and Industry Perceptions of Horticultural Trends and Issues, Production and Financial Figures.* Wellington. New Zealand.

Mistriotis, A., Arcidiacono, C., Picuno, P., Bot, G.P.A. & Scarascia-Mugnozza, G. (1997a). Computational analysis of ventilation in greenhouses at zero- and low-wind-speeds. *Agricultural and forest meteorology,* **88:** 121-135.

Mistriotis, A, Dong, T.D., Wagemans, M.J.M. & Bot, G.P.A. (1997b). Computational fluid dynamics (CFD) as a tool for analysis of ventilation and indoor microclimate in agricultural buildings. *Netherlands Journal of Agricultural Science,* **45:** 81-96.

Mitchell, F.G. (1992). Cooling Horticultural Commodities. In *Postharvest Technology of Horticultural Crops*, Kader, A. A., ed. University of California, Davis, California.

Murthy, P.V.S.N. & Singh, P. (1997). Effect of viscous dissipation on non-Dracian natural convection regime. *International Journal of Heat and Mass Transfer,* **40:** 1251-1260.

Nakayama, A. & Kuwahara, F. (1999). A macroscopic turbulence model for flow in a porous medium. *Journal of Fluid Engineering,* **121:** 427-433.

Narayana, K.B. & Murthy, M.V.K. (1981). Heat and mass transfer characteristics and the evaluation of thermal properties of moist food materials. *Transactions of the ASAE,* **24:** 789-793.

Neale, G. & Nader, W. (1974). Practical significance of Brinkman's extension of Darcy's law: coupled parallel flows within a channel and a bounding porous medium. *Canadian Journal of Chemistry Engineering*, **52:** 475-478.

Neale, M.A. & Messer, H.J.M. (1976). Resistance of root and bulk vegetables to airflow. *Journal of Agricultural Engineering Research*, **21:** 221-231.

Nield, D.A. & Bejan, A. (1992). *Convection in Porous Media.* Springer-Verlag, New York.

Nithiarasu, P., Seetharamu, K.N. & Sundararajan, T. (1997). Natural convective heat transfer in a fluid saturated variable porosity medium. *International Journal of Heat and Mass Transfer,* **40:** 3955-3967.

NZAPMB (New Zealand Apple and Pear Marketing Board). (1996). *1996 Annual Report.* Wellington, New Zealand.

Ochoa-Tapia, J.A. & Whitaker, S. (1995a). Momentum transfer at the boundary between a porous medium and a homogeneous fluid-I. theoretical development. *International Journal of Heat and Mass Transfer*, **38:** 2635-2646.

Ochoa-Tapia, J.A. & Whitaker, S. (1995b). Momentum transfer at the boundary between a porous medium and a homogeneous fluid-II. comparison with experiment. *International Journal of Heat and Mass Transfer*, **38:** 2647-2655.

Ochoa-Tapia, J.A. & Whitaker, S. (1997). Heat transfer at the boundary between a porous medium and a homogeneous fluid. *International Journal of Heat and Mass Transfer*, **40:** 2691-2707.

Pala, M. & Devers, Y.O. (1988). Computer simulated model for power consumption and weight loss in a cold store, *Refrigeration Science & Technology*., **1988-1:** 233-241.

Pan, J.C. & Bhowmik, S.R. (1991). The finite element analysis of transient heat transfer in fresh tomatoes during cooling. *Transactions of the ASAE*, **34:** 972-976.

Parry, J.L. (1985). Mathematical modelling and computer simulation of heat and mass transfer in agricultural grain drying: a review. *Journal of Agricultural Engineering Research,* **32:** 1-29.

Parson, D.J. (1991). Modelling gas flow in a silage clamp after opening. *Journal of Agricultural Engineering Research*, **50:** 209-218.

Patankar, S.V. (1980). *Numerical Heat Transfer and Fluid Flow.* Hemisphere Publishing Co., Washington.

Patankar, S.V. & Spalding, D.B. (1972). A calculation procedure for heat, mass and momentum transfer in three-dimensional parabolic flows, *International Journal of Heat and Mass Transfer,* **15:** 1787-1806.

Patel, P.N.& Sastry, S.K. (1988a). Effects of temperature, relative humidity and storage time on the transpiration coefficients of selected perishables. *ASHRAE Transactions,* **94(1):** 1563-1587.

Patel, P.N., Pai, T.K. & Sastry, S.K. (1988a). Effects of temperature fluctuation on transpiration of selected perishables: mathematical models and experimental studies. *ASHRAE Transactions,* **94(1):** 1588-1601.

Peyret, R. & Taylor, T.D. (1985). *Computational Methods for Fluid Flow*. Springer-Verlag, New York.

Poulikakos, D. & Renken, K. (1987). Forced convection in a channel filled with porous medium, including the effects of flow inertia, variable porosity, and Brinkman Friction. *ASME Journal of Heat Transfer*, **109:** 880-888.

Reddy, J.N. & Gartling, D.K. (1994). *The finite element method in heat transfer and fluid dynamics.* CRC Press, Boca Raton.

Reinartz, A. & Renz, U. (1984). Calculations of the temperature and flow field in a room ventilated by a radial air distributor. *International Journal of Refrigeration,* **7:** 308-312.

Reynolds, A.M. (1997). A model for predicting airborne dust concentrations within a ventilated airspace. *Journal of Agricultural Engineering Research*, **66:** 103-109.

Reynoso, R.O. & de Michelis, A. (1988). Simulation of batch cryogenic freezers. *International Journal of Refrigeration,* **11:** 6-10.

Roblee, L.H.S., Baurd, R.M. & Tierney, J.W. (1958). Radial porosity variations in packed beds. *A.I.Ch.E. Journal*, **4:** 460-464.

Rodi, W. (1979*). Turbulence Models and Their Application in Hydraulics - A State of the Art Review.* International Association for Hydraulic Research, Delft, the Netherlands.

Romero, R.A & Chau, K.V. (1987). A mathematical simulation for transpiration from fruits and vegetables in bulk storage. *ASAE Paper No. 87-6007.*

Sahraoui, M. & Kaviany, M. (1992). Slip and no-slip boundary condition at interface of porous, plain media. *International Journal of Heat and Mass Transfer*, **35:** 927-943.

Sahraoui, M. & Kaviany, M. (1993). Slip and no-slip boundary condition at interface of porous, plain media: conduction. *International Journal of Heat and Mass Transfer*, **36:** 1019-1033.

Sahraoui, M. & Kaviany, M. (1994). Slip and no-slip boundary condition at interface of porous, plain media: convection. *International Journal of Heat and Mass Transfer*, **37:** 1028-1044.

Sastry, S.K. & Buffington, D.E. (1983). Transpiration rates of stored perishable commodities: a mathematical model and experiments on tomatoes. *International Journal of Refrigeration,* **6:** 85-96.

Sastry, S.K., Baird, C.D. & Buffington, D.E. (1978). Transpiration rates of certain fruits and vegetables. *ASHRAE Transactions,* **84:** 237-255.

Sastry, S.K., Zuritz, C.A. & Anantheswaran, R.C. (1985). Interaction between heat and mass transfer in foods. *ASHRAE Transactions,* **91(1B):** 353-370.

Schertz, W.M. & Bischoff, K.B. (1969). Thermal and material transport in non-isothermal packed beds. *A.I.Ch.E. Journal,* **15:** 597-604.

Scott, G. & Richardson, P. (1997). The application of computational fluid dynamics in the food industry. *Trends in Food Science & Technology*, **8:** 119-124.

Slimi, K., Nasrallah, S.B. & J. Fohr. (1998). Transient natural convection in a vertical cylinder opened at the extremities and filled with a fluid saturated porous medium:

validity of Darcy flow model and thermal boundary layer approximations. *International Journal of Heat and Mass Transfer,* **41:** 1113-1125.

Smith, E.A. (1982). Three-dimensional analysis of air velocity and pressure in beds of grain and hay. *Journal of Agricultural Engineering Research*, **27:** 101-117.

Smith, R.E & Nelson, G.L. (1969). Transient heat transfer in solids: theory versus experimental. *Transactions of the ASAE*, **12:** 833-836, 844.

Smith, R.E., Nelson, G.L. & Henrichson, R.L. (1967). Analysis on transient heat transfer from anomalous shapes. *Transactions of the ASAE,* **10:** 236-245.

Smith, R.E., Nelson, G.L. & Henrichson, R.L. (1968). Application of geometry analysis of anomalous shapes to problems in transient heat transfer. *Transactions of the ASAE,* **11:** 296-302.

Szczechowiak, E. & Rainczak, J. (1987). The cooling chamber and the air-cooler operation in unsteady states, *Proceeding of 17th International. Congress of Refrigeration*, **2:** 864-869.

Tanner, J. D. (1998). *Mathematical modelling for design of horticultural packaging.* PhD thesis, Massey University, Palmerston North, New Zealand.

Tassou, S.A & Xiang, W. (1998). Modelling the environment within a wet air-cooled vegetable store. *Journal of Food Science,* **38:** 169-187.

Tennekes, H. & Lumley, J.L. (1973). *A First Course in Turbulence.* The MIT Press, Cambridge, USA.

Timmons, M.B., Albright, L.D., Furry, R.B. & Torrance, K.E. (1980). Experimental and numerical study of air movement in slot-ventilated enclosures. *ASHRAE Transactions*, **86:** 221-240.

Touber,S. (1984). Principles and methods for mathematical modelling the steady-state and dynamics behaviour of refrigeration components and installations, *Refrigeration Science & Technology*, **1984-2**: 163-175.

Vafai, K., Alkire, R.L. & Tien, C.L. (1985). An experimental investigation of heat transfer in varaible porosity media. *ASME Journal of Heat Transfer*, **107:** 642-647.

Vafai, K. & Sozen, M. (1990). Analysis of energy and momentum transport for fluid flow through a porous bed. *ASME Journal of Heat Transfer,* **112:** 690-698.

Vafai, K. & Thiyagaraja, R. (1987). Analysis of flow and heat transfer at the interface region of a porous medium. *International Journal of Heat and Mass Transfer*, **30:** 1391-1405.

Vafai, K. & Tien, C.L. (1981). Boundary and inertia effects on flow and heat transfer in porous media. *International Journal of Heat and Mass Transfer,* **24:** 195-203.

Van Gerwen, R.J.M., Van der Sluis, S.M. & Van Oort, H. (1991). Computer modelling of carcass chilling models, *Proceedings of 18th International. Congress of Refrigeration*, **4:** 1893-1897.

Versteeg, H.K. & Malalaaekera, W. (1995). *An Introduction to Computational Fluid Dynamics, The Finite Volume Method.* Longman, Harlow, England.

Wakao, N. & Kaguei, S. (1982). *Heat and Mass Transfer in Packed Beds.* Gordon and Breach Science Publisher, New York.

Wang, H. & Touber, S. (1990). Distributed dynamic modelling of a refrigerated room. *International Journal of Refrigeration,* **13:** 214-222.

Wang, H. & Touber, S. (1991). Distributed and non-steady-state modelling of an air cooler. *International Journal of Refrigeration,* **14:** 98-111.

Wang, J., and Tunpun, K. 1969. Forced-air precooling of tomatoes in cartons. *Transactions of the ASAE*, **12:** 804-806.

Watkins, J.B. (1989). *Forced-Air Cooling* (2nd Ed). Queensland Department of Primary Industries, Brisbane, Australia.

Weiner, K.L. & Parkin, C.S. (1993). The use of computational fluid dynamics code for modelling spray from a mist-blower. *Journal of Agricultural Engineering Research*, **55:** 313-324.

Wells, C.M. (1992). *Modelling the Greenhouse Environment and the Growth of Cucumbers*. PhD Thesis, Massey University, Palmerston North, New Zealand.

Whitaker, S. (1997). Volume averaging of transport equations. In *Fluid Transport in Porous Media*, Prieur du Plessis, J., ed. Computational Mechanics Publications, Southampton, UK.

Wills, R., McGlasson, B., Graham, D. & Joyce, D. (1998). *Postharvest: An Introduction to the Physiology and Handling of Fruit, Vegetables, and Ornamentals* (4th Ed). Cab International, New York.

Woods, J.L. (1990). Moisture loss from fruits and vegetables. *Postharvest News and Information* **1:** 159-199.

Worley, M.S. & Manbeck, H.B. (1995). Modelling particle transport and air flow in ceiling inlet ventilation systems. *Transactions of the ASAE*, **38:** 231-239.

Xu, Y. & Burfoot, D. (1999). Simulating the bulk storage of foodstuffs. *Journal of Food Engineering*, **39:** 23-29.

Xu, Z.G., Walklate, P.J. & McLeod, A. (1997). Numerical study of a full-size free-air fumigation system. *Agricultural and Forest Meteorology*, **85:** 149-158.

Yuan, S.W. (1967). *Foundations of Fluid Mechanics.* Prentice-Hall International, Inc. London.

Zou, Q. (1998). *CFD Modelling of Airflow and Heat Transfer in a Ventilated Carton.* Master thesis, Massey University, Palmerston North.

Appendix A
Derivation of Discretisation Equations

A.1 Discretisation Equations for PDEs in the Airflow Model for Bulk Packaging Systems

A.1.1 Numerical Schemes

The conventions for representing a quantity in a location of the calculation domain are shown in Figures 6.2, 6.10-6.12 and A.1. The location was described with respect to the cell type and the position in the cell. In an equation, all vector cells have a common scalar cell of current grid node.

- **Discretisation equations**

Using the SIMPLER method to solve the airflow models, five types of discretisation equations are needed.

1) X-momentum discretisation equations were derived by integrating the momentum equations in the direction of x-axis over the corresponding x-momentum cells:

$$a_{uL-P-u}u_{L-u}^{current} + a_{uW-P-u}u_{W-u}^{current} + a_{uS-P-u}u_{S-u}^{current} + a_{uP-P-u}u_{P-u}^{cu\ rent} + a_{uN-P-u}u_{N-u}^{current} + a_{uE-P-u}u_{E-u}^{current} + a_{uH-P-u}u_{H-u}^{current} = S_{u-P-u} + (\phi_{p-scalar}p_{P-scalar} - \phi_{E-scalar}p_{E-scalar})A_{e-u} \quad \text{(A.1)}$$

where:

u = velocity component at x-axis (m s^{-1}).

p = pressure (N m^{-2}).

ϕ = porosity

A = cell surface area (m^2).

a_{uE} = coefficient in x-momentum discretisation equation for east node.

a_{uW} = coefficient in x-momentum discretisation equation for west node.

a_{uN} = coefficient in x-momentum discretisation equation for north node.

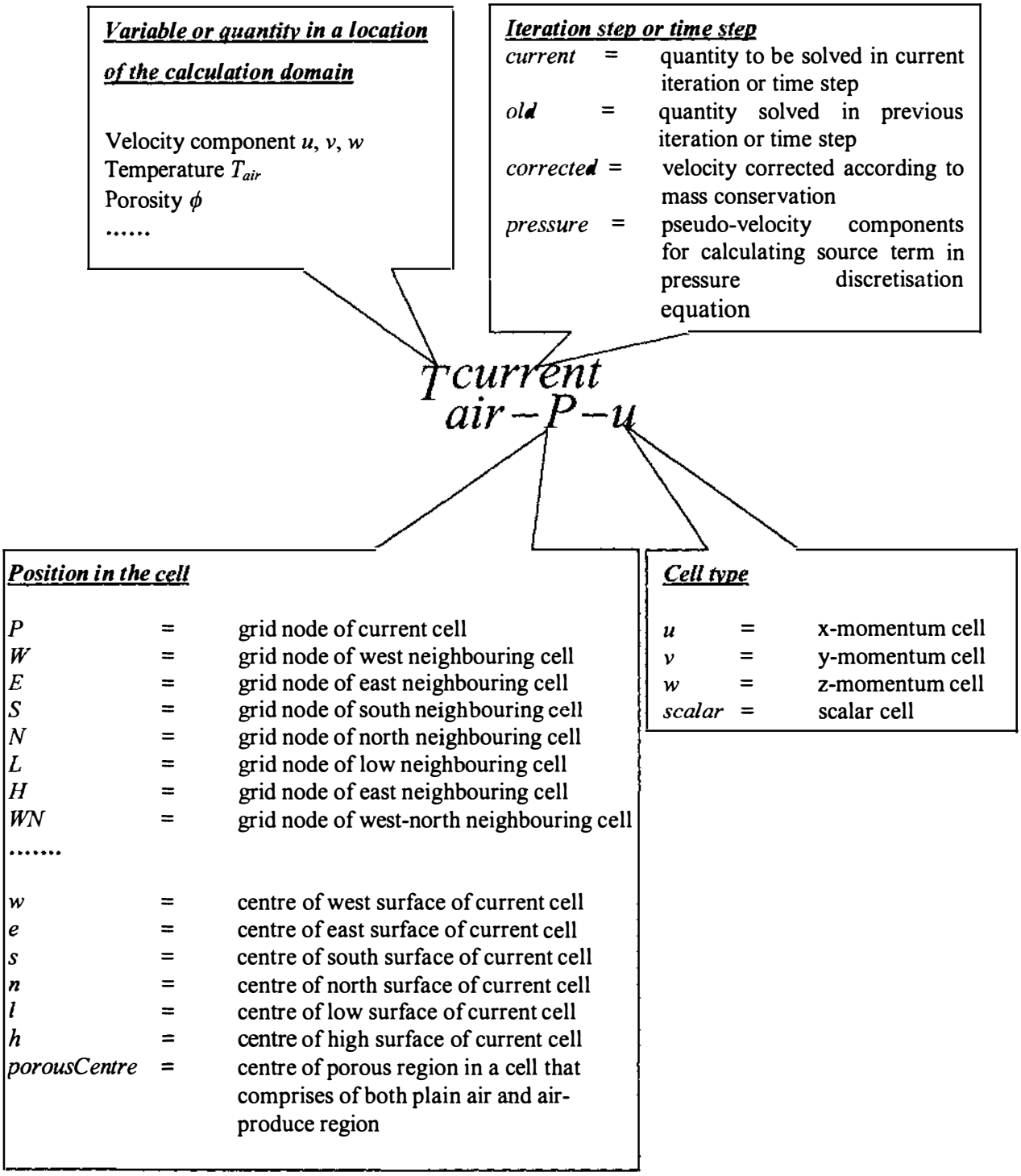

Figure A.1 Convention for representing a quantity in a location of the calculation domain.

a_{uS} = coefficient in x-momentum discretisation equation for south node.

a_{uH} = coefficient in x-momentum discretisation equation for high node.

a_{uL} = coefficient in x-momentum discretisation equation for low node.

a_{uP} = coefficient in x-momentum discretisation equation for current node.

S_u = source term for x-momentum discretisation equation (N).

For each x-momentum cell, an x-momentum discretisation equation was formed, so the number of algebraic equations in the system of x-momentum discretisation equations is equal to the number of x-momentum cells.

2) Y-momentum discretisation equations were derived by integrating the momentum equations in the direction of y-axis over the corresponding y-momentum cells:

$$a_{vL-P-v}v_{L-v}^{current} + a_{vW-P-v}v_{W-v}^{current} + a_{vS-P-v}v_{S-v}^{current} + a_{vP-P-v}v_{P-v}^{current} + a_{vN-P-v}v_{N-v}^{current} + a_{vE-P-v}v_{E-v}^{current} + a_{vH-P-v}v_{H-v}^{current} = S_{v-P-v} + (\phi_{P-scalar}p_{P-scalar} - \phi_{N-scalar}p_{N-scalar})A_{n-v} \quad \text{(A.2)}$$

where:

v = velocity component at y-axis (m s^{-1}).

p = pressure (N m^{-2}).

ϕ = porosity

a_{vE} = coefficient in y-momentum discretisation equation for east node.

a_{vW} = coefficient in y-momentum discretisation equation for west node.

a_{vN} = coefficient in y-momentum discretisation equation for north node.

a_{vS} = coefficient in y-momentum discretisation equation for south node.

a_{vH} = coefficient in y-momentum discretisation equation for high node.

a_{vL} = coefficient in y-momentum discretisation equation for low node.

a_{vP} = coefficient in y-momentum discretisation equation for current node.

S_v = source term for y-momentum discretisation equation (N).

For each y-momentum cell, a y-momentum discretisation equation was formed, so the number of algebraic equations in the system of y-momentum discretisation equations is equal to the number of y-momentum cells.

3) Z-momentum discretisation equations were derived by integrating the momentum equations in the direction of z axis over the corresponding z-momentum cells:

$$a_{wL-P-w}w_{L-w}^{current}+a_{wW-P-w}w_{W-w}^{current}+a_{wS-P-w}w_{S-w}^{current}+a_{wP-P-w}w_{P-w}^{current}+a_{wN-P-w}w_{N-w}^{current}+ a_{wE-P-w}w_{E-w}^{urrent}+a_{wH-P-w}w_{N-w}^{current}=S_{w-P-w}+(\phi_{P-scalar}p_{P-scalar}-\phi_{H-scalar}p_{H-scalar})A_{h-w} \quad (A.3)$$

where:

w = velocity component at z-axis (m s^{-1}).

a_{wE} = coefficient in z-momentum discretisation equation for east node.

a_{wW} = coefficient in z-momentum discretisation equation for west node.

a_{wN} = coefficient in z-momentum discretisation equation for north node.

a_{wS} = coefficient in z-momentum discretisation equation for south node.

a_{wH} = coefficient in z-momentum discretisation equation for high node.

a_{wL} = coefficient in z-momentum discretisation equation for low node.

a_{wP} = coefficient in z-momentum discretisation equation for current node.

S_w = source term for z-momentum discretisation equation (N).

For each z-momentum cell, a z-momentum discretisation equation was formed, so the number of algebraic equations in the system of z-momentum discretisation equations is equal to the number of z-momentum cells.

4) Pressure correction discretisation equations were derived by enforcing mass conservation over scalar cells with velocity corrections obtained from the momentum discretisation equations:

$$a_{pL-P-scalar}\Delta p_{L-scalar}+a_{pW-P-scalar}\Delta p_{W-scalar}+a_{pS-P-scalar}\Delta p_{S-scalar}+a_{pP-P-scalar}\Delta p_{P-scalar} +a_{pN-P-scalar}\Delta p_{N-scalar}+a_{pE-p-scalar}\Delta p_{E-scalar}+a_{pH-P-scalar}\Delta p_{H-scalar}=S_{\Delta p-P-scalar} \quad (A.4)$$

where:

Δp = pressure correction (N m^{-2}).

a_{pE} = coefficient in pressure correction discretisation equation for east node.

a_{pW} = coefficient in pressure correction discretisation equation for west node.

a_{pN} = coefficient in pressure correction discretisation equation for north node.

a_{pS} = coefficient in pressure correction discretisation equation for south node.

a_{pH} = coefficient in pressure correction discretisation equation for high node.

a_{pL} = coefficient in pressure correction discretisation equation for low node.

a_{pP} = coefficient in pressure correction discretisation equation for current node.

$S_{\Delta p}$ = source term for pressure correction discretisation equation (N).

For each scalar cell, a pressure correction discretisation equation was formed, so the number of algebraic equations in the system of pressure correction discretisation equations is equal to the number of scalar cells.

5) Pressure discretisation equations have the same coefficients as their corresponding pressure correction equations, and were derived by enforcing mass conservation over scalar cells with velocity components obtained from the momentum discretisation equations:

$$a_{pL-P-scalar}p_{L-scalar} + a_{pW-P-scalar}p_{W-scalar} + a_{pS-P-scalar}p_{S-scalar} + a_{pP-P-scalar}p_{P-scalar} + a_{pN-P-scalar}p_{N-scalar} + a_{pE-p-scalar}p_{E-scalar} + a_{pH-P-scalar}p_{H-scalar} = S_{p-P-scalar} \quad \text{(A.5)}$$

where:

p = pressure (N m^{-2}).

S_p = source term for pressure discretisation equation (N).

For each scalar cell, a pressure discretisation equation was formed, so the number of algebraic equations in the system of pressure discretisation equations is equal to the number of scalar cells.

A.1.2 X-Momentum Discretisation Equations

- **Types of x-momentum cells**

There are eight types of x-momentum cells, which are summarised in Figure A.2 and Table A.1. For each type of x-momentum cell, a set of expressions was derived for the coefficients and source term in the x-momentum discretisation equation (Equation A.1).

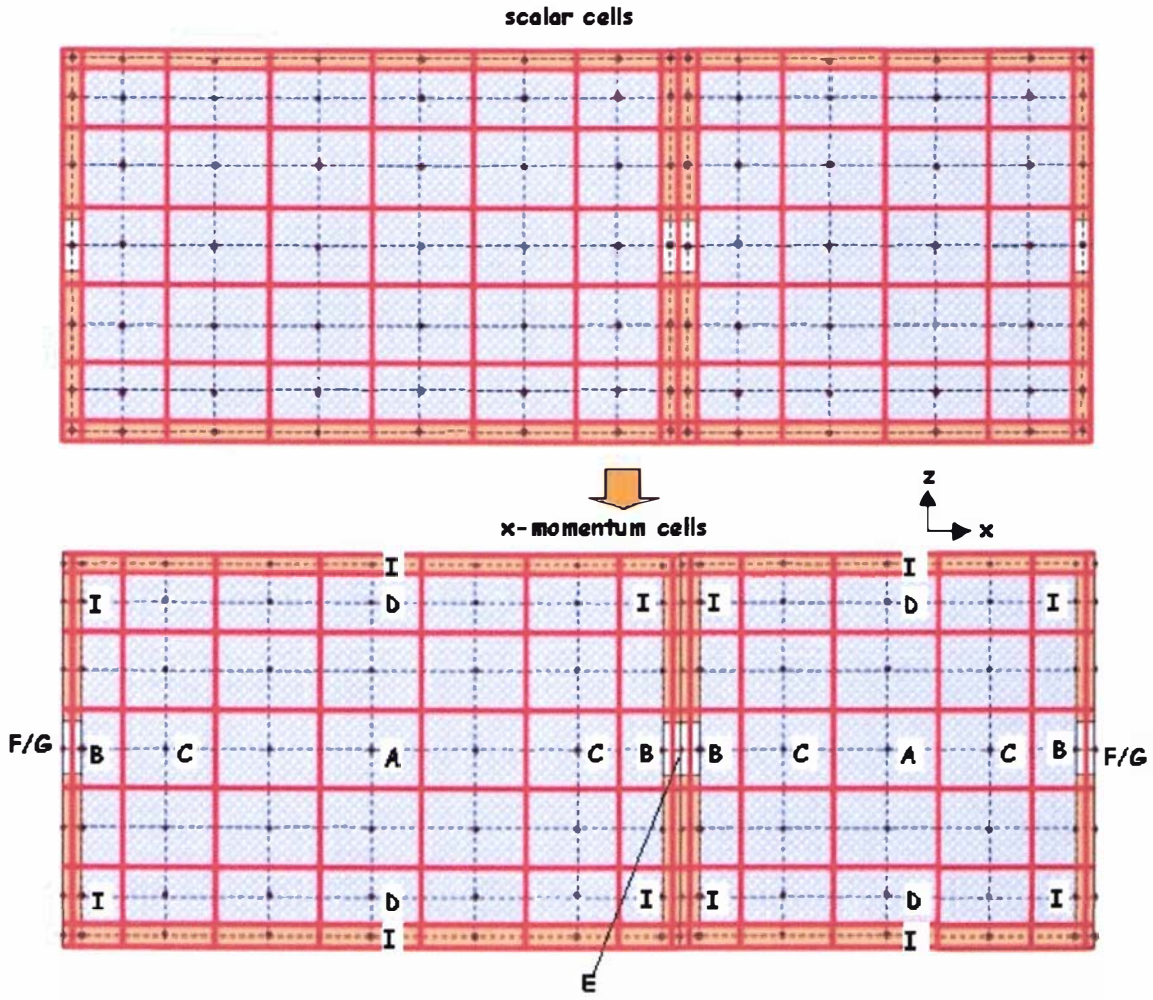

Figure A.2 Grids for the x-momentum discretisation equations in bulk packaging systems (the capital letters indicate the types of x-momentum cells, which are explained in Table A.1)

Table A.1 Types of x-momentum cells in bulk packaging systems

Type	Location	Transport equations
A	Middle of produce-air region	• Generalised volume-averaged momentum equation (Equation 4.4a)
B	On the interface between plain air region and west/east package walls with vents	• Generalised volume-averaged momentum equation (Equation 4.4a) • One-dimensional Navier-Stokes equation (Equation 4.3 a)
C	In produce-air region and on the east or west side of the cells of type B	• Generalised volume-averaged momentum equation (Equation 4.4a)
D	In produce-air region and next to south, north, bottom, and top package walls	• Wall boundary conditions
E	On the interface between a vented east wall in one package and a vented west wall in another package	• One-dimensional Navier-Stokes equation (Equation 4.3 a)
F	On the interface between outside environment and the west/east walls with fixed-pressure vents.	• Fixed-pressure boundary conditions
G	On the interface between outside environment and the west/east walls with fixed-velocity vents.	• Fixed-velocity boundary conditions
I	In south, north, bottom, and top package wall, or in the interface between produce-air region and west/east package wall without vents	• Velocity component in the direction of x-axis is set to zero

- **X-momentum discretisation equations for x-momentum cells in the middle of air-produce region**

The momentum equation in the direction of x axis for the air-produce region in a bulk package (Equation 4.4a) was presented in following simplified form:

$$\frac{\partial}{\partial x}(\rho_a \phi u u)+\frac{\partial}{\partial y}(\rho_a \phi v u)+\frac{\partial}{\partial z}(\rho_a \phi w u)-\frac{\partial}{\partial x}\left(\mu\phi\frac{\partial u}{\partial x}\right)-\frac{\partial}{\partial y}\left(\mu\phi\frac{\partial u}{\partial y}\right)-\frac{\partial}{\partial z}\left(\mu\phi\frac{\partial u}{\partial z}\right)= \frac{\partial(\phi p)}{\partial x}-\frac{\mu\phi^2 u}{K}-\frac{F\phi^3\rho_a}{\sqrt{K}}|u|u \quad \text{(A.6)}$$

where:

u = intrinsic phase average of air velocity component in the direction of x-axis (m s^{-1}).

v = intrinsic phase average of air velocity component in the direction of x-axis (m s^{-1}).

w = intrinsic phase average of air velocity component in the direction of x-axis (m s^{-1}).

p = intrinsic phase average of air pressure (N m^{-2}).

ϕ = porosity.

K = permeability (m^2).

F = Forcheimer coefficient.

μ = air dynamic viscosity (N s m^{-2}).

ρ_a = air density (kg m^{-3}).

The first step for deriving the discretisation equation is to integrate the differential equation over an x-momentum cell in the air-produce region (index convection was shown in Figure 6.10):

$$\begin{aligned}
&\int_{A_{e-u}}\left((\rho_a\phi uu)-\left(\mu\phi\frac{\partial u}{\partial x}\right)\right)ds-\int_{A_{w-u}}\left((\rho_a\phi uu)-\left(\mu\phi\frac{\partial u}{\partial x}\right)\right)ds+\\
&\int_{A_{n-u}}\left((\rho_a\phi vu)-\left(\mu\phi\frac{\partial u}{\partial y}\right)\right)ds-\int_{A_{s-u}}\left((\rho_a\phi vu)-\left(\mu\phi\frac{\partial u}{\partial y}\right)\right)ds+\\
&\int_{A_{h-u}}\left((\rho_a\phi wu)-\left(\mu\phi\frac{\partial u}{\partial z}\right)\right)ds-\int_{A_{l-u}}\left((\rho_a\phi wu)-\left(\mu\phi\frac{\partial u}{\partial z}\right)\right)ds=\\
&\int_{A_{w-u}}(\phi p)ds-\int_{A_{e-u}}(\phi p)ds+\int_{V_{P-u}}\left(-\frac{\mu\phi^2u}{K}-\frac{F\phi^3\rho_a}{\sqrt{K}}|u|u\right)dv
\end{aligned}\qquad \text{(A.7)}$$

where:

A = cell surface area (m^2).

$V_{P\text{-}u}$ = volume of x-momentum cell (m^3).

(1) Treatment of convection and diffusion terms

Approximating the momentum flux due to both convection and diffusion out of the east surface with the second-order midpoint rule (Ferziger & Peric, 1999):

$$\int_{A_{e-u}}\left((\rho_a\phi uu)-\left(\mu\phi\frac{\partial u}{\partial x}\right)\right)ds=\left((\rho_a\phi uu)_{e-u}-\left(\mu\phi\frac{\partial u}{\partial x}\right)_{e-u}\right)A_{e-u} \tag{A.8}$$

The upwind interpolation scheme (UDS) with central difference scheme (CDS) deferred correction was used to approximate the convection term (Ferziger & Peric, 1999):

$$\begin{aligned}(\rho_a\phi uu)_{e-u}&=\max(\rho_a\phi_{e-u}u_{e-u},0)u_{P-u}^{current}+\min(\rho_a\phi_{e-u}u_{e-u},0)u_{E-u}^{current}+\\&\rho_a\phi_{e-u}u_{e-u}\left(\frac{x_{E-u}-x_{e-u}}{x_{E-u}-x_{P-u}}u_{P-u}+\frac{x_{e-u}-x_{P-u}}{x_{E-u}-x_{P-u}}u_{E-u}\right)-\max(\rho_a\phi_{e-u}u_{e-u},0)u_{P-u}-\min(\rho_a\phi_{e-u}u_{e-u},0)u_{E-u}\end{aligned} \tag{A.9}$$

In Equation (A.9), the first two terms were derived according to UDS, the last three terms were from CDS deferred correction. The mass flow rate was approximated as follows:

$$\rho_a\phi_{e-u}u_{e-u}=\frac{\rho_a\phi_{P-u}u_{P-u}+\rho_a\phi_{E-u}u_{E-u}}{2} \tag{A.10}$$

Substituting Equation (A.10) into Equation (A.11) gives:

$$\begin{aligned}(\rho_a\phi uu)_{e-u}&=\max\left(\frac{\rho_a\phi_{P-u}u_{P-u}+\rho_a\phi_{E-u}u_{E-u}}{2},0\right)u_{P-u}^{current}+\min\left(\frac{\rho_a\phi_{P-u}u_{P-u}+\rho_a\phi_{E-u}u_{E-u}}{2},0\right)u_{E-u}^{current}\\&+\frac{\rho_a\phi_{P-u}u_{P-u}+\rho_a\phi_{E-u}u_{E-u}}{2}\left(\frac{x_{E-u}-x_{e-u}}{x_{E-u}-x_{P-u}}u_{P-u}+\frac{x_{e-u}-x_{P-u}}{x_{E-u}-x_{P-u}}u_{E-u}\right)-\\&\max\left(\frac{\rho_a\phi_{P-u}u_{P-u}+\rho_a\phi_{E-u}u_{E-u}}{2},0\right)u_{P-u}-\min\left(\frac{\rho_a\phi_{P-u}u_{P-u}+\rho_a\phi_{E-u}u_{E-u}}{2},0\right)u_{E-u}\end{aligned} \tag{A.11}$$

The diffusion term was approximated by a central difference scheme:

$$\left(\mu\phi\frac{\partial u}{\partial x}\right)_{e-u} = \mu\phi_{e-u}\frac{u_{E-u}^{current} - u_{P-u}^{current}}{x_{E-u} - x_{P-u}} \tag{A.12}$$

The convection-diffusion terms on other surfaces of the x-momentum cell were approximated using the same schemes.

(2) Treatment of pressure terms

The pressure terms were approximated using the midpoint rule:

$$\int_{A_{w-u}} (\phi p) ds - \int_{A_{e-u}} (\phi p) ds + = (\phi_{P-scalar} p_{P-scalar} - \phi_{E-scalar} p_{E-scalar}) A_{e-u} \tag{A.13}$$

(3) Treatment of source term

Using the values at grid node to approximate the average value over the cell, the source term due to the porous structure was written:

$$\int_{V_{P-u}} \left(-\frac{\mu\phi^2 u}{K} - \frac{F\phi^3\rho_a}{\sqrt{K}}|u|u\right) dv = -\left(\frac{\mu\phi_{P-u}^{\ 2}}{K_{P-u}} + \frac{F_{P-u}\phi_{P-u}^{\ 3}\rho_a}{\sqrt{K_{p-u}}}|u_{P-u}|\right) V_{P-u} u_{P-u}^{current} \tag{A.14}$$

where:

V_{P-u} = volume of x-momentum cell (m^3).

Combining the above treatments, the coefficients in the x-momentum discretisation equation (Equation A.1) were derived to be:

$$a_{uE-P-u} = \left(\min\left(\frac{\rho_a\phi_{E-u}u_{E-u} + \rho_a\phi_{P-u}u_{P-u}}{2}, 0\right) - \frac{\phi_{e-u}\mu}{x_{E-u} - x_{P-u}}\right) A_{e-u} \tag{A.15}$$

$$a_{uW-P-u} = \left(-\max\left(\frac{\rho_a\phi_{W-u}u_{W-u} + \rho_a\phi_{P-u}u_{P-u}}{2}, 0\right) - \frac{\phi_{w-u}\mu}{x_{P-u} - x_{W-u}}\right) A_{w-u} \tag{A.16}$$

$$a_{uN-p-u} = \left(\min\left(\frac{\rho_a\phi_{P-v}v_{P-v} + \rho_a\phi_{E-v}v_{E-v}}{2}, 0\right) - \frac{\phi_{n-u}\mu}{y_{N-u} - y_{P-u}}\right) A_{n-u} \tag{A.17}$$

$$a_{uS-P-u} = \left(-\max\left(\frac{\rho_a \phi_{S-v} v_{S-v} + \rho_a \phi_{SE-v} v_{SE-v}}{2}, 0 \right) - \frac{\phi_{s-u}\mu}{y_{P-u} - y_{S-u}} \right) A_{s-u} \tag{A.18}$$

$$a_{uH-p-u} = \left(\min\left(\frac{\rho_a \phi_{P-w} w_{P-w} + \rho_a \phi_{E-w} w_{E-w}}{2}, 0 \right) - \frac{\phi_{h-u}\mu}{z_{H-u} - z_{P-u}} \right) A_{h-u} \tag{A.19}$$

$$a_{uL-P-u} = \left(-\max\left(\frac{\rho_a \phi_{L-w} w_{L-w} + \rho_a \phi_{LE-w} w_{LE-w}}{2}, 0 \right) - \frac{\phi_{l-u}\mu}{z_{P-u} - z_{L-u}} \right) A_{l-u} \tag{A.20}$$

$$a_{uP-P-u} = -\left(a_{uL-P-u} + a_{uW-P-u} + a_{uS-P-u} + a_{uN-P-u} + a_{uE-P-u} + a_{uH-P-u}\right) + \left(\frac{\mu \phi_{P-u}^{\ 2}}{K_{P-u}} + \frac{F_{P-u} \phi_{P-u}^{\ 3} \rho_a}{\sqrt{K_{p-u}}} \left| u_{P-u} \right| \right) V_u \tag{A.21}$$

The source term in Equation (A.1) was due to the terms for CDS deferred correction:

$$S_{u-P-u} = S_{duw-P-u} + S_{due-P-u} + S_{dus-P-u} + S_{dun-P-u} + S_{dul-P-u} + S_{duh-P-u} \tag{A.22}$$

$$S_{due-P-u} = \frac{\rho_a \phi_{P-u} u_{P-u} + \rho_a \phi_{E-u} u_{E-u}}{2} \left(\frac{x_{E-u} - x_{e-u}}{x_{E-u} - x_{P-u}} u_{P-u} + \frac{x_{e-u} - x_{P-u}}{x_{E-u} - x_{P-u}} u_{E-u} \right) A_{e-u} + \max\left(\frac{\rho_a \phi_{P-u} u_{P-u} + \rho_a \phi_{E-u} u_{E-u}}{2}, 0 \right) A_{e-u} u_{P-u} + \min\left(\frac{\rho_a \phi_{P-u} u_{P-u} + \rho_a \phi_{E-u} u_{E-u}}{2}, 0 \right) A_{e-u} u_{E-u} \tag{A.23}$$

$$S_{duw-P-u} = \frac{\rho_a \phi_{W-u} u_{W-u} + \rho_a \phi_{P-u} u_{P-u}}{2} \left(\frac{x_{w-u} - x_{W-u}}{x_{P-u} - x_{W-u}} u_{P-u} + \frac{x_{P-u} - x_{w-u}}{x_{P-u} - x_{W-u}} u_{W-u} \right) A_{w-u} - \min\left(\frac{\rho_a \phi_{W-u} u_{W-u} + \rho_a \phi_{P-u} u_{P-u}}{2}, 0 \right) A_{w-u} u_{P-u} - \max\left(\frac{\rho_a \phi_{W-u} u_{W-u} + \rho_a \phi_{P-u} u_{P-u}}{2}, 0 \right) A_{w-u} u_{W-u} \tag{A.24}$$

$$S_{dun-P-u} = \frac{\rho_a \phi_{P-v} v_{P-v} + \rho_a \phi_{E-v} v_{E-v}}{2} \left(\frac{y_{N-u} - y_{n-u}}{y_{N-u} - y_{P-u}} u_{P-u} + \frac{y_{n-u} - y_{P-u}}{y_{N-u} - y_{P-u}} u_{N-u} \right) A_{n-u} + \max\left(\frac{\rho_a \phi_{P-v} v_{P-v} + \rho_a \phi_{E-v} v_{E-v}}{2}, 0 \right) A_{n-u} u_{P-u} + \min\left(\frac{\rho_a \phi_{P-v} v_{P-v} + \rho_a \phi_{E-v} v_{E-v}}{2}, 0 \right) A_{n-u} u_{N-u} \tag{A.25}$$

$$S_{dus-P-u}=\frac{\rho_a\phi_{S-v}v_{S-v}+\rho_a\phi_{SE-v}v_{SE-v}}{2}\left(\frac{y_{s-u}-y_{S-u}}{y_{P-u}-y_{S-u}}u_{P-u}+\frac{y_{P-u}-y_{s-u}}{y_{P-u}-y_{S-u}}u_{S-u}\right)A_{s-u}-$$
$$min\left(\frac{\rho_a\phi_{S-v}v_{S-v}+\rho_a\phi_{SE-v}v_{SE-v}}{2},0\right)A_{s-u}u_{P-u}-max\left(\frac{\rho_a\phi_{S-v}v_{S-v}+\rho_a\phi_{SE-v}v_{SE-v}}{2},0\right)A_{s-u}u_{S-u}$$

(A.26)

$$S_{duh-P-u}=\frac{\rho_a\phi_{P-w}w_{P-w}+\rho_a\phi_{E-w}w_{E-w}}{2}\left(\frac{z_{H-u}-z_{h-u}}{z_{H-u}-z_{P-u}}u_{P-u}+\frac{z_{h-u}-z_{P-u}}{z_{H-u}-z_{P-u}}u_{H-u}\right)A_{h-u}+$$
$$max\left(\frac{\rho_a\phi_{P-w}w_{P-w}+\rho_a\phi_{E-w}w_{E-w}}{2},0\right)A_{h-u}u_{P-u}+min\left(\frac{\rho_a\phi_{P-w}w_{P-w}+\rho_a\phi_{E-w}w_{E-w}}{2},0\right)A_{h-u}u_{H-u}$$

(A.27)

$$S_{dul-P-u}=\frac{\rho_a\phi_{L-w}w_{L-w}+\rho_a\phi_{LE-w}w_{LE-w}}{2}\left(\frac{z_{l-u}-z_{L-u}}{z_{P-u}-z_{L-u}}u_{P-u}+\frac{z_{P-u}-z_{l-u}}{z_{P-u}-z_{L-u}}u_{L-u}\right)A_{l-u}-$$
$$min\left(\frac{\rho_a\phi_{L-w}w_{L-w}+\rho_a\phi_{LE-w}w_{LE-w}}{2},0\right)A_{l-u}u_{P-u}-max\left(\frac{\rho_a\phi_{L-w}w_{L-w}+\rho_a\phi_{LE-w}w_{LE-w}}{2},0\right)A_{l-u}u_{L-u}$$

(A.28)

where:

S_{due} = source term due to CDS deferred correction at east surface in x-momentum discretisation equation (N).

S_{duw} = source term due to CDS deferred correction at west surface in x-momentum discretisation equation (N).

S_{dun} = source term due to CDS deferred correction at north surface in x-momentum discretisation equation (N).

S_{dus} = source term due to CDS deferred correction at south surface in x-momentum discretisation equation (N).

S_{duh} = source term due to CDS deferred correction at high surface in x-momentum discretisation equation (N).

S_{dul} = source term due to CDS deferred correction at low surface in x-momentum discretisation equation (N).

- **X-momentum discretisation equation for the x-momentum cells on the interface between produce-air region and the west or east package wall with vents**

As shown in Figure A.3, the x-momentum cell at the boundary between produce-air region and west package wall was divided into two parts, the middle part contains the vent, and the surrounding part has zero velocity on the boundary. The discretisation equation was derived from the middle part. Extending the assumption of one-dimensional flow in vents, it was assumed that the airflow in the middle part of the x-momentum cell is one-dimensional. Therefore only the convection and diffusion fluxes on west and east surface need to be considered. The areas of the west and east surfaces are the vent areas that are calculated with the porosity of the scalar cell in the package wall. To match the momentum and mass flux in the interface between the package wall and the produce-air region, the porosity in the interface was set to one so that the microscopic velocity at the plain air region side matches the intrinsic velocity at the produce-air region. Based on the above treatments, the convection and diffusion fluxes on the west and east surfaces of the middle part of the x-momentum cell were approximated with the numerical schemes presented in the previous section, giving the Equations (A.29)-(A.30):

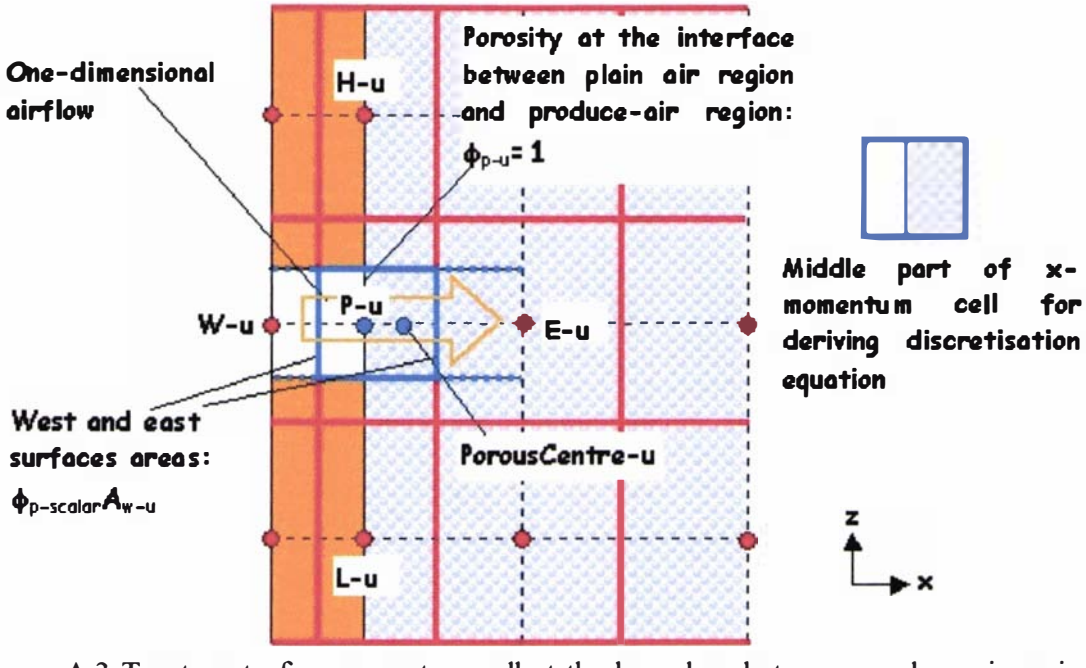

Figure A.3 Treatment of x-momentum cell at the boundary between produce-air region and west package wall

$$\int_{A_{e-u}}\left[\left(\rho_a\phi uu\right)-\left(\mu\phi\frac{\partial u}{\partial x}\right)\right]ds=\left\{\begin{array}{l}\max\left(\frac{\rho_a u_{P-u}+\rho_a\phi_{E-u}u_{E-u}}{2},0\right)u_{P-u}^{current}+\\ \min\left(\frac{\rho_a u_{P-u}+\rho_a\phi_{E-u}u_{E-u}}{2},0\right)u_{E-u}^{current}+\\ \frac{\rho_a u_{P-u}+\rho_a\phi_{E-u}u_{E-u}}{2}\left(\frac{x_{E-u}-x_{e-u}}{x_{E-u}-x_{P-u}}u_{P-u}+\frac{x_{e-u}-x_{P-u}}{x_{E-u}-x_{P-u}}u_{E-u}\right)-\\ \max\left(\frac{\rho_a u_{P-u}+\rho_a\phi_{E-u}u_{E-u}}{2},0\right)u_{P-u}-\\ \min\left(\frac{\rho_a u_{P-u}+\rho_a\phi_{E-u}u_{E-u}}{2},0\right)u_{E-u}-\frac{\mu\phi_{e-u}\left(u_{E-u}^{current}-u_{P-u}^{current}\right)}{x_{E-u}-x_{P-u}}\end{array}\right\}A_{e-u}\phi_{P-scalar}$$

(A.29)

$$\int_{A_{e-u}}\left[\left(\rho_a\phi uu\right)-\left(\mu\phi\frac{\partial u}{\partial x}\right)\right]ds=\left\{\begin{array}{l}\max\left(\frac{\rho_a u_{P-u}+\rho_a u_{W-u}}{2},0\right)u_{W-u}^{current}+\\ \min\left(\frac{\rho_a u_{P-u}+\rho_a u_{W-u}}{2},0\right)u_{P-u}^{current}+\\ \frac{\rho_a u_{P-u}+\rho_a u_{W-u}}{2}\left(\frac{x_{P-u}-x_{w-u}}{x_{P-u}-x_{W-u}}u_{W-u}+\frac{x_{w-u}-x_{W-u}}{x_{P-u}-x_{W-u}}u_{P-u}\right)-\\ \max\left(\frac{\rho_a u_{P-u}+\rho_a u_{W-u}}{2},0\right)u_{W-u}-\\ \min\left(\frac{\rho_a u_{P-u}+\rho_a u_{W-u}}{2},0\right)u_{P-u}-\frac{\mu\left(u_{P-u}^{current}-u_{W-u}^{current}\right)}{x_{P-u}-x_{W-u}}\end{array}\right\}A_{w-u}\phi_{P-scalar}$$

(A.30)

The resistance due to the porous structure exists only in the air-produce region (Figure A.3), and therefore the velocity and porosity at the centre of the air-produce region within the middle part of the x-momentum cell was approximated as follows:

$$u_{porousCentre-u}=\frac{3u_{P-u}+u_{E-u}}{4} \tag{A.31}$$

$$\phi_{porousCentre-u}=\frac{3+\phi_{E-u}}{4} \tag{A.32}$$

Using the above equations to approximate the average value over the produce-air region within the middle part of the x-momentum cell, the source term due to porous structure was written:

$$\int_{Vu}\left(-\frac{\mu\phi^2 u}{K}-\frac{F\phi^3\rho_a}{\sqrt{K}}|u|u\right)dv=-\left(\frac{\mu\phi_{porousCentre-u}{}^2}{K_{porousCentre-u}}+\frac{F_{porouseCentre-u}\phi_{porousCentre-u}{}^3\rho_a\left|\frac{3u_{P-u}+u_{E-u}}{4}\right|}{\sqrt{K_{porousCentre-u}}}\right)$$
$$A_{w-u}(x_{e-u}-x_{P-u})\phi_{P-scalar}\left(\frac{3u_{P-u}^{current}+u_{E-u}^{current}}{4}\right) \quad \text{(A.33)}$$

Based on the above calculation for flux and source term, the coefficients were calculated as follows:

$$a_{uW-P-u}=\left(-\max\left(\frac{(\rho_a u_{W-u}+\rho_a u_{P-u})}{2},0\right)-\frac{\mu}{x_{P-u}-x_{W-u}}\right)A_{w-u}\phi_{P-scalar} \quad \text{(A.34)}$$

$$a_{uE-P-u}=\left(\min\left(\frac{(\rho_a\phi_{E-u}u_{E-u}+\rho_a u_{P-u})}{2},0\right)-\frac{\phi_{e-u}\mu}{x_{E-u}-x_{P-u}}\right)A_{w-u}\phi_{P-scalar}+$$
$$\left(\frac{\mu\phi_{porousCentre-u}{}^2}{K_{porousCentre-u}}+\frac{F_{porouseCentre-u}\phi_{porousCentre-u}{}^3\rho_a\left|\frac{3u_{P-u}+u_{E-u}}{4}\right|}{\sqrt{K_{porousCentre-u}}}\right)\frac{A_{w-u}(x_{e-u}-x_{P-u})\phi_{P-scalar}}{4} \quad \text{(A.35)}$$

$$a_{uN-P-u}=0 \quad \text{(A.36)}$$

$$a_{uS-P-u}=0 \quad \text{(A.37)}$$

$$a_{uH-P-u}=0 \quad \text{(A.38)}$$

$$a_{uL-P-u}=0 \quad \text{(A.39)}$$

$$a_{uP-P-u}=-\left(a_{uW-P-u}+\left(\min\left(\frac{(\rho_a\phi_{E-u}u_{E-u}+\rho_a u_{P-u})}{2},0\right)-\frac{\phi_{e-u}\mu}{x_{E-u}-x_{P-u}}\right)A_{w-u}\phi_{P-scalar}\right)+$$
$$\left(\frac{\mu\phi_{porousCentre-u}{}^2}{K_{porousCentre-u}}+\frac{F_{porouseCentre-u}\phi_{porousCentre-u}{}^3\rho_a\left|\frac{3u_{P-u}+u_{E-u}}{4}\right|}{\sqrt{K_{porousCentre-u}}}\right)\frac{3A_{w-u}(x_{e-u}-x_{P-u})\phi_{P-scalar}}{4} \quad \text{(A.40)}$$

To simplify the calculation, the source term due to deferred CDS correction was ignored:

$$S_{u-P-u} = 0 \tag{A.41}$$

The x-momentum discretisation equation for the x-momentum cell at the boundary between produce-air region and east package wall was derived in the same way.

- **X-momentum discretisation equation for the x-momentum cells next to the x-momentum cells at the boundary between produce-air region and west/east package walls with vents**

As shown in Figure A.4, the x-momentum cell next to the x-momentum cell at the boundary between produce-air region and west package wall is the same as the x-momentum cells in the middle of produce regions apart from the treatment of velocity and porosity at the west node. To maintain mass conservation, velocity at the west node was modified as follows:

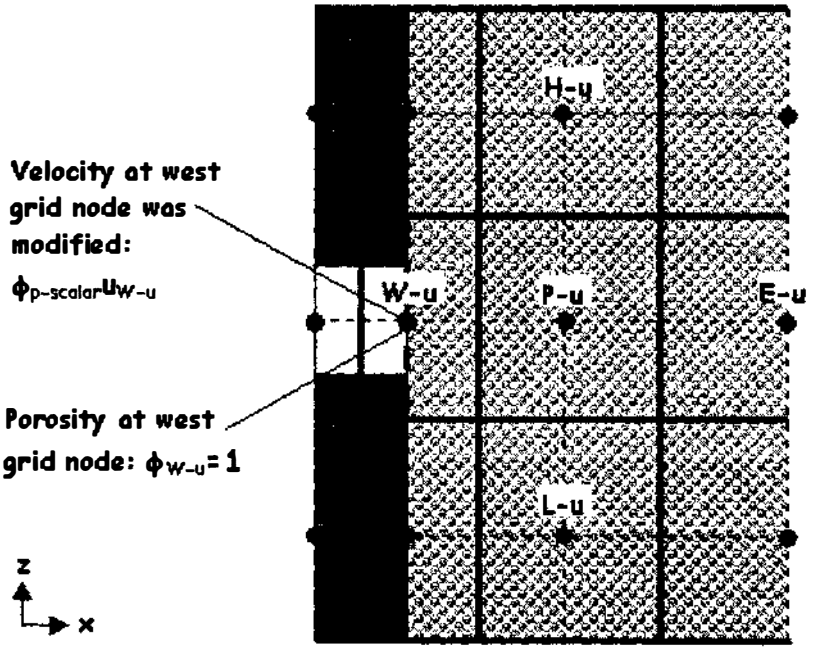

Figure A.4 Treatment of the x-momentum cell next to the x-momentum cell at the boundary between produce-air region and west package wall with vent

$$u^{m}_{W-u} = \phi_{W-scalar} u_{W-u} \tag{A.42}$$

As discussed in the previous section, the porosity at the interface between produce-air region and west package wall with vent was set to one. Therefore Equation (A.16) was modified as follows:

$$a_{uW-P-u} = \left(-\max\left(\frac{\rho_a \phi_{W-scalar} u_{W-u} + \rho_a \phi_{P-u} u_{P-u}}{2}, 0 \right) - \frac{\phi_{w-u} \phi_{W-scalar} \mu}{x_{P-u} - x_{W-u}} \right) A_{w-u} \tag{A.43}$$

Consequently the coefficient for current node was modified as follows:

$$a_{uP-P-u} = \left(-\max\left(\frac{\rho_a \phi_{W-scalar} u_{W-u} + \rho_a \phi_{P-u} u_{P-u}}{2}, 0 \right) - \frac{\phi_{w-u} \mu}{x_{P-u} - x_{W-u}} \right) A_{w-u} -$$
$$\left(a_{uL-P-u} + a_{uS-P-u} + a_{uN-P-u} + a_{uE-P-u} + a_{uH-P-u}\right) + \left(\frac{\mu \phi_{P-u}^{2}}{K_{P-u}} + \frac{F_{P-u} \phi_{P-u}^{3} \rho_a}{\sqrt{K_{p-u}}} |u_{P-u}| \right) V_u \tag{A.44}$$

Other coefficients were calculated with Equations (A.15) and (A.17)-(A.20). To simplify the calculation, the CDS deferred correction from west surface was removed from source term equation (Equation A.22):

$$S_u = S_{due-P-u} + S_{dus-P-u} + S_{dun-P-u} + S_{dut-P-u} + S_{duh-P-u} \tag{A.45}$$

The x-momentum discretisation equation for the x-momentum cell next to the x-momentum cell at the boundary between produce-air region and east package wall was derived in the same way.

- **X-momentum discretisation equation for the x-momentum cells in air-produce region and next to south/north/bottom/top package walls**

For the x-momentum cells along the south package wall, the convection term is zero. Even if the cell is next to the south package wall with vent, the convection flux for momentum at x-axis is still zero due to one-dimensional nature of airflow in the vent. Therefore the diffusion term for south surface was approximated as follows:

$$-\left(\phi\mu\frac{\partial u}{\partial y}A\right)_{s-u} = -\phi_{P-u}\mu\frac{u_{P-u}}{y_{P-u}-y_{s-u}}A_{s-u} \tag{A.46}$$

Consequently the coefficients for south grid node and current grid node were modified as follows:

$$a_{uS-P-u} = 0 \tag{A.47}$$

$$a_{uP-P-u} = -\left(a_{uL-P-u} - \frac{\phi_{P-u}\mu A_{s-u}}{y_{P-u}-y_{s-u}} + a_{uW-P-u} + a_{uN-P-u} + a_{uE-P-u} + a_{uH-P-u}\right) \tag{A.48}$$

Other coefficients were calculated with Equations (A.15)-(A.17) and (A.19)-(A.20).

The CDS deferred correction from south surface was removed from source term equation (Equation A.22).

$$S_{u-P-u} = S_{due-u} + S_{duw-u} + S_{dun-u} + S_{dul-u} + S_{duh-u} \tag{A.49}$$

The x-momentum discretisation equations for the x-momentum cell next to north, bottom, and top package walls were derived in the same way.

- **X-momentum discretisation equation for x-momentum cells between a vented east wall in one package and a vented west wall in another package**

As shown in Figure A.5, the x-momentum cell between two package walls is in plain air region. For one-dimensional airflow, only the convection and diffusion fluxes on west and east surface need to be considered. Integrating one-dimensional momentum equation (Equation 4.3a) over the middle part of the x-momentum cell, the coefficients for x-momentum discretisation equation were derived to be:

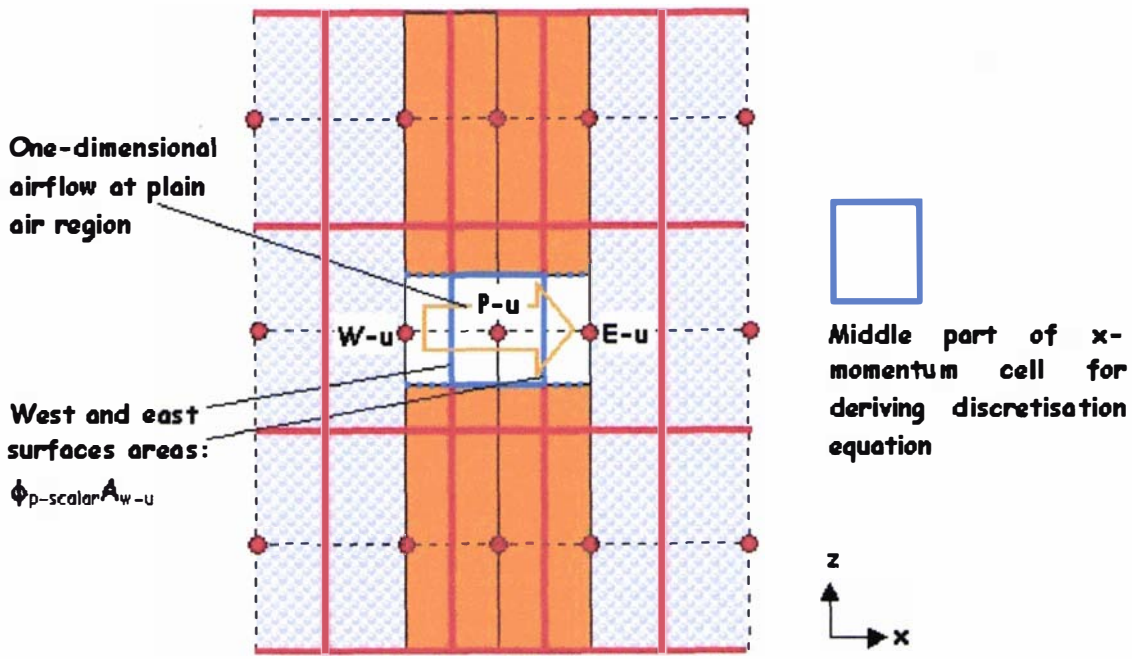

Figure A.5 Treatment of the x-momentum cells between the vented east wall in one package and the vented west wall in another package

$$a_{uW-P-u} = \left(-\max\left(\frac{(\rho_a u_{W-u} + \rho_a u_{P-u})}{2}, 0 \right) - \frac{\mu}{x_{P-u} - x_{W-u}} \right) A_{e-scalar} \phi_{P-scalar} \quad \text{(A.50)}$$

$$a_{uE-P-u} = \left(\min\left(\frac{(\rho_a u_{E-u} + \rho_a u_{P-u})}{2}, 0 \right) - \frac{\mu}{x_{E-u} - x_{P-u}} \right) A_{e-scalar} \phi_{P-scalar} \quad \text{(A.51)}$$

$$a_{uP-P-u} = -(a_{uW-P-u} + a_{uE-P-u}) \quad \text{(A.52)}$$

Other coefficients were set to be zero (Equations A.36-A.39).

To simplify the calculation, the source term due to deferred CDS correction was ignored (Equation A.41).

- **X-momentum discretisation equation for x-momentum cells at the boundary between outside environment and the west/east package walls with fixed-velocity vent**

For fixed-velocity vent, the velocity was set to a predefined value:

$$u_{P-u} = u_{fixed} \tag{A.53}$$

- **X-momentum discretisation equation for x-momentum cells at the boundary between outside environment and the west/east package walls with fixed-pressure vent**

To maintain mass conservation, the velocity at the boundary between west package wall and outside environment was set as follows:

$$u_{P-u} = u_{E-u} \tag{A.54}$$

Similarly, the velocity at the boundary between east package wall and outside environment was set as follows:

$$u_{P-u} = u_{W-u} \tag{A.55}$$

- **X-momentum discretisation equation for the x-momentum cells in south, north, bottom, and top package walls, or in the interfaces between produce-air region and the west/east package walls without vents**

The grid nodes of this type of x-momentum cells are on the solid region, so no-slip boundary condition applies:

$$u_{P-u} = 0 \tag{A.56}$$

A.1.3 Y-Momentum Discretisation Equations

- **Types of y-momentum cells**

There are eight types of y-momentum cells, which are summarised in Figure A.6 and Table A.2. For each type of y-momentum cell, a set of expressions was derived for the coefficients and source term in the y-momentum discretisation equation (Equation A.2).

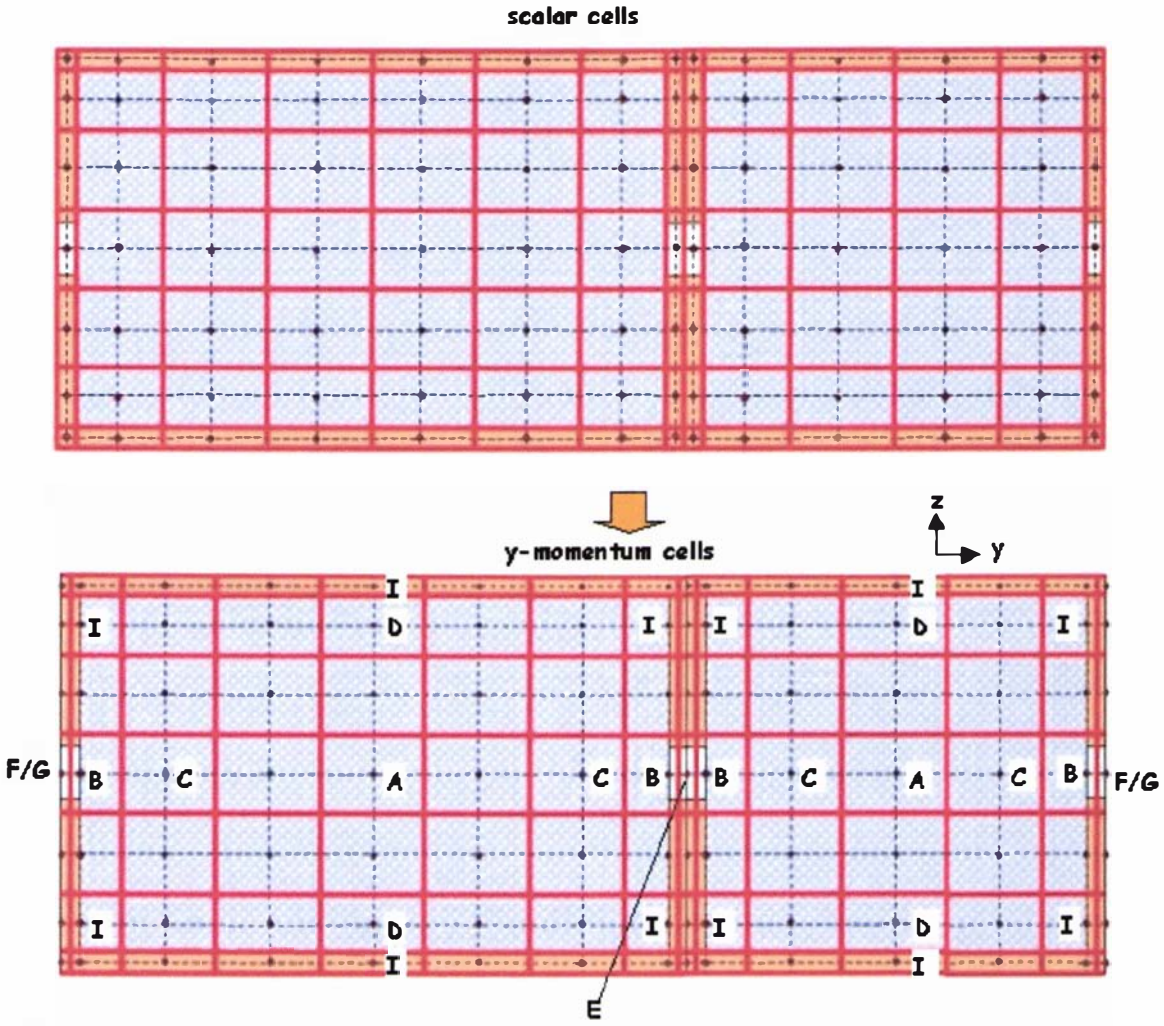

Figure A.6 Grids for the y-momentum discretisation equations in bulk packaging systems (the capital letters indicate the types of the y-momentum cells, which are explained in Table A.2)

Table A.2 Types of y-momentum cells in bulk packaging systems

Type	Location	Transport equations
A	Middle of produce-air region	• Generalised volume-averaged momentum equation (Equation 4.4b)
B	On the interface between plain air region and south/north package walls with vents	• Generalised volume-averaged momentum equation (Equation 4.4b) • One-dimensional Navier-Stokes equation (Equation 4.3 b)
C	In produce-air region and on the north or south side of the cells of type B	• Generalised volume-averaged momentum equation (Equation 4.4b)
D	In produce-air region and next to west, east, bottom, and top package walls	• Wall boundary conditions
E	On the interface between a vented north wall in one package and a vented south wall in another package	• One-dimensional Navier-Stokes equation (Equation 4.3 b)
F	On the interface between outside environment and the south/north walls with fixed-pressure vents.	• Fixed-pressure boundary conditions
G	On the interface between outside environment and the south/north walls with fixed-velocity vents.	• Fixed-velocity boundary conditions
I	In west, east, bottom, and top package wall, or in the interface between produce-air region and south/north package walls without vent	• Velocity component at y-axis is set to zero

- **Y-momentum discretisation equations**

Since the types of y-momentum cells are very similar to that of x-momentum cells, the numerical methods for deriving the x-momentum discretisation equations were used to derive the y-momentum discretisation equations.

A.1.4 Z-Momentum Discretisation Equations

- **Types of z-momentum cells**

There are three types of z-momentum cells, which are summarised in Table A.3 and Figure A7. For each type of z-momentum cells, a set of expressions was derived for the coefficients and source term in z-momentum discretisation equation (Equation A.3).

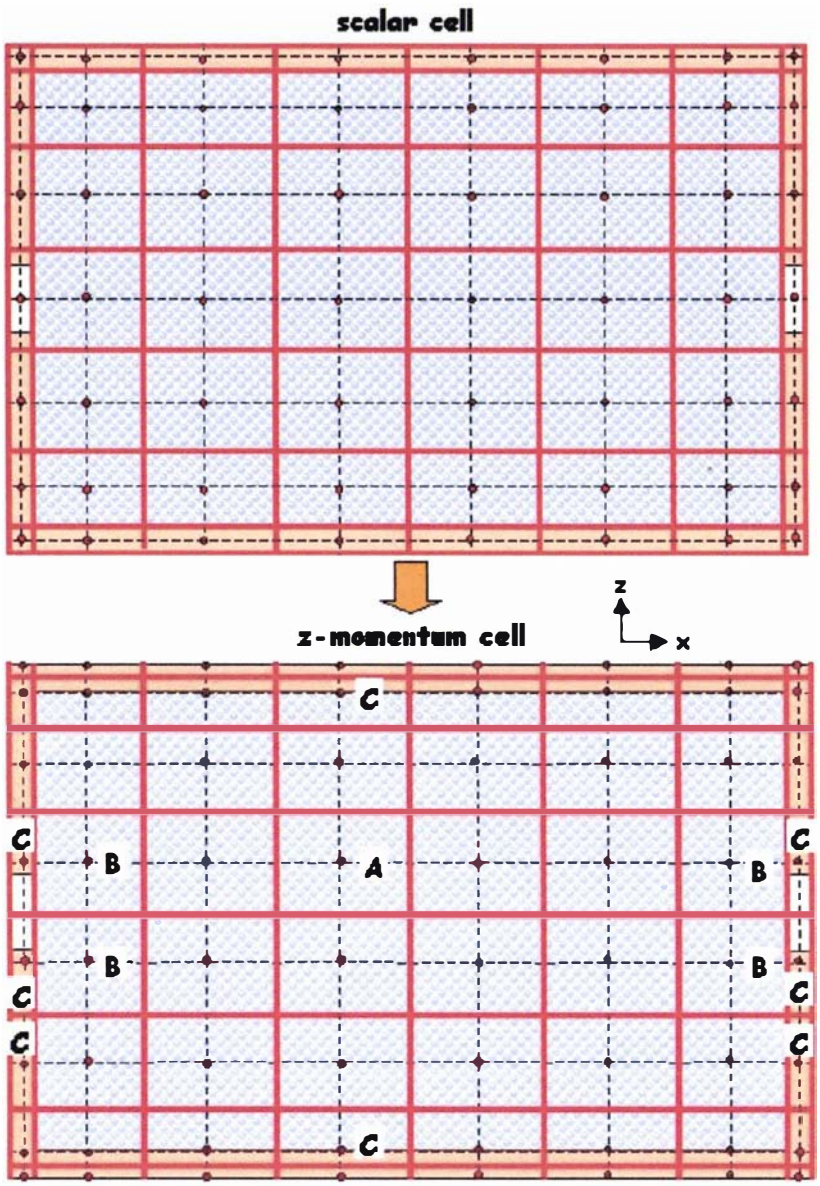

Figure A.7 Grids for the z-momentum discretisation equations in bulk packaging systems (the capital letters indicate the types of z-momentum cells, which are explained in Table A.3)

Table A.3 Types of z-momentum cells in bulk packaging systems

Type	Location	Transport equations
A	Middle of produce-air region	• Generalised volume-averaged momentum equation (Equation 4.4c)
B	In produce-air region and next to west, east, south, and north package walls	• Wall boundary conditions
C	In west/east/north/ south package walls, or in the interface between produce-air region and bottom/top package walls without vent	• Velocity component at z-axis is set to zero

- **Z-momentum discretisation equations**

Since each type of z-momentum cell is similar to the equivalent type of x-momentum cell, the numerical methods for deriving the x-momentum discretisation equations were used to derive the z-momentum discretisation equations.

A.1.5 Pressure Correction and Pressure Discretisation Equations

- **Types of scalar cells in terms of pressure correction and pressure discretisation equation**

There are seven types of scalar cells in terms of pressure correction and pressure, which are summarised in Figure A.8 and Table A.4. For each type of scalar cell, a set of expressions was derived for the coefficients and source terms in pressure correction and pressure discretisation equations (Equations A.4-A.5).

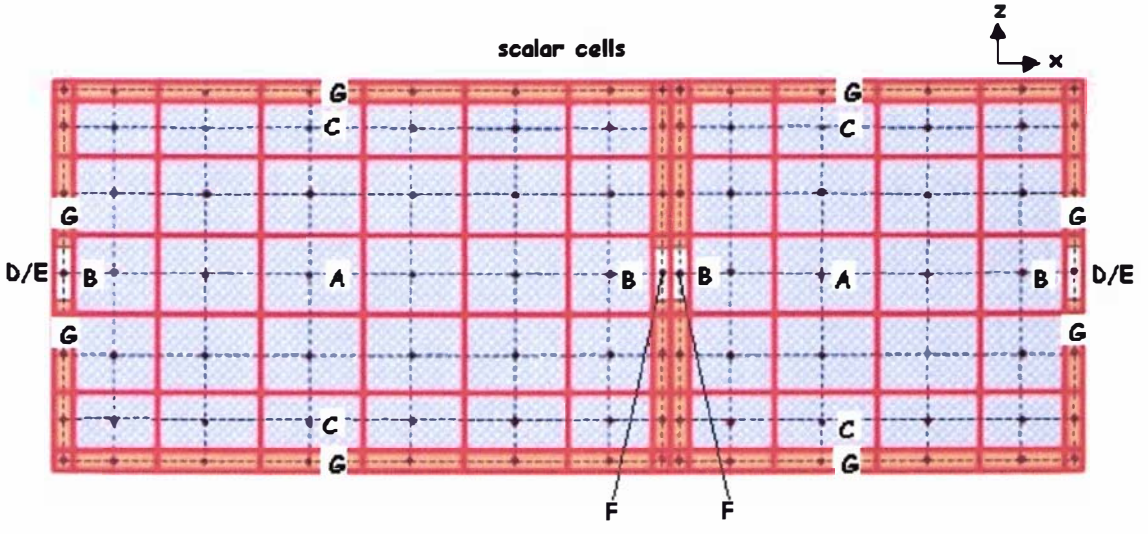

Figure A.8 Grids for the pressure correction and pressure discretisation equations in bulk packaging systems (the capital letters indicate the types of scalar cells in terms of pressure correction and pressure, which are explained in Table A.4)

Table A.4 Types of scalar cells in terms of pressure correction and pressure

Type	Location	Transport equations
A	Middle of produce-air region	• Volume-averaged continuity equation (Equation 4.2)
B	In produce-air region and next to west, east, south, and north package walls with vents	• Volume-averaged continuity equation (Equation 4.2)
C	In produce-air region and next to west, east, south, and north package walls without vents	• Volume-averaged continuity equation (Equation 4.2)
D	In west, east, south, north package walls with fixed-velocity vents	• One-dimensional continuity equation (Equation 4.1a and 41.b) • Fixed-velocity boundary conditions
E	In west, east, south, north package walls with fixed-pressure vents	• No pressure or pressure correction equation is needed
F	In vented west/east/south /north package wall next to another vented package wall	• One-dimensional continuity equation (Equation 4.1a and 4.1b)
G	In west, east, south, north bottom, top package walls without vents	• No pressure or pressure correction equation is needed

- **Pressure correction and pressure discretisation equations for scalar cells in the middle of produce-air region**

The discretisation momentum equations cannot be solved until the pressure field is given. To estimate the pressure field, an imperfect velocity field was calculated according to a guessed pressure field, and then the relations between velocity corrections and pressure corrections were derived as follows (Patankar, 1980):

$$u_{P-u}^{corrected} = u_{P-u} + \frac{(\phi_{P-scalar}\Delta p_{P-scalar} - \phi_{E-scalar}\Delta p_{E-scalar})A_{e-scalar}}{a_{uP-P-u}} \quad \text{(A.57)}$$

$$u_{W-u}^{corrected} = u_{W-u} + \frac{(-\phi_{P-scalar}\Delta p_{P-scalar} + \phi_{W-scalar}\Delta p_{W-scalar})A_{w-scalar}}{a_{uP-W-u}} \quad \text{(A.58)}$$

$$v_{P-v}^{corrected} = v_{P-v} + \frac{(\phi_{P-scalar}\Delta p_{P-scalar} - \phi_{N-scalar}\Delta p_{N-scalar})A_{n-scalar}}{a_{vP-P-v}} \quad \text{(A.59)}$$

$$v_{S-v}^{corrected} = v_{S-v} + \frac{(-\phi_{P-scalar}\Delta p_{P-scalar} + \phi_{S-scalar}\Delta p_{S-scalar})A_{s-scalar}}{a_{vP-S-v}} \quad \text{(A.60)}$$

$$w_{P-w}^{corrected} = w_{P-w} + \frac{(\phi_{P-scalar}\Delta p_{P-scalar} - \phi_{H-scalar}\Delta p_{H-scalar})A_{h-scalar}}{a_{wP-P-w}} \quad \text{(A.61)}$$

$$w_{L-w}^{corrected} = w_{L-w} + \frac{(-\phi_{P-scalar}\Delta p_{P-scalar} + \phi_{L-scalar}\Delta p_{L-scalar})A_{l-s\_lar}}{a_{wP-L-w}} \quad \text{(A.62)}$$

where:

Δp = pressure correction ($N \cdot m^{-2}$).

a_{uP} = coefficient in x-momentum discretisation equation for current node.

a_{vP} = coefficient in y-momentum discretisation equation for current node.

a_{wP} = coefficient in z-momentum discretisation equation for current node.

The following equation was from mass conservation over a scalar cell (continuity equation):

$$\rho_a\phi_{e-scalar}A_{e-scalar}u_{P-u}^{corrected} - \rho_a\phi_{w-scalar}A_{w-scalar}u_{W-u}^{corrected} + \rho_a\phi_{n-scalar}A_{n-scalar}v_{P-v}^{corrected} - \rho_a\phi_{s-scalar}A_{s-scalar}v_{S-v}^{corrected} + \rho_a\phi_{h-scalar}A_{h-scalar}w_{P-w}^{corrected} - \rho_a\phi_{le-scalar}A_{l-scalar}w_{L-w}^{corrected} = 0 \quad \text{(A.63)}$$

Substituting Equations (A.57)-(A.62) into Equation (A.63), the coefficients and source term in pressure correction equation (Equation A.4) were calculated as follows:

$$a_{pE-P-scalar} = -\frac{\rho_a\phi_{e-scalar}\phi_{E-scalar}A_{e-scalar}^2}{a_{uP-P-u}} \quad \text{(A.64)}$$

$$a_{pW-P-scalar} = -\frac{\rho_a\phi_{w-scalar}\phi_{W-scalar}A_{w-scalar}^2}{a_{uP-W-u}} \quad \text{(A.65)}$$

$$a_{pH-P-scalar} = -\frac{\rho_a\phi_{h-scalar}\phi_{H-scalar}A_{h-scalar}^2}{a_{wP-P-w}} \quad \text{(A.66)}$$

$$a_{pL-P-scalar} = -\frac{\rho_a\phi_{l-scalar}\phi_{L-scalar}A_{l-scalar}^2}{a_{wP-L-w}} \quad \text{(A.67)}$$

$$a_{pN-P-scalar} = -\frac{\rho_a\phi_{n-scalar}\phi_{N-scalar}A_{n-scalar}^2}{a_{vP-P-v}} \quad \text{(A.68)}$$

$$a_{pS-P-scalar} = -\frac{\rho_a \phi_{s-scalar} \phi_{S-scalar} A^2_{s-scalar}}{a_{vP-S-v}} \tag{A.69}$$

$$a_{pP-P-scalar} = \frac{\rho_a \phi_{l-scalar} \phi_{P-scalar} A^2_{l-scalar}}{a_{wP-L-w}} + \frac{\rho_a \phi_{h-scalar} \phi_{P-scalar} A^2_{h-scalar}}{a_{wP-P-w}} + \frac{\rho_a \phi_{w-scalar} \phi_{P-scalar} A^2_{w-scalar}}{a_{uP-W-u}} + \frac{\rho_a \phi_{e-scalar} \phi_{P-scalar} A^2_{e-scalar}}{a_{uP-P-u}} + \frac{\rho_a \phi_{s-scalar} \phi_{P-scalar} A^2_{s-scalar}}{a_{vP-S-v}} + \frac{\rho_a \phi_{n-scalar} \phi_{P-scalar} A^2_{n-scalar}}{a_{vP-P-v}} \tag{A.70}$$

$$S_{\Delta p-P-scalar} = \rho_a \phi_{l-scalar} w_{L-w} A_{l-scalar} - \rho_a \phi_{h-scalar} w_{P-w} A_{h-scalar} + \rho_a \phi_{w-scalar} u_{W-u} A_{w-scalar} - \rho_a \phi_{e-scalar} u_{P-u} A_{e-scalar} + \rho_a \phi_{s-scalar} v_{S-v} A_{s-scalat} - \rho_a \phi_{n-scalar} v_{P-v} A_{n-scalar} \tag{A.71}$$

The velocity fields were corrected by the calculated pressure corrections using Equations (A.57)-(A.62).

The pressure was calculated with a pressure equation that has the same coefficients as the pressure correction equation. The source term in pressure equation was calculated from pseudo-velocity components:

$$S_{p-P-scalar} = \rho_a \phi_{l-scalar} w^{pressure}_{L-w} A_{l-scalar} - \rho_a \phi_{h-scalar} w^{pressure}_{P-w} A_{h-scalar} + \rho_a \phi_{w-scalar} u^{pressure}_{W-u} A_{w-scalar} - \rho_a \phi_{e-scalar} u^{pressure}_{P-u} A_{e-scalar} + \rho_a \phi_{s-scalar} v^{pressure}_{S-v} A_{s-scalar} - \rho_a \phi_{n-scalar} v^{pressure}_{P-v} A_{n-scalar} \tag{A.72}$$

The pseudo-velocity components were calculated from the momentum discretisation equations as follows:

$$u^{pressure}_{P-u} = \frac{S_{u-P-u} - a_{uN-P-u} u_{N-u} - a_{uE-P-u} u_{E-u} - a_{uH-P-u} u_{H-u} - a_{uL-P-u} u_{L-u} - a_{uW-P-u} u_{W-u} - a_{uS-P-u} u_{S-u}}{a_{uP-P-u}} \tag{A.73}$$

$$v^{pressure}_{P-v} = \frac{S_{v-P-v} - a_{vN-P-v} v_{N-v} - a_{vE-P-v} v_{E-v} - a_{vH-P-v} v_{H-v} - a_{vL-P-v} v_{L-v} - a_{vW-P-v} v_{W-v} - a_{vS-P-v} v_{S-v}}{a_{vP-P-v}} \tag{A.74}$$

$$w_{P-w}^{pressure} = \frac{S_{w-P-w} - a_{wN-P-w}w_{N-w} - a_{wE-P-w}w_{E-w} - a_{wH-P-w}w_{H-w} - a_{wL-P-w}w_{L-w} - a_{wW-P-w}w_{W-w} - a_{wS-P-w}w_{S-w}}{a_{wP-P-w}} \quad \text{(A.75)}$$

- **Pressure and pressure correction discretisation equations for scalar cells in air-produce region and next to west /east/south/north package walls with vents**

Based on the x-momentum discretisation equation for x-momentum cells at the boundary between produce-air region and west package wall, the velocity correction equation was derived:

$$u_{W-u}^{corrected} = u_{W-u} + \frac{(-\phi_{P-scalar}\Delta p_{P-scalar} + \Delta p_{W-scalar})\phi_{W-scalar}A_{w-scalar}}{a_{uP-W-u}} \quad \text{(A.76)}$$

Equation (A.63) was modified to account for the vent structure as shown in Figure A.9.

$$\rho_a\phi_{e-scalar}A_{e-scalar}u_{P-u}^{corrected} - \rho_a\phi_{W-scalar}A_{w-scalar}u_{W-u}^{corrected} + \rho_a\phi_{n-scalar}A_{n-scalar}v_{P-v}^{corrected} - \rho_a\phi_{s-scalar}A_{s-scalar}v_{S-v}^{corrected} + \rho_a\phi_{h-scalar}A_{h-scalar}w_{P-w}^{corrected} - \rho_a\phi_{le-scalar}A_{l-scalar}w_{L-w}^{corrected} = 0 \quad \text{(A.77)}$$

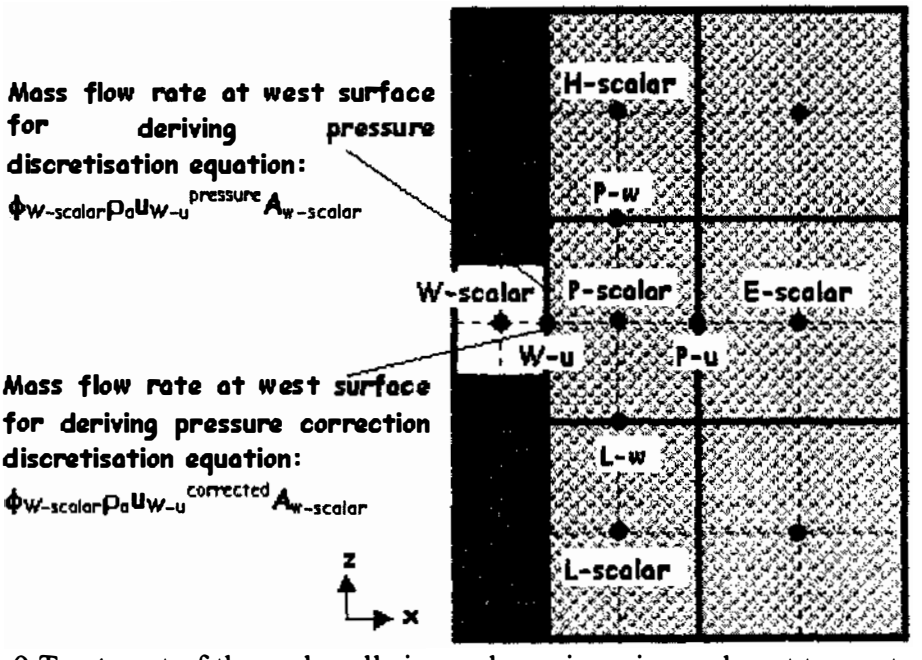

Figure A.9 Treatment of the scale cells in produce-air region and next to west package wall with vents for derivation of pressure correction and pressure discretisation equations.

Consequently the following modified coefficients and source terms in pressure correction and pressure discretisation equations for the scalar cell next to west wall with vent were derived:

$$a_{pW-P-scalar} = -\frac{\rho_a \phi_{W-scalar}^2 A_{w-scalar}^2}{a_{uP-W-u}} \tag{A.78}$$

$$a_{pP-P-scalar} = \frac{\rho_a \phi_{l-scalar} \phi_{P-scalar} A_{l-scalar}^2}{a_{wP-L-w}} + \frac{\rho_a \phi_{h-scalar} \phi_{P-scalar} A_{h-scalar}^2}{a_{wP-P-w}} + \frac{\rho_a \phi_{W-scalar}^2 \phi_{P-scalar} A_{w-scalar}^2}{a_{uP-W-u}} + \frac{\rho_a \phi_{e-scalar} \phi_{P-scalar} A_{e-scalar}^2}{a_{uP-P-u}} + \frac{\rho_a \phi_{s-scalar} \phi_{P-scalar} A_{s-scalar}^2}{a_{vP-S-v}} + \frac{\rho_a \phi_{n-scalar} \phi_{P-scalar} A_{n-scalar}^2}{a_{vP-P-v}} \tag{A.79}$$

$$S_{\Delta p-P-scalar} = \rho_a \phi_{l-scalar} w_{L-w} A_{l-scalar} - \rho_a \phi_{h-scalar} w_{P-w} A_{h-scalar} + \rho_a \phi_{W-scalar} u_{W-u} A_{w-scalar} - \rho_a \phi_{e-scalar} u_{P-u} A_{e-scalar} + \rho_a \phi_{s-scalar} v_{S-v} A_{s-scalar} - \rho_a \phi_{n-scalar} v_{P-v} A_{n-scalar} \tag{A.80}$$

$$S_{p-P-scalar} = \rho_a \phi_{l-scalar} w_{L-w}^{pressure} A_{l-scalar} - \rho_a \phi_{h-scalar} w_{P-w}^{pressure} A_{h-scalar} + \rho_a \phi_{W-scalar} u_{W-u}^{pressure} A_{w-scalar} - \rho_a \phi_{e-scalar} u_{P-u}^{pressure} A_{e-scalar} + \rho_a \phi_{s-scalar} v_{S-v}^{pressure} A_{s-scalar} - \rho_a \phi_{n-scalar} v_{P-v}^{pressure} A_{n-scalar} \tag{A.81}$$

Other coefficients were calculated with Equations (A.64) and (A.66)-(A.69).

The pressure correction and pressure discretisation equations for the scalar cells next to the east/south/north package walls with vents were derived in the same way.

- **Pressure correction and pressure discretisation equations for scalar cells in air-produce region and next to the package wall without vents**

For the scalar cells next to the west wall, no pressure and velocity corrections for west grid node are needed as the wall velocity (u_W=0) is known, Therefore the coefficient for west node in pressure and pressure correction equations were modified as follows:

$$a_{pW-P-scalar} = 0 \tag{A.82}$$

Other coefficients were calculated with Equations (A.64) and (A.66)-(A.69).

The pressure correction and pressure discretisation equations for the scalar cells next to east/south/north/bottom/top package walls were derived in the same way.

- **Pressure correction and pressure discretisation equations for scalar cells in package walls with fixed velocity vents**

As shown in Figure A.10, the middle part of the scalar cell, which contains the vent in west package wall, was used to implement mass conversation for derivation of the pressure correction and pressure discretisation equations. Since the velocities at all surfaces except the east surface are either zero or the fixed velocity, no pressure and velocity corrections are needed. The coefficients for these grid nodes in pressure and pressure correction equations were modified as follows:

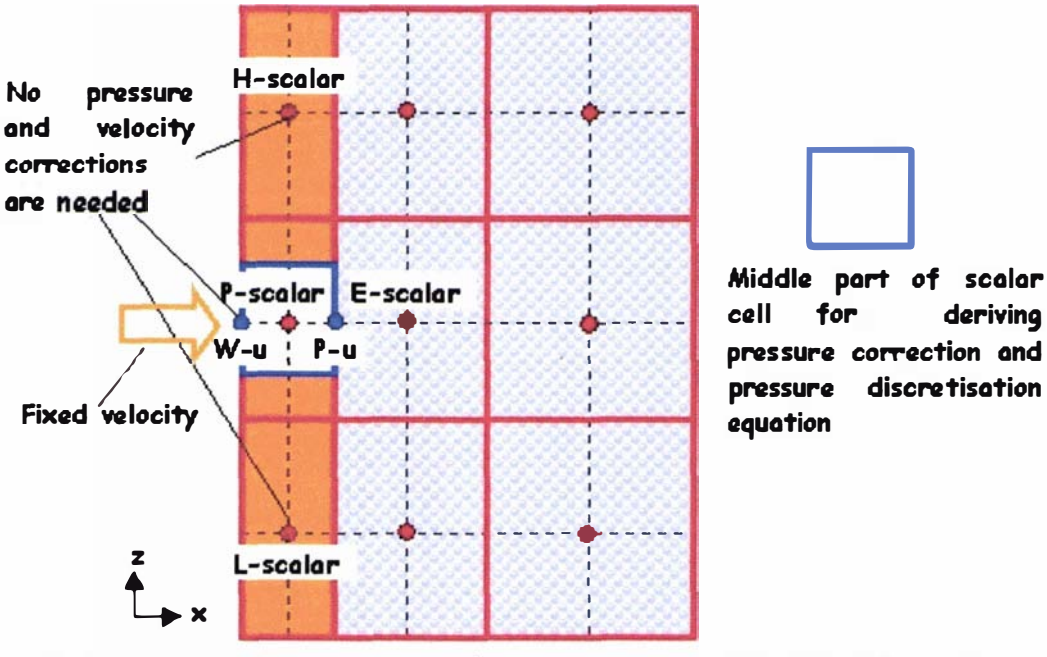

Figure A.10 Treatment of the scale cell in the west package wall with vent for derivation of pressure correction and pressure discretisation equations.

$$a_{pW-P-scalar} = 0 \tag{A.83}$$

$$a_{pN-P-scalar} = 0 \tag{A.84}$$

$$a_{pS-P-scalar} = 0 \tag{A.85}$$

$$a_{pH-P-scalar} = 0 \tag{A.86}$$

$$a_{pL-P-scalar} = 0 \tag{A.87}$$

The velocity correction equation at east surface was derived as follows:

$$u_{P-u}^{corrected} = u_{P-u} + \frac{(\Delta p_{P-scalar} - \phi_{E-scalar}\Delta p_{E-scalar})\phi_{P-scalar}A_{e-scalar}}{a_{uP-P-u}} \tag{A.88}$$

Consequently the coefficients for east and current nodes and source terms were derived as follows:

$$a_{pE-P-scalar} = -\frac{\rho_a \phi_{P-scalar}^2 \phi_{E-scalar} A_{e-scalar}^2}{a_{uP-P-u}} \tag{A.89}$$

$$a_{pP-P-scalar} = \frac{\rho_a \phi_{P-scalar}^2 A_{e-scalar}^2}{a_{uP-P-u}} \tag{A.90}$$

$$S_{\Delta p-P-scalar} = \rho_a \phi_{P-scalar} u_{W-u} A_{e-scalar} - \rho_a \phi_{P-scalar} u_{P-u} A_{e-scalar} \tag{A.91}$$

$$S_{p-P-scalar} = \rho_a \phi_{P-scalar} u_{W-u}^{pressure} A_{e-scalar} - \rho_a \phi_{P-scalar} u_{P-u}^{pressure} A_{e-scalar} \tag{A.92}$$

The pressure correction and pressure discretisation equations for the scalar cells in the east/south/north package walls with fixed velocity vents were derived in the same way.

- **Pressure correction and pressure discretisation equations for scalar cells in package walls with fixed pressure vents or scalar cells in package walls without vents**

As the pressure in the scalar cell is fixed, no pressure correction is needed.

$$\Delta p_{P-scalar} = 0 \tag{A.93}$$

$$p_{P-scalar} = p_{fixed} \tag{A.94}$$

- **Pressure correction and pressure discretisation equations for scalar cells in one vented wall in one package and next to another vented wall in another package**

As shown in Figure A.11, the middle part of the scale cell, which contains the vent in east package wall, was used to implement mass conversation for derivation of pressure correction and pressure discretisation equations. The velocity correction equations for east and west surfaces were derived:

$$u_{P-u}^{corrected} = u_{P-u} + \frac{(\Delta p_{P-scalar} - \Delta p_{E-scalar})\phi_{P-scalar} A_{e-scalar}}{a_{uP-P-u}} \tag{A.95}$$

$$u_{W-u}^{corrected} = u_{W-u} + \frac{(\Delta p_{P-scalar} - \phi_{W-scalar} \Delta p_{W-scalar})\phi_{P-scalar} A_{e-scalar}}{a_{uP-W-u}} \tag{A.96}$$

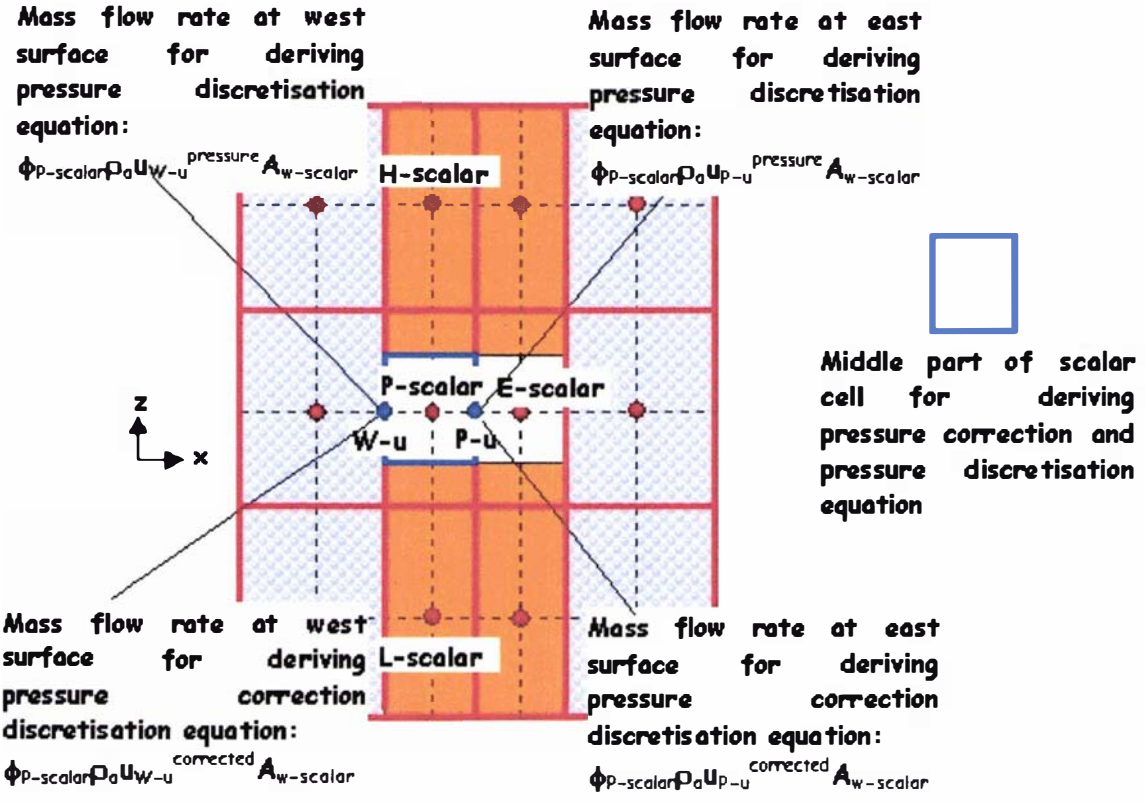

Figure A.11 Treatment of the scalar cell in a vented east package wall next to a west wall in another package for derivation of pressure correction and pressure discretisation equations.

Based on mass conservation, the following coefficients and source terms were derived (other coefficients are zero):

$$a_{pW-P-scalar} = -\frac{\rho_a \phi^2_{P-scalar} \phi_{W-scalar} A^2_{e-scalar}}{a_{uP-W-u}} \quad \text{(A.97)}$$

$$a_{pE-P-scalar} = -\frac{\rho_a \phi^2_{P-scalar} A^2_{e-scalar}}{a_{uP-P-u}} \quad \text{(A.98)}$$

$$a_{pP-P-scalar} = \frac{\rho_a \phi^2_{P-scalar} A^2_{e-scalar}}{a_{uP-W-u}} + \frac{\rho_a \phi^2_{P-scalar} A^2_{e-scalar}}{a_{uP-P-u}} \quad \text{(A.99)}$$

$$S_{\Delta p-P-scalar} = \rho_a \phi_{P-scalar} u_{W-u} A_{e-scalar} - \rho_a \phi_{P-scalar} u_{P-u} A_{e-scalar} \quad \text{(A.100)}$$

$$S_{p-P-scalar} = \rho_a \phi_{P-scalar} u^{pressure}_{W-u} A_{e-scalar} - \rho_a \phi_{P-scalar} u^{pressure}_{P-u} A_{e-scalar} \quad \text{(A.101)}$$

The pressure correction and pressure discretisation equations for the scalar cells in the vented west/south/north package walls and next to the walls in another package were derived in the same way.

A.2 Discretisation Equations for PDEs in the Airflow Model for Layered Packaging Systems

A.2.1 Numerical Schemes

The same numerical schemes used for discretisation of the airflow model in bulk packaging system were applied to derive the discretisation equations for the airflow model in layered packaging system, which have the same forms as that in bulk packaging systems (Equations A.1-A.5).

A.2.2 X-momentum Discretisation Equations

- **Types of x-momentum cells**

There are eight types of x-momentum cells, which are summarised in Figure A.12 and Table A.5. For each type of x-momentum cell, a set of expressions was derived for the coefficients and source term in the x-momentum discretisation equation (Equation A.1).

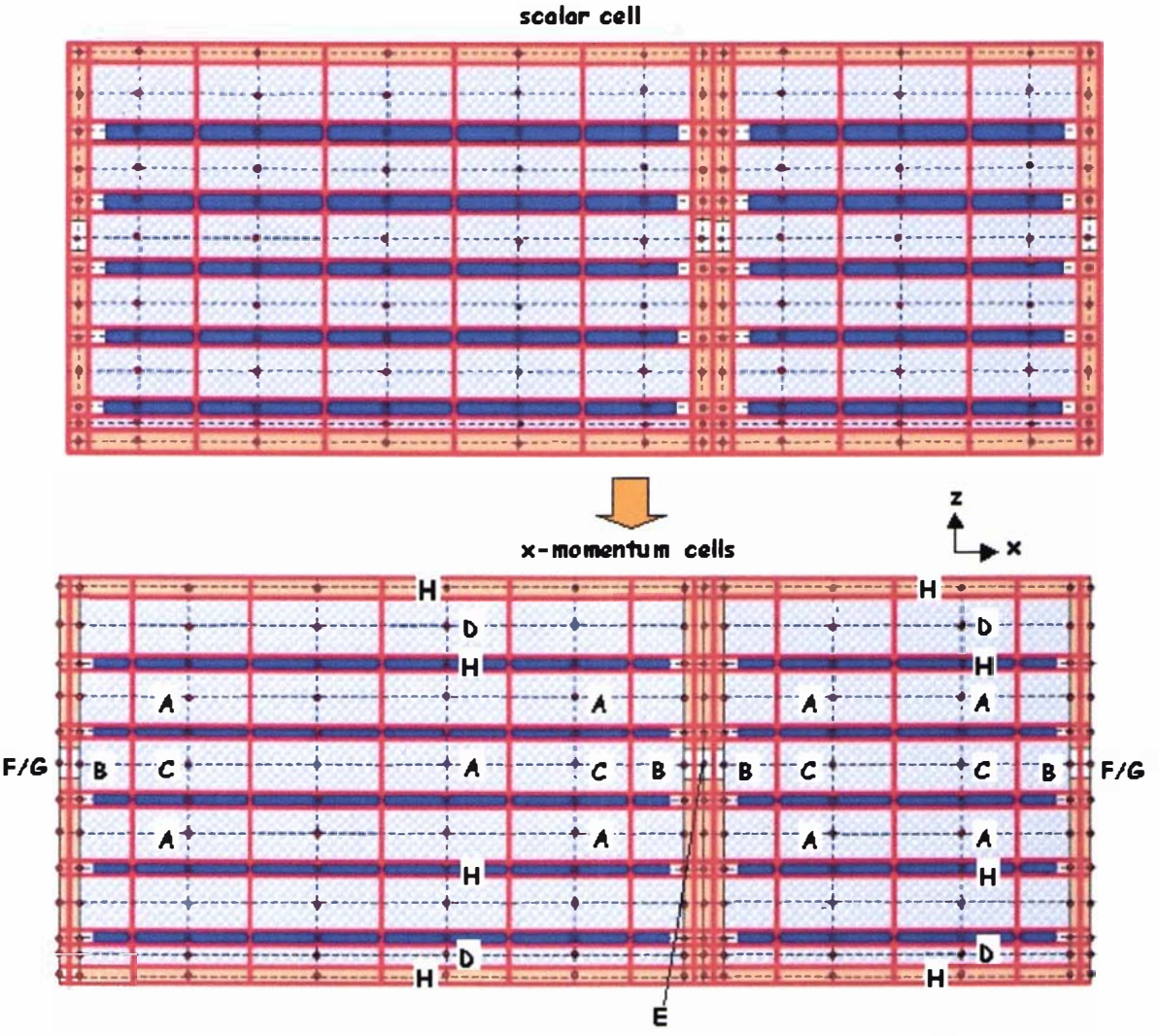

Figure A.12 Grids for the x-momentum discretisation equations for the layered packaging systems (the capital letters indicate the types of x-momentum, which are explained in Table A.5)

Table A.5 Types of x-momentum cells in layered packaging systems

Type	Location	Transport equations
A	Middle of produce-air regions	• Generalised volume-averaged momentum equation (Equation 4.15a)
B	On the interface between plain air region and west/east package walls with vents	• Generalised volume-averaged momentum equation (Equation 4.15a) • One-dimensional Navier-Stokes equation (Equation 4.3 a)
C	In produce-air region and on the east or west side of the cells of type B	• Generalised volume-averaged momentum equation (Equation 4.15a)
D	In produce-air region and next to south, north, bottom, and top package walls	• Wall boundary conditions
E	On the interface between a vented east wall in one package and a vented west wall in another package	• One-dimensional Navier-Stokes equation (Equation 4.3 a)
F	On the interface between outside environment and the west/east walls with fixed-pressure vents.	• Fixed-pressure boundary conditions
G	On the interface between outside environment and the west/east walls with fixed-velocity vents.	• Fixed-velocity boundary conditions
H	In south/north/bottom/top package walls and trays, or in the interface between produce-air region and west/east package wall without vents	• Velocity component at x-axis is set to zero

- **X-momentum discretisation equations in the x-momentum cells in air-produce regions**

The x-momentum discretisation equations for the x-momentum cells in the produce-air regions of the layered packaging systems are very similar to that of the bulk packaging systems. The main difference is that the momentum fluxes on low and high surfaces of the cells in the layered packages are only caused by diffusion, as air movements are horizontal.

The coefficients for low and high nodes in the discretisation equations were modified, and the items for the low and high nodes in source terms of discretisation equations were set to zero:

$$a_{uL-P-u} = 0 \tag{A.102}$$

$$a_{uH-P-u} = 0 \tag{A.103}$$

$$a_{uP-P-u} = -\left(-\frac{\phi_{P-u}\mu A_{l-u}}{z_{P-u}-z_{l-u}} + a_{uW-P-u} + a_{uS-P-u} + a_{uE-P-u} + a_{uN-P-u} - \frac{\phi_{P-u}\mu A_{h-u}}{z_{h-u}-z_{P-u}} \right) \tag{A.104}$$

$$S_{u-P-u} = S_{due-u} + S_{duw-u} + S_{dus-u} + S_{dun-u} \tag{A.105}$$

- **X-momentum discretisation equations in the x-momentum cells in package walls and trays**

The grid nodes of these types of x-momentum cells are on the solid region, so no-slip boundary condition applies.

$$u_{P-u} = 0 \tag{A.106}$$

- **X-momentum discretisation equations in the x-momentum cells in boundary between package walls and air-produce regions**

The x-momentum discretisation equations in these types of x-momentum cells for layered packaging systems are the same as that for the bulk packaging systems.

A.2.3 Y-momentum discretisation equations

- **Types of y-momentum cells**

There are eight types of y-momentum cells, which are summarised in Figure A.13 and Table A.6. For each type of y-momentum cell, a set of expressions was derived for the coefficients and source term in the y-momentum discretisation equation (Equation A.2).

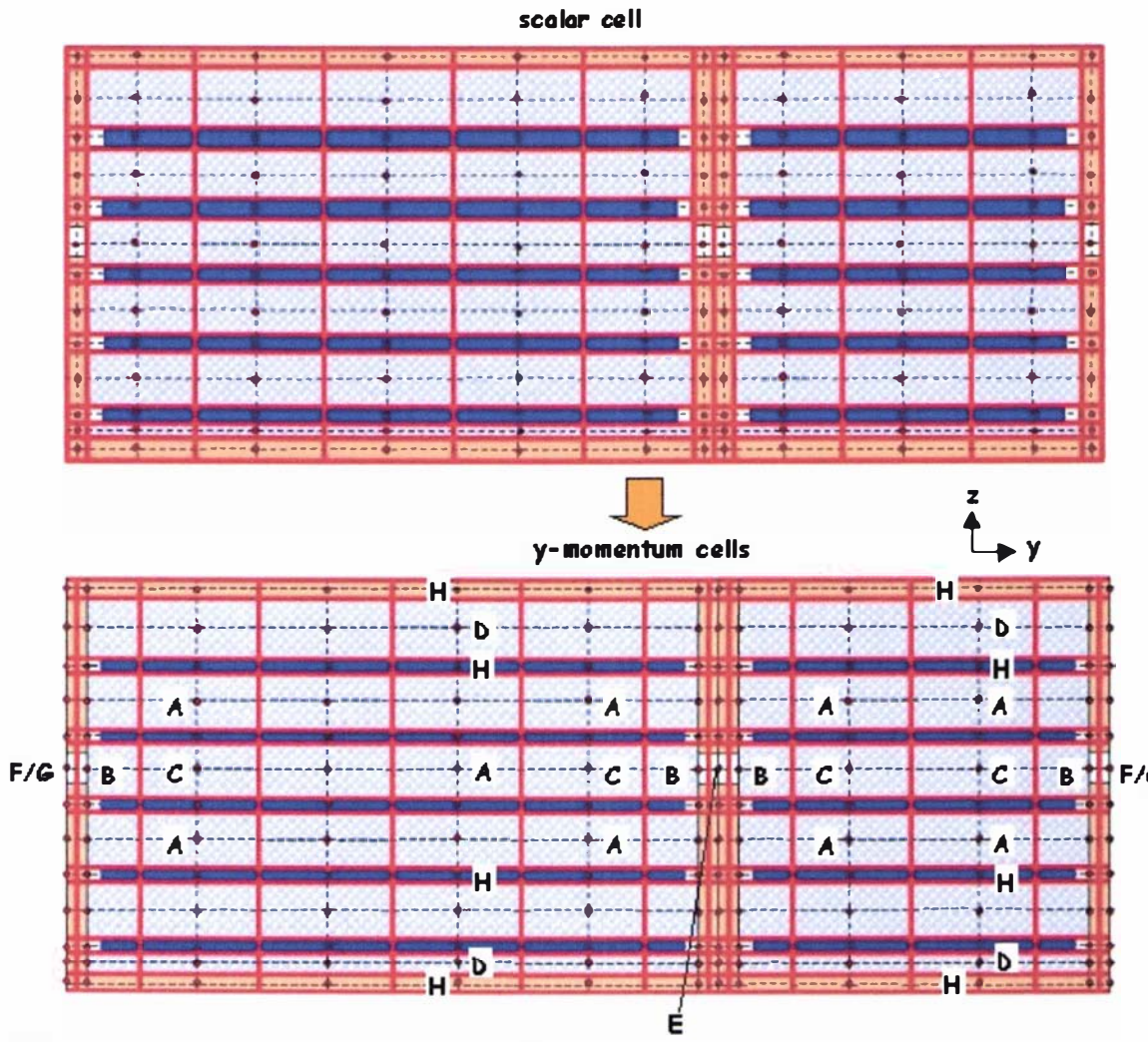

Figure A.13 Grids for the y-momentum discretisation equations in the layered packaging systems (the capital letters indicate the types of y-momentum, which are explained in Table A.6)

- **Y-momentum discretisation equations**

Since the types of y-momentum cells are very similar to that of x-momentum cells, the numerical methods for deriving the x-momentum discretisation equations were used to derive the y-momentum discretisation equations

Table A.6 Types of y-momentum cells in layered packaging systems

Type	Location	Transport equations
A	Middle of produce-air regions	• Generalised volume-averaged momentum equation (Equation 4.15b)
B	On the interface between plain air region and south/north package walls with vents	• Generalised volume-averaged momentum equation (Equation 4.15b) • One-dimensional Navier-Stokes equation (Equation 4.3 b) • Boundary conditions between plain air region and produce-air region
C	In produce-air region and on the south or north side of the cells of type B	• Generalised volume-averaged momentum equation (Equation 4.15b)
D	In produce-air region and next to west, east, bottom, and top package walls	• Wall boundary conditions
E	On the interface between a vented north wall in one package and a vented south wall in another package	• One-dimensional Navier-Stokes equation (Equation 4.3 b)
F	On the interface between outside environment and the south/north walls with fixed-pressure vents.	• Fixed-pressure boundary conditions
G	On the interface between outside environment and the south/north walls with fixed-velocity vents.	• Fixed-velocity boundary conditions
I	In west/east/bottom/top package walls and trays, or in the interface between air-produce region and south/north package wall without vents	• Velocity component at y-axis is set to zero

A.2.4 Z-momentum discretisation equations

- **Types of z-momentum equations**

There are three types of z-momentum cells, which are summarised in Figure A.14 and Table A.7. For each type of z-momentum cell, a set of expressions was derived for the coefficients and source term in z-momentum discretisation equation (Equation A.3).

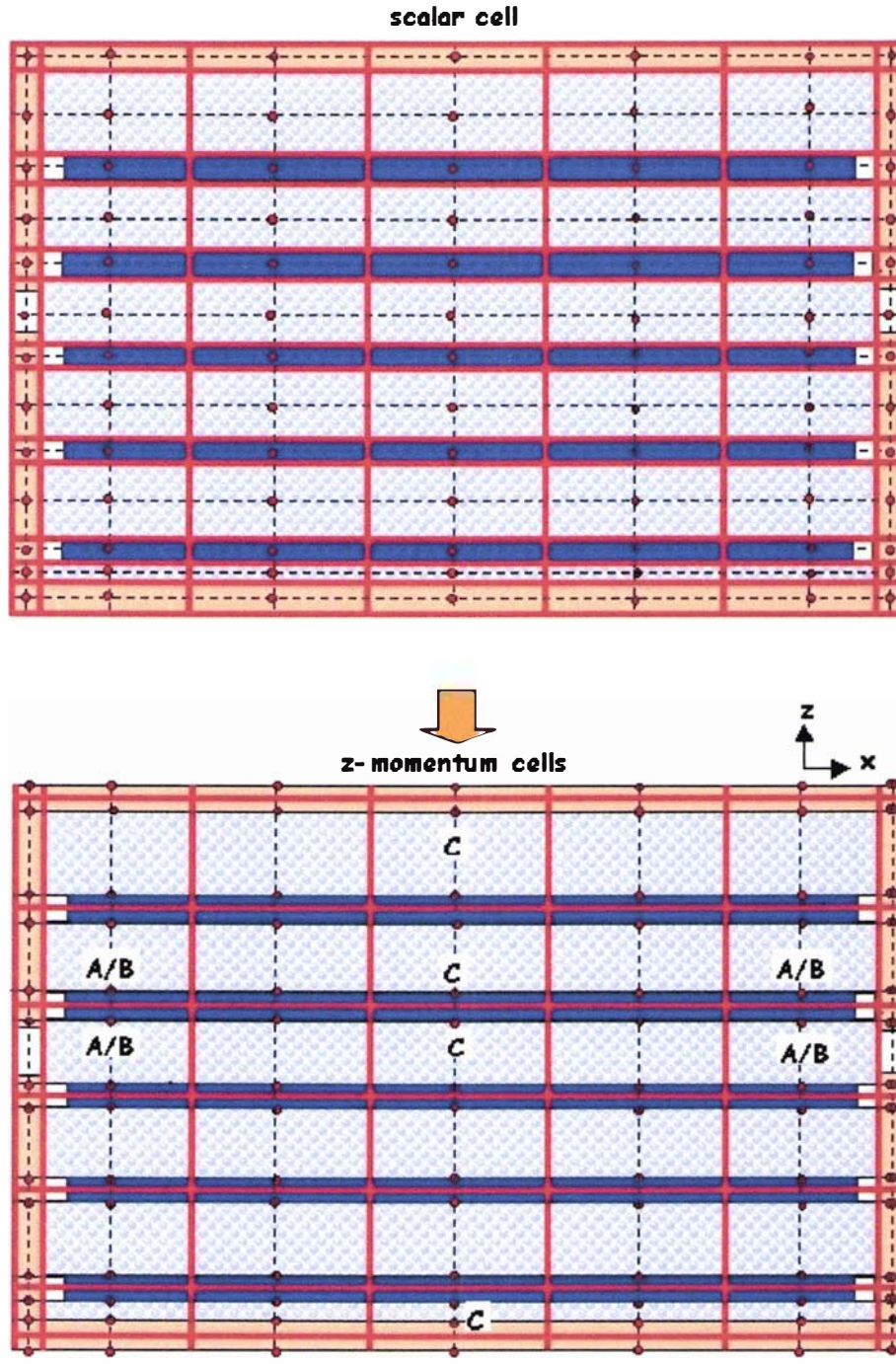

Figure A.14 Grids for the z-momentum discretisation equations in the layered packaging systems (the capital letters indicate the types of z-momentum, which are explained in Table A.7)

Table A.7 Types of z-momentum cells in layered packaging systems.

Type	Location	Transport equations
A	Next to package walls	• One-dimensional momentum equation (Equation 4.17)
B	At the corners of package	• One-dimensional momentum equation (Equation 4.17)
C	Other places	• Velocity component at z-axis is set to zero

- **Z-momentum discretisation equations for z-momentum cells along the package walls**

As shown in Figure A.15, the z-momentum cell along the west package wall was divided into two parts, the narrow part next to the wall contains the gap between package wall and tray end, and the other part has zero velocity on the boundary. Therefore discretisation equation was derived from the narrow part.

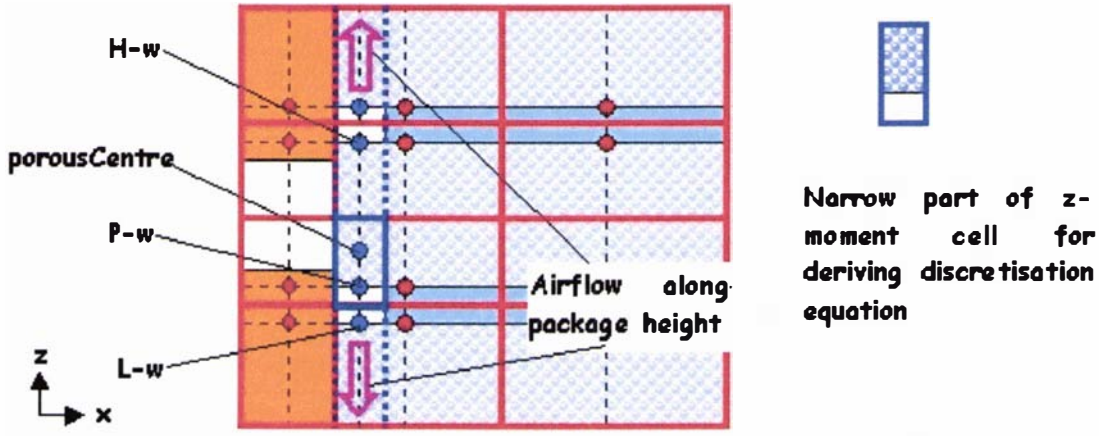

Figure A.15 Treatment of the z-momentum cells next to package walls in layered packages

Integrating Equations 4.17 over the narrow part of the z-momentum cell, the coefficients and source terms in z-momentum discretisation equation were derived:

$$a_{wE-P-w} = 0 \tag{A.107}$$

$$a_{wW-P-w} = 0 \tag{A.108}$$

$$a_{wN-P-w} = -\frac{\mu}{y_{N-w} - y_{P-w}}\left(z_{h-w} - z_{l-w}\right)W_{gap-w} \tag{A.109}$$

$$a_{wS-P-w} = -\frac{\mu}{y_{P-w} - y_{S-w}}\left(z_{h-w} - z_{l-w}\right)W_{gap-w} \tag{A.110}$$

$$a_{wH-P-w}=\left(\min\left(\frac{\rho_a w_{P-w}+\rho_a w_{H-w}}{2},0\right)-\frac{\mu}{z_{H-w}-z_{P-w}}\right)(y_{n-w}-y_{s-w})W_{gap-w} \tag{A.111}$$

$$a_{wL-P-w}=\left(-\max\left(\frac{\rho_a w_{L-w}+\rho_a w_{P-w}}{2},0\right)-\frac{\mu}{z_{P-w}-z_{L-w}}\right)(y_{n-w}-y_{s-w})W_{gap-w} \tag{A.112}$$

$$a_{wP-P-w}=-\left(a_{wL-P-w}\frac{\mu}{x_{P-w}-x_{w-w}}A_{w-w}+a_{wS-P-w}+a_{wN-P-w}\frac{\mu}{x_{e-w}-x_{P-w}}A_{e-w}+a_{wH-P-w}\right)$$
$$+\left(\frac{\mu\phi_{gap}^{\ 2}}{K_{gap}}+\frac{F_{gap}\phi_{gap}^{\ 3}\rho_a}{\sqrt{K_{gap}}}|w_{P-w}|\right)(z_{h-w}-z_{l-w})(y_{n-w}-y_{s-w})W_{gap-w} \tag{A.113}$$

$$S_{w-P-w}=S_{dwl-P-w}+S_{dwh-P-w} \tag{A.114}$$

$$S_{dwh-P-w}=\left(\begin{array}{l}-\frac{\rho_a w_{P-w}+\rho_a w_{H-w}}{2}\left(\frac{z_{H-w}-z_{h-w}}{z_{H-w}-z_{P-w}}w_{P-w}+\frac{z_{h-w}-z_{P-w}}{z_{H-w}-z_{P-w}}w_{H-w}\right)+\\ \max\left(\frac{\rho_a w_{P-w}+\rho_a w_{H-w}}{2},0\right)w_{P-w}+\min\left(\frac{\rho_a w_{P-w}+\rho_a w_{H-w}}{2},0\right)w_{H-w}\end{array}\right)(y_{n-w}-y_{s-w})W_{gap-w} \tag{A.115}$$

$$S_{dwl-P-w}=\left(\begin{array}{l}\frac{\rho_a w_{L-w}+\rho_a w_{P-w}}{2}\left(\frac{z_{l-w}-z_{L-w}}{z_{P-w}-z_{L-w}}w_{P-w}+\frac{z_{P-w}-z_{l-w}}{z_{P-w}-z_{L-w}}w_{L-w}\right)-\\ \min\left(\frac{\rho_a w_{L-w}+\rho_a w_{P-w}}{2},0\right)w_{P-w}-\max\left(\frac{\rho_a w_{L-w}+\rho_a w_{P-w}}{2},0\right)w_{L-w}\end{array}\right)(y_{n-w}-y_{s-w})W_{gap-w} \tag{A.116}$$

where:

$W_{gap\text{-}w}$	=	width of gap between package west wall and tray end (m).
ϕ_{gap}	=	porosity in the near wall region (~=0.9).
K_{gap}	=	permeability calculated from ϕ_{gap} (m^2).
F_{gap}	=	Forcheimer coefficient calculated from ϕ_{gap}.

Similar schemes were used to derive the z-momentum discretisation equations for z-momentum cells along the east, north, and south package walls

- **Z-momentum discretisation equations for z-momentum cells at package corners**

As shown in Figure A.16, the z-momentum cell at the west-south package corner has two narrow parts with one along the west wall, and the other along the south wall. To simplify the derivation of the discretisation equation, for momentum fluxes on horizontal directions, only the diffusion along package walls was considered. Therefore the following coefficients and source terms were derived as follows:

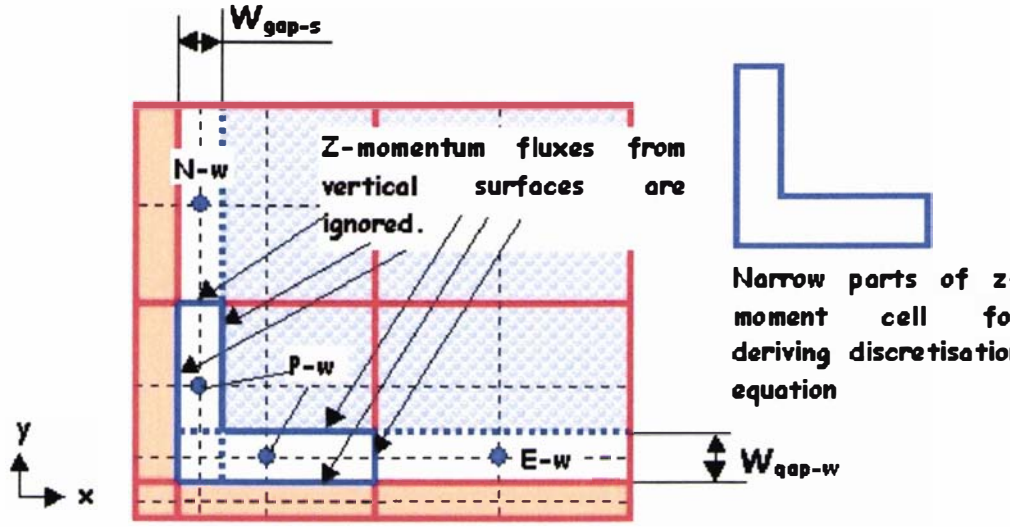

Figure A.16 Treatment of the z-momentum cell at west-south package corner in layered packages

$$a_{wE-P-w} = 0 \tag{A.117}$$

$$a_{wW-P-w} = 0 \tag{A.118}$$

$$a_{wN-P-w} = 0 \tag{A.119}$$

$$a_{wS-P-w} = 0 \tag{A.120}$$

$$a_{wH-P-w} = \left(\min\left(\frac{\rho_a w_{P-w} + \rho_a w_{H-w}}{2}, 0 \right) - \frac{\mu}{z_{H-w} - z_{P-w}} \right) \left((y_{n-w} - y_{s-w}) W_{gap-w} + (x_{e-w} - x_{w-w}) W_{gap-s} \right) \tag{A.121}$$

$$a_{wL-P-w} = \left(-\max\left(\frac{\rho_a w_{L-w} + \rho_a w_{P-w}}{2}, 0 \right) - \frac{\mu}{z_{P-w} - z_{L-w}} \right) \left((y_{n-w} - y_{s-w}) W_{gap-w} + (x_{e-w} - x_{w-w}) W_{gap-s} \right) \tag{A.122}$$

$$a_{wP-P-w} = -\left(a_{wL-P-w} - \frac{\mu}{x_{P-w} - x_{w-w}} A_{w-w} - \frac{\mu}{y_{P-w} - y_{s-w}} A_{s-w} + a_{wH-P-w} \right)$$
$$+ \left(\frac{\mu \phi_{gap}^{\ 2}}{K_{gap}} + \frac{F_{gap} \phi_{gap}^{\ 3} \rho_a}{\sqrt{K_{gap}}} |w_{P-w}| \right) (z_{h-w} - z_{l-w}) \left((y_{n-w} - y_{s-w}) W_{gap-w} + (x_{e-w} - x_{w-w}) W_{gap-s} \right) \tag{A.123}$$

$$S_{w-P-w} = S_{dwl-P-w} + S_{dwh-P-w} \tag{A.124}$$

$$S_{dwh-P-w} = \left(\begin{array}{l} \frac{\rho_a w_{P-w} + \rho_a w_{H-w}}{2} \left(\frac{z_{H-w} - z_{h-w}}{z_{H-w} - z_{P-w}} w_{P-w} + \frac{z_{h-w} - z_{P-w}}{z_{H-w} - z_{P-w}} w_{H-w} \right) + \\ max\left(\frac{\rho_a w_{P-w} + \rho_a w_{H-w}}{2}, 0 \right) w_{P-w} + min\left(\frac{\rho_a w_{P-w} + \rho_a w_{H-w}}{2}, 0 \right) w_{H-w} \end{array} \right) \tag{A.125}$$
$$\left((y_{n-w} - y_{s-w}) W_{gap-w} + (x_{e-w} - x_{w-w}) W_{gap-s} \right)$$

$$S_{dwl-P-w} = \left(\begin{array}{l} \frac{\rho_a w_{L-w} + \rho_a w_{P-w}}{2} \left(\frac{z_{l-w} - z_{L-w}}{z_{P-w} - z_{L-w}} w_{P-w} + \frac{z_{P-w} - z_{l-w}}{z_{P-w} - z_{L-w}} w_{L-w} \right) + \\ min\left(\frac{\rho_a w_{L-w} + \rho_a w_{P-w}}{2}, 0 \right) w_{P-w} - max\left(\frac{\rho_a w_{L-w} + \rho_a w_{P-w}}{2}, 0 \right) w_{L-w} \end{array} \right) \tag{A.126}$$
$$\left((y_{n-w} - y_{s-w}) W_{gap-w} + (x_{e-w} - x_{w-w}) W_{gap-s} \right)$$

where:

W_{gap-s} = width of gap between package south wall and tray end (m).

Similar schemes were used to derive the z-momentum discretisation equations for z-momentum cells at other corners.

A 2.5 Pressure correction and pressure discretisation equations

- **Types of scalar cells in terms of pressure correction and pressure discretisation equation**

There are seven types of scalar cells in terms of pressure correction and pressure, which are summarised in Figure A.17 and Table A.8. . For each type of scalar cell, a set of expressions was derived for the coefficients and source terms in pressure correction and pressure discretisation equations (Equations A.4-A.5).

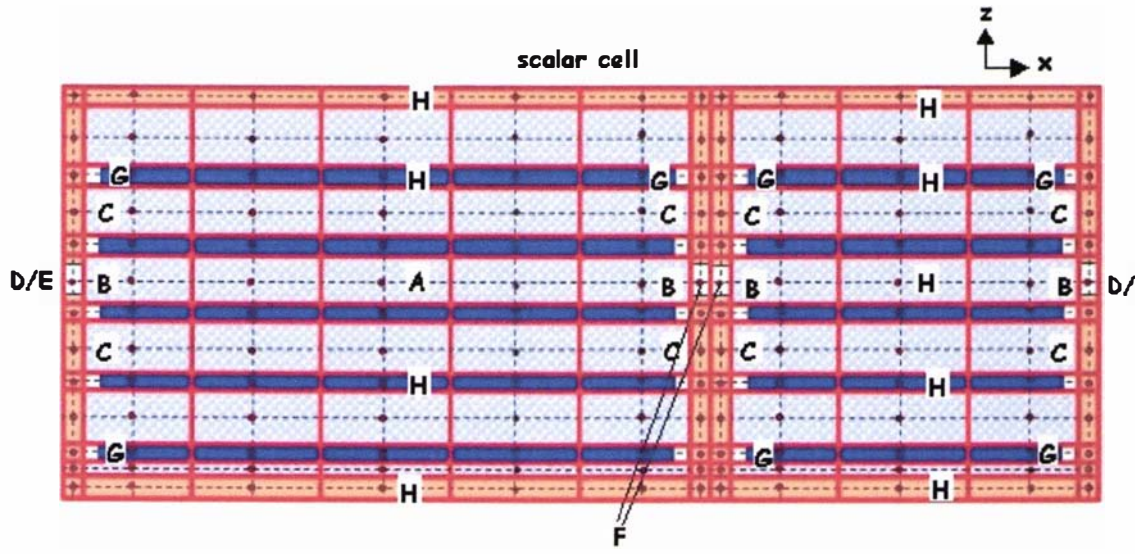

Figure A.17 Grids for the pressure correction and pressure discretisation equations in the layered packaging systems (the capital letters indicate the types of scalar cells in terms of pressure correction and pressure, which are explained in Table A.8)

- **Pressure correction and pressure discretisation equations for scalar cells in the middle of produce-air regions**

The pressure correction and pressure discretisation equations for scalar cells in the middle of air-produce region in layered packaging systems are the same as that in bulk package, except that no pressure and velocity corrections are needed for low and high nodes:

Table A.8 Types of scalar cells in terms of pressure correction and pressure

Type	Location	Transport equations
A	Middle of produce-air regions	• Volume-averaged continuity equation (Equation 4.14)
B	In produce-air regions and next to west, east, south, and north package walls with vents	• Volume-averaged continuity equation (Equation 4.14)
C	In produce-air regions and next to west, east, south, and north package walls without vents	• Volume-averaged continuity equation (Equation 4.14)
D	In west, east, south, north package walls with fixed-velocity vents	• One-dimensional continuity equation (Equation 4.1a and 41.b) • Fixed-velocity boundary conditions
E	In west, east, south, north package walls with fixed-pressure vents	• No pressure or pressure correction equation is needed
F	In vented west/east/south /north package wall next to another vented package wall	• One-dimensional continuity equation (Equation 4.1a and 4.1b)
G	In trays with gaps between tray edges and package walls	• One-dimensional continuity equation (Equation 4.15)
H	In west, east, south, north bottom, top package walls without vents and trays	• No pressure or pressure correction equation is needed

$$a_{pH-P-scalar} = 0 \tag{A.127}$$

$$a_{pL-P-scalar} = 0 \tag{A.128}$$

$$a_{pP-P-scalar} = \frac{\rho_a \phi_{w-scalar} \phi_{P-scalar} A^2_{w-scalar}}{a_{uP-W-u}} + \frac{\rho_a \phi_{e-scalar} \phi_{P-scalar} A^2_{e-scalar}}{a_{uP-P-u}} + \frac{\rho_a \phi_{s-scalar} \phi_{P-scalar} A^2_{s-scalar}}{a_{vP-S-v}} + \frac{\rho_a \phi_{n-scalar} \phi_{P-scalar} A^2_{n-scalar}}{a_{vP-P-v}} \tag{A.129}$$

- **Pressure and pressure correction discretisation equations for scalar cells in produce-air region and along the package walls**

As shown in Figure A.18, the velocity correction equation at west surface of the scalar cell was derived from x-momentum discretisation equation:

$$u^{corrected}_{W-u} = u_{W-u} + \frac{(-\phi_{P-scalar} \Delta p_{P-scalar} + \Delta p_{W-scalar}) \phi_{W-scalar} A_{w-scalar}}{a_{uP-W-u}} \tag{A.130}$$

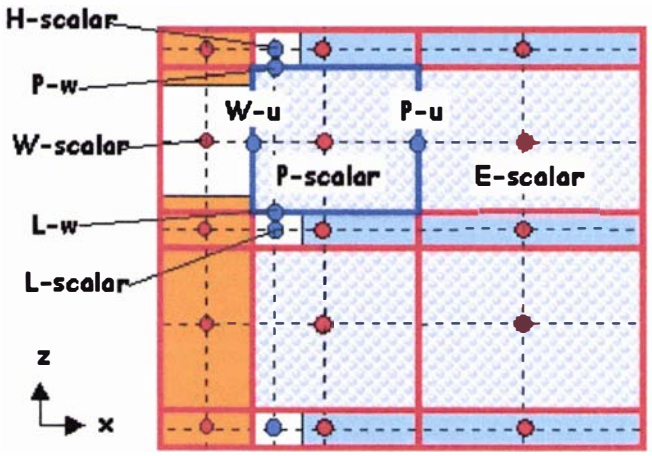

Scalar cell for deriving pressure correction and pressure discretisation equation

Figure A.18 Treatment of the scale cells in produce-air region and next to west wall in layered package with vents for derivation of pressure correction and pressure discretisation equations.

The velocity correction equations at low and high surfaces of the scalar cell were derived from z-momentum discretisation equations:

$$w_{P-w}^{corrected} = w_{P-w} + \frac{(\Delta p_{P-scalar} - \Delta p_{H-scalar})(y_{n-w} - y_{s-w})W_{gap-w}}{a_{wP-P-w}} \tag{A.131}$$

$$w_{L-w}^{corrected} = w_{L-w} + \frac{(-\Delta p_{P-scalar} + \Delta p_{L-scalar})(y_{n-w} - y_{s-w})W_{gap-w}}{a_{wP-L-w}} \tag{A.132}$$

Equation (A.63) was modified to account for the vent and gap structure:

$$\rho_a \phi_{e-scalar} A_{e-scalar} u_{P-u}^{corrected} - \rho_a \phi_{W-scalar} A_{w-scalar} u_{W-u}^{corrected} + \rho_a \phi_{n-scalar} A_{n-scalar} v_{P-v}^{corrected} - \rho_a \phi_{s-scalar} A_{s-scalar} v_{S-v}^{corrected} + \rho_a (y_{n-w} - y_{s-w}) W_{gap-w} w_{P-w}^{corrected} - \rho_a (y_{n-w} - y_{s-w}) W_{gap-w} w_{L-w}^{corrected} = 0 \tag{A.133}$$

Consequently, the following modified coefficients and source term were employed:

$$a_{pW-P-scalar} = -\frac{\rho_a \phi_{W-scalar}^2 A_{w-scalar}^2}{a_{uP-W-u}} \tag{A.134}$$

$$a_{pL-P-scalar} = -\frac{\rho_a (y_{n-w} - y_{s-w})^2 W_{gap-w}^2}{a_{wP-L-w}} \tag{A.135}$$

$$a_{pH-P-scalar} = -\frac{\rho_a (y_{n-w} - y_{s-w})^2 W_{gap-w}^2}{a_{wP-P-w}} \tag{A.136}$$

$$a_{pP-P-scalar} = -a_{pL-P-scalar} - a_{pH-P-scalar} + \frac{\rho_a \phi_{W-scalar}^2 \phi_{P-scalar} A_{w-scalar}^2}{a_{uP-W-u}} + \frac{\rho_a \phi_{e-scalar} \phi_{P-scalar} A_{e-scalar}^2}{a_{uP-P-u}} + \frac{\rho_a \phi_{s-scalar} \phi_{P-scalar} A_{s-scalar}^2}{a_{vP-S-v}} + \frac{\rho_a \phi_{n-scalar} \phi_{P-scalar} A_{n-scalar}^2}{a_{vP-P-v}} \tag{A.137}$$

$$S_{\Delta p-P-scalar} = \rho_a w_{L-w} (y_{n-w} - y_{s-w}) W_{gap-w} - \rho_a w_{P-w} (y_{n-w} - y_{s-w}) W_{gap-w} + \rho_a \phi_{W-scalar} u_{W-u} A_{w-scalar} - \rho_a \phi_{e-scalar} u_{P-u} A_{e-scalar} + \rho_a \phi_{s-scalar} v_{S-v} A_{s-scalat} - \rho_a \phi_{n-scalar} v_{P-v} A_{n-scalar} \tag{A.138}$$

$$S_{p-P-scalar} = \rho_a w_{L-w}^{pressure} (y_{n-w} - y_{s-w}) W_{gap-w} - \rho_a w_{P-w}^{pressure} (y_{n-w} - y_{s-w}) W_{gap-w} + \rho_a \phi_{W-scalar} u_{W-u}^{pressure} A_{w-scalar} - \rho_a \phi_{e-scalar} u_{P-u}^{pressure} A_{e-scalar} + \rho_a \phi_{s-scalar} v_{S-v}^{pressure} A_{s-scalar} - \rho_a \phi_{n-scalar} v_{P-v}^{pressure} A_{n-scalar} \tag{A.139}$$

Other coefficients were calculated with Equations (A.64) and (A.66)-(A.67).

Similar schemes were used to derive the pressure correction and pressure discretisation equations for scalar cells along other surfaces and at package corners.

- **Pressure and pressure correction discretisation equations in the scalar cells in package walls and trays**

The pressure correction and pressure discretisation equations in these types of scalar cells for layered packaging systems are the same as that for the bulk packaging systems. Particularly for the scalar cells in trays containing the gaps between walls and tray edges, the same treatment for the vents in package walls was employed.

- **Pressure and pressure correction discretisation equations in the scalar cells in package walls and trays**

The pressure correction and pressure discretisation equations in these types of scalar cells for layered packaging systems are the same as that for the bulk packaging systems. Particularly for the scalar cells in trays containing the gaps between walls and tray edges, the same treatment for the vents in package walls was employed.

A.3 Discretisation Equations for PDEs in the Heat Transfer Model for the Bulk Packaging Systems

A.3.1 Numerical Schemes

The PDEs for energy conservation of air and solid (produce and packaging materials) were discretised in the same way as for deriving the momentum discretisation equations outlined in previous sections. The same conventions were employed to represent the quantities in the calculation domains. The energy discretisation equations were derived over scalar cells. As the energy equations are to be solved based on the results of the solved velocity field, the velocity components on the surface centres of the scalar cells are treated as known.

- **Discretisation equations**

In general, for each scalar cell in bulk package two discretisation energy equations were derived:

1) Solid energy discretisation equation was derived from the energy conservation equation for package walls in solid region (Equation 5.2) or the volume-averaged energy conservation equation for produce in produce-air region (Equation 5.4):

$$a_{TsL-P-scalar}T^{current}_{s-L-scalar} + a_{TsW-P-scalar}T^{current}_{s-W-scalar} + a_{TsS-P-scalar}T^{current}_{s-S-scalar} + a_{TsP-P-scalar}T^{current}_{s-P-scalar} + a_{TsN-P-scalar}T^{current}_{s-N-scalar} + a_{TsE-P-scalar}T^{current}_{s-E-scalar} + a_{TsH-P-scalar}T^{current}_{s-H-scalar} = S_{Ts-P-scalar} \quad \text{(A.140)}$$

where:

T_s = solid temperature (K).

a_{TsE} = coefficient in solid energy discretisation equation for east node (W K^{-1}).

a_{TsW} = coefficient in solid energy discretisation equation for west node (W K^{-1}).

a_{TsN} = coefficient in solid energy discretisation equation for north node (W K^{-1}).

a_{TsS} = coefficient in solid energy discretisation equation for south node (W K^{-1}).

a_{TsH} = coefficient in solid energy discretisation equation for high node (W K^{-1}).

a_{TsL} = coefficient in solid energy discretisation equation for low node (W K^{-1}).

a_{TsP} = coefficient in solid energy discretisation equation for current node (W K^{-1}).

S_{Ts} = source term for solid energy discretisation equation (W).

The number of algebraic equations in the system of solid energy discretisation equations is equal to the number of scalar cells.

2) Air energy discretisation equation that was derived from the energy conservation equation for air in vents (Equations 5.1a & 5.1b) or the volume-averaged energy conservation equation for air in produce-air region (Equation 5.3):

$$a_{TaL-P-scalar}T^{current}_{a-L-scalar} + a_{TaW-P-scalar}T^{current}_{a-W-scalar} + a_{TaS-P-scalar}T^{current}_{a-S-scalar} + a_{TaP-P-scalar}T^{current}_{a-P-scalar} + a_{TaN-P-scalar}T^{current}_{a-N-scalar} + a_{TaE-P-scalar}T^{current}_{a-E-scalar} + a_{TaH-P-scalar}T^{current}_{a-H-scalar} = S_{Ta-P-scalar} \quad \text{(A.141)}$$

where:

T_a = air temperature (K).

a_{TaE} = coefficient in air energy discretisation equation for east node (W K^{-1}).

a_{TaW} = coefficient in air energy discretisation equation for west node (W K^{-1}).

a_{TaN} = coefficient in air energy discretisation equation for north node (W K^{-1}).

a_{TaS} = coefficient in air energy discretisation equation for south node (W K^{-1}).

a_{TaH} = coefficient in air energy discretisation equation for high node (W K^{-1}).

a_{TaL} = coefficient in air energy discretisation equation for low node (W K^{-1}).

a_{TaP} = coefficient in air energy discretisation equation for current node (W K^{-1}).

S_{Ta} = source term for air energy discretisation equation (W).

For each scalar cell in produce-air region, as shown in Figure 6.13, a representative produce item was divided into four sub-cells. For each sub-cell, a discretisation equation was derived from the energy equation for produce item (Equation 5.5).

1) The produce item energy discretisation equation for sub-cell1 has the following form:

$$a_{Tp1-sub1}T^{current}_{p-sub1} + a_{Tp2-sub1}T^{current}_{p-sub2} = S_{Tp-sub1} \quad \text{(A.142)}$$

where:

$T_{p\text{-}sub1}$ = temperature of sub-cell1 of representative produce item (K).

$T_{p\text{-}sub2}$ = temperature of sub-cell2 of representative produce item (K).

$a_{Tp1\text{-}sub1}$ = coefficient for produce temperature in sub-cell1 in produce item energy discretisation for sub-cell1 (W K^{-1}).

$a_{Tp2\text{-}sub1}$ = coefficient for produce temperature in sub-cell2 in produce item energy discretisation for sub-cell1 (W K^{-1}).

$S_{Tp\text{-}sub1}$ = source term in produce item energy discretisation for sub-cell1 (W).

2) The produce item energy discretisation equation for sub-cell2 has the following form:

$$a_{Tp1-sub2}T^{current}_{p-sub1} + a_{Tp2-sub2}T^{current}_{p-sub2} + a_{Tp3-sub2}T^{current}_{p-sub3} = S_{Tp-sub2} \quad \text{(A.143)}$$

where:

$T_{p\text{-}sub3}$ = temperature of sub-cell3 of representative produce item (K).

$a_{Tp1\text{-}sub2}$ = coefficient for produce temperature in sub-cell1 in produce item energy discretisation for sub-cell2 (W K^{-1}).

$a_{Tp2\text{-}sub2}$ = coefficient for produce temperature in sub-cell2 in produce item energy discretisation for sub-cell2 (W K^{-1}).

$a_{Tp3\text{-}sub2}$ = coefficient for produce temperature in sub-cell3 in produce item energy discretisation for sub-cell2 (W K^{-1}).

$S_{Tp\text{-}sub2}$ = source term in produce item energy discretisation for sub-cell2 (W).

3) The produce item energy discretisation equation for sub-cell3 has the following form:

$$a_{Tp2-sub3}T^{current}_{p-sub2} + a_{Tp3-sub3}T^{current}_{p-sub3} + a_{Tp4-sub3}T^{current}_{p-sub4} = S_{Tp-sub3} \quad \text{(A.144)}$$

where:

$T_{p\text{-}sub4}$ = temperature of sub-cell4 of representative produce item (K).

$a_{Tp2\text{-}sub3}$ = coefficient for produce temperature in sub-cell2 in produce item energy discretisation for sub-cell3 (W K^{-1}).

$a_{Tp3\text{-}sub3}$ = coefficient for produce temperature in sub-cell3 in produce item energy discretisation for sub-cell3 (W K^{-1}).

$a_{Tp4\text{-}sub3}$ = coefficient for produce temperature in sub-cell4 in produce item energy discretisation for sub-cell3 (W K^{-1}).

$S_{Tp\text{-}sub3}$ = source term in produce-item energy discretisation for sub-cell3 (W).

4) The produce item energy discretisation equation for sub-cell3 has the following form:

$$a_{Tp3-sub4}T_{p-sub3}^{current} + a_{Tp4-sub4}T_{p-sub4}^{current} = S_{Tp-sub4} \quad \text{(A.145)}$$

where:

$a_{Tp3\text{-}sub4}$= coefficient for produce temperature in sub-cell3 in produce item energy discretisation for sub-cell4 (W K^{-1}).

$a_{Tp3\text{-}sub4}$= coefficient for produce temperature in sub-cell4 in produce item energy discretisation for sub-cell4 (W K^{-1}).

$S_{Tp\text{-}sub4}$ = source term in produce item energy discretisation for sub-cell4 (W).

- **Types of scalar cells in terms of derivation of energy discretisation equations**

There are seven types of scalar cells in terms of derivation of energy discretisation equations, which are summarised in Figure A.19 and Table A.9.

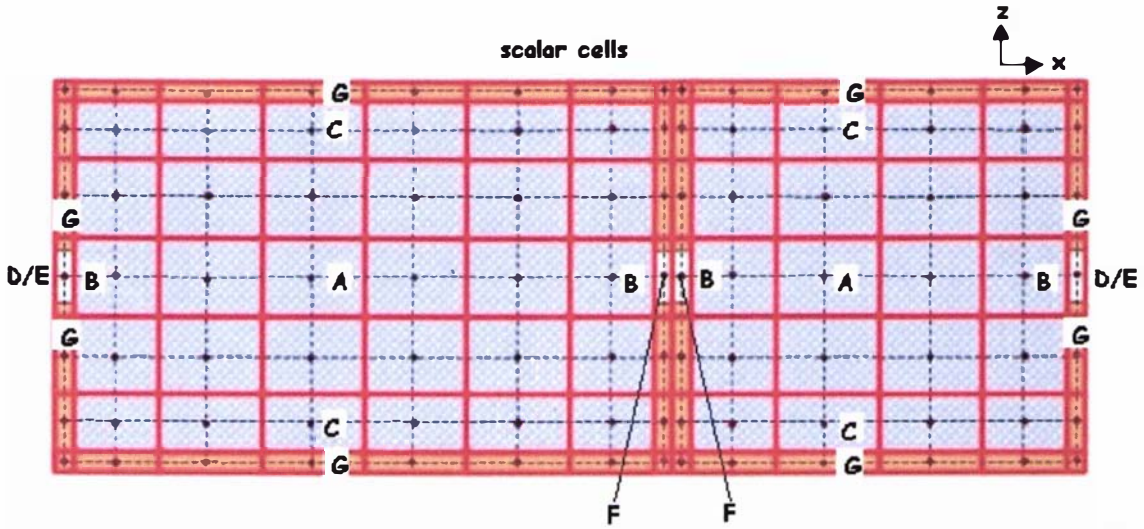

Figure A.19 Grids for deriving the energy discretisation equations in the bulk packaging systems (the capital letters indicate the types of scalar cells in terms of derivation of energy discretisation equations, which are explained in Table A.9)

Table A.9 Types of scalar cells in terms of derivation of energy discretisation equations

Type	Location	Transport equations
A	Middle of produce-air region	• Volume-averaged energy equation for air (Equation 5.3) • Volume-averaged energy equation for produce (Equation 5.4) • Energy equation for single item of produce (Equation 5.5)
B	In produce-air region and next to west, east, south, and north package walls with vents	• Volume-averaged energy equation for air (Equation 5.3) • Volume-averaged energy equation for produce (Equation 5.4) • Energy equation for single item of produce (Equation 5.5)
C	In produce-air region and next to west, east, south, and north package walls without vents	• Volume-averaged energy equation for air (Equation 5.3) • Volume-averaged energy equation for produce (Equation 5.4) • Energy equation for single item of produce (Equation 5.5)
D	In west, east, south, north package walls with vents where airflow enters package from outside environment	• One-dimensional energy conservation equation for air (Equation 5.1a and 5.1b) • Energy conservation equation for package walls (Equation 5.2)
E	In west, east, south, north package walls with vents where airflow leaves package from outside environment	• One-dimensional energy conservation equation for air (Equation 5.1a and 5.1b) • Energy conservation equation for package walls (Equation 5.2)
F	In west, east, south, north package walls with vents where airflow moves from one package to another	• One-dimensional energy conservation equation for air (Equation 5.1a and 5.1b) • Energy conservation equation for package walls (Equation 5.2)
G	In west, east, south, north bottom, top package walls without vents	• Energy conservation equation for package walls (Equation 5.2)

A.3.2 Energy Discretisation Equations for Scalar Cells in Produce-Air Region

- **Energy discretisation equations for scalar cells in the middle of produce-air region**

(1) Air energy discretisation equation

Volume-averaged energy equation for air in bulk package (Equation 5.3) was presented in following simplified form:

$$\frac{\partial(\rho_a\phi C_a T_a)}{\partial t}+\frac{\partial(\rho_a\phi u C_a T_a)}{\partial x}+\frac{\partial(\rho_a\phi v C_a T_a)}{\partial y}+\frac{\partial(\rho_a\phi w C_a T_a)}{\partial x}-\frac{\partial}{\partial x}\left((\phi K_a+K_{dis})\frac{\partial T_a}{\partial x}\right)$$
$$-\frac{\partial}{\partial y}\left((\phi K_a+K_{dis})\frac{\partial T_a}{\partial y}\right)-\frac{\partial}{\partial z}\left((\phi K_a+K_{dis})\frac{\partial T_a}{\partial z}\right)=h_t a_{aP}(T_{PSurface}-T_a) \quad \text{(A.146)}$$

where:

u	=	intrinsic phase average of air velocity component in the direction of x-axis (m s^{-1}).
v	=	intrinsic phase average of air velocity component in the direction of y-axis (m s^{1}).
w	=	intrinsic phase average of air velocity component in the direction of z-axis (m s^{1}).
Ta	=	intrinsic phase average of air temperature (K).
$T_{PSurface}$	=	produce surface temperature (K).
ρ_a	=	air density (kg m^{-3}).
C_a	=	air specific heat at constant pressure (J kg^{-1} K^{-1}).
K_a	=	air thermal conductivity (W m^{-1} K^{-1}).
K_{dis}	=	dispersion conductivity (W m^{-1} K^{-1}).
ϕ	=	porosity.
a_{ap}	=	specific interstitial surface area (m^{-1}).
h_t	=	heat transfer coefficient between air and solid surface (W m^{-2} K^{-1}).

The air energy discretisation equation was derived by integrating Equation A.146 over a scalar cell. The unsteady term was approximated with an implicit two time level scheme (Patankar, 1980):

$$\int_{V_{P-scalar}}\frac{\partial(\rho_a\phi C_a T_a)}{\partial t}dV=\frac{\rho_a\phi_{P-scalar}C_a V_{P-scalar}}{\Delta t}(T^{current}_{a-P-scalar}-T^{old}_{a-P-scalar})=a_{TaT-P-scalar}T^{current}_{a-P-scalar}-S_{TaT-P-scalar} \quad \text{(A.147)}$$

$$a_{TaT-P-scalar}=\frac{\rho_a\phi_{P-scalar}C_a V_{P-scalar}}{\Delta t} \quad \text{(A.148)}$$

$$S_{TaT-P-scalar} = \frac{\rho_a \phi_{P-scalar} C_a V_{P-scalar}}{\Delta t} T^{old}_{a-P-scalar} \quad \text{(A.149)}$$

where:

a_{TaT} = coefficient of time term in air energy discretisation equation (W K^{-1}).

V = volume of scalar cell (m^3).

Δt = time step (s).

S_{TaT} = source term in air energy discretisation equation due to time discretisation (W).

The convection, diffusion, and source terms were approximated using the same numerical schemes for deriving the x-momentum discretisation equation (Section A.1.2). Combining these treatments, and using the produce temperature in sub-cell1 to approximate surface temperature, the coefficients and source term for air energy discretisation equation were derived.

$$a_{TaE-P-scalar} = \left(\min(\rho_a C_a \phi_{e-scalar} u_{P-u}, 0) - \frac{\phi_{e-scalar} K_a + K_{dis-e-scalar}}{x_{E-scalar} - x_{P-scalar}} \right) A_{e-scalar} \quad \text{(A.150)}$$

$$a_{TaW-P-scalar} = \left(-\max(\rho_a C_a \phi_{w-scalar} u_{W-u}, 0) - \frac{\phi_{w-scalar} K_a + K_{dis-w-scalar}}{x_{P-scalar} - x_{W-scalar}} \right) A_{w-scalar} \quad \text{(A.151)}$$

$$a_{TaN-P-scalar} = \left(\min(\rho_a C_a \phi_{n-scalar} v_{P-v}, 0) - \frac{\phi_{n-scalar} K_a + K_{dis-n-scalar}}{y_{N-scalar} - y_{P-scalar}} \right) A_{n-scalar} \quad \text{(A.152)}$$

$$a_{TaS-P-scalar} = \left(-\max(\rho_a C_a \phi_{s-scalar} v_{S-v}, 0) - \frac{\phi_{s-scalar} K_a + K_{dis-s-scalar}}{y_{P-scalar} - y_{S-scalar}} \right) A_{s-scalar} \quad \text{(A.153)}$$

$$a_{TaH-P-scalar} = \left(\min(\rho_a C_a \phi_{h-scalar} w_{P-w}, 0) - \frac{\phi_{h-scalar} K_a + K_{dis-h-scalar}}{z_{H-scalar} - z_{P-scalar}} \right) A_{h-scalar} \quad \text{(A.154)}$$

$$a_{TaL-P-scalar} = \left(-\max(\rho_a C_a \phi_{l-scalar} w_{L-w}, 0) - \frac{\phi_{l-scalar} K_a + K_{dis-l-scalar}}{z_{P-scalar} - z_{L-scalar}} \right) A_{l-scalar} \quad \text{(A.155)}$$

$$a_{TaP-P-scalar} = -\left(a_{TaL-P-scalar} + a_{TaW-P-scalar} + a_{TaS-T-scalar} + a_{TaN-P-scalar} + a_{TaE-P-scalar} + a_{TaH-P-scalar}\right) + a_{TaT-P-scalar} + h_{t-P-scalar} a_{aP} V_{p-scalar} \tag{A.156}$$

$$S_{Ta-P-scalar} = S_{dTaw-P-scalar} + S_{dTae-P-scalar} + S_{dTas-P-scalar} + S_{dTan-P-scalar} + S_{dTal-P-scalar} + S_{dTah-P-scalar} + S_{TaT-P-scalar} + h_{t-P-scalar} a_{aP} V_{p-scalar} T_{P-subl} \tag{A.157}$$

$$S_{dTae-P-scalar} = -\rho_a C_a \phi_{e-scalar} u_{P-u} \left(\frac{x_{E-scalar} - x_{e-scalar}}{x_{E-scalar} - x_{P-scalar}} T_{a-P-scalar} + \frac{x_{e-scalar} - x_{P-scalar}}{x_{E-scalar} - x_{P-scalar}} T_{a-E-scalar} \right) A_{e-scalar} + \max\left(\rho_a C_a \phi_{e-scalar} u_{P-u}, 0\right) T_{a-P-scalar} A_{e-scalar} + \min\left(\rho_a C_a \phi_{e-scalar} u_{P-u}, 0\right) T_{a-E-scalar} A_{e-scalar} \tag{A.158}$$

$$S_{dTaw-P-scalar} = \rho_a C_a \phi_{w-scalar} u_{W-u} \left(\frac{x_{w-scalar} - x_{W-scalar}}{x_{P-scalar} - x_{W-scalar}} T_{a-P-scalar} + \frac{x_{P-scalar} - x_{w-scalar}}{x_{P-scalar} - x_{W-scalar}} T_{a-W-scalar} \right) A_{w-scalar} - \min\left(\rho_a C_a \phi_{w-scalar} u_{W-u}, 0\right) T_{a-P-scalar} A_{w-scalar} - \max\left(\rho_a C_a \phi_{w-scalar} u_{W-u}, 0\right) T_{a-W-scalar} A_{w-scalar} \tag{A.159}$$

$$S_{dTan-P-scalar} = -\rho_a C_a \phi_{n-scalar} v_{P-v} \left(\frac{y_{N-scalar} - y_{n-scalar}}{y_{N-scalar} - y_{P-scalar}} T_{a-P-scalar} + \frac{y_{n-scalar} - y_{P-scalar}}{y_{N-scalar} - y_{P-scalar}} T_{a-N-scalar} \right) A_{n-scalar} + \max\left(\rho_a C_a \phi_{n-scalar} v_{P-v}, 0\right) T_{a-P-scalar} A_{n-scalar} + \min\left(\rho_a C_a \phi_{n-scalar} v_{P-v}, 0\right) T_{a-N-scalar} A_{n-scalar} \tag{A.160}$$

$$S_{dTas-P-scalar} = \rho_a C_a \phi_{s-scalar} v_{S-v} \left(\frac{y_{s-scalar} - y_{S-scalar}}{y_{P-scalar} - y_{S-scalar}} T_{a-P-scalar} + \frac{y_{P-scalar} - y_{s-scalar}}{y_{P-scalar} - y_{S-scalar}} T_{a-S-scalar} \right) A_{s-scalar} - \min\left(\rho_a C_a \phi_{s-scalar} v_{S-v}, 0\right) T_{a-P-scalar} A_{s-scalar} - \max\left(\rho_a C_a \phi_{s-scalar} v_{S-v}, 0\right) T_{a-S-scalar} A_{s-scalar} \tag{A.161}$$

$$S_{dTah-P-scalar} = -\rho_a C_a \phi_{h-scalar} w_{P-w} \left(\frac{z_{H-scalar} - z_{h-scalar}}{z_{H-scalar} - z_{P-scalar}} T_{a-P-scalar} + \frac{z_{h-scalar} - z_{P-scalar}}{z_{H-scalar} - z_{P-scalar}} T_{a-H-scalar} \right) A_{h-scalar} + \max\left(\rho_a C_a \phi_{h-scalar} w_{P-w}, 0\right) T_{a-P-scalar} A_{h-scalar} + \min\left(\rho_a C_a \phi_{h-scalar} w_{P-w}, 0\right) T_{a-H-scalar} A_{h-scalar} \tag{A.162}$$

$$S_{dTal-P-scalar}=\rho_a C_a \phi_{l-scalar} w_{L-w}\left(\frac{z_{l-scalar}-z_{L-scalar}}{z_{P-scalar}-z_{L-scalar}}T_{a-P-scalar}+\frac{z_{P-scalar}-z_{l-scalar}}{z_{P-scalar}-z_{L-scalar}}T_{a-L-scalar}\right)A_{l-scalar}-$$
$$min(\rho_a C_a \phi_{l-scalar} w_{L-w},0)T_{a-P-scalar}A_{l-scalar}-max(\rho_a C_a \phi_{l-scalar} w_{L-w},0)T_{a-L-scalar}A_{l-scalar}$$

(A.163)

where:

$T_{p\text{-}subl}$ = temperature of sub-cell1 of representative produce item (K).

S_{dTae} = source term due to CDS deferred correction at east surface in air energy discretisation equation (W).

S_{sTaw} = source term due to CDS deferred correction at west surface in air energy discretisation equation (W).

S_{dTan} = source term due to CDS deferred correction at north surface in air energy discretisation equation (W).

S_{sTas} = source term due to CDS deferred correction at south surface in air energy discretisation equation (W).

S_{dTah} = source term due to CDS deferred correction at high surface in air energy discretisation equation (W).

S_{sTal} = source term due to CDS deferred correction at low surface in air energy discretisation equation (W).

(2) Solid energy discretisation equation

The volume-averaged energy equation for produce in bulk package (Equation 5.5) was presented in following simplified form:

$$\frac{\partial\left(\rho_p C_p (1-\phi)T_s\right)}{\partial t}-\frac{\partial}{\partial x}\left((1-\phi)K_p\frac{\partial T_s}{\partial x}\right)-\frac{\partial}{\partial y}\left((1-\phi)K_p\frac{\partial T_s}{\partial y}\right)-\frac{\partial}{\partial z}\left((1-\phi)K_p\frac{\partial T_s}{\partial z}\right)$$
$$=-a_{sp}h_t(T_{PSurface}-T_a)+(1-\phi)\rho_p R_P$$

(A.164)

where:

t = time(s).

ρ_p = product density (kg m^{-3}).

T_s = intrinsic phase average of solid temperature (K).

K_p = product thermal conductivity (W K^{-1} m^{-1}).

C_p = product specific heat (J kg^{-1} K^{-1}).

R_p = product respiration heat (W kg^{-1}).

ϕ = porosity.

a_{ap} = specific interstitial surface area (m^{-1}).

h_t = heat transfer coefficient between air and solid surface (W m^{-2} K^{-1}).

Applying the same numerical schemes used to derive the air energy discretisation equation, the coefficients and source term for the solid discretisation equation were derived:

$$a_{TsE-P-scalar} = -\frac{(1-\phi_{e-scalar})K_p}{x_{E-scalar} - x_{P-scalar}} A_{e-scalar} \quad \text{(A.165)}$$

$$a_{TsW-P-scalar} = -\frac{(1-\phi_{w-scalar})K_p}{x_{P-scalar} - x_{W-scalar}} A_{w-scalar} \quad \text{(A.166)}$$

$$a_{TsN-P-scalar} = -\frac{(1-\phi_{n-scalar})K_p}{y_{N-scalar} - y_{P-scalar}} A_{n-scalar} \quad \text{(A.167)}$$

$$a_{TsS-P-scalar} = -\frac{(1-\phi_{s-scalar})K_p}{y_{P-scalar} - y_{S-scalar}} A_{s-scalar} \quad \text{(A.168)}$$

$$a_{TsH-P-scalar} = -\frac{(1-\phi_{h-scalar})K_p}{z_{H-scalar} - z_{P-scalar}} A_{h-scalar} \quad \text{(A.169)}$$

$$a_{TsL-P-scalar} = -\frac{(1-\phi_{l-scalar})K_p}{z_{P-scalar} - z_{L-scalar}} A_{l-scalar} \quad \text{(A.170)}$$

$$a_{TsT-P-scalar} = \frac{\rho_a(1-\phi_{P-scalar})C_p V_{P-scalar}}{\Delta t} \quad \text{(A.171)}$$

$$S_{TsT-P-scalar} = \frac{\rho_a(1-\phi_{P-scalar})C_p V_{P-scalar}}{\Delta t} T^{old}_{s-P-scalar} \quad \text{(A.172)}$$

$$a_{TsP-P-scalar} = -\left(a_{TsL-P-scalar} + a_{TsW-P-scalar} + a_{TsS-T-scalar} + a_{TsN-P-scalar} + a_{TsE-P-scalar} + a_{TsH-P-scalar}\right) + a_{TsT-P-scalar} \tag{A.173}$$

$$S_{Ts-P-scalar} = S_{TsT-P-scalar} + h_{t-P-scalar} a_{aP} V_{p-scalar} (T_{a-P-scalar} - T_{p-subl}) + (1-\phi_{P-scalar}) \rho_p R_{p-P-scalar} V_{p-scalar} \tag{A.174}$$

where:

a_{TsT} = coefficient of time term in solid energy discretisation equation (W K^{-1}).

V = volume of scalar cell (m^3).

Δt = time step (s).

S_{TsT} = source term in solid energy discretisation equation caused by time discretisation (W).

T_{p-subl} = temperature of sub-cell1 of representative produce item (K).

(3) Produce item energy discretisation equations

As shown in Figure 6.13, the produce item energy discretisation equation for sub-cell1 was derived over sub-cell1 from the energy equation for produce item (Equation 5.5):

$$\int_{V_{subl}} \left(\frac{\partial(\rho_p C_p T_p)}{\partial t} \right) dv - \int_{A_{subl}} \left(\frac{1}{r^2} \frac{\partial}{\partial r} (K_p r^2 \frac{\partial T_p}{\partial r}) \right) ds + \int_{A_{sub2}} \left(\frac{1}{r^2} \frac{\partial}{\partial r} (K_p r^2 \frac{\partial T_p}{\partial r}) \right) ds = \int_{V_{subl}} (\rho_p R_p) dv \tag{A.175}$$

where:

A_{subl} = outer surface area of sub-cell1 (m^2).

A_{sub2} = outer surface area of sub-cell2 (m^2).

The unsteady term was approximated as follows:

$$\int_{V_{subl}} \left(\frac{\partial(\rho_p C_p T_p)}{\partial t} \right) dv = \frac{\rho_p C_p V_{subl}}{\Delta t} (T_{p-subl}^{current} - T_{p-subl}^{old}) \tag{A.176}$$

where:

T_{p-subl} = temperature of sub-cell1 of representative produce item (K).

V_{subl} = volume of sub-cell1 (m^3).

Δt = time step (s).

The diffusion term on the outer surface of sub-cell1 (surface of produce item) was calculated according to the convection heat transfer between air and produce item surface, and the conduction heat transfer between the produce items in current scalar cell with the produce items in neighbouring scalar cells:

$$-\int_{A_{sub1}}\left(\frac{1}{r^2}\frac{\partial}{\partial r}(K_p r^2\frac{\partial T_p}{\partial r})\right)ds = -A_{sub1}(T_{a-P-scalar}-T_{p-sub1})h_{t-P-scalar} + \frac{V_{produce}}{V_{p-scalar}(1-\phi_{P-scalar})}\begin{pmatrix} a_{TsE-P-scalar}(T_{s-E-scalar}-T_{s-P-scalar})-a_{TsW-P-scalar}(T_{s-P-scalar}-T_{s-W-scalar}) \\ a_{TsN-P-scalar}(T_{s-N-scalar}-T_{s-P-scalar})-a_{TsS-P-scalar}(T_{s-P-scalar}-T_{s-S-scalar}) \\ a_{TsH-P-scalar}(T_{s-H-scalar}-T_{s-P-scalar})-a_{TsL-P-scalar}(T_{s-P-scalar}-T_{s-L-scalar}) \end{pmatrix} \quad \text{(A.177)}$$

where:

$V_{produce}$ = volume of produce item (m^3).

The diffusion term on the surface between sub-cell1 and sub-cell2 was approximated as follows:

$$\int_{A_{sub2}}\left(\frac{1}{r^2}\frac{\partial}{\partial r}(K_p r^2\frac{\partial T_p}{\partial r})\right)ds = \frac{A_{sub2}K_p\left(T_{p-sub1}^{current}-T_{p-sub2}^{current}\right)}{(r_{sub1}-r_{sub2})} \quad \text{(A.178)}$$

where:

$T_{p\text{-}sub1}$ = temperature of sub-cell1 of representative produce item (K).

$T_{p\text{-}sub2}$ = temperature of sub-cell2 of representative produce item (K).

r_{sub1} = radium of grid node in sub-cell1 (m).

r_{sub2} = radium of grid node in sub-cell2 (m).

The source term was approximated using Equation 5.14:

$$\int_{V_{sub1}}(\rho_P R_p)dv = \rho_p c(T_{p-sub1}-255.35)^d V_{sub1} \quad \text{(A.179)}$$

where:

c = constant.

d = constant.

Based on the above analysis, the coefficients and source terms in the produce item discretisation equation for sub-celll were derived:

$$a_{Tp1-sub1} = \frac{A_{sub2} K_p}{(r_{sub1} - r_{sub2})} + \frac{\rho_p C_p V_{sub1}}{\Delta t} \tag{A.180}$$

$$a_{Tp1-sub2} = -\frac{A_{sub2} K_p}{(r_{sub1} - r_{sub2})} \tag{A.181}$$

$$S_{Tp-sub1} = \rho_p c\left(T_{p-sub1} - 255.35\right)^d V_{sub1} + \frac{\rho_p C_p V_{sub1}}{\Delta t} T^{old}_{p-sub1} + A_{sub1}\left(T_{a-P-scalar} - T_{p-sub1}\right) h_{t-P-scalar} -$$
$$\frac{V_{produce}}{V_{p-scalar}\left(1-\phi_{P-scalar}\right)} \begin{pmatrix} a_{TsE-P-scalar}\left(T_{s-E-scalar} - T_{s-P-scalar}\right) - a_{TsW-P-scalar}\left(T_{s-P-scalar} - T_{s-W-scalar}\right) \\ a_{TsN-P-scalar}\left(T_{s-N-scalar} - T_{s-P-scalar}\right) - a_{TsS-P-scalar}\left(T_{s-P-scalar} - T_{s-S-scalar}\right) \\ a_{TsH-P-scalar}\left(T_{s-H-scalar} - T_{s-P-scalar}\right) - a_{TsL-P-scalar}\left(T_{s-P-scalar} - T_{s-L-scalar}\right) \end{pmatrix} \tag{A.182}$$

As long as the time step and sub-cells are set, the coefficients are decided, so there is no need to update the coefficients during calculation.

The same numerical schemes were applied to derive produce-item energy discretisation equations for other sub-cells.

- **Energy discretisation equations for scalar cells in the produce-air region and next to a package wall with vent**

As shown in Figure A.20, the scalar cell next to west package wall with vent is the same as the scalar cells in the middle of produce regions apart from derivation of the coefficients for the west node.

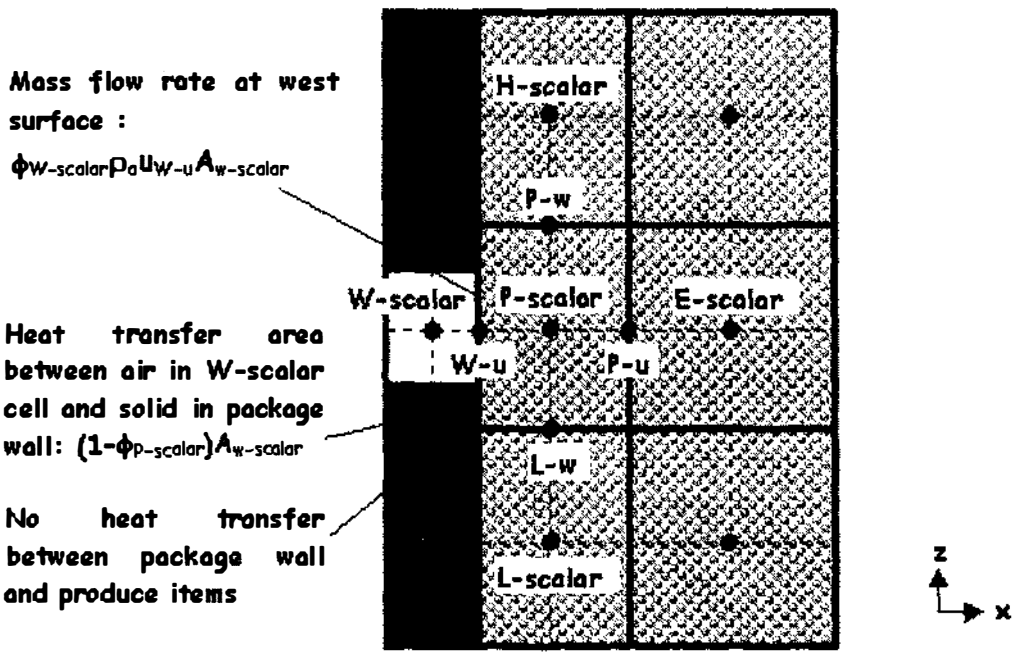

Figure A.20 Treatment of scalar cell next to west package wall with vent for deriving energy discretisation equations

(1) Air energy discretisation equation

At the interface between plain air region and produce-air region, the porosity was set as one for maintaining mass and energy conservation similar to the treatment for momentum and pressure discretisation equations. Therefore for the scalar cell next to west package wall with vent, the energy flux at west surface from plain air region to the air in produce-air region was calculated as follows:

$$\int_{A_{w-scalar}} \left(\rho_a \phi u C_a T_a - (\phi K_a + K_{dis}) \frac{\partial T_a}{\partial x} \right) ds = \left(\begin{array}{l} \max(\rho_a C_a u_{W-u}, 0) T_{a-W-scalar}^{current} + \min(\rho_a C_a u_{W-u}, 0) T_{a-P-scalar}^{current} \\ - \dfrac{K_a \left(T_{a-P-scalar}^{current} - T_{a-W-scalar}^{current} \right)}{x_{P-scalar} - x_{W-scalar}} \end{array} \right) A_{w-scalar} \phi_{W-scalar} \quad \text{(A.183)}$$

The energy flux at west surface from package wall into the air in the scalar cell was calculated using Equation (5.19):

$$Q_{pack-air} = h_{t-P-scalar}(T_{s-W-scalar} - T^{current}_{a-P-scalar})(1-\phi_{W-scalar})A_{w-scalar} \quad \text{(A.184)}$$

Based on the above analysis, the coefficients were modified as follows:

$$a_{TaW-P-scalar} = \left(-\max(\rho_a C_a u_{W-u},0) - \frac{K_a}{x_{P-scalar} - x_{W-scalar}}\right) A_{w-scalar}\phi_{W-scalar} \quad \text{(A.185)}$$

$$a_{TaP-P-scalar} = -(a_{TaL-P-scalar} + a_{TaW-P-scalar} + a_{TaS-T-scalar} + a_{TaN-P-scalar} + a_{TaE-P-scalar} + a_{TaH-P-scalar}) + a_{TaT-P-scalar} + h_{t-P-scalar}a_{aP}V_{p-scalar} + h_{t-P-scalar}(1-\phi_{W-scalar})A_{w-scalar} \quad \text{(A.186)}$$

$$S_{Ta-P-scalar} = S_{dTa-P-scalar} + S_{dTae-P-scalar} + S_{dTas-P-scalar} + S_{dTan-P-scalar} + S_{dTal-P-scalar} + S_{dTah-P-scalar} + S_{TaT-P-scalar} + h_{t-P-scalar}a_{aP}V_{p-scalar}T_{p-subl} + h_{t-P-scalar}T_{s-W-scalar}(1-\phi_{W-scalar})A_{-scalar} \quad \text{(A.187)}$$

The same method was applied for the scalar cells next to other package walls.

(2) Solid energy discretisation equation

For the scalar cell next to west package wall with vent, the energy flux at west surface to the solid (produce) in the scalar cell was zero since the heat transfer between produce and package walls was assumed negligible. Therefore the coefficient for west grid node was set to zero.

$$a_{TaW-P-scalar} = 0 \quad \text{(A.188)}$$

The same method was applied for the scalar cells next to other package walls.

(3) Produce item energy discretisation equations

Since the coefficient for west node was set to zero, the produce item energy discretisation equations for the scalar cell in the middle of produce-air region are equally applicable and can be used.

- **Energy discretisation equations for scalar cells in the produce-air region and next to a package wall without vent**

Since the porosity of the cells in package walls without vent was set to zero, all discretisation equations derived in the previous section were used ($\phi_{W\text{-}scalar}$ in these equations is 0).

A.3.3 Energy Discretisation Equations for Scalar Cells in Package Walls

- **Energy discretisation equations for scalar cells on package walls with vents where airflow moves from one package to another**

(1) Air energy discretisation equation

As shown in Figure A.21, the middle part of the scale cell, which contains the vent in east package wall, was used to derive air energy discretisation equation from the one-dimensional energy conservation equation for air (Equation 5.1a). The energy flux between plain air region and produce-air region at the west surface was discussed in Section A.3.2 (Equation A.183). The energy fluxes form south, north, top, and bottom surfaces of the vent were ignored.

The air energy flux at the east surface was derived from the one-dimensional air energy conservation equation (Equation 5.1a):

$$\int_{A_{e-scalar}} \left(\rho_a u C_a T_a - K_a \frac{\partial T_a}{\partial x} \right) ds = \left(\begin{array}{l} \max(\rho_a C_a u_{P-u}, 0) T_{a-P-scalar}^{current} + \min(\rho_a C_a u_{P-u}, 0) T_{a-E-scalar}^{current} \\ - \dfrac{K_a \left(T_{a-E-scalar}^{current} - T_{a-P-scalar}^{current} \right)}{x_{E-scalar} - x_{P-scalar}} \end{array} \right) A_{e-scalar} \phi_{P-scalar} \tag{A.189}$$

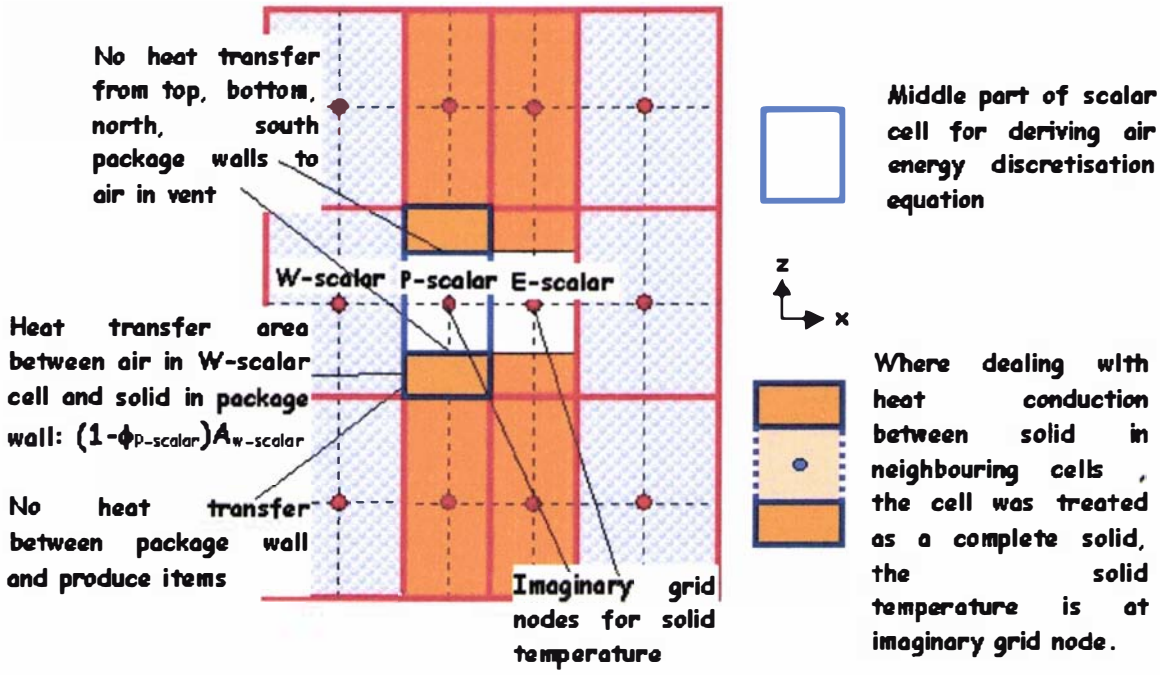

Figure A.21 Treatment of the scalar cell in a vented east wall of one package next to a vented west wall of another package for deriving energy discretisation equations.

Based on the above analysis, the coefficients in air energy discretisation equation were derived:

$$a_{TaE-P-scalar} = \left(\min\left(\rho_a C_a u_{P-u}, 0\right) - \frac{K_a}{x_{E-scalar} - x_{P-scalar}} \right) A_{e-scalar} \phi_{P-scalar} \tag{A.190}$$

$$a_{TaW-P-scalar} = \left(-\max\left(\rho_a C_a u_{W-u}, 0\right) - \frac{K_a}{x_{P-scalar} - x_{W-scalar}} \right) A_{w-scalar} \phi_{P-scalar} \tag{A.191}$$

$$a_{TaN-P-scalar} = 0 \tag{A.192}$$

$$a_{TaS-P-scalar} = 0 \tag{A.193}$$

$$a_{TaH-P-scalar} = 0 \tag{A.194}$$

$$a_{TaL-P-scalar} = 0 \tag{A.195}$$

$$a_{TaT-P-scalar} = \frac{\rho_a \phi_{P-scalar} C_a V_{P-scalar}}{\Delta t} \tag{A.196}$$

$$a_{TaP-P-scalar} = a_{TaW-P-scalar} + a_{TaE-P-scalar} + a_{TaT-P-scalar} \tag{A.197}$$

$$S_{TaT-P-scalar} = \frac{\rho_a \phi_{P-scalar} C_a V_{P-scalar}}{\Delta t} T^{old}_{a-P-scalar} \tag{A.198}$$

$$S_{Ta-P-scalar} = S_{TaT-P-scalar} \tag{A.199}$$

(2) Solid energy discretisation equations

As shown in Figure A.21, to avoid dealing with the complicated geometry of the solid part around the vent, the scalar cell was treated as a complete solid region while approximating heat conduction between neighbouring cells. The solid temperature was calculated at the imaginary grid node.

The heat transfer between the solid part of scalar cell in a package wall and the air and produce in produce-air region was discussed earlier in Section A.4.2 (Equation A.184 and Equation A.188).

Based on the above analysis, the coefficients and source terms for solid discretisation equation in package wall were derived:

$$a_{TsE-P-scalar} = -\frac{K_p}{x_{E-scalar} - x_{P-scalar}} A_{e-scalar} (1 - \phi_{P-scalar}) \tag{A.200}$$

$$a_{TsW-P-scalar} = 0 \tag{A.201}$$

$$a_{TsN-P-scalar} = -\frac{K_p}{y_{N-scalar} - y_{P-scalar}} A_{n-scalar} \tag{A.202}$$

$$a_{TsS-P-scalar} = -\frac{K_p}{y_{P-scalar} - y_{S-scalar}} A_{s-scalar} \tag{A.203}$$

$$a_{TsH-P-scalar} = -\frac{K_p}{z_{H-scalar} - z_{P-scalar}} A_{h-scalar} \quad \text{(A.204)}$$

$$a_{TsL-P-scalar} = -\frac{K_p}{z_{P-scalar} - z_{L-scalar}} A_{l-scalar} \quad \text{(A.205)}$$

$$a_{TsT-P-scalar} = \frac{\rho_a (1-\phi_{P-scalar}) C_p V_{P-scalar}}{\Delta t} \quad \text{(A.206)}$$

$$S_{TsT-P-scalar} = \frac{\rho_a (1-\phi_{P-scalar}) C_p V_{P-scalar}}{\Delta t} T^{old}_{s-P-scalar} \quad \text{(A.207)}$$

$$a_{TsP-P-scalar} = -(a_{TsL-P-scalar} + a_{TsW-P-scalar} + a_{TsS-T-scalar} + a_{TsN-P-scalar} + a_{TsE-P-scalar} + a_{TsH-P-scalar}) + a_{TsT-P-scalar} + h_{t-W-scalar}(1-\phi_{P-scalar}) A_{w-scalar} \quad \text{(A.208)}$$

$$S_{Ts-P-scalar} = S_{TsT-P-scalar} + h_{t-P-scalar} A_{w-scalar} T_{a-W-scalar} (1-\phi_{P-scalar}) \quad \text{(A.209)}$$

This same method was employed to derive the air and solid discretisation equations for the scalar cells in other vented package walls that are adjacent to a vented wall in another package.

- **Energy discretisation equations for scalar cells in package walls with vents where airflow enters package from outside environment**

As shown in Figure A.22, the same methods described in the previous section were employed to derive the solid energy discretisation equation for the scalar cells in package walls where air enters package. In this scenario there is no need for the air energy discretisation equation, as the temperature at grid node was simply set as the temperature of air entering package according to the boundary condition outlined in Chapter 5 (Equation 5.16).

$$T_{a-P-scalar} = T_{a-enter} \quad \text{(A.210)}$$

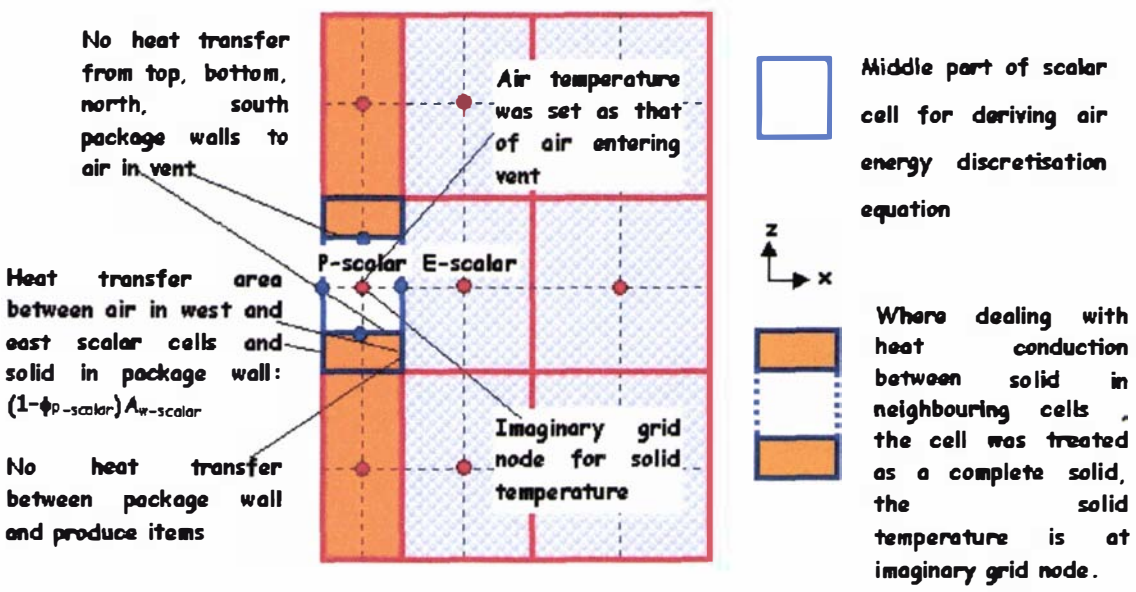

Figure A.22 Treatment of the scalar cell in a vented west wall where air enters the package

where:

$T_{a\text{-}enter}$ = temperature of air entering a vent (K).

- **Energy discretisation equations for scalar cells in package walls with vents where airflow leaves package to outside environment**

As shown in Figure A.23, the same methods described in the previous section were employed to derive solid energy discretisation equation for the scalar cells in package walls where air enters package.

Similarly there is no need for the air energy discretisation equation, as the temperature at grid node was simply set as the temperature of down stream airflow according to the boundary condition outlined in Chapter 5 (Equation 5.17):

$$T_{a-P-scalar} = T_{a-E-scalat} \qquad \text{(A.211)}$$

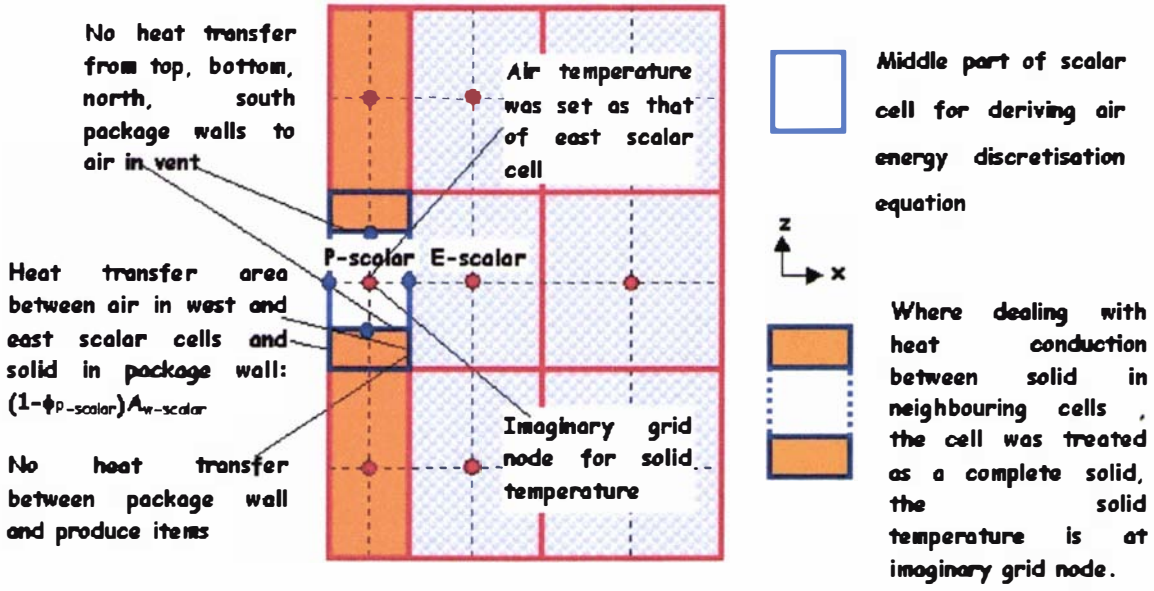

Figure A.23 Treatment of the scalar cell in a vented west wall where air leaves the package

- **Energy discretisation equations for scalar cells in package walls without vents**

The solid energy discretisation equations for this type of scalar cells were treated as special cases of that for the scalar cells in package walls with vents, while the porosity was set to zero. Therefore, there is no need for the air energy discretisation equation for the scalar cells in package walls without vents.

A.4 Discretisation Equations for PDEs in the Heat Transfer Model for Layered Packaging Systems

A.4.1 Numerical Schemes

- **Discretisation equations**

In general, for each scalar cell in layered package two discretisation energy equations were derived.

1) Solid energy discretisation equation was derived from the energy conservation equation for package walls in solid region (Equation 5.2). The solid energy

discretisation equations for layered packages have the same form as that for bulk packages (Equation A.140).

2) Air energy discretisation equation was derived from the energy conservation equation for air in vents (Equations 5.1a and 5.1b) or the volume-averaged energy conservation equation for air in produce-air region (Equations 5.22). The air energy discretisation equations for layered packages have the same form as that for bulk packages (Equation A.141).

Similar to bulk packages, for each scalar cell in produce-air region, a representative produce item was divided into four sub-cells. For each sub-cell, a discretisation equation was derived from the energy equation for produce item (Equations A.142-A.145).

- **Types of scalar cells in terms of derivation of energy discretisation equations**

There are seven types of scalar cells in terms of derivation of the energy discretisation equations, which are summarised in Figure A.24 and Table A.10.

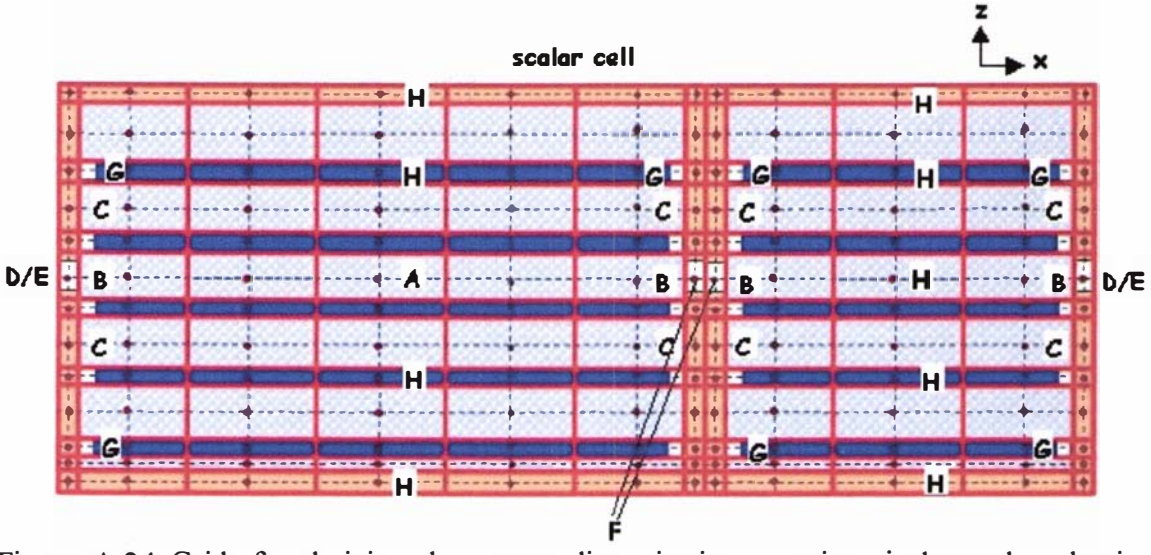

Figure A.24 Grids for deriving the energy discretisation equations in layered packaging systems (the capital letters indicate the types of scalar cells in terms of derivation of the energy discretisation equations, which are explained in Table A.10)

Table A.10 Types of scalar cells in terms of derivation of energy discretisation equations in layered packaging systems

Type	Location	Transport equations
A	Middle of produce-air regions	• Volume-averaged energy equation for air (Equation 5.22) • Energy equation for single item of produce (Equation 5.5)
B	In produce-air regions and next to west, east, south, and north package walls with vents	• Volume-averaged energy equation for air (Equation 5.22) • Energy equation for single item of produce (Equation 5.5)
C	In produce-air regions and next to west, east, south, and north package walls without vents	• Volume-averaged energy equation for air (Equation 5.22) • Energy equation for single item of produce (Equation 5.5)
D	In west, east, south, north package walls with fixed-velocity vents	• One-dimensional energy conservation equation for air (Equation 5.1a and 5.1b) • Energy conservation equation for package walls (Equation 5.2)
E	In west, east, south, north package walls with fixed-pressure vents	• One-dimensional energy conservation equation for air (Equation 5.1a and 5.1b) • Energy conservation equation for package walls (Equation 5.2)
F	In vented west/east/south /north package wall next to another vented package wall	• One-dimensional energy conservation equation for air (Equation 5.1a and 5.1b) • Energy conservation equation for package walls (Equation 5.2)
G	In trays with gaps between tray edges and package walls	• One-dimensional energy conservation equation for air (Equation 5.21) • Energy conservation equation for package walls (Equation 5.2)
H	In trays and package walls without vents and trays	• Energy conservation equation for package walls (Equation 5.2)

A.4.2 Energy Discretisation Equations for Scalar Cells in Produce-Air Regions

- **Energy discretisation equations for scalar cells in the middle of produce-air regions**

(1) Air energy discretisation equation

The air energy discretisation equations for scalar cells in air-produce regions for layered packaging systems are very similar to that for the bulk packaging systems. However, the main difference is that the energy flux on the low and high surfaces of the cells in the layered packaging system are only caused by heat transfer between trays and air as shown in Figure A.25.

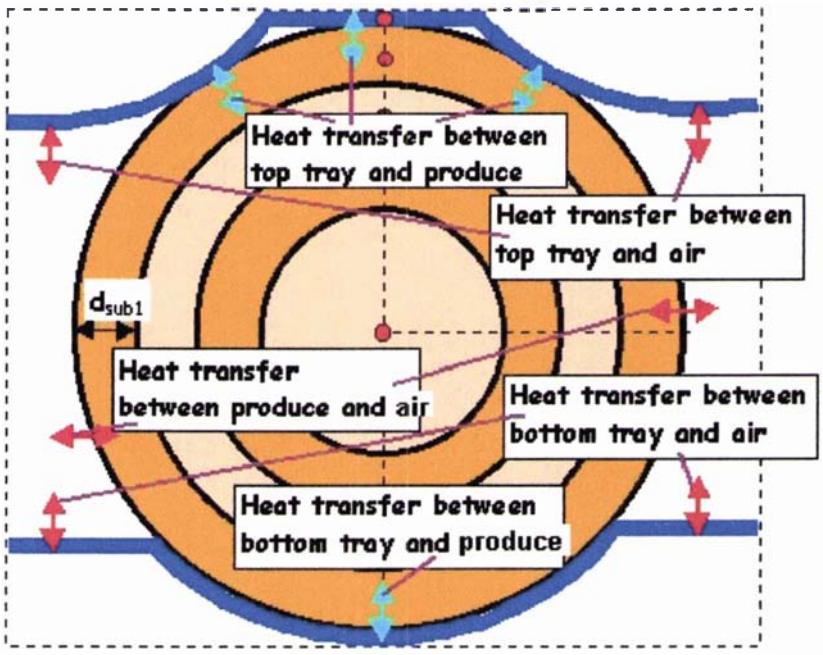

Figure A.25 Heat transfer within the scalar cell in produce-air region

$$Q_{l-scalar} = h_{t-P-scalar}(T_{s-L-scalar} - T_{a-P-scalar}^{current})\frac{(1-\phi_{P-scalar})V_{P-scalar}A_{bottom-tray-air}}{V_{produce}} \quad \text{(A.212)}$$

$$Q_{h-scalar} = h_{t-P-scalar}(T_{s-H-scalar} - T_{a-P-scalar}^{current})\frac{(1-\phi_{P-scalar})V_{P-scalar}A_{top-tray-air}}{V_{produce}} \quad \text{(A.213)}$$

where:

Q	=	energy flux entering scalar cell at a surface (W).
$A_{top\text{-}tray\text{-}air}$	=	area of top tray portion exposed to air per produce item (m^2).
$A_{bottom\text{-}tray\text{-}air}$	=	area of bottom tray portion exposed to air per produce item (m^2).
$V_{produce}$	=	produce item volume (m3).

The coefficients for low and high nodes in the discretisation equations were modified, and the items for low and high nodes in source terms of discretisation equations were set to zero:

$$a_{TaH-P-scalar} = 0 \quad \text{(A.214)}$$

$$a_{TaL-P-scalar} = 0 \quad \text{(A.215)}$$

$$a_{TaP-P-scalar} = -\left(a_{TaW-P-scalar} + a_{TaS-T-scalar} + a_{TaN-P-scalar} + a_{TaE-P-scalar}\right) + a_{TaT-P-scalar} + h_{t-P-scalar}\frac{(1-\phi_{P-scalar})V_{P-scalar}A_{produce-air}}{V_{produce}} + h_{t-P-scalar}\frac{(1-\phi_{P-scalar})V_{P-scalar}A_{bottom-tray-air}}{V_{produce}} + h_{t-P-scalar}\frac{(1-\phi_{P-scalar})V_{P-scalar}A_{top-tray-air}}{V_{produce}} \quad \text{(A.216)}$$

$$S_{Ta-P-scalar} = S_{dTaw-P-scalar} + S_{dTae-P-scalar} + S_{dTas-P-scalar} + S_{dTan-P-scalar} + S_{TaT-P-scalar} + T_{PSurface-P-scalar}h_{t-P-scalar}\frac{(1-\phi_{P-scalar})V_{P-scalar}A_{produce-air}}{V_{produce}} + h_{t-P-scalar}T_{s-L-scalar}\frac{(1-\phi_{P-scalar})V_{P-scalar}A_{bottom-tray-air}}{V_{produce}} + h_{t-P-scalar}T_{s-h-scalar}\frac{(1-\phi_{P-scalar})V_{P-scalar}A_{top-tray-air}}{V_{produce}} \quad \text{(A.217)}$$

where:

$A_{produce-air}$ = area of produce item surface portion exposed to air (m^2).

Other coefficients and terms in Equations A.217-6.218 were calculated with the coefficient expressions for bulk packages (Equations A.150-A.163).

(2) Produce item discretisation equations

The energy fluxes entering to the surface of produce item consist of energy fluxes from air, top tray, and bottom tray, which were approximated as follows:

$$Q_{air-produce} = h_{t-P-scalar}(T_{a-L-scalar} - T_{p-subl})A_{produce-air} \quad \text{(A.218)}$$

$$Q_{top-tray-produce} = \left(\frac{d_{subl}}{d_{subl}+d_{tray}}K_{tray} + \frac{d_{tray}}{d_{subl}+d_{tray}}K_p\right)\frac{2(T_{s-H-scalar} - T_{subl}^{current})A_{top-tray-produce}}{d_{subl}+d_{tray}} \quad \text{(A.219)}$$

$$Q_{top-tray-produce} = \left(\frac{d_{subl}}{d_{subl}+d_{tray}}K_{tray} + \frac{d_{tray}}{d_{subl}+d_{tray}}K_p\right)\frac{2(T_{s-L-scalar} - T_{subl}^{current})A_{bottom-tray-produce}}{d_{subl}+d_{tray}} \quad \text{(A.220)}$$

where:

$Q_{air\text{-}produce}$	=	energy flux from air to representative produce item(W).
$Q_{top\text{-}tray\text{-}produce}$	=	energy flux from top tray to representative produce item(W).
$Q_{bottom\text{-}tray\text{-}produce}$	=	energy flux from bottom tray to representative produce item(W).
$A_{top\text{-}tray\text{-}produce}$	=	contact area between top tray and representative produce item (m^2).
$A_{bottom\text{-}tray\text{-}produce}$	=	contact area between bottom tray and representative produce item (m^2).
K_{tray}	=	tray thermal conductivity (W m^{-1} K^{-1}).
d_{subl}	=	thickness of sub-cells (m).
d_{tray}	=	thickness of tray (m).

Based on the above considerations, the coefficient and source term in produce item discretisation equation for sub-cell1 were modified as follows:

$$a_{Tp1-subl} = \frac{A_{sub2}K_p}{(r_{subl} - r_{sub2})} + \frac{\rho_p C_p V_{subl}}{\Delta t} + \left(\frac{d_{subl}}{d_{subl} + d_{tray}} K_{tray} + \frac{d_{tray}}{d_{subl} + d_{tray}} K_p \right) \frac{2\left(A_{top-try-produce} + A_{bottom-try-produce}\right)}{d_{subl} + d_{tray}} \quad \text{(A.221)}$$

$$S_{Tp-subl} = \rho_p c\left(T_{p-subl} - 255.35\right)^d V_{subl} + \frac{\rho_p C_p V_{subl}}{\Delta t} T_{p-subl}^{old} + A_{subl}(T_{a-P-scalar} - T_{p-subl})h_{t-P-scalar} - \left(\frac{d_{subl}}{d_{subl} + d_{tray}} K_{tray} + \frac{d_{tray}}{d_{subl} + d_{tray}} K_p \right) \frac{2\left(T_{s-H-scalar}A_{top-try-produce} + T_{s-L-scalar}A_{bottom-try-produce}\right)}{d_{subl} + d_{tray}} \quad \text{(A.222)}$$

Other coefficients and source terms in the produce-item discretisation equations were the same as those for bulk packages.

- **Energy discretisation equations for scalar cells in the produce-air region and next to a package wall with vent**

As shown in Figure A.26, for the scalar cell next to vented west package wall, energy flux at low and high surfaces should account for the flux from the gaps between package wall

and tray edges. The energy flows from the gaps and vents in layered package walls were treated in the same way as for the ones from vent in bulk package wall (Equation A.183). Therefore the coefficients were modified as follows:

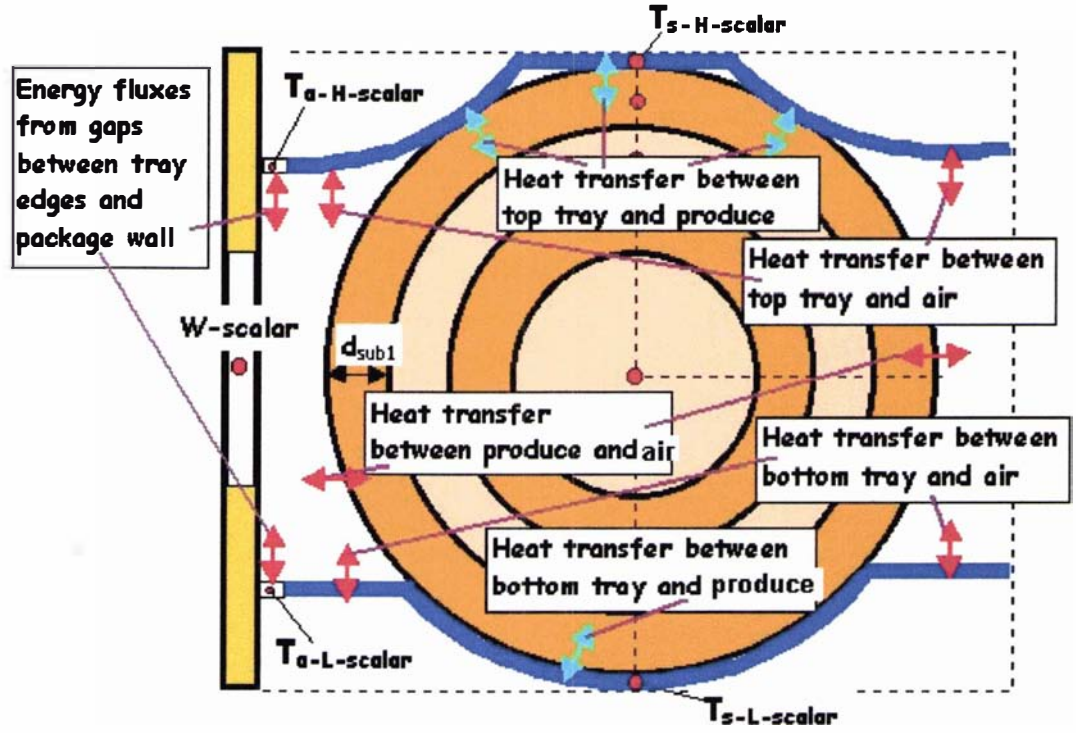

Figure A.26 Treatment of scalar cell next to west wall in layered package with vent for deriving energy discretisation equations

$$a_{TaW-P-scalar} = \left(-\max(\rho_a C_a u_{W-u}, 0) - \frac{K_a}{x_{P-scalar} - x_{W-scalar}} \right) A_{w-scalar} \phi_{W-scalar} \qquad \text{(A.223)}$$

$$a_{TaL-P-scalar} = \left(-\max(\rho_a C_a w_{L-w}, 0) - \frac{K_a}{z_{P-scalar} - z_{L-scalar}} \right) A_{l-scalar} \phi_{L-scalar} \qquad \text{(A.224)}$$

$$a_{TaH-P-scalar} = \left(\min(\rho_a C_a w_{H-w}, 0) - \frac{K_a}{z_{H-scalar} - z_{P-scalar}} \right) A_{h-scalar} \phi_{H-scalar} \qquad \text{(A.225)}$$

$$a_{TaP-P-scalar} = -\left(a_{TaW-P-scalar} + a_{TaS-T-scalar} + a_{TaN-P-scalar} + a_{TaE-P-scalar} + a_{TaL-P-scalar} + a_{TaH-P-scalar}\right) + a_{TaT-P-scalar} + h_{t-P-scalar}\frac{(1-\phi_{P-scalar})V_{P-scalar}A_{produce-air}}{V_{produce}} + h_{t-P-scalar}\frac{(1-\phi_{P-scalar})V_{P-scalar}A_{bottom-tray-air}}{V_{produce}} + h_{t-P-scalar}\frac{(1-\phi_{P-scalar})V_{P-scalar}A_{top-tray-air}}{V_{produce}}$$

(A.226)

Other coefficients and source term in the air energy discretisation equations for the scalar cells next to vented package walls were the same as the ones for the scalar cells in the middle of produce-air regions.

The produce item energy discretisation equations are the same as the ones for the scalar cells in the middle of produce-air regions.

- **Energy discretisation equations for scalar cells in the produce-air region and next to a package wall without vent**

Similar to the situation for bulk package, all discretisation equations derived in the previous section are applicable and can be used when the porosity for the cells in package walls was set to zero.

A.4.3 Energy Discretisation Equations for Scalar Cells in Package Walls

The air and solid discretisation equations in these types of scalar cells for layered packaging systems are the same as the ones for the bulk packaging systems. Particularly for the scalar cells in trays containing the gaps between walls and tray edges, the same treatment for the vents in package walls were employed (see Section A.3).

A.5 Convergence criteria

The residual of x-momentum equation over a cell was defined as follows:

$$R_{u-P-u} = a_{uL-P-u}u_{L-u}^{current} + a_{uW-P-u}u_{W-u}^{current} + a_{uS-P-u}u_{S-u}^{current} + a_{uP-P-u}u_{P-u}^{current} + a_{uN-P-u}u_{N-u}^{current} + a_{uE-P-u}u_{E-u}^{current} + a_{uH-P-u}u_{H-u}^{current} - S_{u-P-u} - (\phi_{p-scalar}p_{P-scalar} - \phi_{E-scalar}p_{E-scalar})A_{e-u}$$

(A.227)

where:

R_u = residual of momentum at x-axis over a cell (kg m s^{-1}).

The whole field residual was defined as the norm of residuals in all cells:

$$R_{u-field} = \sqrt{\sum_P R_{u-P-u}^2} \tag{A.228}$$

where:

$R_{u\text{-}field}$ = whole field residual of momentum at x-axis (kg m s^{-1}).

The norm of difference between two successive iterations was defined as:

$$\left|\Delta u^n\right| = \sqrt{\sum_p \left(u_{p-u}^{n+1} - u_{p-u}^n\right)^2} \tag{A.229}$$

where:

$u_{p-scalar}^{n+1}$ = $u_{p\text{-}scalar}$ calculated u at a x-momentum cell at n+1 iteration.

$u_{p-scalar}^{n}$ = $u_{p\text{-}scalar}$ calculated u at a x-momentum cell at n iteration.

$\left|\Delta u^n\right|$ = normalised difference between two successive iterations.

NOMENCLATURE

μ	=	air dynamic viscosity (N s m^{-2}).
μ_{eff}	=	effective viscosity of fluid in porous medium (kg m^{-1} s^{-1}).
ψ	=	quantity ψ of β phase in porous medium.
ψ'	=	spatial deviation of ψ.
φ	=	quantity φ of β phase in porous medium.
φ'	=	spatial deviation of φ.
ϕ	=	porosity.
ϕ_∞	=	free stream porosity.
ϕ_{gap}	=	estimated porosity of the vertical tunnel along package wall.
ρ_a	=	air density (kg m^{-3}).
ρ_B	=	bulk density of container packed with products (kg m^{-3}).
ρ_f	=	fluid density (kg m^{-3}).
ρ_p	=	product density (kg·m^{-3}).
ρ_{pack}	=	packaging material density (kg m^{-3}).
ρ_s	=	solid density (kg m^{-3}).
Δp	=	pressure correction (N m^{-2}).
Δt	=	time step (s).
$\lvert \Delta u^n \rvert$	=	normalised difference between two successive iterations.
$\langle \psi \rangle$	=	superficial average of ψ.
$\langle \psi \rangle_\beta$	=	intrinsic phase average of ψ.
$\langle p \rangle_a$	=	intrinsic phase average of air pressure (N m^{-2}).
$\langle T_a \rangle_a$	=	intrinsic phase average of air temperature (K).
$\langle T_p \rangle_p$	=	intrinsic phase average of product temperature (K).
$\langle u \rangle_a$	=	intrinsic phase average of air velocity component in the direction of x-axis (m s^{-1}).
$\langle \mathbf{v} \rangle$	=	superficial velocity (m s^{-1}).
$\langle v \rangle_a$	=	intrinsic phase average of air velocity component in the direction of y-axis (m s^{-1}).
$\langle w \rangle_a$	=	intrinsic phase average of air velocity component in the direction of z-axis (m s^{-1}).

a	=	empirical constant.
A	=	empirical parameter.
A	=	cell surface area (m^2).
$A_{\beta\sigma}$	=	interfacial area between β-phase and σ-phase contained within REV (m^2).
a_{ap}	=	specific interstitial surface area (m^{-1}).
$A_{bottom\text{-}tray\text{-}air}$	=	area of bottom tray portion exposed to air per produce item (m^2).
$A_{bottom\text{-}tray\text{-}produce}$	=	contact area between bottom tray and representative produce item (m^2).
A_{cell}	=	area of the cell (m^2).
A_{fs}	=	interfacial area between fluid phase and solid phase contained within REV (m^2).
a_{pE}	=	coefficient in pressure correction discretisation equation for east node.
$a_{p\text{-}exposed}$	=	exposed-to-air produce surface area per unit volume of air-produce region (m^{-1}).
a_{pH}	=	coefficient in pressure correction discretisation equation for high node.
a_{pL}	=	coefficient in pressure correction discretisation equation for low node.
a_{pN}	=	coefficient in pressure correction discretisation equation for north node.
a_{pP}	=	coefficient in pressure correction discretisation equation for current node.
$A_{produce\text{-}air}$	=	area of produce item surface portion exposed to air (m^2).
a_{pS}	=	coefficient in pressure correction discretisation equation for south node.
a_{pW}	=	coefficient in pressure correction discretisation equation for west node.
a_{sf}	=	specific surface area (m^{-1}).
A_{sub1}	=	outer surface area of sub-cell1 (m^2).
a_{TaE}	=	coefficient in air energy discretisation equation for east node ($W\,K^{-1}$).

a_{TaH} = coefficient in air energy discretisation equation for high node (W K^{-1}).

a_{TaL} = coefficient in air energy discretisation equation for low node (W K^{-1}).

a_{TaN} = coefficient in air energy discretisation equation for north node (W K^{-1}).

a_{TaP} = coefficient in air energy discretisation equation for current node (W K^{-1}).

a_{TaS} = coefficient in air energy discretisation equation for south node (W K^{-1}).

a_{TaT} = coefficient of time term in air energy discretisation equation (W K^{-1}).

a_{TaW} = coefficient in air energy discretisation equation for west node (W K^{-1}).

$A_{top\text{-}tray\text{-}air}$ = area of top tray portion exposed to air per produce item (m^2).

$A_{top\text{-}tray\text{-}produce}$ = contact area between top tray and representative produce item (m^2).

$a_{Tp1\text{-}sub1}$ = coefficient for produce temperature in sub-cell1 in produce item energy discretisation for sub-cell1 (W K^{-1}).

$a_{Tp1\text{-}sub2}$ = coefficient for produce temperature in sub-cell1 in produce item energy discretisation for sub-cell2 (W K^{-1}).

$a_{Tp2\text{-}sub1}$ = coefficient for produce temperature in sub-cell2 in produce item energy discretisation for sub-cell1 (W K^{-1}).

$a_{Tp2\text{-}sub2}$ = coefficient for produce temperature in sub-cell2 in produce item energy discretisation for sub-cell2 (W K^{-1}).

$a_{Tp2\text{-}sub3}$ = coefficient for produce temperature in sub-cell2 in produce item energy discretisation for sub-cell3 (W K^{-1}).

$a_{Tp3\text{-}sub2}$ = coefficient for produce temperature in sub-cell3 in produce item energy discretisation for sub-cell2 (W K^{-1}).

$a_{Tp3\text{-}sub3}$ = coefficient for produce temperature in sub-cell3 in produce item energy discretisation for sub-cell3 (W K^{-1}).

$a_{Tp3\text{-}sub4}$ = coefficient for produce temperature in sub-cell3 in produce item energy discretisation for sub-cell4 (W K^{-1}).

$a_{Tp3\text{-}sub4}$ = coefficient for produce temperature in sub-cell4 in produce item energy discretisation for sub-cell4 (W K^{-1}).

$a_{Tp4\text{-}sub3}$ = coefficient for produce temperature in sub-cell4 in produce item energy discretisation for sub-cell3 (W K^{-1}).

a_{TsE} = coefficient in solid energy discretisation equation for east node (W K^{-1}).

a_{TsH} = coefficient in solid energy discretisation equation for high node (W K^{-1}).

a_{TsL} = coefficient in solid energy discretisation equation for low node (W K^{-1}).

a_{TsN} = coefficient in solid energy discretisation equation for north node (W K^{-1}).

a_{TsP} = coefficient in solid energy discretisation equation for current node (W K^{-1}).

a_{TsS} = coefficient in solid energy discretisation equation for south node (W K^{-1}).

a_{TsT} = coefficient of time term in solid energy discretisation equation (W K^{-1}).

a_{TsW} = coefficient in solid energy discretisation equation for west node (W K^{-1}).

a_{uE} = coefficient in x-momentum discretisation equation for east node.

a_{uH} = coefficient in x-momentum discretisation equation for high node.

a_{uL} = coefficient in x-momentum discretisation equation for low node.

a_{uN} = coefficient in x-momentum discretisation equation for north node.

a_{uP} = coefficient in x-momentum discretisation equation for current node.

a_{uS} = coefficient in x-momentum discretisation equation for south node.

a_{uW} = coefficient in x-momentum discretisation equation for west node.

a_{vE}	=	coefficient in y-momentum discretisation equation for east node.
A_{vent}	=	area of the vent portion in a cell (m^2).
a_{vH}	=	coefficient in y-momentum discretisation equation for high node.
a_{vL}	=	coefficient in y-momentum discretisation equation for low node.
a_{vN}	=	coefficient in y-momentum discretisation equation for north node.
a_{vP}	=	coefficient in y-momentum discretisation equation for current node.
a_{vS}	=	coefficient in y-momentum discretisation equation for south node.
a_{vW}	=	coefficient in y-momentum discretisation equation for west node.
a_{wE}	=	coefficient in z-momentum discretisation equation for east node.
a_{wH}	=	coefficient in z-momentum discretisation equation for high node.
a_{wL}	=	coefficient in z-momentum discretisation equation for low node.
a_{wN}	=	coefficient in z-momentum discretisation equation for north node.
a_{wP}	=	coefficient in z-momentum discretisation equation for current node.
a_{wS}	=	coefficient in z-momentum discretisation equation for south node.
a_{wW}	=	coefficient in z-momentum discretisation equation for west node.
$\mathbf{B}$	=	body-force related to solid matrix ($N\ m^{-3}$).
b	=	empirical constant.
B	=	empirical parameter.
c	=	constant.
C_a	=	air specific heat at constant pressure ($J\ kg^{-1}\ K^{-1}$).

C_{dis}	=	empirical constant (~ 0.2).
ceil	=	function that rounds a number toward plus infinity.
C_l	=	empirical parameter (~ 0.5).
C_P	=	fluid constant-pressure specific heat capacity (J K^{-1} kg^{-1}).
C_p	=	product specific heat (J kg^{-1} K^{-1}).
C_{pack}	=	packaging material specific heat capacity (J K^{-1} m^{-1})
C_s	=	solid specific heat capacity (J kg^{-1} K^{-1}).
C_t	=	empirical parameter (~ 0.1).
D	=	constant tensor.
d	=	constant.
D*	=	constant tensor.
$D_{cell\text{-}est}$	=	estimated cell width (m).
d_{eq}	=	equivalent mean diameter (m).
d_p	=	diameter of particles (m).
d_{subl}	=	thickness of sub-cells (m).
D_t	=	empirical constant.
d_{tray}	=	thickness of tray (m).
F	=	Forcheimer coefficient.
F_{gap}	=	Forcheimer coefficient calculated from ϕ_{gap}.
g	=	gravitational constant (m s^{-2}).
H_{cell}	=	height of global cell (dimension of cell along z-axis) (m).
h_e	=	surface heat transfer coefficient (W m^{-2} K^{-1}).
H_{pack}	=	height of package (dimension of package along z-axis) (m).
h_{sf}	=	interfacial heat transfer coefficient (J K^{-1} m^{-2}).
h_t	=	heat transfer coefficient between air and solid surface (W m^{-2} K^{-1}).
$h_{t\text{-}out}$	=	heat transfer coefficient between outside airflow and package walls (W m^{-2} K^{-1}).
I	=	second-order identity tensor.
K	=	permeability of porous medium (m^2).
K_a	=	air thermal conductivity (W m^{-1} K^{-1}).
$\mathbf{K_d}$	=	dispersion conductivity tensor (W K^{-1} m^{-1}).
K_{dis}	=	dispersion conductivity (W K^{-1} m^{-1}).
K_{dl}	=	longitudinal dispersion conductivity (W K^{-1} m^{-1}).

K_{dt}	=	transverse dispersion conductivity (W K^{-1} m^{-1}).
$\mathbf{K_e}$	=	effective thermal conductivity tensor (W K^{-1} m^{-1}).
K_f	=	fluid thermal conductivity (W K^{-1} m^{-1}).
K_{gap}	=	permeability calculated from ϕ_{gap} (m^2).
K_p	=	product thermal conductivity ($W \cdot K^{-1} \cdot m^{-1}$).
K_{pack}	=	packaging material thermal conductivity (W K^{-1} m^{-1}).
K_s	=	solid thermal conductivity (W m^{-1} K^{-1}).
K_{tray}	=	tray thermal conductivity (W m^{-1} K^{-1}).
l	=	dimensionless dispersion length.
L_{cell}	=	length of global cell (dimension of package along x-axis) (m).
L_{pack}	=	length of package (dimension of package along x-axis) (m).
min	=	function that finds the minimum among several variables.
$m_{product\_total}$	=	total mass of products in the package (kg).
n	=	surface normal direction coordinate (m).
$\mathbf{n}$	=	unit vector in direction of fluid superficial velocity.
$\mathbf{n}_{\beta\sigma}$	=	unit normal vector pointing from β-phase to σ-phase.
n_1	=	integer.
n_2	=	integer.
$\mathbf{n}_{fs}$	=	unit normal vector pointing from fruit phase to solid phase.
Nu_d	=	Nusselt number.
n_x	=	number of global cells along x-axis.
n_y	=	number of global cells along y-axis.
n_z	=	number of global cells along z-axis.
p	=	pressure (N m^{-2}).
Pe_d	=	Peclet number based on particle dimension.
p_{fixed}	=	value of pressure at the vent (N m^{-2}).
Pr	=	Prandtl Number.
Q	=	energy flux entering scalar cell at a surface (W).
$q_{air\text{-}pack}$	=	heat flux from air to packaging material (W m^{-2}).
$Q_{air\text{-}produce}$	=	energy flux from air to representative produce item(W).
$q_{air\text{-}tray}$	=	heat flux from air to tray (W m^{-2}).
$Q_{bottom\text{-}tray\text{-}produce}$	=	energy flux from bottom tray to representative produce item(W).

$q_{out\text{-}pack}$ = heat flux from outside airflow to packaging material (W m^{-2}).

$q_{produce\text{-}air}$ = heat flux from air to produce item (W m^{-2}).

$Q_{top\text{-}tray\text{-}produce}$ = energy flux from top tray to representative produce item(W).

r = spatial variable along sphere radius (m).

$R_{cell\text{-}produce}$ = ratio between global cell horizontal dimension and produce equivalent diameter (m).

Re_d = Reynolds number.

R_p = product respiration heat (W kg^{-1}).

R_u = residual of momentum at x-axis over a cell (kg m s^{-1}).

$R_{u\text{-}field}$ = whole field residual of momentum at x-axis (kg m s^{-1}).

$S_{\Delta p}$ = source term for pressure correction discretisation equation (N).

S_{dTae} = source term due to CDS deferred correction at east surface in air energy discretisation equation (W).

S_{dTah} = source term due to CDS deferred correction at high surface in air energy discretisation equation (W).

S_{dTan} = source term due to CDS deferred correction at north surface in air energy discretisation equation (W).

S_{due} = source term due to CDS deferred correction at east surface in x momentum discretisation equation (N).

S_{duh} = source term due to CDS deferred correction at high surface in x-momentum discretisation equation (N).

S_{dul} = source term due to CDS deferred correction at low surface in x-momentum discretisation equation (N).

S_{dun} = source term due to CDS deferred correction at north surface in x-momentum discretisation equation (N).

S_{dus} = source term due to CDS deferred correction at south surface in x-momentum discretisation equation (N).

S_{duw} = source term due to CDS deferred correction at west surface in x-momentum discretisation equation (N).

S_p = mean surface area of produce item (m^2).

S_p = source term for pressure discretisation equation (N).

S_{sTal} = source term due to CDS deferred correction at low surface in air energy discretisation equation (W).

S_{sTas}	=	source term due to CDS deferred correction at south surface in air energy discretisation equation (W).
S_{sTaw}	=	source term due to CDS deferred correction at west surface in air energy discretisation equation (W).
S_{Ta}	=	source term for air energy discretisation equation (W).
S_{TaT}	=	source term in air energy discretisation equation due to time discretisation (W).
$S_{Tp\text{-}sub1}$	=	source term in produce item energy discretisation for sub-cell1 (W).
$S_{Tp\text{-}sub2}$	=	source term in produce item energy discretisation for sub-cell2 (W).
$S_{Tp\text{-}sub3}$	=	source term in produce-item energy discretisation for sub-cell3 (W).
$S_{Tp\text{-}sub4}$	=	source term in produce item energy discretisation for sub-cell4 (W).
S_{Ts}	=	source term for solid energy discretisation equation (W).
S_{TsT}	=	source term in solid energy discretisation equation caused by time discretisation (W).
S_u	=	source term for x-momentum discretisation equation (N).
S_v	=	source term for y-momentum discretisation equation (N).
S_w	=	source term for z-momentum discretisation equation (N).
t	=	time(s).
T_a	=	air temperature (K).
$T_{a\text{-}enter}$	=	temperature of air entering a vent (K).
T_{am}	=	ambient temperature (K).
$T_{a\text{-}out}$	=	outside airflow temperature (K).
T_f	=	fluid temperature (K).
$T_{f'}$	=	spatial deviation of fluid temperature (K).
T_p	=	produce temperature (K).
T_{pack}	=	packaging material temperature (K).
$T_{p\text{-}sub1}$	=	temperature of sub-cell1 of representative produce item (K).
$T_{p\text{-}sub2}$	=	temperature of sub-cell2 of representative produce item (K).
$T_{p\text{-}sub3}$	=	temperature of sub-cell3 of representative produce item (K).

$T_{p\text{-}sub4}$	=	temperature of sub-cell4 of representative produce item (K).
$T_{PSurface}$	=	produce surface temperature (K).
T_s	=	solid temperature (K).
T_s'	=	spatial deviation of solid temperature (K).
$T_{s\text{-}surface}$	=	solid surface temperature (K).
$T_{traySurface}$	=	tray surface temperature (K).
u	=	air velocity component in the direction of x-axis (m s^{-1}).
u_{fixed}	=	value of air velocity at the vent (m s^{-1}).
$u^{n}_{p-scalar}$	=	$u_{p\text{-}scalar}$ calculated u at a x-momentum cell at n iteration.
$u^{n+1}_{p-scalar}$	=	$u_{p\text{-}scalar}$ calculated u at a x-momentum cell at n+1 iteration.
v	=	air velocity component in the direction of y-axis (m s^{-1}).
$\mathbf{v}'$	=	spatial deviation of fluid velocity (m s^{-1}).
$\mathbf{v}$	=	velocity vector (m·s^{-1}).
V	=	volume of representative element volume (m^3).
V	=	volume of scalar cell (m^3).
V_β	=	volume of β phase in representative element volume (m^3).
V_p	=	mean particle volume (m^3).
V_p	=	mean volume of produce item (m^3).
$V_{produce}$	=	volume of produce item (m^3).
$V_{P\text{-}u}$	=	volume of x-momentum cell (m^3).
V_{sub1}	=	volume of sub-cell1 (m^3).
w	=	air velocity component in the direction of z-axis (m s^{-1}).
w	=	empirical constant.
W_{cell}	=	width of global cell (dimension of package along y-axis) (m).
$W_{gap\text{-}s}$	=	width of gap between package south wall and tray end (m).
$W_{gap\text{-}w}$	=	width of gap between package west wall and tray end (m).
W_{pack}	=	width of package (dimension of package along y-axis) (m).
y	=	distance from the nearest boundary (m).